Regulation of Cardiomyocyte Proliferation by microRNAs and Small Molecules

Thesis

Regulation of cardiomyocyte proliferation by microRNAs and small molecules

Consuelo Torrini

A Thesis submitted in fulfilment of the requirements of the Open University (UK) for the degree of Doctor of Philosophy

International Centre for Genetic Engineering and Biotechnology
ICGEB, Trieste, Italy

Director of the studies: Prof. Mauro Giacca
External supervisor: Prof Manuel Mayr

Submitted February, 2018

Abstract

Understanding the molecular mechanisms regulating cardiac cell proliferation during the embryonic, fetal and adult life holds a paramount importance in view of developing innovative strategies aimed at inducing myocardial regeneration after cardiac damage. Previous high throughput screening studies in our laboratory identified a series of microRNAs able to trigger cardiomyocyte proliferation and stimulate cardiac regeneration after myocardial infarction.

In the first part of this project, we investigated the mechanism of action of the top ten most effective of these miRNAs, revealing an involvement of the Hippo-YAP pathway in their action. We found that all the investigated miRNAs activated YAP-mediated transcription, nuclear localization of active YAP and increased expression of YAP responsive genes. Of notice, miR-199a-3p, one of the most effective miRNAs exerted its direct effect on two mRNA targets impinging on the Hippo pathway, the inhibitory kinase TAOK1 and the E3 ubiquitin ligase, β−TrCP. Most of the miRNAs inducing proliferation (including miR-199a-3p) also modulated the dynamics of the actin cytoskeleton in the treated cardiomyocytes, which displayed a rounded shape and gross bundles of actin fibers at the cytoplasm periphery. Consistent with these observations, we found that the Cofilin2 mRNA was a direct target of four of the investigated miRNAs and that downregulation of Cofilin2 itself was sufficient to promote cardiomyocyte proliferation, activate nuclear translocation of YAP and stimulate transcription of TEAD-responsive genes.

The second part of the project was aimed at identifying small molecules exerting a mitogenic effect on neonatal cardiomyocytes through an unbiased high-throughput screening (HTS) of a library of 780 FDA-registered drugs. The neuroactive alkaloid harmine was identified as the most powerful molecule at inducing cardiomyocyte proliferation *in vitro* and heart regeneration after myocardial infarction *in vivo*. Harmine exerted its activity through the inhibition of the dual specificity phosphorylation-regulated tyrosine kinase, Dyrk1a and, again, the activation of YAP nuclear translocation.

Collectively, these results identify both YAP activation and actin cytoskeleton remodelling as major determinants of cardiomyocyte proliferation and establish the molecular basis for the development of pharmacological therapies to promote heart regeneration through the stimulation of the endogenous capacity of cardiomyocytes to proliferate.

Acknowledgements

First, I would like to thank my mentor, Prof. Mauro Giacca, for giving me the opportunity to work in such an inspiring environment as his laboratory and to always incite me to do my best. His strict supervision pushed me above and beyond my limits. Thank you.

I would like to thank my external supervisor Prof. Manuel Mayr for his advice and Dr. Lawrence Banks for his support and his precious suggestions.

In ICGEB I have met extraordinary people, who contributed to making my PhD period a full-life-experience from both scientific and personal points of view. Thanks to the great Molecular Medicine team, which was always supporting me in the long working hours as well as Molecular Cardiology and Cardiovascular Biology groups.
A special thank goes to Dr. Maria Ines Gutierrez and Dr. Valentina Martinelli for their patient and fundamental help during these intense working-years. A big thank you goes to Prof. Chiara Collesi for the precious help and the great support, especially during the last period. I would also like to thank the above, as well as Luca, Francesca, Ambra, Giulia P, Ilaria, Nadja, Edoardo, Silvia, Michele, Giulia R, Hashim and Elena for sharing with me the enthusiasm for research.
I also thank ICGEB for the financial support.

Finally, I wish to thank my family for teaching me the meaning of "If you want, you can".

CONTRIBUTIONS

For the work reported in the present Thesis, I would like to acknowledge the essential contribution of:

- Dr. Ellen Dirkx for sharing with me the results of the FDA-registered drug screening and for letting me continue to work on this project. I really appreciate her guidance and the great scientific debates that we shared.
- Dr. Miguel Mano for performing the drug screening at the High-Throughput Screening Facility;
- Dr. Danilo Licastro, Dr. Areejit Samal, Ryan Cubero and Dr. Matteo Marsili for performing all the bioinformatics analysis;
- Dr. G. Legname at SISSA for letting me perform some experiments in his laboratory with the help of Dr. M Barbisin.
- the Animal House Facility, and specifically Dr. Serenza Zacchigna and Willy De Mattia;
- Dr Pierluigi Lesizza for performing animal surgery and echocardiography.

ABBREVIATIONS

AAV Adeno-Associated Virus
ATP adenosine triphosphate
A-V atrial-ventricular
BMPs bone morphogenetic proteins
BSA bovine serum albumin
CDK cyclin-dependent kinase
ChIP-Seq chromatin immunoprecipitation-sequencing
cKO conditional knock-out
CM cardiomyocyte
CPCS cardiac progenitor cells
CVD cardiovascular disease
DGC dystrophin glycoprotein complex
DPPH 2, 2-Diphenyl-1-picryl-hydrazyl
ECM extracellular matrix
EDTA ethylene-diamine-tetra acetic acid
EF ejection fraction
EMT epithelial-mesenchymal transition
ESCs embryonic stem cells
FBS foetal bovine serum
GABA gamma-aminobutyric acid
GH growth hormone
GPCRs G-protein-coupled receptor
HBV hepatitis B virus
HF heart failure
HNSCC head and neck squamous cell carcinoma
iPSCs induced pluripotent stem cells
KO knock-out
LV left ventricle
LVAW left ventricular anterior wall
LVEF left ventricular ejection fraction
MAO monoamine oxidase
MAPK mitogen-activated protein kinase
MI myocardial infarction
mRNA messenger RNA
miRNA microRNA
NDRs nuclear Dbf2 related kinases
NMJ neuromuscular junction

NO	nitric oxide
NSCLC	non-small-cell-lung cancer
PBS	phosphate buffer saline
PDZ BD	PDZ binding domain
PE	phenylephrine
PFA	paraformaldehyde
PI3K	phosphatidylinositol-3-kinases
PLC	phospholipase C
rAAV	recombinant adeno associate virus
RISC	RNA induced silencing complex
RNAi	RNA interfering
ROS	reactive oxygen species
siRNA	short interfering RNA
TAC	Transverse aortic constriction
TBE	Tris-borate-EDTA
Tg	transgenic
TRAP	translating ribosomal affinity purification
UTR	untranslated region
WT	wild type

Table of Contents

FIGURE LIST

List of Tables

1 Introduction

1.1 Introduction to cardiovascular diseases

Therapeutic strategies for cardiovascular diseases have been the challenge of the last century. In fact, cardiovascular diseases are one of the leading causes of death worldwide. In USA only, ischemic cardiomyopathies affects 7.1 millions people and 4.5 millions patients suffer of cardiac insufficiency after myocardial infarction, associated with a mortality rate of more than 50% within the follow-up period of 5 years (Writing Group, Mozaffarian et al. 2016).

Ischemic heart failure, as a consequence of myocardial infarction, occurs when cardiac tissue is deprived of oxygen, due to a coronary arterial obstruction. When the ischemic injury is severe enough to cause loss of critical amounts of cardiomyocytes, a series of sequential pathological events occur, including formation of a non-contractile scar, ventricular wall thinning, overload of blood flow that lead to ventricular remodeling, heart failure and most probably to death (Mahmoud and Porrello 2012).

The therapies currently available for patients with myocardial infarction and heart failure, including treatment with ACE-inhibitors, diuretics and beta- blockers, aim at reducing the impact of fibrotic remodeling, thus improving the morphological and functional impairment of the injured heart. However, none of these therapies are able to solve the real critical problem of an infarcted heart, namely the dramatic depletion of cardiomyocytes causing a severe reduction of cardiac contractility and pump function. Therefore, there is a compelling need to explore alternative approaches and new therapeutic strategies aiming at regenerating the injured heart and increasing its physiological functions.

1.2 Heart regeneration

In the animal kingdom, the regenerative potential is not equally distributed among species. Invertebrates, such as insects, planarians and echinoderms, have a strong regenerative ability. Among vertebrates, Axolotl, zebrafish and newts are great examples of regeneration after damage of many different organs, such as limbs or fins. In mammals, this regenerative potential is very limited and restricted to minor parts of the body. The peculiar ability of vertebrates to regenerate is closely related to their capacity to maintain the developmental transcriptional profile ready-to-use. Understanding the peculiar mechanisms of regeneration remains a great challenge in regenerative medicine, especially to face damages to those tissues with poor proliferative capability, including the heart. In this respects, pioneering studies by Poss and Oberpriller reported examples of complete heart regeneration in salamander and zebrafish after heart resection of the left ventricular apex (Poss, Wilson et al. 2002) (Oberpriller and Oberpriller 1974). Regeneration is due to dedifferentiation of pre-existing cardiomyocytes adjacent to the resected area, a process sustained by sarcomere breakdown and cytoskeletal remodeling. A specific gene expression program drives cardiomyocyte differentiation, driven by GATA4 (Lepilina, Coon et al. 2006) and Hand2 (Schindler, Garske et al. 2014). Of note, the newly formed cardiomyocytes are fully able to functionally integrate into the preexisting myocardium.

Multiple recent evidence has demonstrated that the mammalian heart retains its proliferative potential during embryonic development and early post-natal period, while it rapidly looses it after birth (van Amerongen and Engel 2008). In humans, cardiomyocyte cell cycle withdrawal seems to arise around the first year of life, as concluded from recent findings (Li, Wang et al. 1996, Mollova, Bersell et al. 2013) (Bergmann, Zdunek et al. 2015).

A complete functional rescue of cardiac function after acute myocardial ischemia has been recently reported to occur in a two months-old baby with myocardial infarction (Haubner, Schneider et al. 2016). This evidence further strengthen previously published hypotheses, suggesting the possibility of heart regeneration in children and newborns, as observed in rodents (Macmahon 1937, Saker, Walsh-Sukys et al. 1997). In the adult life, injured myocardial tissue is largely replaced by a fibrotic scar, resulting from the lack of proliferative potential of adult cardiomyocytes. However, a limited capacity of cardiac renewal can still occur in adult animals, as demonstrated by using transgenic mice (Hsieh, Segers et al. 2007), the carbon-dating technique in humans (Bergmann, Bhardwaj et al. 2009) or the thymidine-labelling experiments in mice (Soonpaa and Field 1997). A fundamental question was to identify the cell types involved in this regeneration process. Pre-existing cardiomyocytes were identified as the main source of heart regeneration after injury in a model of apical resection in transgenic cmlc2:EGFP zebrafish (Jopling, Sleep et al. 2010) and in rodents (Hsieh, Segers et al. 2007, Senyo, Steinhauser et al. 2013).

In the rodent studies, cardiac cell turnover was estimated to be of 0.76% per year in young adult mice, which decreases with age. This rate resulted significantly increased (4 folds) in the infarct border zone, after myocardial injury. In humans, the measurement by mass spectrometry of carbon-14 incorporated in the DNA during the Cold War in the atomic weapon-testing period was used as a tool to date human cardiomyocytes. Exploiting this technique, it was estimated a cardiomyocyte renewal of about 1% per year in in young adults, which decreases to 0.45% in aged people (Bergmann, Bhardwaj et al. 2009). Although an innate cardiomyocyte turnover has been detected, this is clearly not sufficient to compensate for the critical cardiac cell loss after myocardial infarction. Therefore, understanding the molecular pathways determining the re-entry of cardiomyocytes into the cell cycle remains a critical goal of current research.

1.2.1 Learning from evolution: filling the gap between amphibians and mammals

1.2.1.1 Evolutionary and developmental adaptations in heart regeneration

Morphological differences in heart among species are results of the adaptation from aquatic to terrestrial life. Since these differences correlate with a decreasing heart regeneration capability, it appears important to understand the morphological and physiological changes occurred during this transitions.

The differences between mammals and amphibians consist not only in cardiac chamber morphology, but also in the presence of a complex coronary vasculature, which is not present in amphibians (Reese, Mikawa et al. 2002, Perez-Pomares, Gonzalez-Rosa et al. 2009). Pressure, temperature, hypoxia, metabolism, immune response and blood clotting all parameters that significantly changed during the transition of life to earth.

1.2.1.2 Pressure

The conquest of terrestrial land forced the evolution to supply animals of a closed circulatory system. In the early stage of mammal life, a significant increase in blood pressure correlated with an increase of mechanical load on ventricular walls (Hillman, Kallapur et al. 2012), resulting in cardiomyocyte adaptive changes, with important consequences at the structural and metabolic levels. Recent evidence sustain the hypothesis that the increased mechanical load in adult human heart is responsible for cardiomyocyte cell cycle arrest, as ventricular unloading stimulates cardiomyocyte proliferation (Canseco, Kimura et al. 2015). According to this notion, mammals might have lost their heart regenerative capability to achieve a more functional pumping heart.

1.2.1.3 Body temperature

Another important factor, correlated to the loss of cardiac regeneration ability in vertebrates, is body temperature. In fact, it is known that neonatal mice, similar to fish and amphibians, do not have a thermoregulatory system. Interestingly, this peculiarity is somehow conserved in human infants, who still are not able to maintain constant the body temperature. Thermoregulation is achieved in adult organisms (Tourneux, Libert et al. 2009). The environmental temperature seems to have an effect in many examples of regeneration. For limb regeneration, newts prefer a warmer environment (Tattersall, Tyson et al. 2012). Also in fish, the time frame necessary for completing fin regeneration seems to be dependent from temperature (Sirbulescu and Zupanc 2010). Finally, an *in vivo* model of brain injury suggests an enhanced regeneration after cerebral ischemia in hypothermic conditions (Yenari and Han 2013). No specific data are currently available on temperature in cardiac tissue of various organisms, however, it appears reasonable to conclude that the thermoregulatory system, similar to metabolic efficiency, might have resulted as a consequence of an important evolutionary pressure. This might have influenced the loss of regenerative ability.

1.2.1.4 Oxygen concentration

Another key player in tissue regeneration is oxygen tension. Interestingly, the level of cardiomyocyte oxygenation dramatically changes from embryonic to post-natal life and mimics the shift in oxygen concentration happened in evolution when life moved from water to land. Interestingly, species with high regenerative ability live in a hypoxic habitat. Recent studies (Puente, Kimura et al. 2014) (Nakada, Canseco et al. 2017) have raised the possibility that high oxygen tension is involved in the cardiomyocyte cell cycle arrest, due to the induction of the DNA damage response because of reactive oxygen species. Moreover, it is well accepted that the

subpopulation of CMs responsible for cardiac renewal shows low metabolic activity and a gene expression profile typical of the one detected in hypoxic conditions (Kimura, Xiao et al. 2016). Of note, in the mammalian adult heart, the gradual exposure to a systemic hypoxemia reactivates the endogenous regenerative potential, unveiling the relevance of hypoxia in the regenerative process (Nakada, Canseco et al. 2017).

1.2.1.5 Metabolism

Adaptation of cardiac cells to an oxygen-rich environment triggered important metabolic changes. During fetal life, the glycolytic pathway is the main source of ATP. At birth, cardiomyocytes undergo profound metabolic changes resulting in a more efficient strategy to supply energy through the mitochondrial oxidative phosphorylation process (Gong, Song et al. 2015). Despite its higher efficiency, oxidative phosphorylation generates many reactive oxygen species (ROS), which trigger the activation of the DNA damage response and, consequently, the exit of cardiomyocytes from the cell cycle (Puente, Kimura et al. 2014). Gross metabolic changes occur also in case of heart failure. Since the oxygen tension in the case of ischemic heart damage is very similar to neonatal hypoxic conditions, in a mouse model of myocardial infarction a decrease of fatty acid oxidative phosphorylation has been detected parallel to an increase in glycolysis. These changes are theoretically favorable to regeneration, but, despite the decrease in oxidative phosphorylation, no significant changes in the glycolytic pathway are detected, nor a significant regeneration of the injured tissue (Nakada, Canseco et al. 2017). This evidence suggests that, in order to create a favorable environment for cardiomyocyte cell cycle re-entry, the metabolic switch *per se* is not sufficient, but it requires a complex regulation of different biochemical and biophysical processes, still under intense investigation.

1.2.1.6 Immune system

Another intriguing hypothesis inversely links the tissue regenerative potential along evolution to the development of a mature immune system. In non-mammalian vertebrates a specialized immune system is absent (Buchmann 2014) and, in neonatal mammals, the immune system has very weak pro-inflammatory activity (Sattler and Rosenthal 2016).

The absence of the adaptive immune response in amphibians correlates with the great performance in regenerating limbs as if a more permissive immune surveillance would be required to allow regeneration to happen (Epelman, Liu et al. 2015). Of note, key effectors of the regenerative process in zebrafish, amphibians and in neonatal mice are macrophages (Godwin, Pinto et al. 2013) (Lavine, Epelman et al. 2014). Macrophages are massively recruited at the site of heart damage in both neonatal and adults, and are mainly involved in the neoangiogenesis process of the newly-formed tissue, without any direct role in cardiomyocyte proliferation (Lavine, Epelman et al. 2014). Therefore, even if the adaptive immunity is a potent weapon against infectious diseases, it might be detrimental for regeneration, since it is responsible for the localized inflammatory response at the site of injury, which triggers the release of many cytokines, possibly inhibiting cardiac cell proliferation.

1.2.1.7 Blood clotting

The role of blood clotting is a controversial topic in the field of heart regeneration. . In some conditions, clotting factors are able to induce regeneration. Some examples are given by mouse liver regeneration and salamander lens: in these cases, platelet activation and other coagulation events are able to start the molecular signaling required for the regenerative response (Lesurtel, Graf et al. 2006). Thrombin is a clotting factor responsible for an opposite effect on lens regeneration in newt and axolotl, although it stimulates newt myocyte proliferation *in vitro* (Imokawa, Simon et al. 2004). A different molecule (PDGF-BB), secreted by platelets, induces epicardial cells to start neovascularization in a model of heart regeneration in zebrafish (Kim, Wu et al. 2010). However, since blood clotting is not only involved in tissue regeneration but also in repair, the mechanisms involved in these opposite events are still under debate.

1.2.1.8 Structural organization of cardiac myocytes

The contractile protein apparatus of cardiomyocytes greatly differs between mammalian and non-mammalian vertebrates. A recent proteomic study highlights the differences at protein level between adult zebrafish and mouse hearts and their neonatal counterparts (Gomes, Skroblin et al. 2016). The findings confirmed that neonatal hearts share a similar pattern of immature myofilaments, with a limited number of structural proteins, such as Myh6, Myl2 and Myoz2, expressed in mature cardiomyocytes (Gomes, Skroblin et al. 2016). The innate regenerative potential of zebrafish and mouse neonatal hearts is probably associated with an immature sarcomere structure which renders cardiac cells more prone to divide. Actually, it is well assessed that the ability to disassemble sarcomere is required for cardiomyocytes to proliferate (Ahuja, Perriard et al. 2004). Conversely, the structural rigidity of adult mammalian cardiac cells, acquired during adaptation to the increased workload, is a strong physical barrier for cardiomyocyte proliferation and therefore regeneration.

1.2.1.9 Cardiomyocyte nucleation

Another important feature shared by zebrafish, newt and fetal cardiac cells is the mono-nucleation of myocytes (Senyo, Lee et al. 2014). Among mammals, cardiomyocyte binucleation occurs during the first weeks after birth in rodents and at the end of gestation in sheep and humans (Jonker, Zhang et al. 2007). The rate of binucleation in humans is below the average observed in other species and, after birth, cardiac cells get polyploid, a feature of terminally differentiated cardiomyocytes (Mollova, Bersell et al. 2013). The meaning of this process is unclear: it might be due to the rapid growth occurring after birth in mammalian vertebrates, which results in an increased demand of transcriptional activity, connected to higher energetic requirements of the adult life.

The analysis of the regenerative potential through evolution suggests that, in mammals, postnatal normoxic environment triggered a significant increase of ROS production and possibly the activation of the DNA damage response, might be responsible for the cell cycle arrest of adult

cardiac myocytes. Moreover, structural constrains seem to be greatly involved in the impairment of cardiomyocyte mitosis.

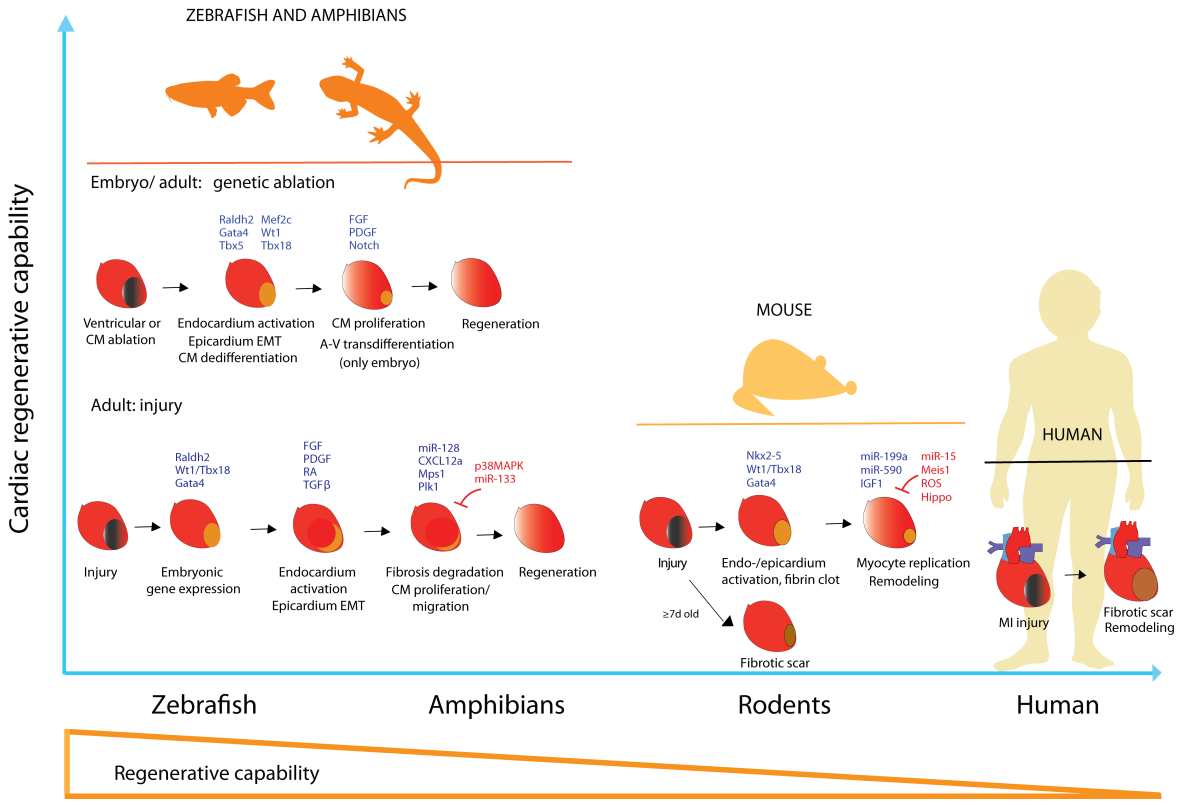

FIGURE 1-1 CARDIAC REGENERATIVE CAPABILITY IN DIFFERENT SPECIES

From zebrafish to humans, heart regenerative potential after injury is significantly diminished. Different pathways lead to recover the damaged tissue in different species. In blue are shown genes , promoting heart regeneration, in red those responsible for inhibition. A-V, atrial-ventricular; EMT, epithelial- mesenchymal transition; MI, myocardial infarction. Adapted from (Sahara, Santoro et al. 2015).

1.2.2 Contributors to heart regeneration: all for one and one for all

If the analysis of morphological and physiological changes of the heart along evolution can contribute to find the reason why heart regeneration does not occur in mammals, deep understanding of organogenesis during embryonic life can give important insight as well. The contribution of several cell types in the repair process strictly resembles the series of events occurring during organogenesis. Indeed, regeneration arises from a complex network of signaling networks aimed at organizing cell proliferation, migration, differentiation and functional integration. In the case of myocardial regeneration, four important processes have been reported as key players: angiogenesis, extracellular matrix signaling (ECM), immune response and innervation.

1.2.2.1 Angiogenesis

In the case of organ regeneration, a newly formed network of vessels is required, in order to give nutrients and oxygen supply to the regenerated tissue. This is the case of zebrafish (Lepilina,

Coon et al. 2006) and mouse heart regeneration, following different types of injury (Porrello, Mahmoud et al. 2011): neo-angiogenesis always parallels the tissutal regenerative response. If angiogenesis is impaired, cardiac regeneration fails (Epelman, 2015). Evidence in zebrafish exists showing a crosstalk through the Fibroblast Growth Factor (FGF) between cardiac and endothelial cells of the epicardium (Lepilina, Coon et al. 2006), having the effect of providing an efficient vascular network to the regenerated heart tissue. Several other growth factors are key regulators of neo-angiogenesis in the case of heart regeneration (Zangi, Lui et al. 2013), supporting the important role of the synergistic regulation of different pathways accomplish a complex process such as tissue regeneration.

1.2.2.2 Extracellular matrix (ECM)

Although the involvement of ECM in cardiac regeneration is still poorly understood, it is known that, in the case of myocardial ischemic injury, a massive ECM deposition followed by remodeling is responsible for fibrotic scar formation and, consequently, for impairment of cardiac function. Interestingly, recent evidence suggests a new role for the fibrotic scar, which not necessarily impairs cardiac regeneration. In zebrafish, if scar formation upon injury is impaired by inhibition of TGF-β signaling, heart tissue regeneration is completely blocked (Chablais and Jazwinska 2012). Moreover, since the cellular component of the connective tissue slightly changes during life, it is possible that different cell types make the tissue environment more permissive to the regenerative response (Chablais and Jazwinska 2012). Moreover, the ECM biochemical composition can impact the efficiency of regeneration, acting as a juxtacrine system to induce cardiac cell proliferation (Ieda, Tsuchihashi et al. 2009).

1.2.2.3 Organ innervation

As it happens for the vascular network, a proper innervation of the newly formed tissue is required to an organ in order to successfully accomplish the regenerative process. Recent data have demonstrated that specific pharmacological repression of cholinergic nerve function results in a reduction in cardiomyocyte proliferation in zebrafish and in neonatal murine heart (Mahmoud, O'Meara et al. 2015). Moreover, experimental evidence shows that, in the presence of mechanical denervation of the vagus nerve in different mouse models of myocardial injury, such as apical resection and myocardial infarction, heart fails to regenerate (Mahmoud, O'Meara et al. 2015) (White, Gordon et al. 2015). Interestingly, regeneration can be partially restored by nerve growth factor (NGF) supply, suggesting that NGF is required to sustain heart regeneration.

1.2.2.4 Immune response

In case of myocardial infarction, an acute inflammatory response is activated, causing a series of pathological events resulting in scar remodeling and consequent heart failure. In this context, macrophages are responsible for massive production of pro-inflammatory cytokines, fibroblast activation and ECM remodeling. The immune response is closely linked to regeneration in injured hearts. Recent information from a model of macrophage depletion in neonatal mice has

demonstrated that monocytes and macrophages are required for both regeneration and neo-angiogenesis in the heart (Aurora, Porrello et al. 2014). Of note, these authors found that the absence of macrophages after infarction did not affect cardiac myocyte proliferation directly, but rather the neo-vascularization of the regenerated tissue, because of the lack of pro-angiogenic cytokines.

1.3.1 Cardiomyocyte identity: from transcriptional profile to structural barriers in development and regeneration

A basic requirement for heart regeneration is the reactivation of an embryonic transcriptional program in cardiac cells, to make them dedifferentiate and be permissive to cell cycle re-entry. Importantly, specific gene expression programs characterize each step of cardiac cell differentiation; the transcription factors Nkx2-5 and ISL1, for example, are markers of cardiac progenitors (Ehrman and Yutzey 1999) (Cai, Liang et al. 2003), while Hopx expression characterizes a subpopulation of cardiac committed progenitors, known as cardiomyoblasts (Jain, Li et al. 2015). Indeed, from ChIP-seq studies on the murine embryonic heart at E9.5, emerged that Hopx localized close to genes related to the WNT signaling pathway. Other studies demonstrated that, Hopx promotes SMAD-mediated BMPs signaling and suppresses WNT signaling, enhancing cardiomyogenesis (Jain, Li et al. 2015). During embryonic heart development, GATA4 regulates the final steps of cardiomyocyte differentiation, driving the expression of a-myosin heavy chain and cardiac troponin C (Molkentin, Lin et al. 1997, Gupta, Gemberling et al. 2013). In the case of heart damage, its de novo expression drives de-differentiation of cardiomyocytes, inducing a phenotype permissive for their division, characterized by less tight and de-structured sarcomeres (Jopling, Sleep et al. 2010). This phenotype is the result of deep changes at chromatin level in failing cardiomyocytes: recent evidences have established that dynamic methylation is a key feature during postnatal growth of cardiomyocytes and interestingly the methylation pattern of cardiac cells in case of injury is very similar to neonatal methylation pattern (Gilsbach, Preissl et al. 2014) . As it happens for GATA4, the fetal transcription factor Hand2 (the heart and neural crest derivatives-expressed protein 2), is re-expressed during heart regeneration (Schindler, Garske et al. 2014). Conversely, some transcriptional factors are involved in cardiomyocyte cell-cycle exit, as p38 kinase and Meis1. Indeed, Meis1 up-regulation during postnatal life is responsible for the activation of CDK inhibitors (p15, p16 and p21) and cardiomyocyte proliferative arrest (Mahmoud, Kocabas et al. 2013).

It is interesting to note that the peculiar transcriptional profile of cardiomyocytes involved in regeneration leads to a partial cell de-differentiation, mainly affecting the sarcomere structure and the actin cytoskeleton, responsible for the contractility and the rigidity of the mature cardiac cells (O'Meara, Wamstad et al. 2015).

1.3.2 Regulation of cardiomyocyte proliferation

Several cell-cycle regulators are expressed during heart development and downregulated in the adulthood (reviewed in (Xin, Olson et al. 2013)). Genetic manipulation of these regulators promotes, to different extents, de-differentiation and proliferation of cardiac cells.

1.3.2.1 FGF1 and inhibition of p38 pathway

The p38 kinase belongs to the MAP kinase family and is a negative regulator of the cell cycle. The inhibition of p38 results in neonatal cardiomyocyte proliferation, while its overexpression has an opposite effect, blocking cardiac cells proliferative ability (Engel, Schebesta et al. 2005). In addition, it was observed that a combination of p38 inhibitors and FGF1, fibroblast growth factor 1, increases mitotic events with an improvement of heart function in a mouse model of myocardial ischemia, due to the impairment of apoptosis at the site of injury (Engel, Hsieh et al. 2006). FGF1 also promotes new vessel formation, while p38 inhibition is associated to the expression of genes involved in cell cycle regulation. However, despite these evidences, the increase in cardiac cell proliferation remains modest.

1.3.2.2 Neuregulin-1 signaling

Neuregulin1 (NRG1) is a growth factor involved in cardiac cell proliferation during embryonic life. NRG1 shows an agonist effect on the ErbB receptor family. It exerts its function binding ErbB4, inducing either ErbB2-ErbB4 or ErbB4-ErbB4 dimerization. Of note, NRG1 is able to induce proliferation only in mononucleated cardiac myocytes (Bersell, Arab et al. 2009). In adult cardiac myocytes, NGR1 treatment induces sarcomere breakdown and an immature sarcomere structure similar to the fetal one. Moreover, NGF1 not only promotes cardiomyocyte proliferation in adult hearts through PI3K activation, but its activation is also required during development for the complete maturation and final differentiation of CMs, under the control of BMP10 (Grego-Bessa, Luna-Zurita et al. 2007).

1.3.2.3 Notch signaling

In Vertebrates, Notch signaling controls mesodermal commitment during development, playing a critical role in mammalian embryonic cardiogenesis; mice lacking the genes encoding either Notch receptors or their ligands show early embryonic lethality, mainly because of cardiovascular abnormalities (Penton, Leonard et al. 2012). In addition to its essential role in heart development and cardiac specification during embryogenesis, Notch regulates proliferation of immature cardiomyocytes during fetal and post-natal life (Collesi, Zentilin et al. 2008) (Campa, Gutierrez-Lanza et al. 2008) (Croquelois, Domenighetti et al. 2008) and is essential for the maintenance of the heart structural and functional integrity after myocardial infarction (Kratsios, Catela et al. 2010) during the response to increased workload or during heart failure (Croquelois, Domenighetti et al. 2008) (Oie, Sandberg et al. 2010). In the species that efficiently regenerate the heart after damage, Notch is essential for postnatal cardiomyocyte proliferation (Raya, Koth et al. 2003) (Zhang, Han et al. 2013), while recent evidence indicates that it is largely ineffective in

driving cardiac regeneration in adults, because of permanent epigenetic modification at main Notch-responsive promoters (Collesi, Zentilin et al. 2008) (Felician, Collesi et al. 2014) .

Among the pathways described as capable to stimulate cardiomyocytes proliferation, the YAP-Hippo signaling pathway is considered the most potent driver in the regulation of cardiomyocyte proliferation.

1.4. A path for regeneration: Hippo Signaling Pathway

The Hippo Pathway was discovered through a genetic screening in Drosophila aimed at identifying genes involved in the control of organ size (Xu, Wang et al. 1995) (Justice, Zilian et al. 1995). It is highly conserved pathway, involved in the maintenance of tissue integrity through a intracellular signaling cascade whose inactivation, through genetic deletion of proteins such as Warts (Wts), Hippo (Hpo), Salvador (Sav) and Mats (Mts), results in a common phenotype of massive proliferation and an overgrowth of the interested tissue (Halder and Johnson 2011).

In the past decade, the Hippo signaling pathway has been described to be involved not only in tissue growth, but also in stem cell pluripotency and cell fate determination (Lian, Kim et al. 2010, Qin, Hejna et al. 2016, Britschgi, Duss et al. 2017). Moreover, it is involved in the control of the balance between proliferation and apoptosis, often associated to the development of solid cancer (Low, Pan et al. 2014).

Actually, solid cancer cells often show a hyperactivation of the Yes-associated protein (YAP), which, together with TAZ, is the main regulator of the Hippo signaling cascade (Zhao, Li et al. 2010). Since proliferation and apoptosis are key regulatory processes in both regenerative medicine and oncology, targeting this pathway has become an attractive clinical strategy for the development of new therapeutics.

The Hippo transduction cascade has a high level of molecular complexity and redundancy, which reflects the importance of this signaling pathway in the regulations of critical cellular processes. Briefly, in humans, the STE20-like protein kinase 1/2 (MST1/2) (Hippo in Drosophila) was described as an upstream kinase, which phosphorylates large tumor suppressor homolog 1/2 (Lats1/2) (Warts in Drosophila); these two kinases are able to directly interact through to the adaptor protein Sav1 (Salvador). MOB1A and MOB1B (Mats in Drosophila) enhance the kinase activity of Lats1/2. Lats1/2 are kinases able to directly regulate YAP/TAZ, the final effectors of the Hippo transduction signaling; upon activation, Lats1/2 phosphorylates the transcriptional co-activator, Yes-associated protein YAP, and its paralogues PDZ-binding domain, TAZ (Yorkie in Drosophila). YAP phosphorylation on Ser127 has two major consequences: it stimulates its binding to the 14-3-3 protein family, preventing YAP translocation to the nucleus and it triggers phosphorylation of CK1d and the recruitment of beta-TRCP, resulting in YAP/TAZ proteasomal degradation (Hariharan 2006, Zhao, Li et al. 2010).

When the MST1/2 kinase cascade gets inactivated, YAP is no longer phosphorylated and translocates into the nucleus to activate the transcription of target genes, including CTGF, CyR61 and Birc5 (Zhao, Ye et al. 2008) (Shimomura, Miyamura et al. 2014).

Since YAP/TAZ are not able to directly bind DNA, their function is mediated by several transcription factors; among these are TEAD1-4 (TEA domain family member- Scalloped in Drosophila) (Zhao, Ye et al. 2008), Runx (Zaidi, Sullivan et al. 2004), FoxO1 (Shao, Zhai et al. 2014), Tbx5 (Murakami, Nakagawa et al. 2005) and SMADs (Ferrigno, Lallemand et al. 2002) but their role in Hippo signaling activation is still not completely understood. The canonical inhibition of the Hippo cascade leads to TEAD1-4-mediated gene expression, preferentially repressed by VGLL4 repressor binding, which is lost in the presence of the YAP/TAZ co-activators (Koontz, Liu-Chittenden et al. 2013).

Consistently, mouse models of knockdown of genes representing the active core of the Hippo pathway, such as MST1/2, SAV1, MOB1A/B or LATS1/2, showed a significant increase of TEAD target gene expression, similar to YAP overexpression models (Dong, Feldmann et al. 2007) (Camargo, Gokhale et al. 2007, Lee, Lee et al. 2010) (Nishio, Hamada et al. 2012).

Downstream target genes of YAP/TAZ signaling were first identified in Drosophila: among them, cyclinE, diap1 and the microRNA bantam are all mediators of cell proliferation and survival (Wu, Liu et al. 2008). Other targets are p73 and ErbB-4; the former is a transcription factor involved in the stimulation of the apoptotic response and in DNA-damage signaling in association with YAP (Downward and Basu 2008); ErbB-4 is a tyrosine kinase receptor, which is able to induce a mitogenic signalling after YAP-mediated transactivation (Komuro, Nagai et al. 2003, Schuchardt, Bhat et al. 2014).

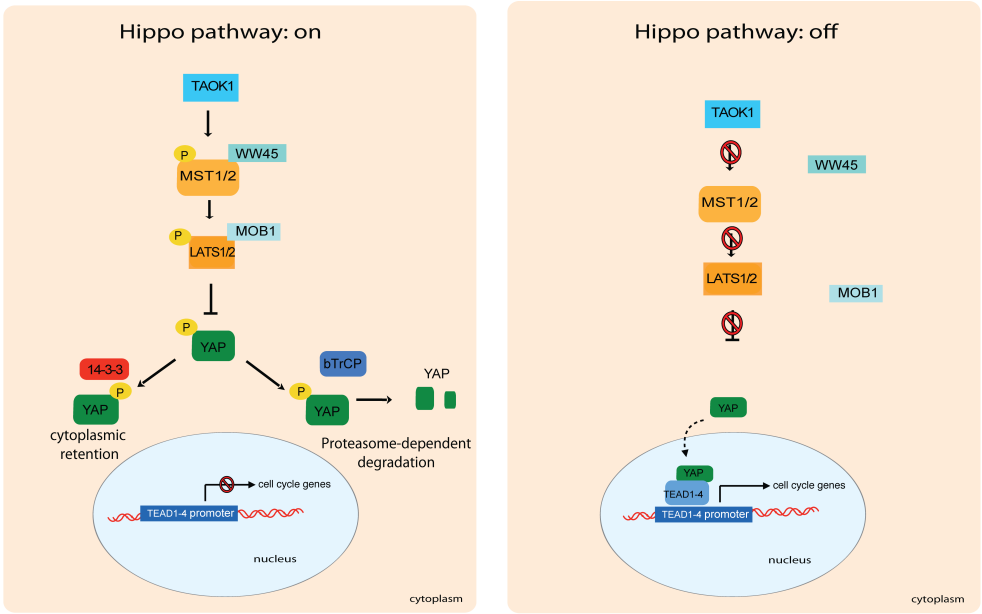

FIGURE 1-2 SCHEMATIC REPRESENTATION OF THE CORE KINASES OF THE HIPPO SIGNALING PATHWAY

A simplified view of the main regulatory kinases of the Hippo pathway are shown in orange (MST1/2 and LATS1/2). When the pathway is turned on, these kinases are activated and lead to downstream

phosphorylation of the final effector of the signaling pathway, YAP, to its consequent cytoplasmic retention or proteasome-dependent degradation. Conversely, when the pathway is turned off, YAP is no longer inhibited, it translocates into the nucleus and, in association with the TEAD transcription factors, induce cell cycle gene expression.

1.4.1 YAP and TAZ protein structure

Both YAP and TAZ show a very conserved protein structure. Both of them show a coiled-coiled and PDZ-binding domain, essential for nuclear translocation (Shimomura, Miyamura et al. 2014). Actually, it was found that the protein zona occludents 2 (ZO2) can bind this region and regulate YAP nuclear translocation via recruitment of some other regulators, or inducing conformational changes, critical for YAP activation (Oka, Schmitt et al. 2012).

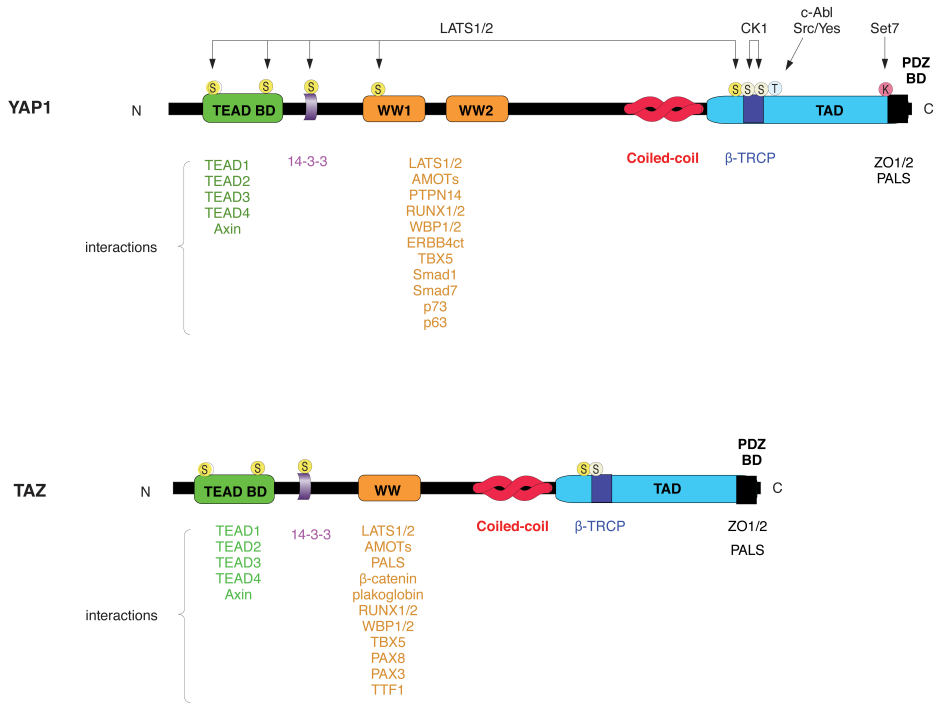

FIGURE 1-3 SCHEMATIC REPRESENTATION OF YAP AND TAZ STRUCTURE

The functional domains of YAP/TAZ are represented, together with interacting proteins. The PDZ binding domain (PDZ BD) is located at the C-terminus, while the WW domains are in the central region. The TEAD binding domain allows YAP and TAZ to exert their function as transcription factors. The serine residue phosphorylated by upstream protein kinases are indicated in dark yellow, while those target of CK1 phosphorylation are in a lighter yellow; the c-Abl binding site is in light blue. The lysine residue target of Set7 methylation is in pink. Adapted from (Piccolo, Dupont et al. 2014).

Moreover, both YAP and TAZ share other two important motifs: a WW domain in the central region of the protein and a transactivation domain in the C-terminal region (**Fig.1-3).** YAP only shows two interesting domains: the proline rich-domain at N-terminus mediates its interaction with the heterogeneous nuclear ribonuclear protein U (hnRNP U), while the SH3-binding motif, close to the second WW region, mediates its binding with the Yes tyrosine kinase (Sudol 1994,

Howell, Borchers et al. 2004).

The phosphorylation of YAP by LATS on the five serine residues is one of the best-described modifications to regulate YAP activity. The S127A mutation was observed to increase YAP localization inside the nucleus (Basu, Totty et al. 2003). Phosphorylations on Ser127 of YAP and on Ser89 of TAZ create docking sites for 14-3-3 proteins, which promote their cytoplasmic retention (Yu, Zhao et al. 2012) (Basu, Totty et al. 2003). Conversely, phosphorylation on Ser381 has a different functional role, leading to YAP proteasomal degradation (Kim, Kim et al. 2013). Several additional post-translational modifications can occur on YAP/TAZ, such as acetylation, methylation and sumoylation; however, the relevance of most of these modifications is still not completely understood.

1.4.2 YAP signaling pathway: upstream activating stimuli

Among the recently identified proteins involved in the direct regulation of YAP1, the NDR (nuclear Dbf2 related kinase) family members are able to inhibit YAP1/TAZ activation promoting their cytoplasmic retention (Zhang, Tang et al. 2015). NRD1/2 kinases, including LATS1/2, are AGC serine/threonine kinases (STK38/STK38L), which are characterized by a highly conserved NTR domain, the N-terminal regulatory portion, and the functional kinase segment, located between the subdomain VII and VIII (Hergovich, Stegert et al. 2006). NDR1/2 are able to directly interact with MOB through their NTR domain, however different MOB isoforms preferentially interact either with NDR1/2 or with LATS1/2. Actually, MOB2 preferentially binds NDR2, whereas MOB1A/B interact with both NDR1/2 and LATS1/2. Interestingly, their upstream activation can be mediated by MAPK4 and MST kinases via phosphorylation on Thr444/ Thr442 (Stegert, Hergovich et al. 2005) (Hergovich, Kohler et al. 2009). NDR proteins can be functionally regulated by several mechanisms, including phosphorylation or changes in subcellular distribution. Even though the absence of NDR1/2 is associated with a strong increase of YAP activity, their role in the physiological cellular context is poorly understood.

Other kinases have been described to modulate the Hippo pathway, such as the MAP4K family and TAOK1/3, which mediate LATS1/2 activation through phosphorylation (Meng, Moroishi et al. 2015) (Boggiano, Vanderzalm et al. 2011). Of note, TAOK activation can affect the Hippo transduction cascade at two different levels: upstream of MST1/2, mediating their phosphorylation and in parallel to MAP4 kinases and MST1/2, acting directly on LATS1/2 activation (Plouffe, Meng et al. 2016). Moreover NF2, neurofibromatosis type 2, is involved in the activation of LATS1/2, carried out by MAP4Ks and TAOKs. Indeed, NF2 ablation triggers a more relevant decrease of YAP phosphorylation than the absence of MST1/2 (Plouffe, Meng et al. 2016). NF2, is a protein belonging to the FERM domain protein superfamily, whose expression is very abundant in the "zonula adherens", responsible, together with tight junctions, for tissue architecture and integrity (Lallemand, Curto et al. 2003). In this peculiar cellular microenvironment, NF2 and other proteins such as AMOT, Expanded and α-Catenin, are also

involved in the regulation of the Hippo signaling cascade, recruiting LATS at the junctions and consequently inhibiting YAP.

Several different stimuli can modulate the Hippo pathway through G-protein-coupled receptor activation (GPCRs), a class of cell surface receptors able to influence a plethora of biological functions. Due to the different G-proteins, which can be recruited by these receptors, GPCRs are able either to promote or block the Hippo-signaling pathway. In fact, G12/G13, Gq/11 and Gi-coupled receptors inhibit LATS1/2 function, resulting in a positive effect on cell proliferation coherent with YAP activation, while Gs-coupled receptors activate LATS1/2 kinases. Furthermore, Ga proteins exert their effect on Rho GTPases and cytoskeleton remodeling, but how this is linked to LATS activity remains quite obscure (Yu, Zhao et al. 2012).

1.4.3 YAP/ TAZ as mechanosensors

As previously discussed, ECM properties and mechanical cues assume a fundamental role in organ structure development, by influencing cellular transcriptional profiles in adult tissues. At the cellular level, this implies a tight regulation of intra- and extracellular signals, resulting in a dynamic remodeling of actin cytoskeleton. Any alteration of the mechanical forces on cells can actively contribute to the development of pathological conditions such as cancer transformation or fibrosis.

Despite the relevance of cellular mechanoresponse is widely recognized, little information is available on the mechanism of intracellular transduction of these stimuli. In this context, our current knowledge on YAP/TAZ function upon mechanical inputs is also shedding lights on cell mechanobiology.

Actually, YAP and TAZ are mainly regulated by their localization; stiffness of the extracellular matrix or cytoskeletal tension are responsible for their nuclear distribution, which represents their functional activation, while soft substrates induce YAP and TAZ retention inside the cytosol (Aragona, Panciera et al. 2013). Actin cytoskeleton is essential for YAP/TAZ mechanotransduction: indeed, the inhibition of actin polymerization results in YAP/TAZ nuclear exclusion (Dupont, Morsut et al. 2011). These findings have been further supported by evidences obtained using F-actin inhibitory proteins, as CAPZ, ADF/Cofilin, demonstrating YAP activation upon a specific disposition of polymerized actin (Aragona, Panciera et al. 2013). Interestingly, the link between YAP/TAZ activation and changes in cellular geometry seems to be Hippo-independent, implying alternative regulations of YAP/TAZ signaling (Wada, Itoga et al. 2011). FAK, SRC and RHO proteins have been described as molecular links between the extracellular signals (either from other cells or from the ECM) and the intracellular environment, possibly leading to YAP/TAZ activation. The YAP response to mechanical cues is to generate intracellular forces; this implies the formation of contractile actomyosin structures leading to cytoskeleton reorganization. Since in the heart several mechanical cues together with important cell-contact interactions are responsible for tissue integrity and myocardial functionality, the Hippo pathway holds a fundamental role in cardiac development as well as in heart homeostasis.

1.4.4 YAP signaling: between cancer and regeneration

YAP/TAZ involvement in regulation of cell proliferation makes them interesting targets for therapeutic strategies in oncology and regenerative medicine. In non-small-cell-lung-cancer (NSCLC), patients showing high expression of YAP/TAZ have a poor prognosis; however, eventhough YAP/TAZ presence is essential for malignant progression, it is not sufficient to promote the development of NSCL cancer, as well as glioblastoma (Bhat, Salazar et al. 2011) In other types of malignancies, as in colorectal and liver tumors, YAP is required for malignant transformation; in colon and lung cancers arising from K-RAS mutation, both YAP and K-RAS regulate the EMT-related genetic program (Shao, Xue et al. 2014). Moreover, K-RAS is able to promote YAP transcriptional activation, therefore supporting the concept of a Hippo-independent mechanism.

Intriguingly, elevated YAP levels provide several advantages to cancer cells, including enhanced resistance to chemotherapeutic treatments, as observed in breast cancer (reviewed in: (Harvey, Zhang et al. 2013). Moreover, recent findings demonstrate that YAP/TAZ activation, in certain cases, sustains the resistance to oncogene-targeted therapy; elevated levels of YAP correlate with a poor response to RAF and MEK inhibitors in treatment cancer histotypes bearing a BRAF-mutation, acting as a survival stimulus for tumor cells (Lin, Sabnis et al. 2015). Since cell cycle regulation is a crucial process not only in tumor development, but also for organ regeneration, the role of YAP was explored in this context as well. Indeed, the regenerative process occurring in mammalian liver upon different kinds of injury is mediated by Hippo pathway inactivation, specifically by inhibition of Mst1/2 and Lats1/2, associated with a GA-binding protein- dependent YAP overexpression (Wu, Xiao et al. 2013). Neuromuscular junction (NMJ) regeneration is also mediated by YAP activity. Defective NMJ formation was observed in YAP KO mice, with deficit in pre- and postsynaptic distribution and size (Zhao, Shen et al. 2017). Furthermore, YAP absence inhibits muscle re-innervation, again highlighting the fundamental role of YAP in NMJ regeneration. Interestingly, YAP-/- mice showed a decrease in β-catenin levels, suggesting a role of WNT signaling in NMJ regeneration. However, induction of WNT signaling in YAP-/- mice ameliorated, but not completely rescued, the de novo formation of NMJ, demonstrating that β-catenin is not the only player downstream of YAP-mediated NMJ regeneration (Zhao, Shen et al. 2017).

Intestine regeneration requires YAP functional activity too. In fact, a decreased level of cell proliferation was observed in the crypts of YAP KO mice, demonstrating that YAP regulation of intestinal stem cell cycle affects intestinal regeneration. Besides the role of YAP in the regenerative gut response after damage (Gregorieff, Liu et al. 2015) (Barry, Morikawa et al. 2013), the involvement of WNT signaling in intestinal regeneration is commonly accepted.

Another example of the pivotal role of YAP in the regeneration process is bone regenerative response. A dichotomous behavior of YAP in chondrocyte differentiation was described (Deng, Wu et al. 2016). Indeed, YAP is both responsible for early chondrocyte proliferation, through TEAD mediated Sox6 expression, and block of chondrocyte maturation, due to Col10a1

expression inhibition, mediated by Runx2. In addition, YAP drives the early phases of fracture repair, through the suppression of the development of cartilaginous callus tissue.
Finally, YAP was identified as a key player in cardiac regeneration, as discussed below in details.

1.4.5 Hippo pathway: the heart issue

Heart development is a complex process requiring the integration of spatial-temporal signaling pathways and the interaction of different cell types (Brade, Pane et al. 2013). A network of interconnected signaling pathways flow into the nucleus, triggering the activation of a specific set of transcription factors, among which is Tbx5, a major regulator of the gene expression program leading to heart development. The finding that Tbx5 is activated by YAP raised the intriguing possibility that the Hippo pathway might be involved in embryonic cardiac development (Murakami, Nakagawa et al. 2005). Several studies have been performed to better understand the role of the Hippo kinase cascade in the heart. Data suggest that a deficiency of the Hippo pathway during heart development causes cardiac overgrowth; in fact, selective cardiac inactivation of Mst1/2, Sav1, and Lats2, which negatively affect YAP activation, led to marked myocardium enlargement due to an increase in cardiomyocyte number and trabecular expansion (Heallen, Zhang et al. 2011).
The role of YAP in cardiac growth has been investigated using either gain or loss-of-function models (Xin, Kim et al. 2013) (von Gise, Lin et al. 2012). YAP1 activation is fundamental and sufficient to induce proliferation of embryonic cardiomyocytes and is also responsible for the physiological enlargement of the heart during development, via hyperplastic more than hypertrophic growth. These findings suggest that YAP is sufficient to promote cardiomyocyte cell cycle activity. On the contrary, YAP cardiac-specific inactivation, in early stages of the heart development (at E10.5), is lethal, because of a marked reduction of cardiomyocyte number and dramatic hypoplasia (Xin, Kim et al. 2011). Of note, in the heart, YAP signaling is transduced by canonical transcription factors, TEAD1-4, which are fundamental for YAP mitogenic activity in cardiomyocytes (Wu, Liu et al. 2008) (Zhao, Ye et al. 2008). Indeed, lack of expression of TEAD1 results in E11-12 embryonic death, a critical time frame for heart development. Conversely, TEAD1 overexpression in the heart during postnatal period promotes cardiac pathological remodeling, responsible for heart failure (Chen, Friedrich et al. 1994).
Mice overexpressing TEAD1 show age-dependent cardiac dysfunction, associated with. an increase in GSK3β activation associated with decrease levels of both nuclear β-catenin and NFATc3/c4 (Tsika, Ma et al. 2010). These studies show that increased TEAD1 can promote the development of heart defects, typically present in cardiac remodeling following heart failure.
Since, in mammals, both YAP and its paralogue are present, TAZ cardiac-specific KO mice were generated. Surprisingly, postnatal cardiac TAZ deletion did not show any specific phenotype and did not alter mouse lifespan, demonstrating that the role of TAZ in heart development and function is dispensable, compared to YAP (Xin, Kim et al. 2013).
Cardiac-specific Mst1 overexpression sustains a massive cardiomyocyte apoptosis, responsible

for animal death due to dilated cardiomyopathy. Indeed, a dominant-negative MST1 protein exerts a protective function against remodeling in a model of MI (Yamamoto, Yang et al. 2003).

Besides its critical role during heart development, Yap exerts a critical function in heart regeneration upon injury. In a mouse model of myocardial infarction, increased levels of YAP not only prevent cardiac cell loss but also fibrotic scar formation. Consistently, constitutive activation of YAP1 is able to extend the regeneration window, triggering an improvement of cardiac function (Xin, Kim et al. 2013). In a heart-inducible YAP transgenic mouse model, in case of myocardial infarction, YAP activation significantly reduced scar size, with a net improvement of myocardium functionality. These effects were due to adult cardiomyocyte cell cycle re-entry, driven by YAP activation. Of note, sustained expression of YAP triggered significant downregulation of specific genes associated with terminal differentiation of cardiac cells (such as muscle- and oxidative metabolism-related genes), while cell cycle gene expression increased, suggesting that YAP induces a genetic program leading to a less differentiated phenotype, in order to make proliferation possible (Xin, Kim et al. 2013). Hippo signaling deficiency leads to increased cardiomyocyte proliferation and myocardial protection after MI. In fact, Sav1 KO mice show improved cardiac function and smaller scar size after MI (Heallen, Morikawa et al. 2013). These findings suggest that YAP is fundamental for adult heart homeostasis and has a strong cardioprotective function, probably due to its ability to promote both cardiac cell survival and proliferation in response to injury. Recent literature shows a strong interconnection between Yap signaling and other intracellular signal transduction pathways, acting synergistically in the regeneration process (Shao, Zhai et al. 2014) (Lin, Zhou et al. 2015).

Several published studies have analyzed the complex role of YAP in cardiac regeneration and have thus expanded our knowledge on the interaction of YAP-Hippo signaling with other intracellular signal transduction pathways and with the different cellular processes occurring after injury.

An interesting study was performed in conditional cardiac specific Salvador KO mice bearing a dystrophin loss-of-function (Mdx background), in order to explore the link between the Hippo pathway and the dystrophin glycoprotein complex (DGC) (Morikawa, Heallen et al. 2017). Both Salv KO, and Salv;Mdx DKO mice were able to regenerate the apex after heart apical resection. Interestingly, DKO mice were able to repair the resected heart showing an impressive cardiac overgrowth, often resulting in the formation of a second apex. These findings suggest that the Hippo pathway and DGC proteins are both responsible to restrict cell growth after damage, suggesting a key role of the DGC in arraying proliferating cardiomyocytes in a 3D space. When the same mice were analyzed in a TAC model of hypertrophy, the Salv; Mdx DKO myocardium showed milder cardiac fibrotic features than the mdx control mice, associated with a contained dilatation and physiological parameters similar to the Salv KO controls. Moreover, both Salv KO and DKO shared an increased level of nuclear YAP, demonstrating that the cardiomyopathy of mdx mice was abolished by Salvador depletion, resulting in YAP activation, with a consequent boost of cardiomyocyte proliferation and protection from apoptosis (Morikawa, Heallen et al.

2017).

The use of innovative tools, as translating ribosomal affinity purification (TRAP), has allowed the recovery and analysis of cardiomyocyte transcripts in several mouse models. Cardiomyocytes purified from Salv-depleted infarcted hearts express pro-proliferative genes, as well as genes related to vasculogenesis (FGFs and EGFs) and, more importantly, stress-related genes. Among these genes there is Parkin2 (Park2), involved in the quality control of mitochondria, which was also described to be important in cardiac repair, suggesting the need of mitochondrial quality control in the cardiac regenerative process. Park2 is involved in mitochondrial maturation and plays a key role in the cardiomyocyte metabolic transition from the embryonic to the adult age (Dorn 2016). Its absence in Salv KO mice negatively affected heart function, suggesting that Park2 is required not only for myocardial function but also for the resolution of the fibrotic scar (Leach, Heallen et al. 2017).

Recent studies have identified multiple molecular mechanisms exploited by YAP to control heart growth and cardiomyocyte proliferation. In Sav1 KO mice, Sav inactivation triggers β-catenin translocation into the nucleus leading to up-regulation of WNT pathway target genes (Heallen, Zhang et al. 2011). Consistent with these findings, YAP overexpression in fetal hearts caused an increase of WNT signaling (Xin, Kim et al. 2013).

Insulin-like growth factor (IGF) signaling is involved in Yap-dependent cardiomyocyte proliferation as well. Indeed, in a model of YAP constitutive activation, increased levels of IGF1 receptor were detected, with consequent GSK3β functional inhibition. Inactivation of GSK3β stabilizes β-catenin, a final effector of the WNT pathway, resulting in the activation of pro-proliferative genes (Xin, Kim et al. 2011). Moreover, YAP activation in neonatal cardiomyocytes resulted in upregulation of cell cycle regulators such as cyclin D, demonstrating a direct link between cell cycle genes and YAP itself (von Gise, Lin et al. 2012).

Recently, the PI3K-AKT signaling pathway was described to cooperate with YAP-signaling in the control of cardiac cell growth and survival. Through a genome-wide screening approach aimed at identifying genes responsible for YAP-induced pro- proliferative effects, it was found that YAP induces the expression of Pik3cb, the phosphatidilinositol-3phosphate kinase catalytic subunit which is highly expressed during embryonic development and drastically decreases in adulthood. Interestingly, the pattern of expression of Pik3cb superimposes to the one of YAP itself. Strong in vivo evidence supports the requirement of YAP to promote PI3K-AKT mediated cardiomyocyte proliferation. AAV-mediated Pik3cb overexpression in YAP cKO mice after MI triggered a net increase in cardiac function, inducing a net cardiomyocyte proliferative response, paralleled by a reduction of apoptosis (Lin, Zhou et al. 2015).

Collectively, multiple evidence unequivocally demonstrates the pivotal role of YAP as a master gene in cardiac biology. Its effect lasts from embryonic to adult life, since it regulates fetal heart development, induces proliferation in neonatal and adult cardiomyocytes and strengthens the regenerative potential in adult hearts after ischemic injury. Given its central role in heart

regenerative biology, the Hippo-YAP signaling pathway is an attractive target for heart regenerative therapies.

1.4.6 microRNAs targeting YAP1

Cellular processes need a multilayered regulation in order to be straightly modulated. Among the adopted strategies for post-transcriptional regulation of gene expression, microRNAs exploit a pivotal role, given the pleiotropic effect of their action. Several microRNAs have recently been involved in the regulation of the Hippo pathway cascade, mainly as key regulators of tumorigenic transformation. An example is miR-135b in lung cancer, responsible of the metastatic phenotype, given its property to target LATS2, MOB1B and NDR2. Thus, the use of an antagomir, which suppresses miR-135b expression, reduces metastasis and tumor growth (Lin, Chang et al. 2013). Similarly, overexpression of miR-31, a commonly upregulated miRNA in several tumors (Liu, Sempere et al. 2010), is also able to target LATS2, directly binding its 3'UTR as observed in endometrial cancer cell lines (Mitamura, Watari et al. 2014).

Other important miRNAs targeting Hippo pathway members belong to the miR-130 family, whose overexpression has been observed in different cancers, such as bladder, gastric cancer and glioblastoma (Zhu, Wang et al. 2015, Egawa, Jingushi et al. 2016). Of note, YAP exerts a positive feedback on miR-130 expression, which in turn represses VGLL4, an inhibitor of YAP-TEAD complex in hepatocellular carcinoma (Shen, Guo et al. 2015). Interestingly, miR-130a displays a similar function of the fruitfly miRNA bantam, which inhibits the homolog of VGLL4 SdBP/Tgi, further unveiling the evolutionary conservation of YAP molecular signaling. Moreover, upregulation of mir-130b preserves cancer stem cells in glioblastoma, targeting MST1 and SAV1 (Zhu, Wang et al. 2015). On the contrary, both miR-195-5p and miR-186 seem to target YAP with beneficial effects in tumor suppression, specifically on colorectal and hepatic cancer, respectively (Ruan, He et al. 2016, Sun, Song et al. 2017).

Other important insights into the regulation of YAP signaling by miRNAs derived from findings in hepatocellular carcinoma (Liu, Zhang et al. 2015). PreS, a HBV transactivator protein, is able to induce TAZ overexpression by suppressing miR-338-3p. Thus, downregulation of this miRNA, in the presence of preS, causes a reduction in TAZ suppression, resulting in TAZ-mediated promotion of cancer growth (Liu, Zhang et al. 2015). Recently, miR-125a was described to target TAZ in glioblastoma and miR-141 in gastric cancer (Yuan, Xiao et al. 2015, Zuo, Zhang et al. 2015).

A different example is the miR-29 family, upregulated upon YAP overexpression. In this case the pro-proliferative effect is achieved by targeting the 3'UTR of the PTEN transcript. Since PTEN is responsible for inhibition of mTOR, downregulation of PTEN results in mTOR activation and induction of cell proliferation (Tumaneng, Schlegelmilch et al. 2012).

1.5. Gene therapy to promote heart regeneration

Several strategies have been proposed to promote cardiac regeneration. Great excitement was raised in the first decade of this century by the possibility that cells from various derivation might perform as stem cells for cardiac regeneration. This was the case of c-kit-positive cells from the bone marrow (Orlic, Kajstura et al. 2001) and the heart itself (Beltrami, Barlucchi et al. 2003), mesenchymal stromal cells from the bone marrow (Hatzistergos, Quevedo et al. 2010) and heart-derived cardiosphere-forming cells (Smith, Barile et al. 2007). However, when all these cell types have been used for clinical experimentation, the results achieved turned out to be highly disappointing. To date, there is no proof that any cell type with putative stem cell capacity, once injected into the heart, induces real cardiac regeneration (commented in: (Eschenhagen, Bolli et al. 2017) In most instances, implantation of exogenous cells into the heart provides a modest and transitory beneficial effect through the paracrine secretion of factors improving cardiac function, preventing cardiomyocyte apoptosis or inducing neoangiogenesis.

Generation of new myocardial tissue can instead be achieved by the implantation of cardiomyocytes obtained in vitro from ES or iPS cells, as originally shown by the Murry laboratory (Kadota, Pabon et al. 2017). This approach, however, requires the generation of at least one billion cardiomyocytes in culture and their bulk implantation in vivo, with consequent problems related to the electrical and mechanical integration of these cells with the surviving myocardial tissue. An alternative approach would consist in the stimulation of the endogenous capacity of myocardial myocytes to undergo division, therefore achieving endogenous cardiac regeneration. This goal might be achieved by gene therapy.

Gene therapy exploits the idea of modifying cell behavior by delivering nucleic acids. Early attempts of cardiac gene transfer started in ‘90s, with the delivery of angiogenic genes through adenoviral vectors, able to transduce cardiomyocytes at high efficiency and to express high levels of the encoded transgenes. Despite preliminary positive results, most of these studies were prematurely terminated due to the intense inflammatory response and immune rejection elicited by adenoviral vectors (Hedman, Hartikainen et al. 2011). Subsequent attention of the gene therapy community thus turned to the Adeno-Associated Virus (AAV) as a powerful tool for cardiac gene transfer, due to the peculiar tropism of this virus for post-mitotic cells, including cardiomyocytes and the long term episomal persistence of its genome in the infected cells (reviewed in (Zacchigna, Zentilin et al. 2014)) Over 100 clinical trials with AAV vectors have been performed to date (http://www.abedia.com/wiley/), of which one for a cardiac application (AAV1-Serca2a for heart failure (Hulot, Salem et al. 2017).

While the use of viral vectors is essential to transfer large genes into the heart, shorter nucleic acids could be delivered through simple chemical methods. This is the case of the delivery of short interfering RNAs (siRNAs), miRNA mimics and inhibitors, which are currently largely used in RNAi-based therapeutics (Zhou, Zhang et al. 2014) (**Fig.1-4**). Inded, microRNAs might also play a role in cardiac regeneration (Eulalio, Mano et al. 2012) and are key regulators of heart

remodelling, representing a new class of therapeutic targets in heart failure patients (Philippen, Dirkx et al. 2015).

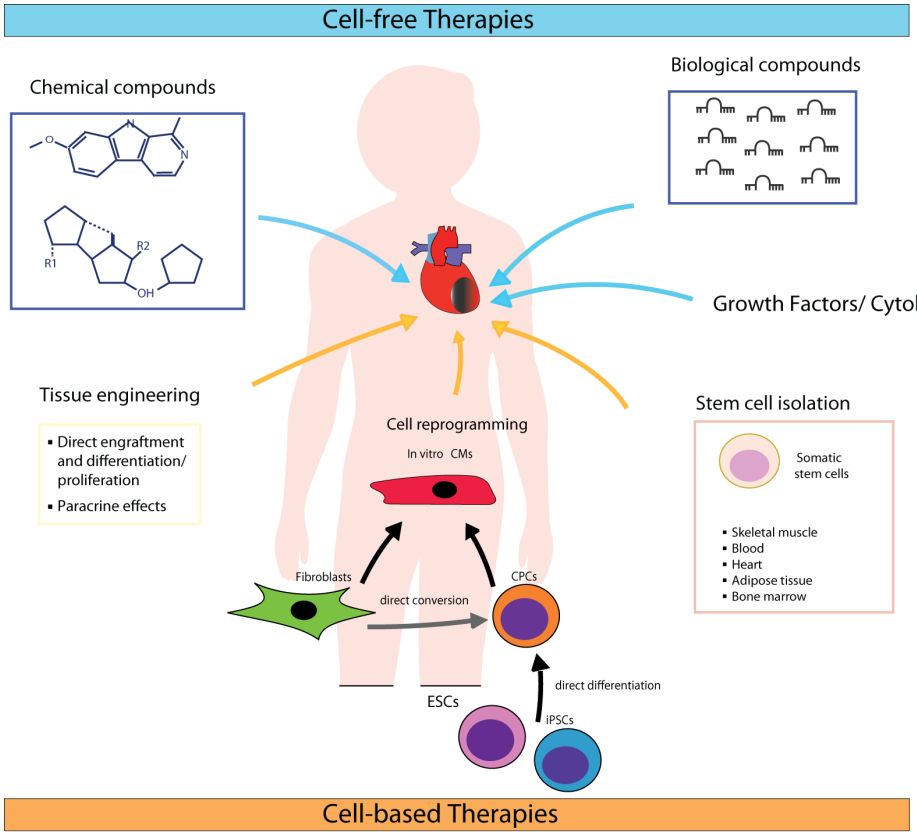

FIGURE 1-4 SCHEMATIC OVERVIEW OF STRATEGIES AVAILABLE FOR HEART REGENERATIVE THERAPY

On the top, cell-free therapies are represented by the use of chemical compounds, cytokines, growth factors and microRNAs. At the bottom, cell-based therapies are based on the use of cardiomyocytes derived from different sources such as embryonic stem cells (ESCs), cardiac progenitor cells (CPCs) and induced pluripotent stem cells (iPSCs). Adapted from (Sahara, Santoro et al. 2015).

1.5.1 Biological compounds for heart regeneration: microRNAs, as regulators of gene expression

Among all non-coding RNAs, microRNAs (miRNAs) are endogenous -22nt long RNA molecules which act as post-transcriptional regulators of gene expression in plants and animals (Bartel 2004). They exert their function by binding the 3' UTR of target messenger RNA, leading to either its degradation or the inhibition of protein translation (Humphreys, Westman et al. 2005). MiRNA target recognition is restricted to a short sequence, known as the "seed" sequence (Rhoades, Reinhart et al. 2002, Vasudevan and Steitz 2007) shared by all micro-RNAs belonging to the same family. Interestingly, the length of 3' UTRs correlates with the number of miRNA-binding sites, therefore with the complexity of gene expression modulation (Osada and Takahashi 2007) (Cheng, Bhardwaj et al. 2009). Moreover, a single miRNA can control the expression of several target mRNAs, therefore enabling the modulation of an entire signaling pathway (van

Rooij and Kauppinen 2014).

1.5.1.1 MicroRNA biosynthesis and processing

MicroRNAs have several peculiar features if compared to other functional RNA species in the cell. Most of them are encoded by polycistronic transcripts, suggesting that members of the same family evolved as a cluster (Du and Zamore 2005). In eukaryotic cells, microRNAs are processed in a sequence of steps (reviewed by (Cai, Hagedorn et al. 2004) (Du and Zamore 2005).

The precursor microRNA, also known as pre-microRNA, is an approximately 60 nt long hairpin RNA generated by excision from the primary transcript by Drosha (Lee, Ahn et al. 2003) Drosha is a class III endonucleases, which produces duplex RNA products containing a 5' phosphate and a 3'-OH, with usually a 2 nt overhang at the 3' end (Zeng, Yi et al. 2005). Drosha exhibits low enzymatic efficiency, therefore a regulatory subunit, DGCR8, helps the enzyme in the recognition of its targets (**Fig.1-5**).

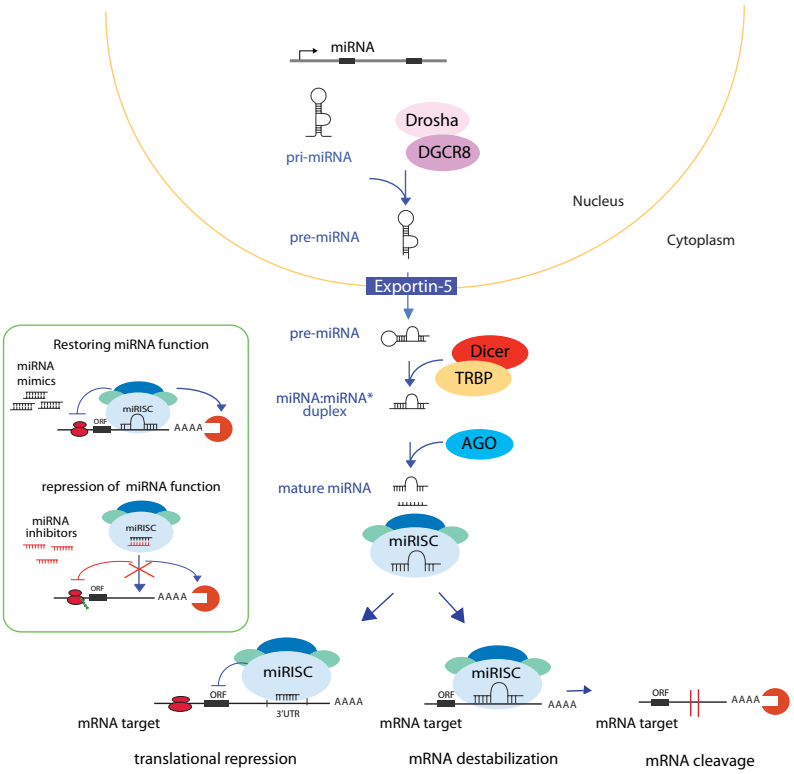

FIGURE 1-5 BIOGENESIS OF MICRORNAS, PROCESSING AND MATURATION.

A primary miRNA transcript is produced by RNA polymerase II or III and is cleaved by the Drosha–DGCR8 complex in the nucleus. Exportin-5–Ran-GTP mediates the export of the pre-miRNA to the cytoplasm, where Dicer, in complex with TRBP, further processes it to a mature miRNA. The functional strand is then loaded with Argonaute (Ago2) into the RNA-induced silencing complex (miRISC). RISC is guided to silence target mRNAs and to induce mRNA cleavage or translational repression. miRNA function can be artificially mimicked using double-stranded miRNA mimics or inhibited by single-stranded antimiR oligonucleotides, as illustrated in the green box. Adapted from: (van Rooij and Kauppinen 2014).

Once pre-miRNAs are produced, exportin5 (Exp5) is responsible for their export into the cytoplasm (Khvorova, Reynolds et al. 2003), where Dicer, a RNaseIII-type enzyme, recognize the 3' overhang via its PAZ domain and produces a duplex intermediate miRNA; usually only one of the two strands can be detected in cells, while the other is degraded. How the choice is mechanistically achieved is not known, although it likely involves differential binding and retention of one of the two RNA strands by Dicer and its associated proteins (Tomari, Matranga et al. 2004). The functional strand is bound by Argonaute and loaded into the RNA-induced silencing complex (RISC) (Meister, Landthaler et al. 2004). RISC is guided to silence target mRNAs and to induce mRNA cleavage or translational repression (**Fig.1-5**).

1.5.1.2 miRNAs controlling cardiomyocyte proliferation

Several microRNAs have been described as powerful regulators of different biological processes. During zebrafish heart regeneration, both mir-99 and mir-100 are downregulated (Aguirre, Montserrat et al. 2014). Interestingly, they both target Smarca5 and Fntb, key factors involved in dedifferentiation and proliferation of adult cardiomyocytes, suggesting that miR-99 and 100 are involved in cardiac cell cycle withdrawal. Other examples are the miR-1 and miR-133 families, part of the same bi-cistronic transcript and both regulators of cardiac cell proliferation. Actually, miR-1 and miR-133a are specifically expressed in cardiac and skeletal muscle, while miR-133b is expressed in skeletal muscle only. Multiple evidence strongly supports a fundamental role for this miRNA cluster during heart development(Zhao, Samal et al. 2005). In fact, Hand2, a crucial transcription factor in cardiac morphogenesis, is a direct miR-1 target. Of note, when an altered expression of miR-1 and miR-133 occurs in adult cardiac tissue, heart failure arises both in mice and humans. This finding can be explained by the fact that miR-133 silencing results in the suppression of genes as Cdc42 and RhoA, which induce the cardiac hypertrophic phenotype (Care, Catalucci et al. 2007). Similar function is exerted by miR-1, whose overexpression decreases cell death and fibrotic cardiac remodeling (Karakikes, Chaanine et al. 2013). MiR-133-1 and miR-133-2 are inhibitors of cardiomyocyte proliferation, since they both target Cyclin D1 and SRF. MiR-133 also regulates the expression of Mps1, a kinase involved in several cell cycle checkpoints, as the mitotic spindle-assembly checkpoint (Mattison, Stumpff et al. 2011).

The miR-15 family is also involved in cardiomyocyte cell cycle withdrawal. MiR-195 targets Chek1, a checkpoint kinase known to negatively regulate cell cycle progression. As a consequence, miR-15 suppression boosts cardiac cell proliferation and improves cardiac function after MI (Porrello, Mahmoud et al. 2013).

Other microRNAs exert their function in cardiac myocyte differentiation during embryonic heart development, as is the case of the miR-17-92 cluster. The expression of this cluster is under BMP regulation and its direct targets are Isl1 and Tbx1. In mice, their overexpression is sufficient to promote cell cycle entry of cardiac cells and tissue protection in case of MI (Chen, Huang et al. 2013).

Taken together, these findings support the use of miRNA as therapeutic tools to target multiple genes at the same time, in light of the final goal to force cardiomyocyte cell cycle re-entry. In this context, a high-throughput screening performed in our laboratory revealed several human miRNAs able to induce cardiomyocyte proliferation. Among them, hsa-miR 199a-3p and hsa-miR 590-3p were able to induce cardiac regeneration after myocardial infarction, by boosting cardiomyocyte proliferation *in vivo* (Eulalio, Mano et al. 2012).

1.5.1.3 MicroRNAs in heart regeneration: the role of YAP

The Morrisey's group (Tian, Liu et al. 2015) recently described the miR-302~367 cluster, which is early expressed during cardiac development in mice and plays an important role in cardiac myocyte proliferation during heart embryogenesis. Main targets of this cluster of miRNAs are several proteins of the Hippo pathway. The sustained expression of miR-302~367 in a transgenic mouse model induced long lasting cardiomyocyte proliferation, finally leading to cardiomegaly and heart failure. Conversely, transient in vivo overexpression of this cluster using miR-302~367 mimics induced heart regeneration, with a significant improvement of cardiac function (Tian, Liu et al. 2015). These observations further support the role of the Hippo pathway as a master regulator of cardiomyocyte proliferation and heart regeneration and validate the use of miRNA mimics as tools to reproduce the effects of specific miRNAs in vivo in a limited time frame, avoiding the adverse effects of their prolonged overexpression.

1.5.2 Chemical compounds for heart regeneration

Parallel to the significant advances in the understanding of key regulatory processes leading to cardiac regeneration, an increasing interest is focused on the development of new, small molecules to be used as therapeutic tools in heart regenerative medicine. Small chemical compounds would significantly improve the impact of heart therapy, with a net reduction in costs and increase of benefits, since already approved drugs have been tested for safety and pharmacokinetics in patients, and they have established manufacturing and distribution networks.

To date, only a few chemical compounds have been studied in order to stimulate heart muscle repair. The isoxazole family (Isx) was described to promote cardiac repair after myocardial infarction, activating Notch signaling in progenitors of epicardial origin. Moreover, these organic compounds were able to protect cardiomyocytes after myocardial infarction by inhibiting the proton sensing GPCR-68, a highly controlled receptor during cardiac ischemia. These preliminary encouraging results were not paralleled by a rescue in cardiac function, suggesting a role of Isx in the protection from cardiac remodeling after infarction, rather than in the acute phase of the ischemic damage (Russell, Goetsch et al. 2012).

Another pathway deeply studied as a potential therapeutic target for heart regeneration is the WNT/β-catenin pathway because of its involvement in the cell cycle regulation in the embryonic cardiac precursors (Ueno, Weidinger et al. 2007). ICG-001 is a small WNT modulator molecule, which selectively disrupts the interaction of β-catenin with CREB binding protein (CBP)

(Willems, Spiering et al. 2011). However, ICG-001 ability of improving the cardiac contractile function in an *in vivo* model of myocardial infarction is mainly associated with its effect on epicardial cells rather then on ventricular cardiomyocytes (Sasaki, Hwang et al. 2013).

More recently, MSI-1436, a strong allosteric inhibitor of the protein tyrosine phosphatase 1B (PTP1b), was also described as a promising candidate for heart regeneration. This small molecule, also known as Trodusquemine, showed good tolerance in patients in phase 1 clinical trials for type-2 diabetes and for the treatment of obesity (*ClinicalTrials.gov identifier NCT number: NCT00606112*). Besides these applications, MSI-1436 is able to successfully induce cardiac muscle regeneration in a mouse model of myocardial infarction, with no detectable side effects at a dosage well below the minimum dose tolerated by patients (Smith, Maguire-Nguyen et al. 2017). The regenerative effect of this compound was also observed during regeneration of other tissues, as the caudal fin of zebrafish. This evidence suggests that MSI-1436 could act as a powerful trigger of tissue regeneration in a broad spectrum of putative targets (Smith, Maguire-Nguyen et al. 2017).

Last, but not least, harmine is a compound showing a regenerative effect on pancreatic beta cells; it is a FDA-registered compound, which shares with MSI-1436 the peculiar property to act on many tissues with relevant beneficial effects as discussed below in details.

1.5.2.1 Harmine: a versatile compound

The 7-methoxy-1-methyl-9H-pyrido[3, 4-b] indole, also known as harmine, is a tricyclic beta-carboline alkaloid, found in many plants. It was originally extracted from the seeds and root of *Peganum harmala*, a plant broadly used in North Africa, Middle East and Central Asia. It is also present in the stem of the *Banisteriopsis Caapi* vine, the main component of the ayahusca, a hallucinogen infusion prepared in Brazilian Amazon during tribal spiritual ceremonies.

Harmine is not only present in the vegetable kingdom but also in marine organisms, insects and mammals, as well as in human tissues and fluids. It was traditionally used as a drug with a broad spectrum of features, including antimicrobial, anti-inflammatory, antimycotic, anti-oxidative, antitumor, anti-depressive and analgesic effects (Moloudizargari, Mikaili et al. 2013) (Patel, Gadewar et al. 2012).

1.5.2.3 Harmine in biology and its potential therapeutic value

The molecular mechanism of action of harmine is only partially described. It is known that this drug binds type A receptors of the gamma-aminobutyric acid (GABA) in the same site used by benzodiazepine, but with an opposite effect. These chemicals are also known as MAO Inhibitors, due to their ability to inhibit a metabolic enzyme, the monoamine oxidase (MAO), in order to prevent direct activation of monoamine receptors (Farzin, Haghparast et al. 2011).

MAO is responsible for the oxidative deamination of amines and is directly involved in the metabolism of vasoactive and neuroactive amines in many tissues. MAO exists in two different isoforms: MAO-A and MAO-B. Both isoenzymes are able to oxidize dopamine, but MAO-A preferentially acts on serotonin and norepinephrine, while MAO-B on phenylethylamine (Shih,

Chen et al. 1999). In particular, harmala alkaloids reversibly bind the enzymatic site of MAO, resulting in an enhanced and prolonged effect of neurotransmitters, due to the fact that MAO physiological function is to degrade endogenous neurotransmitters and dietary amines. Indeed, at the periphery, MAOs catalyze the oxidative catabolism of circulating amines, blocking the effect of dietary amines. In the central nervous system, MAOs inactivate amine neurotransmitters, guaranteeing the protection of neurons from exogenous amines and monitoring the intracellular reservoir of amines. Genetic depletion of MAO genes results in higher reactivity in stress conditions (Grimsby, Toth et al. 1997). Interestingly, MAO-A-deficient animals show cognitive deficit and reduced control of impulses with behavior disturbances, while a deficiency of MAO-B is not associated with any evident clinical defect, indicating that MAO-A has a more relevant role in amine metabolism (Lenders, Eisenhofer et al. 1996).

Harmine is also a potent inhibitor of a dual specificity tyrosine-phosphorylation-regulated kinase (Dyrk1a), which regulates cell proliferation, apoptosis and brain development (Matsuki, Hori et al. 2005). Dyrk1a belongs to a family of kinases (Dyrk1b, Dyrk2, Dyrk3, Dyrk4a and Dyrk4b), which share the same activation mechanism (Walte, Ruben et al. 2013); they undergo auto-phosphorylation on residue Y321 in order to achieve full activation and phosphorylate their substrates on serines and threonines (Himpel, Panzer et al. 2001). Dyrk1a is also overexpressed in several cancers, such as glioblastoma and lung cancer (Pozo, Zahonero et al. 2013) (Gao, Zheng et al. 2009). A complete overview of Dyrk1a's downstream molecular mechanism remains a topic of debate.

1.5.2.3.1 Cardiovascular responses

Harmala compounds have a strong impact on the cardiovascular apparatus: bradycardia, alterations in arterial blood pressure and in myocardial contractile force are just a few of several effects on heart and blood vessels.

The vasorelaxant effect induced by harmala drugs is due to their effect on the alpha 1-adrenergic receptors of the vascular smooth muscle cells, and to the increased NO levels, produced by endothelial cells because of the increased levels of external Ca2+. In fact, both harmine and harmaline (10^-6 to 3x10^-4 M) are able to inhibit muscle contractile response in a concentration-dependent manner in the presence of stimulatory agents (Berrougui, Martin-Cordero et al. 2006). However, neither harmine nor harmaline showed any effect on the endothelium-independent relaxation.

Interestingly, hamaline and harmine are able to reduce free radicals generated by DPPH, suggesting that the decrease in oxidative stress correlates with an increase of the relaxation effect on aortic rings. Indeed, harmine as well as harmaline are able to reduce the arterial pressure systemically and vascular resistance in peripheral tissues (Berrougui, Martin-Cordero et al. 2006).

Little is known about the direct effect of harmine on the myocardium. Pioneering studies described a ionotropic effect and induced reduction in cardiac contractility (Aarons, Rossi et al. 1977). Interestingly, the short time frame of cardiovascular effects is not compatible with the

timing of MAO inhibition by harmala alkaloids, therefore suggesting a MAO-independent mechanism of action (Aarons, Rossi et al. 1977).

Another interesting feature of harmine is its strong anti-angiogenic action in tumors both *in vivo* and *in vitro,* in a model of gastric cancer, through the downregulation of COX-2 and NO synthase (Hamsa and Kuttan 2010). Harmine is able to inhibit endothelial cell proliferation and induce the production of pro-angiogenic cytochines (VEGF, NO and cytokines such as IL-1b and TNF-a) in a dose-dependent manner. These anti-angiogenic effects were detected at micromolar concentrations (2 μM), supporting the potential therapeutic use of harmine at low dosage.

1.5.2.3.2 Nervous System responses

Traditionally, harmala alkaloids have been described to have psychoactive properties with a broad spectrum of effects on both the central and peripheral nervous system. In addition to their effect on MAO inhibition, described above, another important feature of these compounds is related to their anti-depressant effect. Indeed, the acute administration of harmine at 15 mg/kg body weight, in rat hippocampal neurons induced a massive secretion of brain-derived neurotrophic factor (BDNF) (Fortunato, Reus et al. 2009), the levels of which are dramatically reduced in depressed patients.

In the beginning of 1920s, multiple findings brought to evidence the involvement of beta-carboline in Parkinson's disease development. In particular, patients affected by Parkinson's disease showed increased levels of β-carbolines with dopaminergic cytotoxicity mediated by DAT (dopaminergic active transporter) (Storch, Hwang et al. 2004). Another neurodegenerative disorder, Alzheimer's disease, has recently been linked to both MAO activation and Dyrk1a kinase activity. In fact, Dyrk1a contributes to Tau phosphorylation (on Ser396) and consequently to the formation of the neurotoxic tau aggregates (Frost, Meechoovet et al. 2011), responsible for the pathological progression of Alzheimer's disease. In this context, harmine treatment was shown to inhibit the formation of these aggregates, due to its suppressing activity on MAO and Dyrk1a (Frost, Meechoovet et al. 2011).

1.5.2.3.3 Anti-cancer properties

In Iran and Morocco, traditional medicine preparations for the treatment of many tumors were based on *P. harmala* seeds. These habits raised the interest of many researchers to understanding the properties of *these s*eeds and, specifically, of β-carboline alkaloid compounds, which are supposed to be partially responsible for the inhibition of cancer cell proliferation. Additionally, their cytotoxic action was also linked to the ability to interact with nucleic acids, therefore inhibiting DNA synthesis (Chen, Chao et al. 2005). Actually, *in vitro*, harmine shows a very strong effect on the inhibition of DNA topoisomerase I purified from human placenta (Sobhani, Ebrahimi et al. 2002). Moreover, harmine mediates DNA conformational changes that interfere with DNA synthesis, resulting in proliferation arrest and genotoxic effect in budding yeast (Li, Liang et al. 2007).

To further strengthen the role of harmine in cell-cycle related processes, recent findings have

shown that, in colon cancer cells, harmine decreases cyclin D1 expression levels, with an opposite increase of cyclin A, E2 and B1 levels as well as of the levels of CDK1/cdc2, myt-1 and p-cdc2. This expression profile is a hallmark of an S-G2/M phase arrest. Moreover, in this model, harmine led to activation of both caspase 3 and PARP and the downregulation of Bcl-2 and Mcl-1; all these events are typically associated with apoptotic death mediated by mitochondrial pathway activation and by inhibition of both Akt and ERK signaling (Liu, Li et al. 2016). In hepatic cancer cell lines, harmine was shown to inhibit Rad51 recruitment, affecting homologous recombination and inhibiting double-strand breaks repair, with consequent cytotoxicity (Zhang, Zhang et al. 2015). This work identified novel potential targets in the homologous recombination pathway to optimize cancer therapy and arrest cancer cell proliferation. Of note, it seems that harmine is able to specifically target proliferating cells, as in hepatoma cell lines, with minimal side effect on post-mitotic cells.

Another example of tumor cells sensitive to harmine treatment is head and neck squamous cell carcinoma (HNSCC). In this model, harmine-mediated inhibition of Dyrk1a decreases phosphorylation of the transcription factor Foxo3a, thus promoting cell death (Radhakrishnan, Nanjappa et al. 2016).

The aforementioned examples are just a few of the several ones supporting harmine as an anticancer drug. Its cytotoxic effect is further strengthened by its anti-angiogenic and anti-inflammatory properties (discussed above), which supported the patent on harmine-anti-tumor effect registered in 2001 (code: CN1358720A).

1.5.2.3.4 Osteogenic effects

The increasing need of new drugs to treat bone-destructive diseases led to the investigation of the properties of natural compounds in bone reabsorption. In this setting, harmine acts on osteoclast progenitors but not on osteoblasts, inhibiting osteoclastogenesis. In particular, harmine downregulates c-Fos and Nfatc1 expression, targeting nuclear factor kappa-B ligand (RANKL) signaling pathway and preventing osteoclast precursor differentiation (Yonezawa, Hasegawa et al. 2011). As a net result, harmine acts on osteoblast differentiation stimulating the activation of Runx2 and BMPs signaling. As in the case of its anti-tumoral effect, a patent for the use of alkyl-amine harmine derivatives to promote bone repair was registered in 2014 (code: EP2968284A2).

1.5.2.3.5 Anti-diabetic actions

Among the alkaloids present in *P. harmala*, harmine is the main responsible of its anti-diabetic effects. Interesting findings show that this compound has an important metabolic effect, promoting the specific expression of PPARγ in adipocytes, resulting in an improvement of glucose metabolism (Waki, Park et al. 2007). Furthermore, harmine is also able to attenuate the expression of pro-inflammatory genes and diminishes macrophage recruitment in the adipose tissue, which is linked to the insulin resistance induced by obesity. The action of harmine on adipocyte metabolism can partially be explained by the inhibition of WNT signaling pathway (Waki, Park et al. 2007).

Since the deficiency of functional pancreatic beta-cells represents the cause of type 1 diabetes, harmine represents a promising therapeutic agent, as it is able to promote beta-cell proliferation, increase islet mass and improve glucose metabolism in *in vivo* models. The inhibition of Dyrk1a and the NFAT transcription factors were reported to be responsible for the harmine pro-proliferative effect in these settings (Wang, Alvarez-Perez et al. 2015).

2 Thesis Aim

The work presented in this Thesis was aimed at identifying the molecular mechanisms by which a few microRNAs and one small molecule are capable to stimulate cardiomyocyte proliferation ex vivo and cardiac regeneration after myocardial infarction in vivo.

First, I concentrated my attention on the effect of 10 microRNAs that had been previously identified by the laboratory for their capacity to stimulate proliferation of neonatal rodent cardiomyocytes. For 6 of these microRNAs, I determined the transcriptional profile induced by their transfection into cardiomyocytes, observing that they all impinge on the Hippo/YAP pathway and determine remodelling of the actin cytoskeleton by targeting one or more of the proteins that control actin polymerization.

Next, I screened a library of FDA-registered drugs in search for small molecules able to activate cardiomyocyte proliferation. I discovered that the neuroactive alkaloid harmine exerted a powerful pro-proliferative effect, which was mediated by the inhibition of the cellular Dyrk1a kinase. Similar to the investigated microRNAs, activation of YAP was also essential to mediate the pro-proliferative effect of harmine.

These findings are discussed in the context of the possibility of inducing cardiac regeneration after myocardial infarction by the stimulation of the endogenous capacity of cardiomyocytes to proliferate.

3 Materials and Methods

3.1. Cell culture methods

3.1.1 Cell lines: HeLa

HeLa cells (ATCC® Cells were taken in a Dulbecco's modified Eagle medium with 1 g/l glucose (DMEM, Life Technologies) supplemented with 10% FBS and 100 U/ml penicillin and 100 mg/ml streptomycin (Sigma).

3.1.2 Primary cells: isolation of ventricular cardiac myocytes from neonatal rats

Ventricular CMs were isolated from neonatal rat as previously described (Collesi, Zentilin et al. 2008). In brief, ventricles from neonatal (P0) rats were separated from the atria, cut into pieces and dissociated in calcium and bicarbonate-free Hanks with Hepes (CBFHH), using mechanical and physical stirring. CBFHH buffer contains 1.75 mg/ml trypsin (BD Difco) and 10 mg/ml DNase II (Sigma). Tissue digestion was performed at room temperature in ten minute steps, with collection of the supernatant to fetal bovine serum (FBS, Life Technologies) after each step. In order to pellet cells, collected supernatant was centrifuged and cardiac cells were then resuspended in Dulbecco's modified Eagle medium 4.5 g/l glucose (DMEM, Life Technologies) supplemented with 5% FBS, 20 mg/ml vitamin B12 (Sigma) and 100 U/ml penicillin and 100 mg/ml streptomycin (Sigma). The collected cells were filtered using a cell strainer (40 mm, BD Falcon) and finally seeded onto four 100-mm plastic dishes for 2 hr at 37°C in 5% CO2 and humidified atmosphere. CMs in the supernatant were then collected, counted and plated at the appropriate density into BD Matrigel Matrix Growth Factor Reduced (356230 BD Bioscience) pre-coated Primaria 96-well plates (BD Falcon) or matrigel-coated Primaria 35-mm dishes (BD Falcon).

Number of cardiac cells seed for each plate/dish:
96-multiwell plate: 15*10^3 cells/ well
35 cm dishes: 5*10^5 cells/ dish
60 cm dishes: 1*10^6 cells/ dish

3.1.3 microRNA/siRNA transfection and EdU incorporation

MicroRNAs and siRNAs (SMARTpool) were obtained from Dharmacon, Thermo Scientific and transfected into neonatal rat CMs using a standard reverse transfection protocol (Eulalio, Mano et al. 2012). Cardiomyocyte transfection efficiency with miRNAs/siRNAs is >90% using Lipofectamine RNAiMAX as lipids. In brief, transfection lipids (Lipofectamine RNAiMAX, Life Technologies) were incubated with OPTIMEM (Life Technologies) for 5 min at RT and added to miRNAs, siRNAs or a combination of the two (at a final concentration of 25 nM each nucleic acid), arrayed on 96-well plates; 30 min later, 1x10^4 cells were seeded in each well. Twenty-four hours after transfection, culture medium was replaced by fresh medium; 28 h later (52 h after

plating), the culture medium was supplementaed with 5 mM 5- ethynyl-29-deoxyuridine (EdU, Life Technologies) for 20 h. Cells were fixed at 72 h after plating and processed for immunofluorescence. Experiments were performed in quadruplicate.

Oligonucleotides		
siRNA targeting sequence: YAP1 NM_001034002.2 sequences: siRNA YAP1sense 5'- GGAGAAGUUUACUACAUAA [dT] [dT] -3' antisense 5'-UUAUGUAGUAAACUUCUCC [dT] [dT] 3'	Sigma	
siGenome SMARTpool against rat Cfl2	Dharmacon, Thermo Scientific	cat# M-099723-01
siGenome SMARTpool against rat Taok1	Dharmacon, Thermo Scientific	cat# M-095482-01
siGenome SMARTpool against rat bTrC	Dharmacon, Thermo Scientific	cat# M-086092-01
siRNA against rat STK38L	Sigma	ID: SASI Rn02_00208859
siRNA against rat Dyrk1a	Ambion	ID: s129286
siRNA against rat Dyrk2	Ambion	ID: s163537
siRNA against rat Dyrk3	Ambion	ID: s156275
siRNA against rat Dyrk4	Ambion	ID: s161980
siRNA negative control	Ambion	
siRNA negative control	Sigma	
siRNA NT4	Dharmacon, Thermo Scientific	

3.1.4 Chemicals

Harmine, harmaline, harmane (Sigma-Aldrich) were dissolved in DMSO and further diluted in culture media at the final concentration of 10 μM.

CytochalasinD (sc_201442, Santa Cruz) was added to CM culture medium at the final concentration of 0.1 μM.

3.1.5 TEAD reporter assay

For luciferase assays, CMs were plated at the concentration of $1.5x10^5$ (day 0) in a double-matrigel coated 96-Multiwell plate and, the day after, were transfected with the selected miRNAs (Dharmacon). At day 3 of culture, cells were transfected with 100 ng of both synthetic TEAD reporter firefly luciferase plasmid (p8xGTIIC-Lux, Plasmid #34615, Addgene) and a renilla luciferase plasmid. The day after transfection, firefly and renilla luciferase activities were measured using the Dual Luciferase Reporter Assay System (Promega), according to the manufacturer's instructions.

3.1.6 Luciferase 3′-UTR reporter assays

Constructs coding for rat 3′-UTR of Cfl2, TAOK1, β-TrCP or STK38L (gBlock) were obtained by gene synthesis from Biomatik (3'UTR-Cfl2) or Genewiz (3'UTR- β- TrCP and 3'UTR-TAOK1) and subcloned into psiCHECK2.1 vector (Promega). HeLa cells were transfected with 100 ng of

the reporter constructs or psiCHECK2 vector (control) using FuGENE HD transfection reagent (Promega). Twenty-four hours later, cells were transfected with the miRNA under investigation at a final concentration of 50 nM in 96-well plates, using a standard forward transfection protocol similar to that described above. Each condition was tested in quadruplicates.

Firefly and renilla luciferase activities were measured 48 hr after plasmid transfection using the Dual Luciferase Reporter Assay System (Promega), according to the manufacturer's instructions.

3.1.61 mutated UTR-luciferase reporters: construct generation

The mutated 3'-UTR of β-TrC and TAOK1 were obtained by gene synthesis (gBlocks) from IDT (Integrated DNA Technology) and sub-cloned into the psiCHECK2.1 vector. The gBlocks terminal regions were implemented with enzymatic restriction sites for XhoI and NotI in addition to flanking regions of stuffer-DNA to increase cut efficiency.

The gBlocks were digested with XhoI and Not-HF (New England Biolabs) as well as the wt UTR-luciferase reporter plasmids.

Briefly, 500 ng of gBlock or 2µg of the vectors were digested with 0.1µl/0.5µl of XhoI (10000U/ml) and 0.1µl/0.5µl of NotI-HF (10000U/ml) in presence of 2µl/3µl of 10x Buffer 2.1 and H20 to final volume of 20 µl/30µl and incubated at 37° for 2 hours; then, heat inactivation for 15' at 65°C.

Both digested vectors were submitted into DNA gel electrophoresis. 1% agarose gel was prepared, placed into an electrophoresis chamber and rinsed in TBE (Tris-Borate-EDTA buffer; Sigma). Samples were loaded into pre-cast wells and placed in an electric field where due to the negatively uniform mass/charge ratio of nucleic acids, DNA fragments migrated according to their molecular weight and secondary structure. The linearized vectors were excised and purified from gel using Wizard SV Gel and PCR Clean-Up System (Promega) according to manufacturer's instruction. Also the digested gBlocks were purified, using the same kit. Finally, the linearized vectors and the digested gBlocks (mutated 3'UTR of β-TrC and TAOK1, respectively) were ligated and transformed into XL10 Gold (Stratagene) recombination deficient bacteria. Colonies were screened for ampicillin resistance as well as insert size by restriction enzyme digestion.

Before using the ligation products to perform the 3'UTR-luciferase assay, we checked the sequence of these plasmids by sequencing (GATC-biotech).

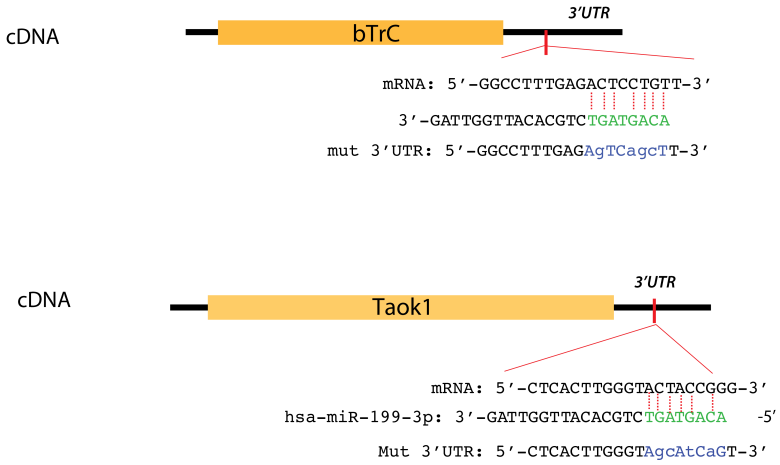

FIGURE 3-1 SCHEMATIC REPRESENTATION OF THE 3'UTR OF TAOK1 AND β-TRC TRANSCRIPTS

The 3'UTR of TAOK1 and bTrC mRNA were mutated as shown in the miR-199a-3p recognized region (in blue). In green the seed sequence of miR-199a-3p.

Recombinant DNA		
p8xGTIIC-Lux plasmid	Gift from S. Piccolo Lab	Addgene, Cat#34615
pRL Renilla Luciferase control plasmid	Promega	cat# E2261
5SA-YAP1 in pCSII-EF-MCS plasmid	Gift from S. Piccolo Lab, Dupont et al. Nature 2011	
psiCheck2.1 plasmid	Promega	Cat# C8021
3'UTR-Cfl2 plasmid	Biomatik	Clone ID T4545-1
3'UTR-bTrc plasmid	Genewiz	Clone ID B28633-1/K28633
3'UTR-Taok1plasmid	Genewiz	
3'UTR-mut Taok1 plasmid	QuikChange II XL Site-Directed Mutagenesis Kit	
3'UTR-mut b-Trc plasmid	QuikChange II XL Site-Directed Mutagenesis Kit	
3'UTR-Stk38L plasmid	IDT gblock	

3.1.7 High-throughput screening: FDA-registered compound screening

The miRNA mimics corresponding to hsa-miR-590-3p, hsa-miR-199a-3p were obtained from Dharmacon, Thermo Scientific. For miRNA transfection in rat CMs, miRNAs were robotically transferred from stock library plates to Primaria 384-well plates (BD Falcon) leaving columns 1 and 24 empty for addition of controls (buffer, cel-miR-67). MiRNAs were transfected into neonatal rat CMs using a standard reverse transfection protocol, at a final miRNA concentration of 25 nM. Briefly, the transfection reagent (Lipofectamine RNAiMAX, Life Technologies) was diluted in OPTI-MEM (Life Technologies) and added to miRNAs on the 384-well plates; 30 min later, 5.000

cells/well were seeded. Twenty-four hours after transfection, culture medium was replaced by fresh medium; 24 h later, that is, 48 h after plating, FDA-registered compounds, 10 mM (or DMSO as control) were robotically arrayed on the 384-well plates and 52h after plating 5 μM 5-ethynyl-2′-deoxyuridine (EdU, Life Technologies) was added for 20 h. Cells were fixed at 48 h after plating and processed for immunofluorescence. Screening was performed in duplicate. Cells were stained according to IF standard protocol as described later.

3.1.8 Immuno-staining: immunofluorescence on primary cell cultures

CMs were fixed with 4% PFA for 10 min, permeabilized with 0.5% Triton X-100 in PBS for 10 min, followed by 1 hr blocking in 2% BSA (Roche). CMs were then stained overnight at 4°C with mouse monoclonal antibody against sarcomeric α-actinin (Abcam) diluted in blocking solution. Cells were washed with PBS and incubated for 2 hr with the secondary antibody conjugated to Alexa Fluor-488 (LifeTechnologies). Cells were further processed using the Click-IT EdU 555 Imaging kit (Life Technologies) to reveal EdU incorporation, according to the manufacturer's instructions, and stained with Hoechst 33342.

3.1.8.1 Image acquisition

In screening experiments, image acquisition was performed using an ImageXpress Micro automated high-content screening fluorescence microscope at ×10 magnification; a total of 16 images were acquired per wavelength, well and replicate, corresponding to approximately 2.500 cells analyzed per condition and replicate. Image analysis was performed using the 'Multi-Wavelenght Cell Scoring' application module implemented in MetaXpress software (Molecular Devices). Cells were scored as proliferating only if positive for the proliferation marker EdU. In all quantifications, CMs were distinguished from other cells present in the primary cultures by their positivity for sarcomeric α-actinin.

3.2 Biochemistry

3.2.1 Nuclear/cytoplasmic fractionation

$1x10^6$ neonatal rat cardiac myocytes were plated on matrigel-coated Primaria 60-mm dishes (BD Falcon) as described above. miRNAs were transfected by a standard forward transfection protocol. Seventy-two hr after transfection, cells were washed with ice-cold PBS and harvested in 80 μl of hypotonic buffer (50 mM Tris pH7.5, 10 mM NaCl, 3 mM MgCl2, 10% glycerol) supplemented with protease inhibitors (complete tablets, Mini EDTA-free, Roche) and phosphatase inhibitors (cocktail 3 Sigma, 2mM orthovanadate, 1 mM NaF). After 1 min, cells were scraped and NP40 was added at 0.1% final concentration. After 5 min on ice, cells were centrifuged at 4000 rpm for 5 min at 4ºC; the supernatant and cytosolic fractions were then recovered. Pellets were resuspended in 70 μl IPLS buffer (50 mM Tris pH 7.5, 120 mM NaCl, 1 mM EDTA, 0.5% NP40, supplemented with the same inhibitors as above) and sonicated with 3 pulses of 10 min each (30 sec on/30sec off) on

ice in a Bioruptor™ Plus (Biosense). Nuclear lysates were centrifuged at 16,000 rpm for 20 min at 4ºC and the supernatant was recovered as nuclear fraction. Concentration of cytoplasmic and nuclear lysates were measured using the Bradford assay (Protein Assay Dye Reagent Concentrate, Bio Rad). Lysates (10 to 20 µg) were loaded for protein separation and subsequent blotting onto a PVDF membrane (Amersham™ Hybond™ PVDF, GE Healthcare).

3.2.2 Antibodies

The following antibodies were used for western blotting analysis.

REAGENT or RESOURCE	**SOURCE**	**IDENTIFIER**
Antibodies		
Rabbit polyclonal anti-YAP	Cell Signaling Tecnology	Cat# 4912S RRID:AB_10694682
Rabbit polyclonal anti-Phospho YAP (Ser 127)	Cell Signaling Tecnology	Cat# 4911S RRID:AB_2218913
Rabbit polyclonal anti-Cofilin 2	Millipore	Cat# 07-300 RRID:AB_2080926
Mouse monoclonal anti-F actin	Abcam	Cat# ab205 RRID:AB_302794 Clone NH3
Rabbit polyclonal anti-actin	Cytoskeleton	Cat# AAN01 also AAN01-B,AAN01-A RRID:AB_10708070
Rabbit polyclonal anti-TAOK1	LifeSpan BioSciences, Inc.	Cat# LS-C146952 Lot# 62983
Rabbit polyclonal anti-beta-TrCP/HOS	Santa Cruz Biotechnology	Cat# sc-15354 RRID:AB_2065916
Rabbit polyclonal anti-GAPDH	Santa Cruz Biotechnology	Cat# sc-25778 RRID:AB_10167668
Rabbit polyclonal anti-PARP-1	Enzo Life Sciences	Cat# ALX-210-302 RRID:AB_2160732
Mouse monoclonal anti-p84	Abcam	Cat# ab487 RRID:AB_304696 Clone 5E10
Mouse monoclonal anti-Sarcomeric Alpha Actinin	Abcam	Cat# ab9465 RRID:AB_307264
Alexa fluor 488 phalloidin	Thermo Fisher Scientific	Cat# A12379 also A-12379 RRID:AB_2315147
rabbit monoclonal anti-Dyrk1a	Cell Signaling	#2771
Mouse monoclonal anti-Dyrk2	Santa Cruz	sc-293487

3.2.3 G/F actin separation and immunoblotting

The amount of G-actin and F-actin in CMs was quantified using G-actin/F-actin in vivo assay kit (Cytoskeleton Inc.) according to the manufacturer's instructions. Briefly, cells were lysed in pre-warmed lysis/F-actin stabilizing buffer supplemented with protease inhibitor and ATP. The cell lysate was centrifuged for 5 min at 350°—g to remove debris. A 100 µl aliquot was then ultracentrifuged at 100,000xg for 1hr at 37°C to pellet F-actin, with G-actin remaining in the supernatant. The pellet was resuspended in 100 µl of F-actin destabilizing buffer on ice for 1 hr

with frequent pipetting. Equal volumes of G-actin and F-actin fractions were mixed with 5x loading buffer and run on SDS-PAGE. Western blot analysis was performed using the anti α-actin antibody provided in the kit. Densitometry analysis was performed using the ImageJ software.

3.3 Molecular Biology Methods

3.3.1 RNA isolation and quantitative Real-Time PCR

Total mRNA was isolated from CMs 72 hr after transfection, or at different time points after cytochalasin D treatment, using a standard TRIZOL RNA isolation protocol. The RNA obtained (1 µg) was reverse-transcribed using MLV-RT (Invitrogen) with random hexamers (10 µM) in a 20 µl reaction, following the manufacturer's instructions. mRNA levels for CTGF, CyR61, BIRC5 and GAPDH were measured by Real-Time PCR using pre-designed TaqMan assays (Thermofisher) and iQ™Supermix (Bio-Rad) according to the manufacturer's instruction.
TaqMan Probes are listed in the table.

Real Time-PCR probes	**SOURCE**	**ID**
CTGF TaqMan Gene Expression Assays	Thermo Scientific	Assay ID Rn01537279_g1
CyR61 TaqMan Gene Expression Assays	Thermo Scientific	Assay ID Rn00580055_m1
Birc5 TaqMan Gene Expression Assays	Thermo Scientific	Assay ID Rn00574012_m1
Taok1 TaqMan Gene Expression Assays	Thermo Scientific	Assay ID Rn00597907_m1
bTrc TaqMan Gene Expression Assays	Thermo Scientific	Assay ID Rn01413748_m1
Cfl2 TaqMan Gene Expression Assays	Thermo Scientific	Assay ID Rn01472820_g1
Stk38l TaqMan Gene Expression Assays	Thermo Scientific	Assay ID Rn01472820_g1
Dyrk2 TaqMan Gene Expression Assays	Thermo Scientific	Assay ID Rn01472820_g1
Dyrk3 TaqMan Gene Expression Assays	Thermo Scientific	Assay ID Rn01472820_g1
Dyrk4 TaqMan Gene Expression Assays	Thermo Scientific	Assay ID Rn01472820_g1
Dyrk1a TaqMan Gene Expression Assays	Thermo Scientific	Assay ID Rn00562940_m1

3.3.2 Transcriptomic analysis

Deep-sequencing of total neonatal rat CM RNA was performed 72 hr after transfection of microRNAs by IGA Technology Services, Udine, Italy as in ref. (Eulalio, Mano et al. 2012). Briefly, RNA purity, integrity and concentration were determined using an Agilent 2100 Bioanalyzer (Agilent Technologies). Only RNA with a RIN value >7 and an rRNA 28S/18S ratio >2 was taken forward for sample preparation. Two µg of total RNA (minimum concentration of 200 ng/µl) per sample were sequenced on an Illumina HiSeq2000. Two lanes in 7-plex were run obtaining 2 millions of single-reads per sample, 50-bp long. The raw sequencing data discussed in this thesis have been deposited in NCBI's Sequence Read Archive (SRA) and are accessible

through SRA STUDY accession SUB2866022.

Real-time image analysis, base calling, de-multiplexing and production of FASTQ sequence files were performed on the HiSeq2000 instrument using the HiSeq Software. Raw sequence files were quality checked using FASTQC software (www.bioinformatics.babraham.ac.uk/projects/fastqc) and trimmed to remove Illumina adaptor using Cutadapt software (Martin, 2011). RNA-seq reads were mapped to Rattus norvegicus reference genome (GCF_000001895.5 Rnor 6.0.82) and to known mature miRNAs using STAR software (Dobin et al., 2013). Rounded Gene counts were used as input and transformed to rpkm using Bioconductor package edgeR rpkm function (McCarthy, Chen et al. 2012) . The CLC Bio Genomic Workbench (Mortazavi et al., 2008) was used to quantify gene expression levels. In particular, sequenced RNA fragments were mapped against the NCBI Rnor_6.0 annotation release 106 (GCF_000001895.5) RefGene genome annotation (O'Leary, Wright et al. 2016). The resulting gene expression levels were then normalized in RPKM (reads per kilobase of exon model per million mapped reads). In case of transfection of a pro-proliferative miRNA, genes whose RPKM values were greater than 1.00 in both miRNA and cel-miR-67 control-transfected rat CMs were considered as expressed. Fold changes were taken with respect to the expression of cel-miR-67 control. Genes whose fold changes were greater than 1.3 (both upregulated and downregulated) were considered as differentially expressed.

3.3.3 Clustering of fold change expression levels

Cluster analysis was performed on the basis of the log2-fold changes in gene expression in respect to cel-miR-67 to classify the pro-proliferative miRNAs according to their effects on CMs upon transfection. In brief, the correlation between the log2-fold changes for all pairs of miRNA was calculated. Clusters were then hierarchically identified using the average linkage criterion with a Euclidean distance metric as implemented in the clustering package of SciPy v0.18.1 (http://www.scipy.org). Dendrograms were then generated to visualize the arrangement of the resulting cluster.

3.3.4 Bioinformatic target prediction

To the best of our knowledge, bioinformatic predictions of seed sequence interactions with rat transcripts are not available. With this constraint, we compiled a list of rat miRNA-gene interactions from mouse predictions. In particular, predicted mouse gene targets of the seed sequences (corresponding to miRNA families) of pro-proliferative miRNAs were collected from TargetScanMouse Release 7.1 (Agarwal, Bell et al. 2015). The mouse genes were then converted to their corresponding rat genes via homology using the HomoloGene database (Coordinators 2016). The list of miRNA-gene interactions was filtered to only include genes that were downregulated by the miRNA upon transfection to CMs according to the transcriptomic data.

3.4 Animal models

Wistar rats and CD1 mice were purchased from Charles River Laboratories Italia Srl. Animal care and treatments were conducted in conformity with institutional guidelines in compliance with national and international laws and policies (EEC Council Directive 86/609, OJL 358, 12 December 1987).

Dyrk1a F/F mice were were received by Prof. John D Crispino from the Robert H Lurie Medical Research Center and MHC-MCM-Dyrk1a F/F mice were generated by breeding Dyrk1a F/F mice and MHC-MCM- mice, which are available in ICGEB Animal House Facility.

3.4.1 Myocardial infarction

Myocardial infarction was produced in adult female CD1 mice (8–12 weeks old), by permanent left anterior descending (LAD) coronary artery ligation. Briefly, mice were anesthetized with an intraperitoneal injection of ketamine and xylazine, endotracheally intubated and placed on a rodent ventilator. Body temperature was maintained at 37°C on a heating pad. Beating heart was accessed via a left thoracotomy. After removing the pericardium, a descending branch of the LAD coronary artery was visualized with a stereomicroscope (Leica) and occluded with a nylon suture. Ligation was confirmed by the whitening of a region of the left ventricle, immediately post-ligation. EdU was administered intraperitoneally (500 µg per animal) every 2 days, for a period of ten days.

3.4.2 Echocardiographical analyses

To evaluate left ventricular function and dimensions, transthoracic two-dimensional echocardiography was performed on mice sedated with 5% isoflurane at 12, 30 and 60 days after myocardial infarction, using a Visual Sonics Vevo 2400 Ultrasound (Visual Sonics) equipped with a 30-MHz linear array transducer. M-mode tracings in parasternal short axis view were used to measure left ventricular anterior and posterior wall thickness and left ventricular internal diameter at end-systole and end-diastole, which were used to calculate left ventricular fractional shortening and ejection fraction. Echocardiography analysis was performed at week 1, 2, 4 and 8 after infarction (in harmine-treated animals) or after the induction of the phenotype (Dyrk1a KO mice) and hearts were collected at 8 week after infarction (n= 6 animals per group).

3.4.3 Heart collection and histological analysis

At the end of the studies, animals were anaesthetized with 5% isoflurane and then killed by injection of 10% KCl, to stop the heart in diastolic phase. The heart was excised, briefly washed in PBS, weighted, fixed in 10% formalin at room temperature, embedded in paraffin and further processed for histology or immunofluorescence. PicusSirius-Red staining were performed according to standard procedures and analyzed for morphology and extent of fibrosis.

3.5 Statistical analysis

Unless otherwise indicated, all data are expressed as mean ± standard error of the mean (SEM). One-way ANOVA followed by post-hoc analysis with the Bonferroni's Multiple Comparison Test was used for the analysis of multiple groups; two-tail Student's t-test was used to compare two individual groups.

4 Results

4.1 Activation of the YAP transcriptional coactivator mediates function of miRNAs inducing cardiomyocyte proliferation

We wanted to explore the involvement of the YAP-Hippo signaling pathway in the biological effect of a series of human microRNAs previously identified to promote cardiac cell proliferation (Eulalio et al 2012). To this aim, we evaluate TEAD activation rate by transfecting neonatal rat cardiomyocytes with a TEAD-responsive reporter plasmid (p8xGTII-Lux) together with the top 10 of microRNAs characterized in our previous work for their pro-proliferative ability (**Fig. 4-1A**). These included human miR-590-3p (the most effective in our original screening in rat cells), miR-199a-3p (the most effective in mouse cells), miR-1825, miR-302c, miR-302d and miR-373 (two miRNAs known to be enriched in embryonic stem cells (Barroso-del Jesus et al., 2009), miR-33b*, miR-18a*, miR-1248, miR-30e*. C. elegans cel-miR-67 was used as a negative control, while constitutively activated YAP (YAP5SA) was used as a positive control. We found that TEAD-luciferase reporter activity was significantly increased upon treatment with all the selected microRNAs compared to the control cel-miR-67 (**Fig. 4-1B**).

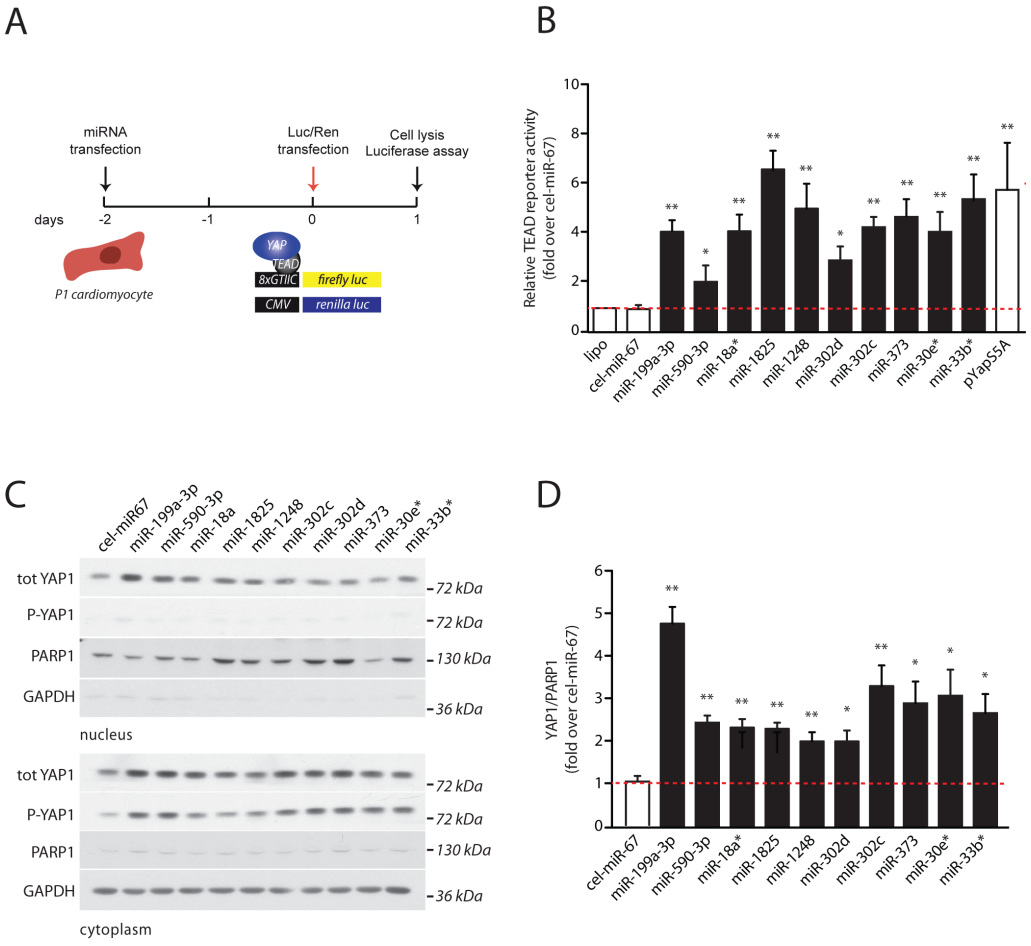

FIGURE 4-1. YAP ACTIVATION IN NEONATAL RAT CARDIOMYOCYTE UPON TREATMENT WITH PRO-PROLIFERATIVE MICRORNAS

A. Experimental scheme to test activation of TEAD-dependent transcription. **B**.TEAD luciferase reporter analysis of CMs transfected with the indicated miRNA mimics. Transfection efficiency was standardized over a constitutively expressed Renilla luciferase reporter. Transfection of a constitutively activated YAP plasmid (pYAP5SA) was used as a

positive control. Data are mean ±SEM (n=5 independent experiments); *$P<0.05$, **$P<0.01$; one-way ANOVA **C.** Increase in YAP nuclear level by CM treatment with proproliferative miRNAs. Western blot of a representative experiment show the levels of nuclear and cytoplasmic YAP1 and phospho-YAP1 (P-YAP1) 72hr after transfection. PARP1 and GAPDH were used for loading control of the nuclear and cytoplasmic fractions respectively. **D**. Quantification of the increase in YAP nuclear level in CMs after miRNA mimics transfection. Results are shown as a ratio of YAP to nuclear PARP1. Data are mean ±SEM (n=5 independent experiments); *$P<0.05$, **$P<0.01$; one-way ANOVA.

To verify that detected TEAD activation corresponded to an increase of nuclear YAP, we investigated YAP1 levels in both cytoplasmic and nuclear fractions of cardiac cells treated with the 10 pro-proliferative microRNAs. In line with the previous evidence, we found that, in all cases, there was a correlation between cell treatment with the pro-proliferative microRNAs and the increase in YAP1 levels in the nucleus as shown in **Fig. 4-1C** and **4-1D.** Finally, to understand whether YAP activation was a crucial event for CM proliferation mediated by these miRNAs, we knocked down YAP1 using a specific siRNA (YAP1 knock down >85% is shown in **Fig. 4-2A**) and simultaneously treated CMs with the investigated miRNAs. We analyzed EdU incorporation level as a marker for cell proliferation and we found that YAP1 knockdown prevented the pro-proliferative effect of all the microRNAs under investigation, as shown in **Fig. 4-2B**. Representative images are shown in **Fig. 4-2C**.

From these results, we conclude that the increase in nuclear YAP activation is a common key event, which mediates CM proliferation by the ten microRNAs under investigation.

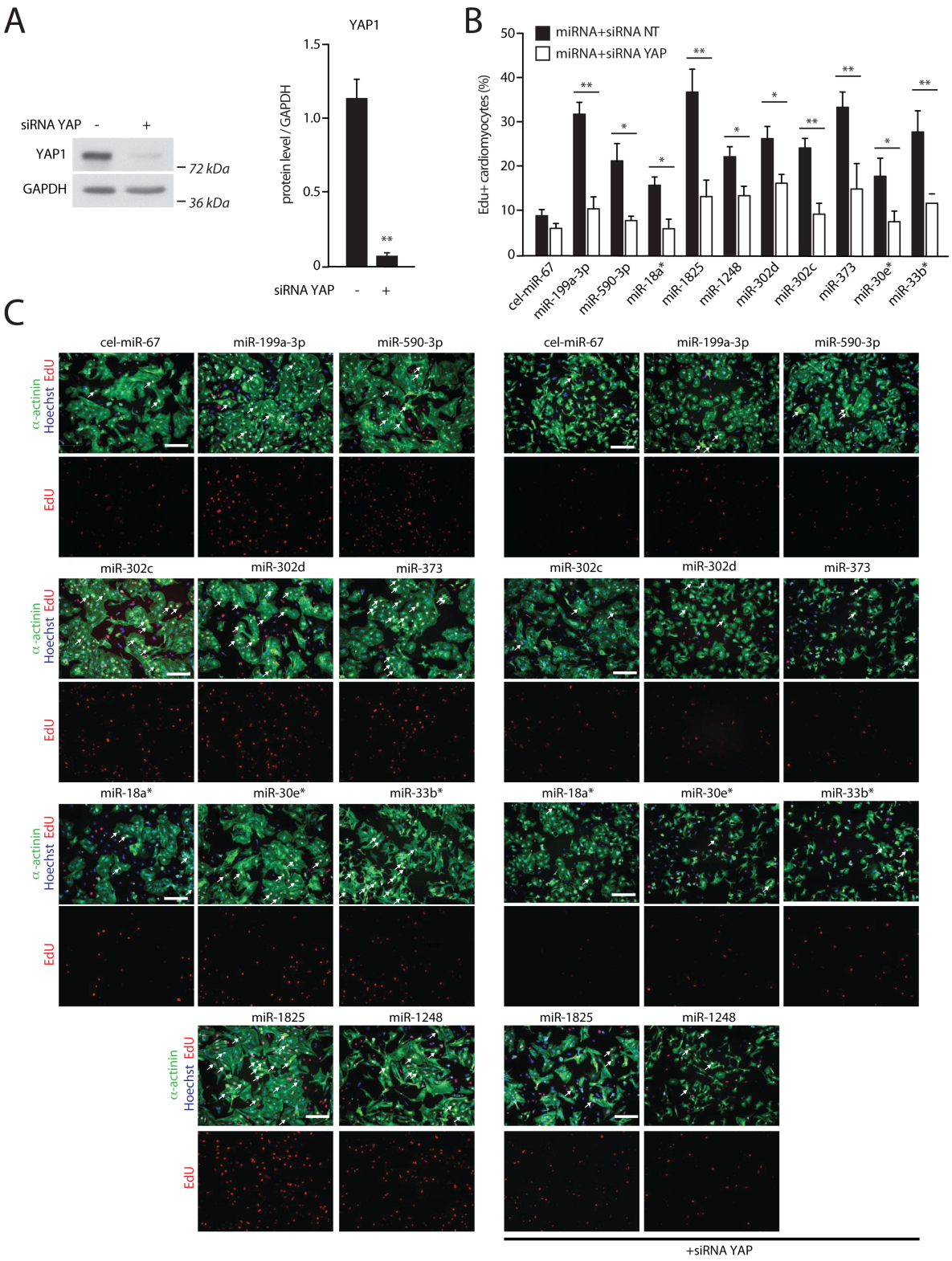

FIGURE 4-2. YAP IS CRUCIAL TO SUSTAIN CARDIOMYOCYTE PRO-PROLIFERATIVE EFFECT EXERTED BY THE MICRORNAS UNDER INVESTIGATION

A. Efficacy of YAP1 downregulation using a specific siRNA. On the left side, representative western blotting. On the right side, quantification of 3 independent experiments. Data are mean ±SEM; ***P<0.01*; t-test **B.** Induction of CM proliferation by miRNA mimics is blunted by YAP knockdown. CMs were transfected with pro-proliferative microRNAs alone or in combination with an anti-YAP siRNA. The graph shows the percentage of sarcomeric α-actinin-positive cells that incorporated EdU. Data are mean ±SEM (n=4 independent experiments); **P<0.05,* ***P<0.01*; one-way ANOVA **C.** Representative images of CMs treated with the indicated miRNAs with out without a siRNA against YAP. CMs are

visualized in green as sarcomere α-actinin-positive cells. Hoechst staining was used for nuclei (blue). EdU incorporation is visualized in red (bottom panels). The arrows indicate example of proliferating CMs. Scale bar: 100 μM.

4.2. Common regulatory pathways mediate the activity of pro-proliferative miRNAs

Next, to understand the mechanisms used by the microRNAs of interest to obtain YAP activation, we first analyzed the transcriptional feature of neonatal rat cardiomyocytes treated with six of these microRNAs, namely human miR-590-3p, miR-199a-3p, miR-1825, miR-302d, miR-373 and miR-33b*; C. elegans cel-miR-67 was used as a negative control. RNA from miRNA-transfected cardiac myocytes was isolated and used for transcriptomic RNA sequencing followed by computational analysis (**Fig. 4-4A** and **-4B)**. Cluster analysis was performed on the obtained results, showing that miR-302d and miR-373-3p had similar effects on target gene regulation (as shown in **Fig. 4-4C**), as predictable from their common seed sequence (**Fig. 4-3)**.

MiRbase accession	MiRbase ID	sequence	Genome context
MIMAT0000232	hsa-miR-199a-3p	5′ ACAGUAGUCUGCACAUUGGUUA 3′	chr1: 172144554-172144614 [-]
MIMAT0004801	hsa-miR-590-3p	5′ UAAUUUUAUGUAUAAGCUAGU 3′	chr7: 74191213-74191273 [+]
MIMAT0006765	hsa-miR-1825	5′ UCCAGUGCCCUCCUCUCC 3′	chr20: 29186400-29186451 [+]
MIMAT0005900	hsa-miR-1248	5′ ACCUUCUUGUAUAAGCACUGUGCUAAA 3′	chr3: 186504461-186504566 [+]
MIMAT0002891	hsa-miR-18a-3p	5′ ACUGCCCUAAGUGCUCCUUCUGG 3′	chr13: 92003005-92003075 [+]
MIMAT0004811	hsa-miR-33b-3p	5′ CAGUGCCUCGGCAGUGCAGCCC 3′	chr17: 17813858-17813916 [-]
MIMAT0000693	hsa-miR-30e-3p	5′ CUUUCAGUCGGAUGUUUACAGC 3′	chr1: 41220027-41220118 [+]
MIMAT0000718	hsa-miR-302d-3p	5′ UAAGUGCUUCCAUGUUUGAGUGU 3′	chr4: 112648006-112648066 [-]
MIMAT0000717	hsa-miR-302c-3p	5′ UAAGUGCUUCCAUGUUUCAGU 3′	chr4: 112648368-112648423 [-]
MIMAT0000726	hsa-miR-373-3p	5′ GAAGUGCUUCGAUUUUGGGGUGU 3′	chr19: 53788710-53788770 [+]

FIGURE 4.3. MIRNA SEQUENCE AND CHROMOSOMAL LOCALIZATION

Sequence, miRBase accession number, miRBase ID and chromosomal localization of the human miRNAs under investigation. The miRNA seed sequence is in red.

Fig. 4-4A schematically shows the number of genes from NCBI database that were differentially regulated by the miRNAs: a total of 3734 genes were downregulated by at least 1 miRNA (at 1.0 RPKM cutoff and 1.30 fold-change cutoff), while 3326 were upregulated. Next, we performed a pathway analysis using IPA software (Build version: 389077M, Content version: 27821452, 08/08/2016), considering all the tested miRNAs as replicates of the common CM proliferative phenotype. The results showed that the network with the higher score (34) was the cell cycle-cancer and cardiovascular system development and function network, followed by the embryonic - organismal-tissue development network with a score of 22.

Given the involvement of the YAP-Hippo signaling pathway on the regulation of cardiomyocyte

proliferation during embryonic development (Xiao et al., 2016), we focused our attention on genes linked to this pathway. To this aim, we generated an update catalogue of the genes known to have a role in the regulation of YAP-Hippo signaling pathway (203 genes). For each gene we reported fold changes in gene expression for each miRNA treatment along the bioinformatics prediction of miRNA targeting (TargetScan software) (**Table 1)**.

A summary of all this information is reported in **Fig. 4-4D**; the level of each transcripts is indicated by its fold difference over control (green: downregulated genes; red: upregulated genes). Interestingly, five out of six microRNAs upregulated TEAD2 levels, the final effector of the Hippo pathway. Moreover, all the selected microRNAs targeted either LATS1/2 or STK38L kinases, which blunt CM proliferation via YAP1 inactivation (Hergovich, 2016).

Together, these bioinformatics findings on RNA sequencing data indicate that there is a signature of Hippo pathway involvement upon treatment of cardiomyocytes with the six analyzed pro-proliferative microRNAs.

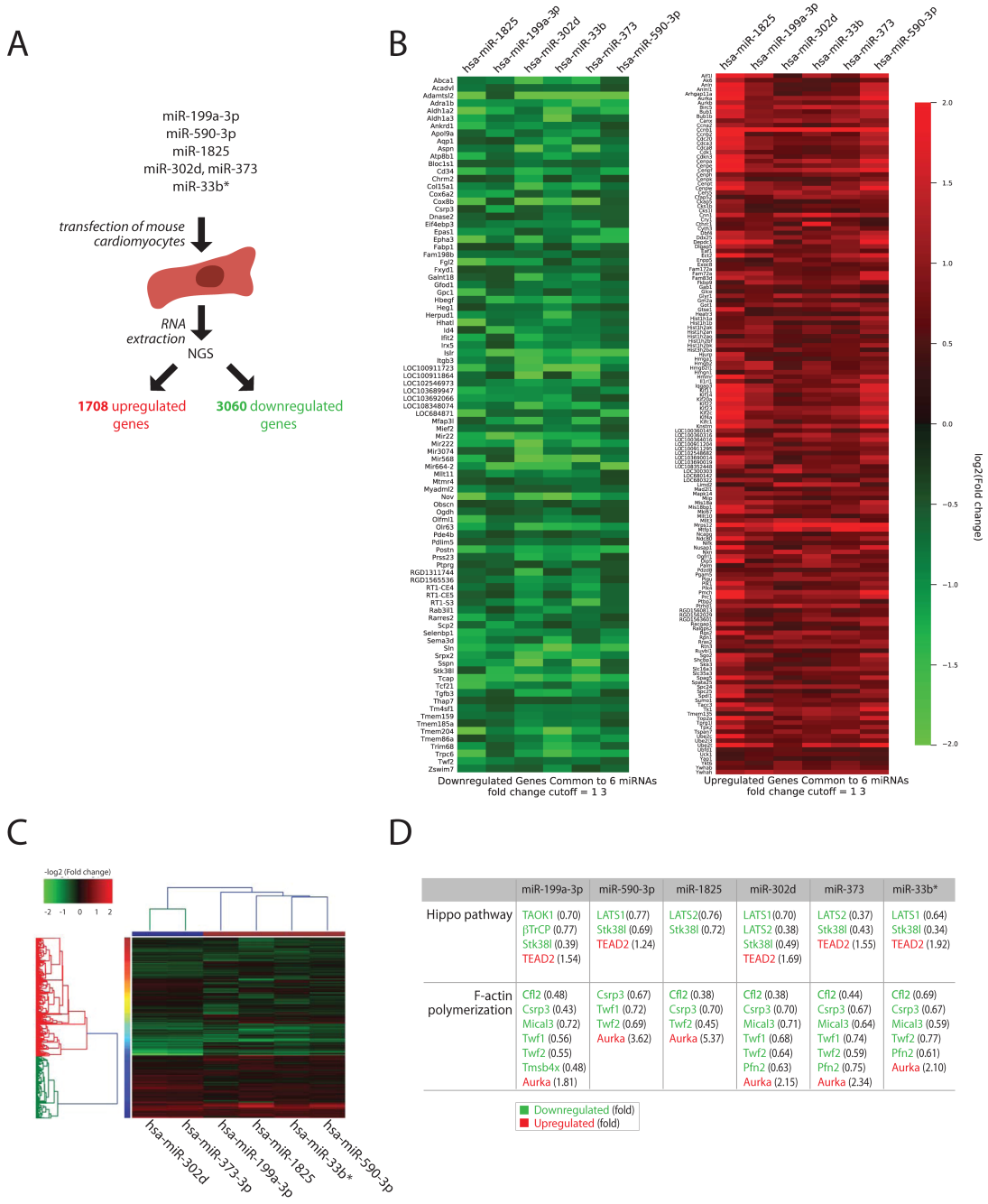

	miR-199a-3p	miR-590-3p	miR-1825	miR-302d	miR-373	miR-33b*
Hippo pathway	TAOK1 (0.70) βTrCP (0.77) Stk38l (0.39) TEAD2 (1.54)	LATS1(0.77) Stk38l (0.69) TEAD2 (1.24)	LATS2(0.76) Stk38l (0.72)	LATS1(0.70) LATS2 (0.38) Stk38l (0.49) TEAD2 (1.69)	LATS2 (0.37) Stk38l (0.43) TEAD2 (1.55)	LATS1 (0.64) Stk38l (0.34) TEAD2 (1.92)
F-actin polymerization	Cfl2 (0.48) Csrp3 (0.43) Mical3 (0.72) Twf1 (0.56) Twf2 (0.55) Tmsb4x (0.48) Aurka (1.81)	Csrp3 (0.67) Twf1 (0.72) Twf2 (0.69) Aurka (3.62)	Cfl2 (0.38) Csrp3 (0.70) Twf2 (0.45) Aurka (5.37)	Cfl2 (0.38) Csrp3 (0.70) Mical3 (0.71) Twf1 (0.68) Twf2 (0.64) Pfn2 (0.63) Aurka (2.15)	Cfl2 (0.44) Csrp3 (0.67) Mical3 (0.64) Twf1 (0.74) Twf2 (0.59) Pfn2 (0.75) Aurka (2.34)	Cfl2 (0.69) Csrp3 (0.67) Mical3 (0.59) Twf2 (0.77) Pfn2 (0.61) Aurka (2.10)

Downregulated (fold)
Upregulated (fold)

FIGURE 4-4. EXPRESSION PROFILE OF GENES IN NEONATAL CMS UPON TREATMENT WITH PRO-PROLIFERATIVE MIRNAS

Total neonatal rat CM RNAs were deep-sequenced and quantified using standard protocols. The gene expression profile mapped on Rattus norvegicus reference genome (GCF_000001895.5 Rnor 6.0.82) was then normalized by RPKM. Fold-changes in gene expression upon transfection of pro-proliferating miRNA were taken with respect to cel-miR-67 (negative control). **A.** Schematic representation of RNAseq experiment. Neonatal rat CMs were reverse transfected with the indicated miRNAs and RNA was analyzed by Next Generation Sequencing (NGS). **B.** Heatmap showing differentially expressed genes in response to all 6 miRNAs; downregulated genes are in green, upregulated genes in red. **C.** Cluster analysis was performed on the basis of log2 (fold-change over control, cel-miR-67). The dendrogram shows the arrangement upon hierarchically clustering using an average linkage criterion with a Euclidean distance as a metric. **D**. Common regulatory pathways mediate activity of miRNAs inducing CM proliferation, among which Hippo and F-acting polymerization pathways. Upregulated genes are in red, downregulated genes in green**.**

4.3. Hippo pathway downregulation activates CM proliferation

Interestingly, miR-199a-3p, one of the most effective miRNAs in boosting CM proliferation, lead to the downregulation of three mRNA targets indirectly involved in the Hippo pathway, namely those coding for the TAO kinase1 (TAOK1), the E3 ubiquitin-ligase β-transducing repeat containing protein (β-TrCP) and the serine/threonine kinase, STK38L. TAOK1/3 was described to activate MST1/2 via phosphorylation (Boggiano et al., 2011), as well as LATS1/2 (Plouffe et al., 2016; Poon et al., 2011); β-TrCP mediates YAP ubiquitination and consequently leads to its degradation (Zhao et al., 2010). STK38L, a kinase belonging to the same AGC serine/threonine kinase family as LATS1/2, directly inactivates YAP via phosphorylation (Hergovich, Stegert et al. 2006) (**Fig. 4-5A**). In order to validate these targets and the direct binding of their 3'UTR by the studied miRNAs, we cloned the 3'UTRs of TAOK1, β-TrCP and STK38L mRNAs downstream the firefly luciferase gene and transfected these plasmids into HeLa cells treated with the 10 pro-proproliferative miRNAs (**Fig. 4-5B**). Co-transfection of a Renilla luciferase plasmid served as a control of transfection, while the cloning plasmid (psiCheck2.1) was used for normalization. Analysis of the luciferase activity 48 hours after transfection revealed that only TAOK1 and β-TrCP, but not STK38L, were 3'UTR-direct targets of miR-199a-3p (**Figs. 4-5C, -5D** and **-5E** respectively). The mutated counterparts were no longer able to bind miR-199a-3p as shown in **Fig. 4-5F** and **-5G**. In the case of STK38L, we found a downregulation of its transcript upon miR-199a-3p, miR-302d and miR-373 treatment, possibly due either to an indirect effect or to the binding of miRNAs outside the 3'UTR (western blotting analysis and protein quantification are reported in **4-5M** and **-5N**). To complete this functional characterization, the downregulation of both TAOK1 and the β-TrCP by miR-199a-3p transfection was detected both at protein and mRNA levels (**Fig. 4-5H, -5I** and **-5J** show representative western blots and quantifications**;** gene expression levels are reported in **Fig. 4-5K, -5L**).

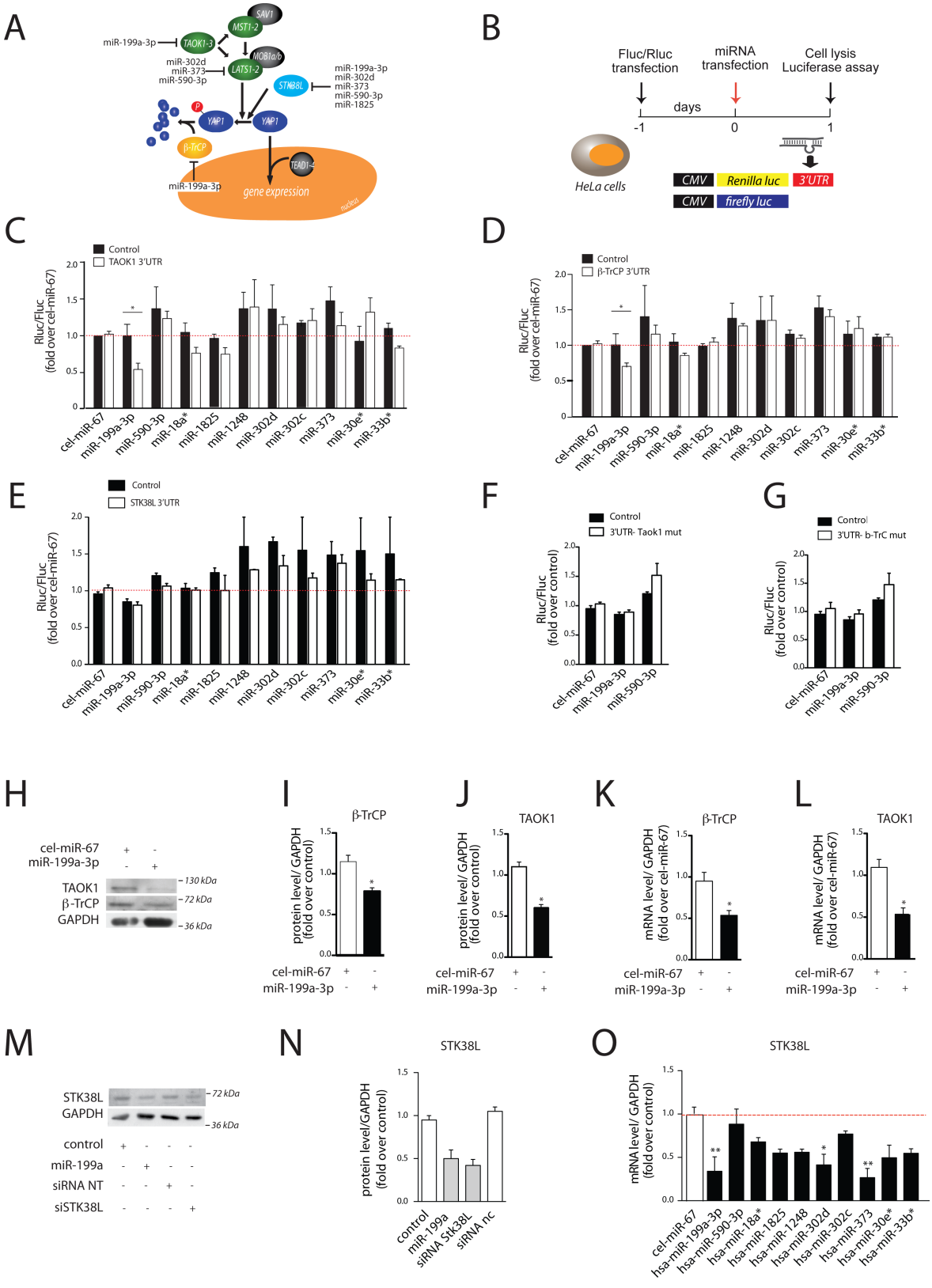

FIGURE 4-5. MECHANISM FOR YAP ACTIVATION BY MIR-199A-3P AND OTHER MIRNAS

A. Schematic representation of the Hippo pathway, with the indication of the predicted target proteins according the TargetScan software. **B**. Experimental flow chart of 3'UTR luciferase assays. Fluc and Rluc: firefly and Renilla luciferase genes, respectively. 3'UTR luciferase assays with the 10 pro-proliferative miRNAs. **C**. TAOK1 and β−TrCP (**D**) 3'-UTRs are direct targets of miR-199a-3p, while STK38L is not (**E**). **F-G** Mutated 3'-UTR luciferase assay of both TAOK1 (**F**) and β−TrCP (**G**). All the Renilla (Rluc) values were normalized over firefly luciferase (Fluc) values. Control refers to transfection of a firefly luciferase gene with no 3'UTR. **H-J**. Representative western blots showing downregulation of TAOK1 and β−TrCP proteins in cells treated with miR-199a-3p mimic (**H**) and the relative

quantifications (**I-J). K-L.** Real-time RT-PCR quantification of TAOK1 and β−TrCP mRNAs in CMs treated with miR-199a-3p mimic. Data are mean ±SEM (n=3 independent experiments); **P<0.05*; t-test. **M.** Western blot showing STK38L levels upon treatment with miR-199a-3p. A siRNA targeting STK38L was used as a negative control. **N.** Protein quantification of western blot shown in panel M. Data are mean ±SEM (n=3 independent experiments); **P<0.05*; t-test. **O.** RT-PCR quantification of STK38L upon pro-proliferative miRNA transfection. Data are mean ±SEM (n=3 independent experiments); **P<0.05, **P<0.01*; one-way ANOVA.

Next we investigated whether the specific silencing of TAOK1, β-TrCP and STK38L had a direct impact on CM proliferation. We co-transfected neonatal CMs with a TEAD luciferase plasmid and with siRNAs targeting TAOK1, β-TrCP or STK38L (**Fig.4-6C**). SiRNA downregulation of each of these targets was evaluated at the protein level; β-TrCP expression was silenced >70% **(Fig. 4-6A)**; TAOK1 expression >90% (**Fig. 4-6B)**; and STK38L >65% (**Fig. 4-5N)**, compared to control. Silencing of these proteins resulted in the transcriptional response of the TEAD-responsive promoter, as shown in **Fig. 4-6C-6D**.

Then, we analysed the effect of TAOK1, STK38L and β-TrCP downregulation on CM proliferation. Of notice, siRNAs against both TAOK1 and β-TrCP significantly enhanced EdU incorporation and this effect was abolished when these siRNAs were combined with the specific silencing of YAP; in contrast, the downregulation of STK38l had no impact on cell proliferation (**Fig**. **4-6E-F)**.

Taken together, these results demonstrate that the mechanism exploited by miR-199a-3p to induce CM proliferation involves the direct targeting of two proteins, TAOK1 and β-TrCP, which regulate YAP activation via different mechanisms. Further analysis, such as rescue experiments in which CM proliferation is evaluated after miR-199a-3p treatment in presence of TAOK1 and β-TrCP overexpression, will clarify the relevance of these miR-199a-3p targets among the others in terms of CM proliferation.

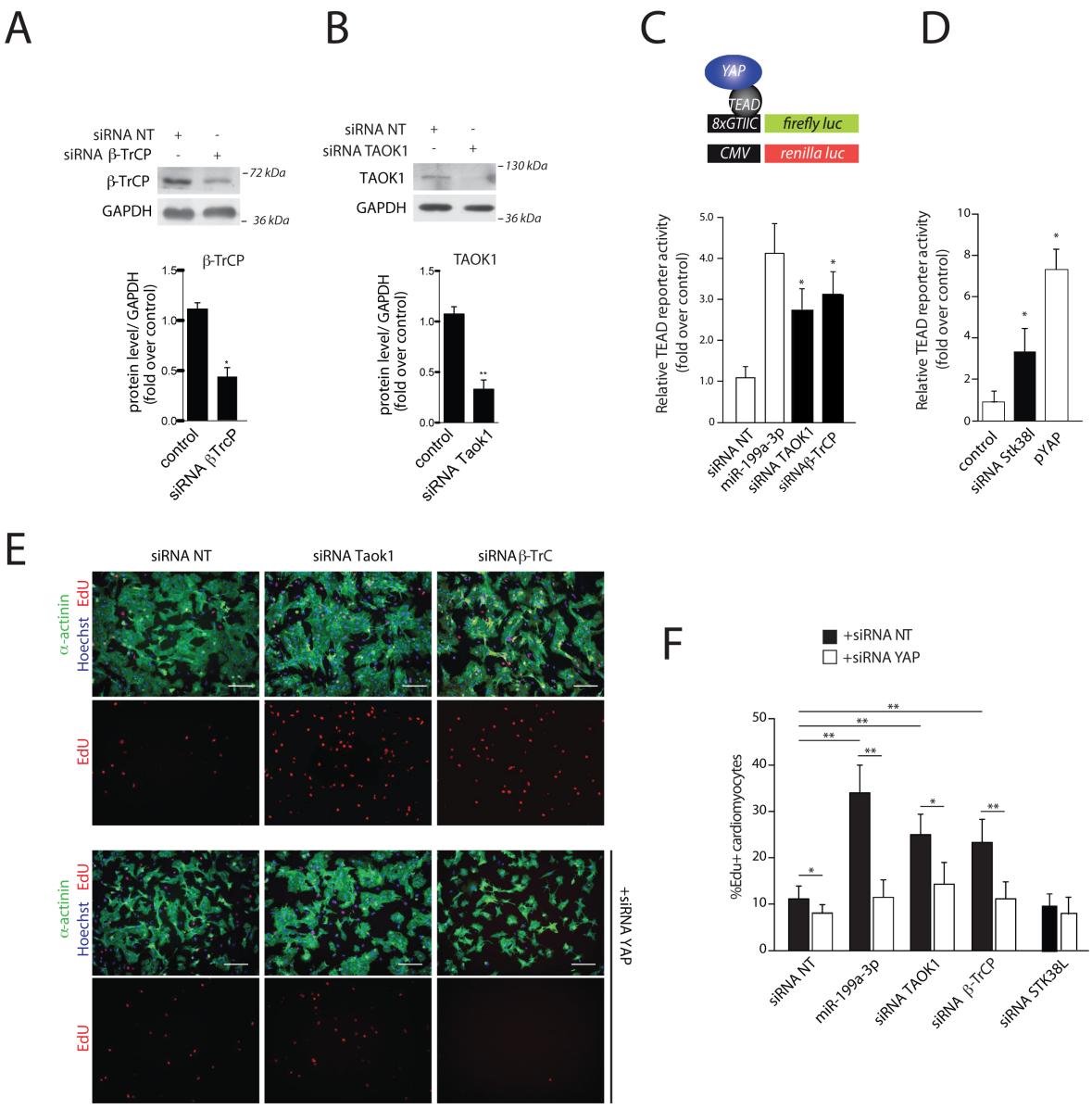

FIGURE 4-6. MECHANISM FOR YAP ACTIVATION BY MIR-199A-3P.

A-B. Representative western blots of β−TrCP and TAOK1 after CM treatment withe the respective siRNAs. Data are mean ±SEM (n=3 independent experiments); *$P<0.05$, **$P<0.01$; t-test. **C-D.** Downregulation of TAOK1, β−TrCP and STK38L stimulate TEAD transcriptional activity. CMs were transfected with siRNAs against TAOK1, β-TrCP or STK38L in combination with a TEAD luciferase reporter. The results were normalized to those obtained by a constitutively expressed Renilla luciferase plasmid. Data were normalized over a non-targeting (NT) siRNA. Data are mean ±SEM (n=5 independent experiments); *$P<0.05$; one-way ANOVA. **E**. Representative images of CMs stained for sarcomeric a-actinin, EdU incorporation and Hoechst (nuclei) after treatment with siRNAs against TAOk1 and β−TrCP transcripts with a siRNA against YAP or a siRNA NT. Scale bar: 100 μm **F.** Percentage of sarcomeric α-actinin-positive cells that had incorporated EdU were analyzed 72 hr after treatment with specific siRNAs in combination with an anti-YAP or a non targeting (NT) siRNA. Data are mean±SEM (n=4 independent experiments); *$P<0.05$, **$P<0.01$; one-way ANOVA.

4.4. Modulation of the actin cytoskeleton by Cofilin-2 regulates cardiomyocyte proliferation

Transfection of neonatal CMs with the selected microRNAs often resulted in relevant cellular morphological changes, including rounding of the cell surface, as shown in **Fig. 4-2C**. Consistent with this observation, our RNAseq study revealed that many differentially expressed genes were involved in actin cytoskeleton remodeling (a list of 79 genes known to be involved in the actin cytoskeleton remodeling is shown in **Table 2,** along with the fold changes upon each miRNAs transfection). **Fig. 6-4B** shows the genes differentially regulated upon miRNA treatment. Several of the downregulated genes encoded for proteins able to directly bind G-actin and prevent actin polymerization (Xue and Robinson, 2013). In particular, Cofilin2 was downregulated by 5 out of 6 investigated miRNAs; Twinfilin1 (Twf1) by 4 miRNAs and Twinfilin2 (Twf2) by all 6 miRNAs; Thymosin β4 (Tmsb4x) by one miRNA and Profilin2 (Pfn2) by 3 miRNAs. Moreover, 5 out of 6 miRNAs also dowregulated Csrp3, a LIM-only domain family protein previously described to be able to bind Cofilin2, enhancing its activity in F-actin depolymerization (Papalouka et al., 2009). Another downregulated target of 4 out of 6 miRNAs is Mical3, a member of the Mical family of proteins also involved in actin depolymerization (Fremont et al., 2017). Finally, Aurora A kinase (Aurka) a serine/threonine kinase playing a critical role during early mitotic stages and spindle formation, known to regulate actin cytoskeleton remodeling through Cofilin phosphorylation (Ritchey and Chakrabarti, 2014), was commonly upregulated by all the investigated miRNAs. **Fig. 4-7A** shows the actin-related proteins that were also predicted as miRNA direct targets according to the TargetScan software.

In particular, we noticed that the Cofilin2 transcript was downregulated by all the miRNAs under investigation, with the exception of miR-590-3p. Furthermore, Cofilin2 was the predicted target of 4 of these miRNAs (miR-199a-3p, miR-1825, miR-302d and miR-373; **Fig. 4-7A**). We demonstrated that all these 4 miRNAs were able to directly bind the Cofilin2 3'UTR in UTR-luciferase assays (**Fig. 4-7B**). Accordingly, from the quantification of Cofilin2 transcript levels in neonatal rat CMs upon miRNA-treatment, a significant downregulation of Cofilin2 transcript was experimentally detected in CMs treated with these 4 miRNAs, in addition to CMs also treated with miR-33b* (**Fig. 4-7C**). Downregulation of Cofilin2 by miR-33b* might be due to an indirect effect, or an effect mediated by the miRNA binding to Cofilin2 transcript outside the 3'UTR. Analysis of Cofilin 2 protein levels in miRNA-treated CMs provided consistent results showing downregulation of this factor after treatment with miR-199a-3p, miR-1825, miR-302d and miR-373 (**Fig. 4-7D**).

Collectively, these results indicate that proteins that regulate the actin cytoskeleton dynamics and, in particular, the inhibitor of F-actin polymerization by Cofilin2, are frequently targeted, either directly or indirectly, by miRNAs inducing CM proliferation.

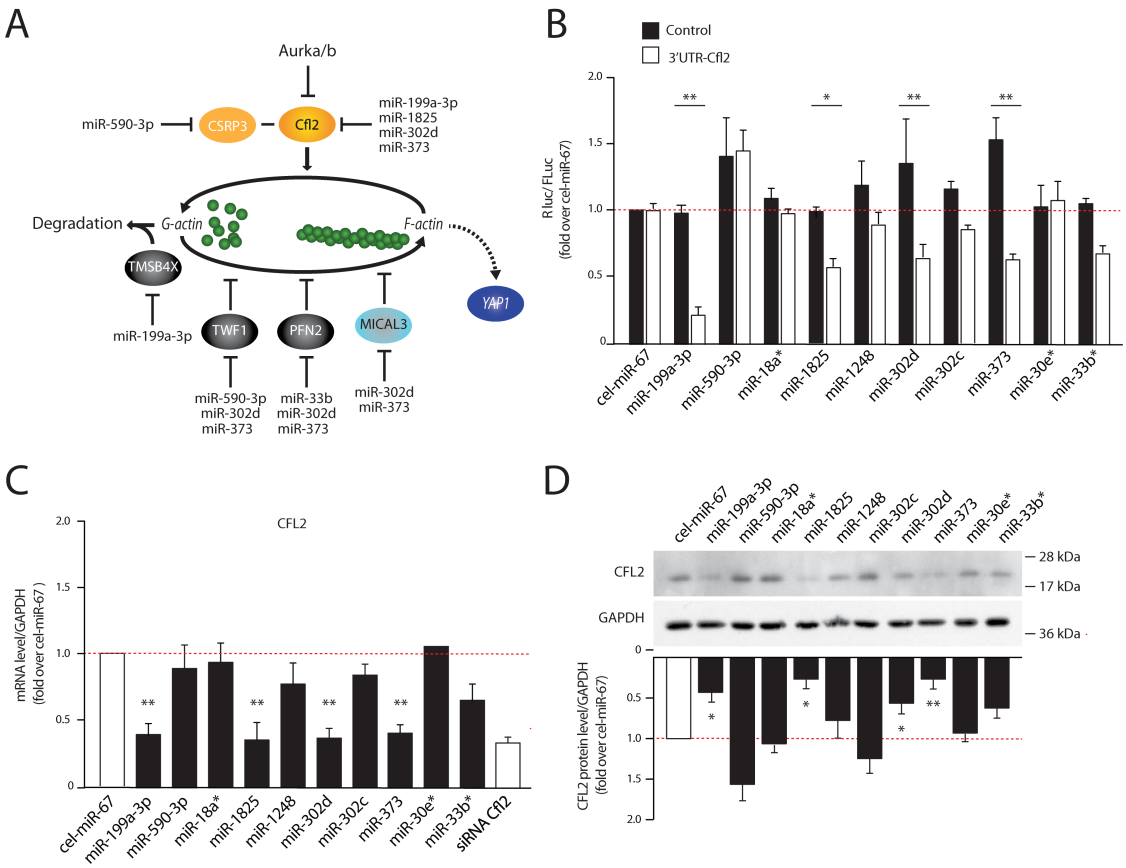

FIGURE 4-7. COFILIN2 IS A COMMON TARGET OF PRO-PROLIFERATIVE MIRNAS.

A. Schematic overview of proteins involved in actin cytoskeleton remodeling which are predicted targets of the pro-proliferative miRNAs **B.** Results of 3'UTR-luciferase assay to evaluate direct targeting of Cofilin2 (Cfl2) by the miRNAs under investigation. Experiments were performed as in Fig. 4-5C-E. Data are mean ±SEM (n=3 independent experiments): *$P<0.05$, **$P<0.01$; one-way ANOVA. **C.** Real-time RT-PCR quantification of the Cofilin2 expression in cardiac cells after miRNA-treatment. A siRNA against Cofilin2 (siCfl2) was used as a positive control. Data are mean±SEM (n=3 independent experiments); *$P<0.05$, **$P<0.01$; one-way ANOVA. **D.** Effect of miRNAs on Cofilin2 protein levels in neonatal rat CMs. Representative western blot shows downregulation of Cfl2 upon pro-proliferative miRNAs. In the lower panel: quantification of Cfl2 levels. Data are mean±SEM (n=3 independent experiments); *$P<0.05$, **$P<0.01$; one-way ANOVA. The red line indicates Cofilin2 levels in CMs treated with the control miRNA, cel-miR-67.

4.5. Remodeling of the actin cytoskeleton in proliferating cardiac myocytes

The actin-severing protein, Cofilin2, regulates actin cytoskeleton dynamics by inducing polymerized actin (F-actin) conversion back into its monomeric form (G-actin). We thus evaluated the ratio between G- and F-actin in cardiomyocytes treated with selected pro-proliferative miRNAs or with a siRNA against Cofilin2; in the presence of this siRNA we obtained a silencing of its target protein of >60% in CMs, which correlated with an upregulation of the levels of F-actin, as shown in **Fig. 4-8A**. The G/F ratio decreased in all the considered miRNA-treated CMs. Importantly, this ratio reached statistical significance for miR-199a-3p, miR-373, miR-302d and miR-33b* when compared to the negative control. The G/F ratio was also decreased in presence of the Cofilin2 silencing, as shown in **Fig. 4-8B** and **Fig. 4-8C** for representative blots and quantification respectively.

Next, we wanted to visualize actin cytoskeleton remodeling in cells treated with some of the pro-proliferative miRNAs or with the anti-Cofilin2 siRNA. For this purpose, we performed immunofluorescence staining using a fluorescein-tagged phalloidin to display F-actin (green). In **Fig. 4-8E,** in control CMs treated with the C. elegans miR-67, actin organization was detected in long threads throughout the cytoplasm, overlapping with those of the cardiac specific, α-actinin (red). In contrast, a round-shaped morphology ì, with actin fibers assembled in gross, round bundles at the cytosol periphery, characterized cells treated with miR-199a-3p and miR-373; these bundles of cortical actin were marked also in α-actinin-negative cells (fibroblasts). CMs treated with the two miRNAs also showed a decreased level of sarcomere organization. On the contrary, no evident morphological effect was detected in cells treated with miR-590-3p. Of notice, the same pattern of F-actin distribution also characterized cells treated with the siRNA against Cofilin2, as shown in **Fig. 4-8D**. Round-shaped CMs after miRNA and siRNA treatments were evaluated using the cell counter tool of the ImageJ software and the relative quantification are presented in **Fig. 4-8F**.

Together, these data are consistent with the conclusion that the pro-proliferative miR-199a-3p and miR-373 determine actin cytoskeleton remodeling and, consequently, CM morphology changes through the direct downregulation of Cofilin2.

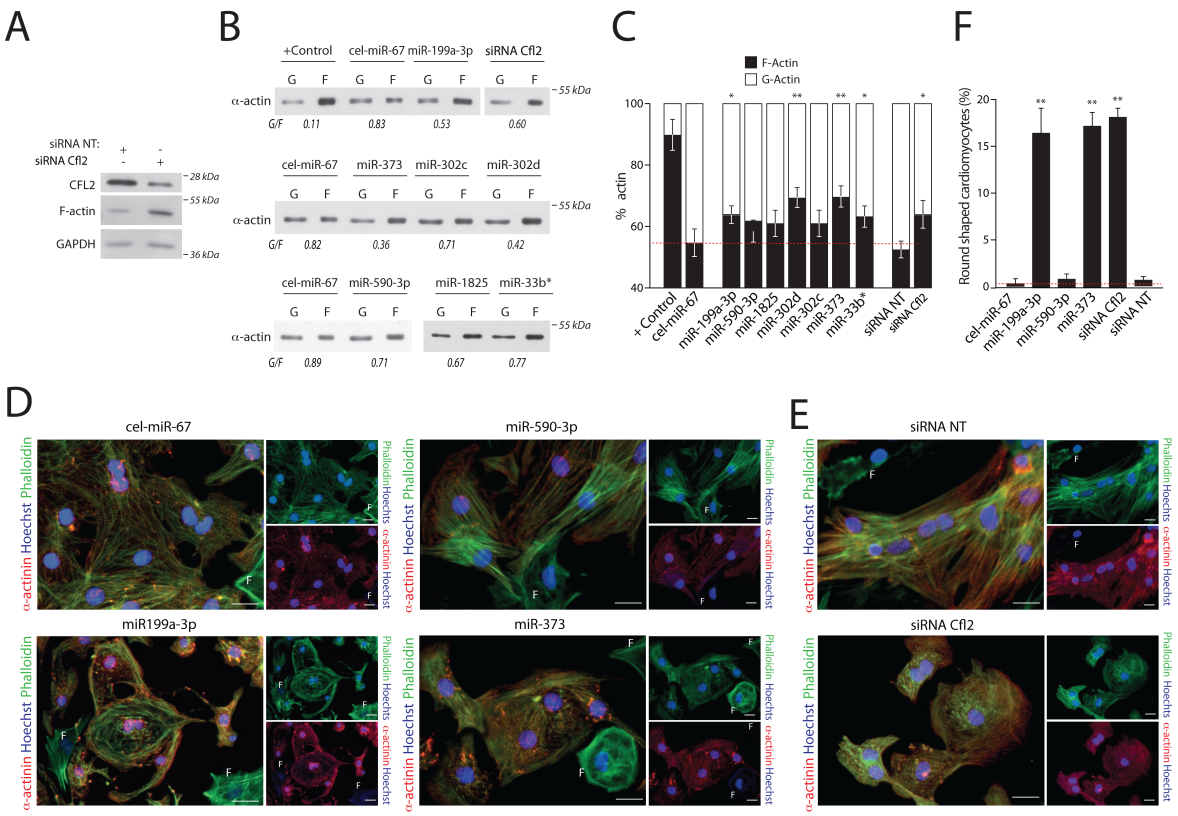

FIGURE 4-8. MIRNA TREATMENT OF CARDIOMYOCYTES INDUCES REMODELLING OF THE ACTIN CYTOSKELETON

A. Representative blots indicating that the downregulation of Cofilin2 changes the G/F actin ratio in favour of the actin polymerized form (F-actin). siRNA NT: non-targeting siRNA control **B.** Quantification of the G-actin/F-actin ratio in CMs upon pro-proliferative miRNAs or anti-Cofilin2 siRNA treatment. Representative western blots, using an anti-a-actin antibody, of supernatants (containing G-actin) and pellets (F-actin) obtained by ultracentrifugation of lysates from the treated CMs. The G/F ratio is shown at the bottom of each band pair. The positive (+) control was provided by the kit manufacturer's. **C.** Quantification of the G/F actin ratio (percentage) obtained as in panel B**.** Data are mean ±SEM (n=3 independent experiments); *$P<0.05$, **$P<0.01$; one-way ANOVA. **D.** Percentage of CMs with a rounded shape (as in the representative images in Panels E and F after treatment of CMs with miR-199a-3p or Cofilin 2 siRNA). Data are from the analysis of over 400 (n=4 independent experiments); shown are mean ±SEM; **$P<0.01$; one-way ANOVA. **E**. Immunofluorescence images showing remodelling of the actin cytoskeleton upon miRNA treatment. Fluorescent phalloidin staining (green) marks F-actin, CMs are visualized with an anti-a-actinin antibody (red), nuclei with Hoechst (blue). F indicates fibroblasts (a-actinin negative cells) **F**. Same as in panel E in CMs treated with an anti-Cofilin2 siRNA or with a nontargeting (NT) siRNA control. Scale bar: 65 μm; Scale bar: 33μm

To evaluate cell cycle progression in cells treated with miR-199a-3p, miR-590-3p, miR-373 or the anti-Cofilin2 siRNA, we performed a phospho-histone H3 staining, as shown in the representative pictures in **Fig. 4-9A** for the miRNAs and **Fig. 4-9B** for the siRNA. As shown in in **Fig. 4-9C**, all miRNA treatments induced 5-9% of the cells to move through the G2/M phase. Importantly, mitotic cardiomyocytes showed disruption of the sarcomeric architecture, as concluded from the diffused staining with α-actinin shown in **Fig. 4-9D**. Finally, different mitotic stages are shown in **Fig. 4-9E**; CMs are stained with α-actinin.

Together, these data show significant morphological changes in CM architecture during cell cycle progression, which are recapitulated by the absence of Cofilin2.

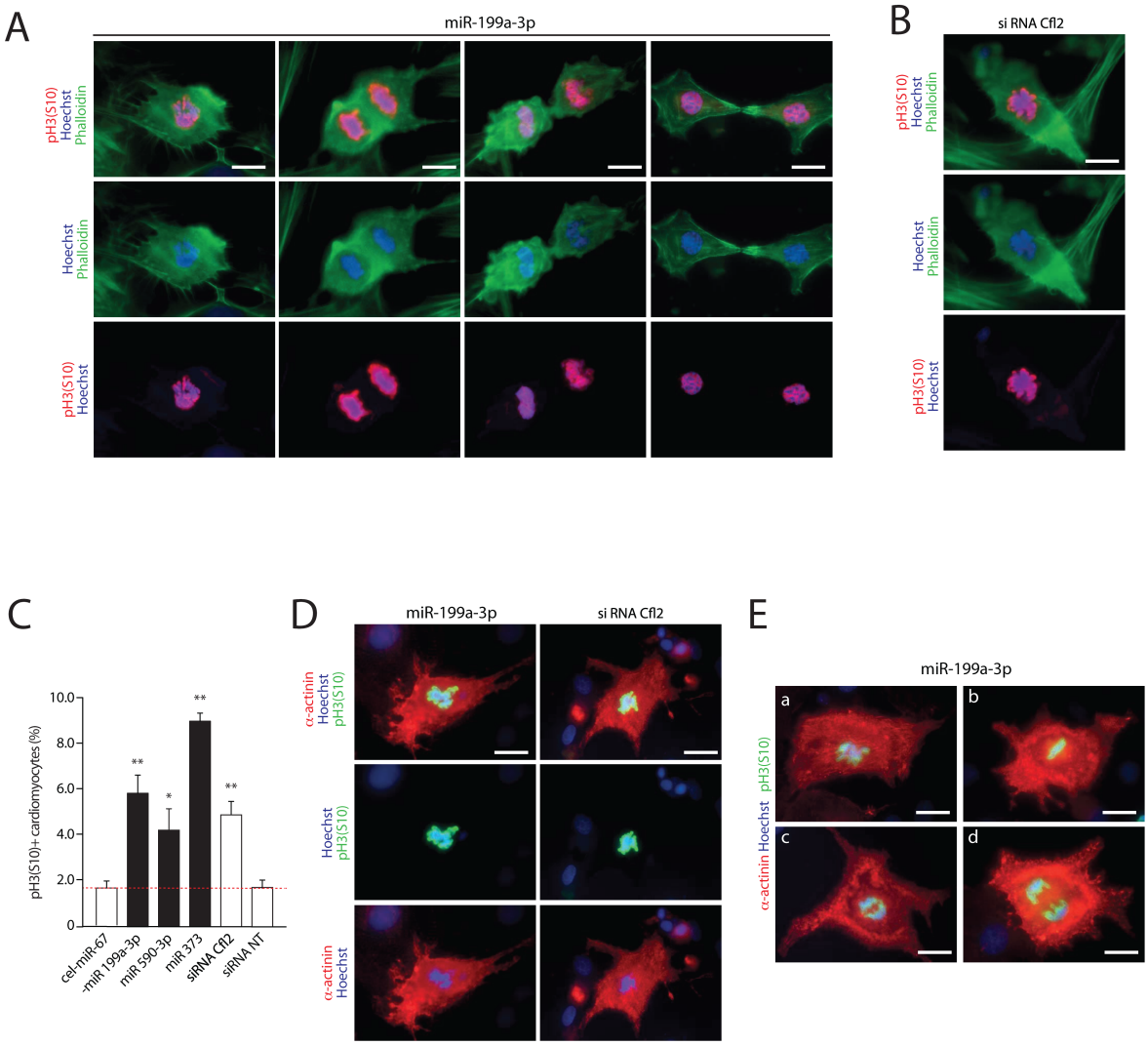

FIGURE 4-9. SARCOMERIC ARCHITECTURE WAS DISRUPTED IN PROLIFERATING CARDIOMYOCYTES UPON BOTH MIR-199A-3P AND COFILIN2 SIRNA TREATMENT

A-B. Representative images showing cells in G2/M phase treated with miR-199a-3p (**A**) or siRNA against Cofilin2 (**B**), showing nuclear staining of phospho-histone H3 (phospho-H3 (S10), red) and diffused cytosolic staining for α-actin (green). Nuclei are visualized with Hoechst 33342 (blue). **C.** Percentage of pH3 (S10)+, α-actinin+ cells (CMs) after treatment with the selected miRNAs or anti-Cofilin2 siRNA. Cel-miR-67 and a non-targeting (NT) siRNA served as negative controls for miRNA and siRNA respectively. Data results from the evaluation of over 400 CMs from four different experiments; shown are mean±SEM;***P<0.01, *P<0.01* one-way ANOVA **D.** Representative images of G2/M cardiomyocytes (defined as in **C**), showing nuclear positivity for phospho-histone H3 (pH3(S10), green) and disruption of the sarcomeric architecture, as suggested by the diffused α-actinin staining (red). Nuclei are counterstained with Hoechst 33342 (blue). **E.** Mitotic CMs in subsequent phases of mitosis (from a to d). Staining corresponds to the one in **D.**

4.6. Downregulation of Cofilin2 activates cardiomyocyte proliferation through YAP activation

We wondered whether cardiac cell proliferation mediated by Cofilin2 inhibition and actin cytoskeleton rearrangements might require YAP activation. In accordance with this possibility, we found that, in CMs, silencing of Cofilin2 mediated by RNAi determined activation of the TEAD-luciferase reporter as shown in **Fig. 4-10A**. In line, cardiomyocyte treatment with anti-Cofilin2 siRNA resulted in a marked upregulation of the transcript levels of two well-established YAP-responsive genes, CTGF and CyR61 (Zhao et al., 2008) as shown in **Fig. 4-10B**.

Moreover, co-transfection of CMs with a siRNA against YAP abolished the pro-proliferative effect exerted by Cofilin2 silencing, similar to the inhibitory effect observed in the presence of miR-199a-3p (**Fig. 4-10C**; representative IF images showing reduction EdU incorporation rate in **Fig. 4-10D**). The obtained data are indicative of a correlation between the actin polymerization process, which is increased by Cofilin2 inhibition, and YAP activation. To investigate this link, we suppressed actin polymerization using cytochalasin D and analysed the levels of both cytosolic and nuclear YAP1. CMs treated with this drug reduced the levels of nuclear YAP1 in a time-dependent manner, whereas increased the amounts of the cytoplasmic, phosphorylated YAP1 (representative western blots in **Fig. 4-10E** and quantification in **Fig. 4-10F**). This effect resulted in the drastic abolishment of the levels of the CTFG and CyR61 gene mRNAs (**Fig. 4-10G**).

Together, these results demonstrate that, in CMs, the extent of actin polymerization regulates YAP nuclear activity and, as a consequence, controls the levels of proliferating cells.

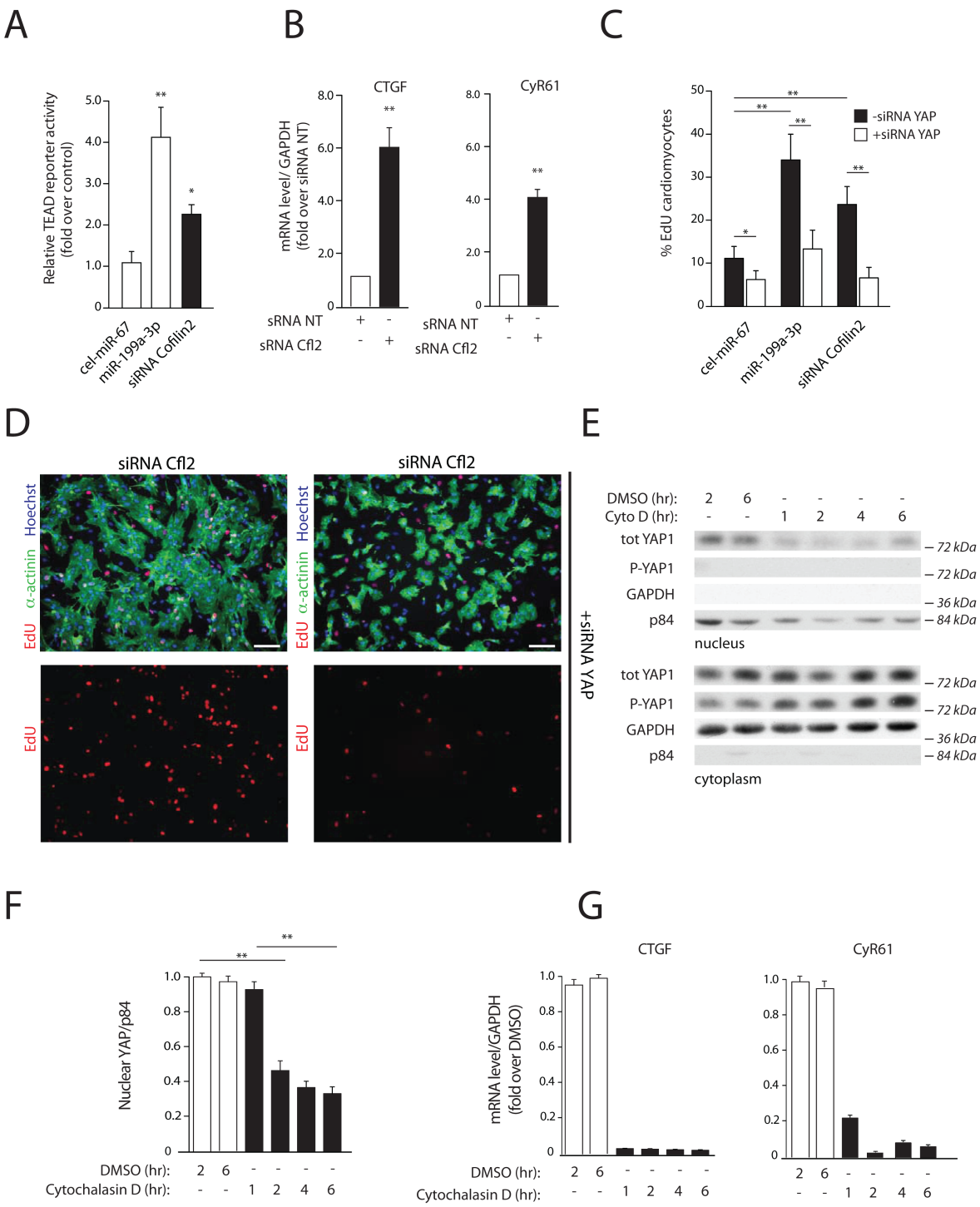

FIGURE 4-10. PERTURBATION OF THE ACTIN CYTOSKELETON ACTIVATES YAP NUCLEAR TRANSLOCATION AND ACTIVITY

A. Downregulation of Cofilin2 activates TEAD reporter activity. The graph reports the results of TEAD-firefly luciferase reporter analysis of CMs transfected with miR-199a-3p and Cofilin2 siRNA. Experiments were performed as in Fig.1C. Transfection efficiency was standardized over a Renilla luciferase reporter. Data are mean±SEM (n=4 independent experiments); *$P<0.05$, **$P<0.01$; one-way ANOVA **B.** Real-time RT-PCR analysis of the levels of the two TEAD responsive genes CTFG and CyR61 in CMs transfected with anti-Cofilin2 siRNA Data are mean±SEM (n=4 independent experiments); **$P<0.01$; t-test. **C**. Downregulation of Cofilin2 activates CM replication in a YAP-dependent manner. The graph shows the percentage of α-actinin-positive cells that have incorporated EdU after 72 h-treatment with anti-Cofilin2 siRNA or miR-199a-3p mimic alone or in combination with an anti-YAP siRNA. **D**. Representative pictures showing CMs incorporating EdU after treatment with an anti-Cofilin2 siRNA as in Panel B in the absence or presence of an anti-YAP siRNA. Scale bar: 100μm **E.** Treatment of CMs with cytochalasin D blocks nuclear translocation of YAP. Representative blots showing the levels of nuclear and cytoplasmic YAP1 and phospho-YAP1 (P-YAP1) in CMs treated

with cytochalasin D for the indicated time points. GAPDH and p84 were used for loading controls of cytoplasmic and nuclear fractions respectively. **F.** Quantification of YAP nuclear translocation in CMs treated with cyochalasin D. Data are mean±SEM (n=3 independent experiments); ***P<0.01*; one-way ANOVA. **G.** Treatment with cytochalasin D blocks transcription of YAP- responsive genes. The graph shows the levels of the CTFG and CyR61 mRNAs, measured by real-time RT-PCR, in CMs treated with cyochalasin D for the indicated time points. Data are mean±SEM (n=3 independent experiments).

4.7. High throughput screening of FDA-registered drugs identifies the neuroactive alkaloid harmine as a powerful inducer of cardiomyocyte proliferation

In addition to mIRNAs, we wondered whether some existing small chemical compounds might also be able to boost CM proliferation, alone or in combination with the pro-proliferative miRNAs miR-199a-3p and miR590-3p. For this aim, we selected a library of 780 FDA-registered compounds (Enzo Life Sciences), which was assembled by the vendor to maximize chemical diversity and thus cover the current full spectrum of pharmacologically active molecules (**Table 3**).

We performed a high-throughput, fluorescence-microscopy-based, screening in neonatal rat CMs to test these molecules for their ability to induce CM proliferation (**Fig. 4-11A**). Primary rat neonatal cardiac cells were prepared with a purity about 90% and reverse transfected with miR-199a-3p and miR-590-3p (or cel-miR-67 as a negative control). After 24 h of transfection, CMs were treated with the library of FDA-registered drugs. Each compound was administered at the final concentration of 10 μM (DMSO was used as a control). After 48 h from plating, cells were fixed and stained using the sarcomeric α-actinin to visualize CMs (green), Hoechst for nuclei (blue) and EdU incorporation (red nuclei) was evaluated as read-out of proliferation. The screening was performed in duplicate.

The most effective molecule in boosting cardiac proliferation was the alkaloid harmine, a component of several psychoactive plant extracts (**Fig 4- 11B, -11C** and **-11D).** Of notice, harmine treatment was able to promote CM proliferation by itself, in the absence of miRNA co-treatment, reaching even higher proliferation levels than miR-199a-3p and miR-590-3p. Simultaneous treatment of cells with harmine and miR-199a-3p did not have synergistic effects; on the contrary, harmine and miR-590-3p treatment determined over 50% of CMs to become EdU-positive (**Fig. 4-11E**). This is in line with the notion, ensuing from our previous experiments, that miR-199a-3p and miR-590-3p act through largely different pathways.

Representative images of CMs after harmine treatment are shown **in Fig 4-11G, -11H** and **-11I** demonstrating a significant increase of the total number of CMs as well as EdU incorporation in CM nuclei. The screening results (**Fig.11B-11D**) are presented using the Z-score, which shows the distance between the raw score and the population mean in units of standard deviation. When the raw score is below the mean, Z is negative, while it becomes

positive when the raw score is above the mean.

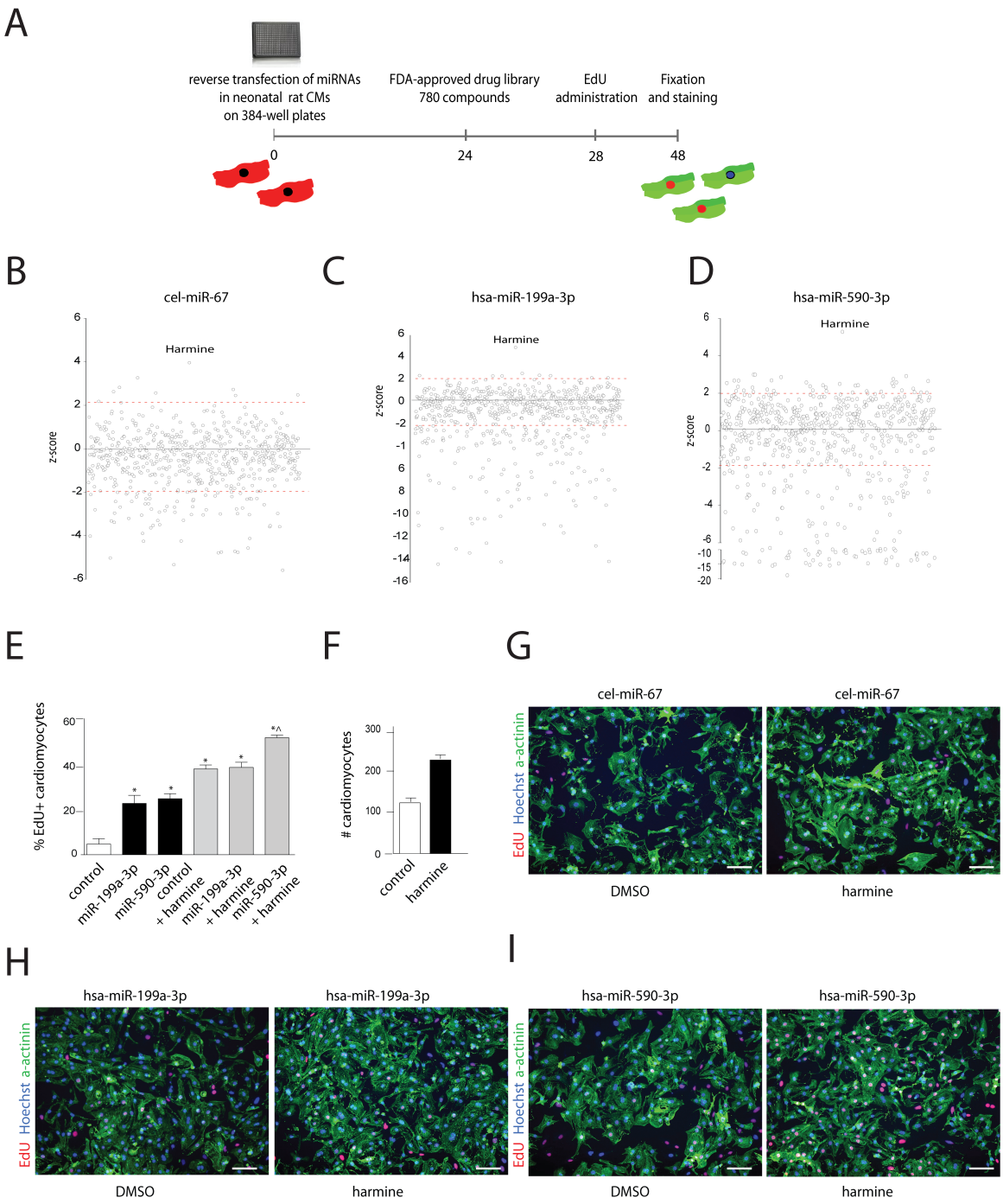

FIGURE 4-11. HIGH THROUGHPUT SCREENING OF SMALL MOLECULES IDENTIFIES THE NEUROACTIVE ALKALOID HARMINE AS A POWERFUL INDUCER OF CM PROLIFERATION

A. Schematic overview of the experimental procedure. A library of 780 FDA-registered compounds was screened in neonatal rat CMs for their ability to induce CM proliferation. Primary cardiac cells were reverse transfected with miR-199a-3p and miR-590-3p (or cel-miR-67 as a control). Twenty-four hour after transfection, CMs were treated with the library of FDA- registered drugs. **B-D**. Results of the screening are presented in the plot as Z-scores (x axis), in which the Z score represents the distance between the raw score and the population mean in units of the standard deviation. Z is negative when the raw score is below the mean, positive when above. Each dot represents a different drug. **E**. EdU quantification (%) of in neonatal rat CMs are reported in the graph**.** Data are mean ±SEM (n=3 independent experiments); *$P<0.05$; one-way ANOVA **F.** The Total number of CMs was increased after harmine treatment as shown

in the graph. **G-I.** Representative images showing CMs visualized using an anti-a-actinin antibody (green); Hoechst identifies nuclei (blue) and EdU detects DNA synthesis (red). Scale bar: 100μm.

4.8. Harmine treatment induces CM proliferation *in vivo*

Next, we investigated the pro-proliferative effect of harmine on cardiac myocytes *in vivo*. Harmine or physiological solution were administrated via intraperitoneal injections in neonatal CD1 mice (P1) for 12 days at the dosage of 1 mg/kg body weight. After 10 days, a single dose of EdU was injected and, 48 hours later, mice were sacrificed and hearts collected for further analyses (**Fig. 4-12A).** Immunofluorescence staining was performed on the total hearts, as shown in **Fig. 4-12B**: EdU incorporation was significant increase in CMs of mice treated with harmine in comparison with the control group (6.7 % EdU+CMs treated mice; 2.5% EdU+CMs controls; ***P<0.01*; t-test). Of note, the presence of increased septum and left ventricular posterior wall thickness, observed in the harmine-injected mice, was an indication of an increase in cardiac mass. Consistent with effect, there was a trend for an increase in cells positive for the proliferation marker phospho-histone 3 (**Fig. 4-12C**). Quantification of phospho-H3 positivity is shown in **Fig**. **12D**.

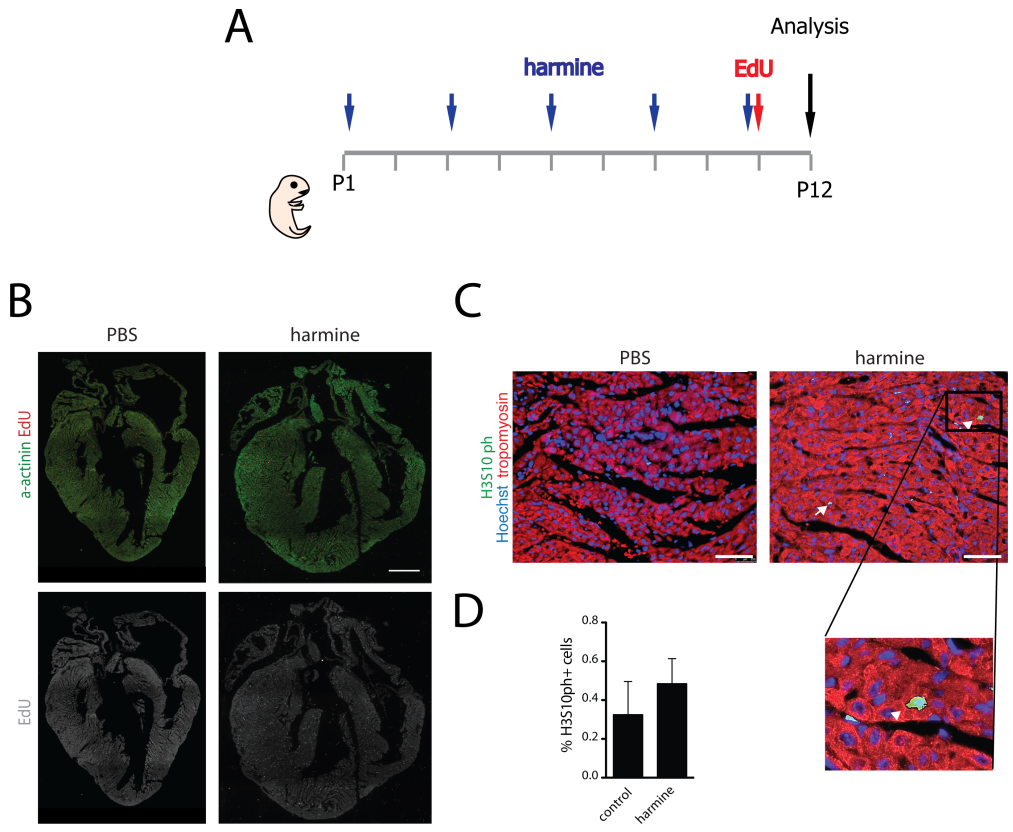

FIGURE 4-12. HARMINE TREATMENT INDUCES CM PROLIFERATION IN VIVO

A. Neonatal mice at postnatal day 1 (p1) were injected with harmine or PBS (control) for 5 times, followed by EdU injection at day 10. Hearts were collected after 12 days and stained for EdU. **B.** EdU and a-actinin staining of murine hearts injected with harmine or PBS. Scale bars, 1mm. **C.** Phospho-H3 (green), tropomyosin (red) positive cells in

paraffin sections of hearts treated with harmine or PBS identify proliferating cardiomyocytes. Relative quantification are shown in panel **D**. Data are mean ±SEM (n=6 mice: 3 controls and 3 treated mice). Hoechst marks nuclei (blue). Bar scale: 250 um

4.9 Harmine promotes heart regeneration in an *in vivo* model of myocardial infarction

Next, we wanted to assess the regenerative potential of harmine in an *in vivo* model of myocardial infarction (MI). For this purpose, PBS or harmine (10 mg/kg body weight) were injected in CD1 mice, which were then monitored for a two-month period (**Fig. 4-13A**). Importantly, since harmine is a neuroactive compound, the drug was administered starting from one week before the permanent ligation of left anterior descending coronary artery, in order for the animals to get exposed to it in advance of treatment.

Two months after MI, harmine-treated mice showed a marked improvement in cardiac contractile function compared to the control group, as shown by a higher left ventricular ejection fraction (LVEF) measured by echocardiography (**Fig. 4-13C**). Consistent with this finding, infarct size in the harmine-treated mice was smaller (1.8 fold reduction in comparison with the control mice, according to ImageJ software measurements), as shown in representative Sirius Red-stained cardiac cross-sections **(Fig. 4-13B)**. Furthermore, the left ventricles of these mice showed a trend toward reduced levels of dilatation as concluded from the echocardiographic analysis of left ventricle volume at the end of systole and diastole (**Figs. 4-13D, -13E)**.

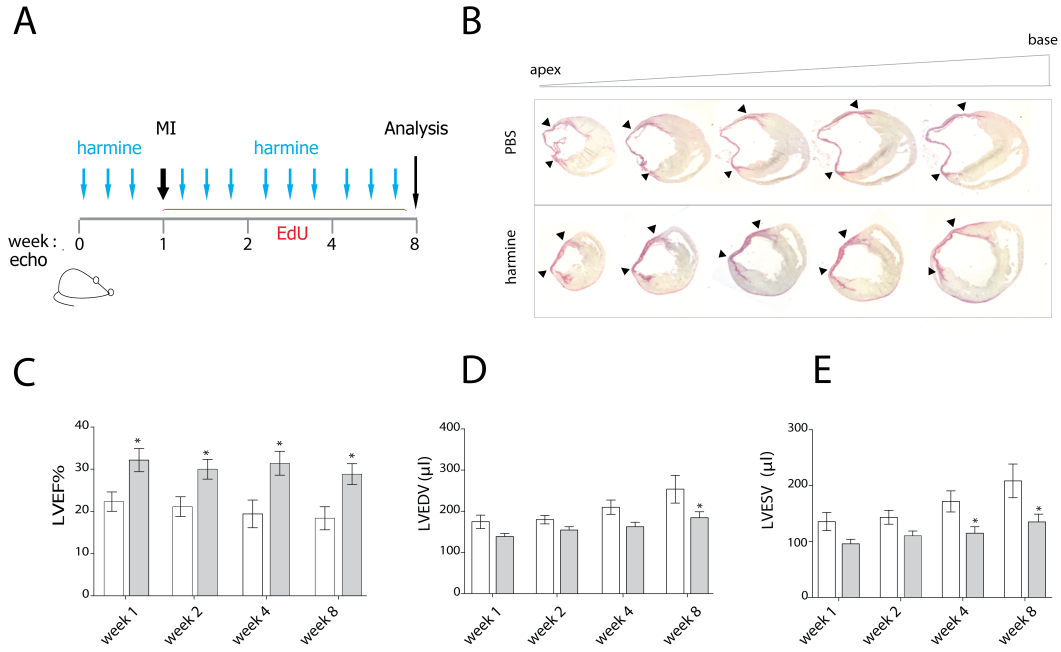

FIGURE 4-13. THE ALKALOIDE HARMINE PROMOTES HEART REGENERATION IN AN IN VIVO MODEL OF MYOCARDIAL INFARCTION

A. Schematic overview of the in vivo experiment. PBS or harmine (10 mg/kg body weight) were injected in CD1 mice, starting from one week before myocardial infarction (MI) and monitored for a period of two months. **B**. Representative

PicusSirius Red-stained cross-sections of hearts at 8 weeks after MI in control and harmine-treated hearts are shown, to evaluate infarct size and fibrotic scar compared to the control hearts. The arrowheads indicate the infarcted area. **C**. From echocardiographic data, % LVEF (left ventricular ejection fraction) was evaluated at 1, 2, 4 and 8 weeks after surgery. **D-E**. Left ventricle dilatation was evaluated by LVESV and LVEDV (left ventricle volume at the end of systole/ diastole) in uL at 0, 1, 2, 4 and 8 weeks.

4.10 Yap-dependent harmine proliferation in neonatal rat CMs

Since from the FDA-registered drug screening it emerged that miR-199a-3p and harmine treatment do not show additive effect on CM proliferation, we reasoned that these molecules might share the same molecular mechanism to promote CM cell cycling. We therefore wondered whether YAP activation was an essential element for harmine to induce CM proliferation. To test this hypothesis, we transfected neonatal rat CMs with the siRNA against YAP1 which was already described above to knockdown the YAP1 transcript. Twenty-four hours before fixing the cells, we treated CMs with harmine and, 4 hours later, with EdU. Analysis of EdU incorporation revealed that the absence of YAP1 in harmine-treated CMs significantly reduced their proliferative ability (**Fig. 4-14A** and **-B**), demonstrating the essential role of YAP in CM cytokinesis mediated by harmine. Representative images of proliferating cardiomyocytes upon harmine administration and their inhibition upon YAP downregulation are shown in **Fig. 4-14A.** Since harmine is a compound belonging to the alkaloid family, we next wondered whether other alkaloids of the same class, such as harmane and harmaline (**Fig. 4-14E**), share the same pro-proliferative capacity. We found that the most potent compound inducing cardiomyocyte proliferation was harmine, as shown in **Fig. 4-14C** and **-14D,** although a modest increase in cardiac myocyte proliferation was also observed in harmaline-treated cells. The effect of harmaline on CM proliferation can be explained by the similar molecular structure of these two drugs, which both have a methoxy and a methyl group that are not present in harmane (**Fig. 4-14E**). Finally, we also tested whether these members of the alkaloid family are also able to induce YAP activity, using a TEAD-luciferase reporter assay. The results obtained demonstrated that only harmine promotes YAP activation in CMs (**Fig. 4-14F**) reaching similar levels as the positive control pYAPS5A (the constitutive activated YAP).

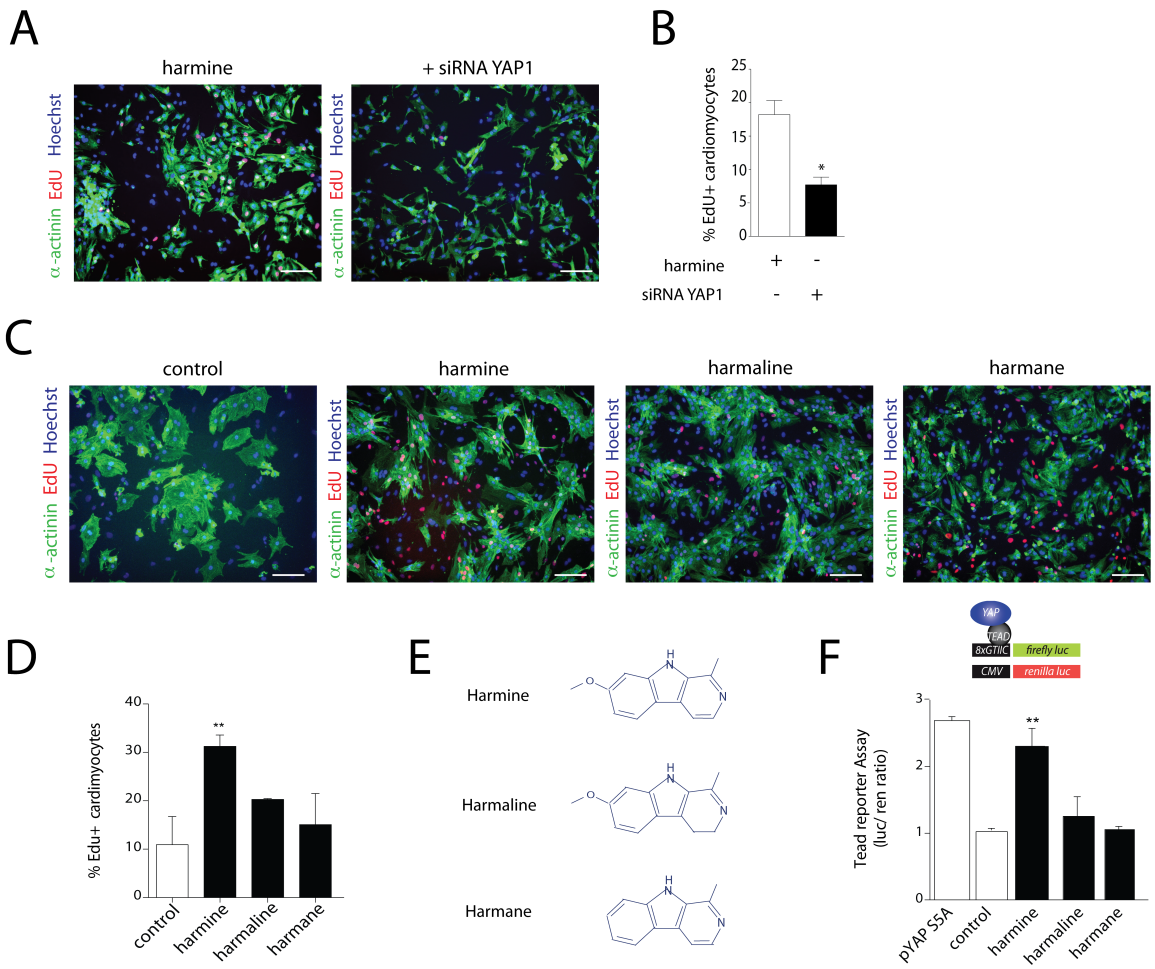

FIGURE 4-14. YAP-DEPENDENT HARMINE-INDUCED PROLIFERATION IN NEONATAL RAT CMS

A. Representative images showing proliferating cells transfected with siRNA anti-Yap1 or a non-targeting (NT) siRNA in the presence of harmine treatment. Cells were stained for a-actinin (green) to visualize CMs, EdU staining (red) to identify proliferating cells. Nuclei are visualized with Hoechst 33342 (blue). **B**. Quantifications of EdU+ CMs (%) are shown in the graph. Data are mean ±SEM (n=3 independent experiments); *$P<0.05$; t-test. Scale bar: 100µm **C-E.** Harmine analogues, harmaline and harmane (molecules structure in **E**), were tested for their ability to induce CM proliferation (**C**). Quantification of EdU+ CMs (%) are shown in the graph **D**. Data are mean ±SEM (n=3 independent experiments); **$P<0.01$; one-way ANOVA. **F.** CMs were treated with harmine analogues in combination with a TEAD luciferase reporter. Data were analyzed as in Fig. 4-6C. Data are mean ±SEM (n=5 independent experiments); **$P<0.01$; one-way ANOVA.

4.12 Dyrk1a inhibition and Yap activation mediate the pro-proliferative effect of harmine in cardiomyocytes

It is known that harmine is also able to inhibit the dual specificity tyrosine phosphorylation regulated kinase (Dyrk1a), while both harmane and harmaline specifically inhibit MAO-A (Herraiz, Gonzalez et al. 2010) (Herraiz and Chaparro 2006) .We therefore investigated whether the mechanism by which harmine induces CM proliferation might require Dyrk1a kinase inhibition.

To investigate the role of Dyrk1a in the harmine-mediated CM proliferation, we silenced Dyrk1a (>90% protein downregulation; **Fig. 4-15C**) using a specific siRNA against its mRNA and evaluated EdU incorporation in cardiac myocytes. The results obtained showed that suppression of Dyrk1a was sufficient to induce CM proliferation (**Fig. 4-15A**), as concluded by the increase in EdU incorporation observed upon Dyrk1a silencing (**Figs. 4-15A** and **-15B**). On the contrary, we found that adenovirus-mediated overexpression of Dyrk1a reduced proliferation by approximately 50% (**Fig. 4-15D** and **-15E**), correlating with a 50% decreased level of TEAD reporter activity (**Fig. 4-15I).** The overexpression of Dyrk1a mediated by adenovirus was confirmed by the evaluation of Dyrk1a protein level (2.5 fold changes over control) as shown in the **Fig. 4-14F**. An adenovirus carrying GFP was used as a control for these experiments**.** Of notice, TEAD activation levels, boosted by harmine treatment, was markedly reduced when cells were co-treated with harmine and Adeno-Dyrk1a (**Fig. 4-15I)**.

Next, we wanted to understand whether the increased proliferation observed after Dyrk1a silencing was mediated by YAP1. For this aim, we analyzed EdU incorporation in cardiac myocyctes after treatment with siRNA Dyrk1a in combination with a siRNA against YAP1. As shown in **Figs**.**4-15G** and **4-15H,** YAP1 inhibition reduced the CM proliferation induced by Dyrk1a silencing.

Collectively, these data show that Dyrk1a inhibition is responsible for the boost of proliferation triggered by harmine treatment in CMs.

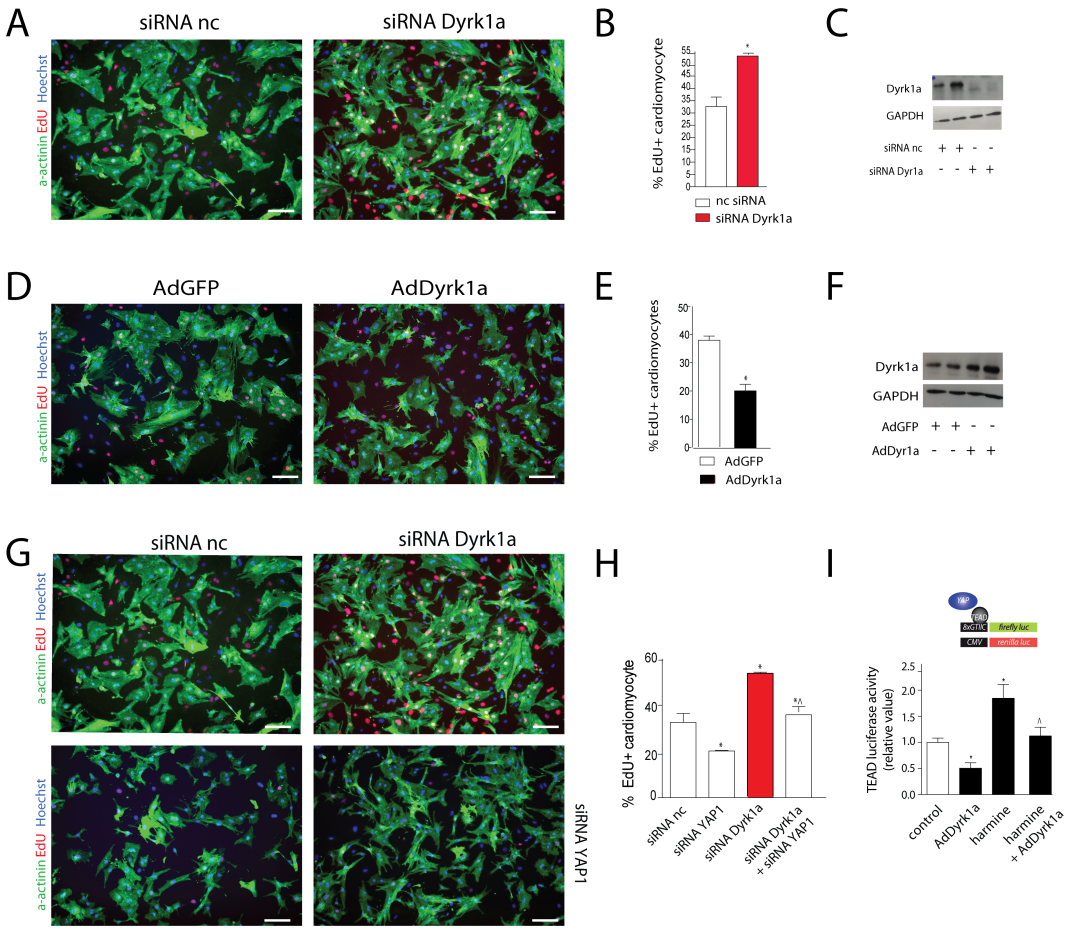

FIGURE 4-15. DYRK1A INHIBITION AND YAP ACTIVATION MEDIATE PRO-PROLIFERATIVE HARMINE EFFECTS IN CMS

A. Representative images of CM proliferation mediated by siRNA-silencing of Dyrk1a. CMs were transfected with a specific siRNA against Dyrk1a or non-coding siRNA (siRNA nc). CMs are visualized in green as α-actinin-positive cells. Hoechst staining was used for nuclei (blue). EdU incorporation is visualized in red. Scale bar: 100μm **B**. The graph shows the percentage of sarcomeric α-actinin-positive cells that have incorporated EdU. Data are mean ±SEM (n=3 independent experiments); *$P<0.01$; t-test. **C**. Western blot showing siRNA-mediated Dyrk1a downregulation. GAPDH was used as loading control. **D**. Representative images of CMs upon overexpression of Dyrk1a mediated by an adenovirus (AdDyrk1a). An adenovirus carrying GFP, adGFP, was used as a control. CMs are stained same as in A. **E.** Percentage of sarcomeric α-actinin-positive cells (green) that have incorporated EdU (red nuclei) are reported in the graph. **F.** Western blot showing overexpression of Dyrk1a protein mediated by the adenovirus **G.** Representative images of CMs transfected with siRNA against Dyrk1a or a non-coding siRNA (siRNA nc) in the presence of Yap1 knockdown. **H**. The graph shows the percentage of sarcomeric α-actinin-positive cells that have incorporated EdU. Data are mean ±SEM (n=3 independent experiments); *$P<0.01$; one-way ANOVA. **I**. CMs treated with adDyrk1a alone and in combination with harmine treatment were transfected with a TEAD luciferase reporter. A constitutively expressed Renilla luciferase plasmid was used to normalize the results. Data are mean ±SEM (n=5 independent experiments); *$P<0.01$; one-way ANOVA.

4.13 The role of the Dyrk family in promoting CM proliferation

To understand whether other Dyrk-family members (**Fig. 4-16A**) had the same capability of Dyrk1a in promoting CM cell cycle activity, we analysed CM proliferation upon transfection with siRNAs against each member of the Dyrk family (Dyrk1a, Dyrk2, Dyrk3, Dyrk4). CMs

were visualized with α-actinin staining (green), EdU staining (red) was used to identify proliferating cells and nuclei were stained with Hoechst 33342 (blue) as shown in **Fig. 4-16C**. The specific silencing of Dyrk1a was the only treatment able to significantly promote an increase in cardiac myocyte proliferation (**Fig. 4-16B**).

Next, CMs treated with siRNAs against Dyrk1a, Dyrk2, Dyrk3 and Dyrk4 were transfected with a TEAD luciferase reporter. The results were normalized to those obtained by a constitutively expressed Renilla luciferase plasmid and calculated as fold over control (non-coding siRNA). Even though Dyrk1a alone was able to induce CM proliferation, it was not the only one able to increase Yap-mediated TEAD activity. Indeed, Dyrk2 also seems to have an effect in inducing Yap activation, as reported in **Fig. 4-16D.**

Finally, the expression of two YAP-responsive genes, CTGF and Birc5, were marked increased upon Dyrk1a silencing or harmine treatment, as shown in **Fig. 4-16E** and **-16F**.

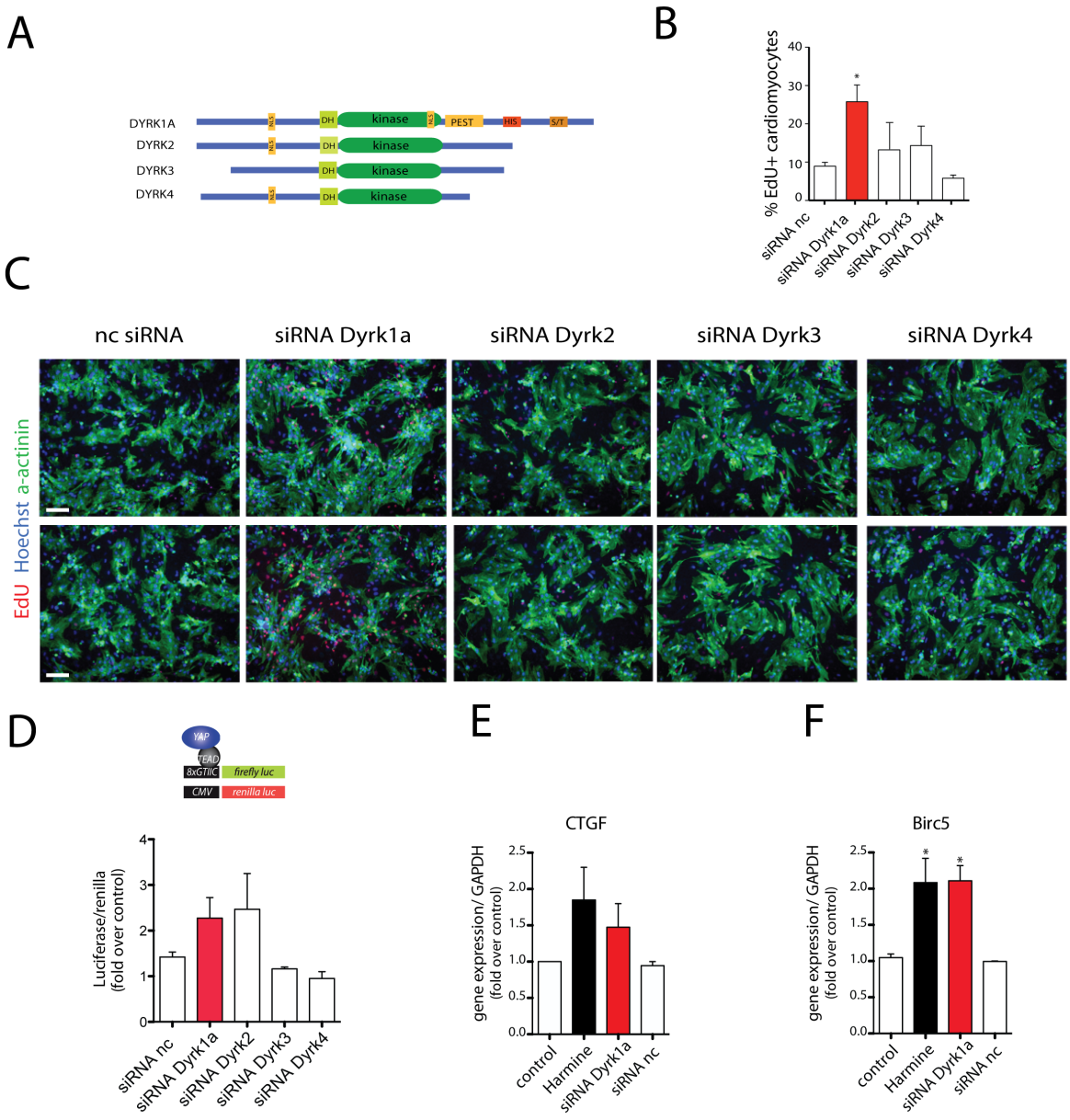

FIGURE 4-16. DYRK1 FAMILY AND YAP EFFECT ON CARDIOMYOCYTE PROLIFERATION

A. Schematic representation of Dyrk family member structure. NSL= nuclear localization sequence; DH: DYRK-homology box; kinase catalytic domain; PEST: proline, glutamic acid, serine, and threonine rich domain; HIS: poly-

histidine domain; S/T: region rich in serines/threonines; NAPA: N-terminal auto-phosphorylation accessory region. **B.** Quantification of EdU+ CMs (%). Data are mean ±SEM (n=3 independent experiments); *$P<0.01$; one-way ANOVA. **C**. Representative images showing CMs transfected with siRNAs against each member of the Dyrk family (Dyrk1a, Dyrk2,Dyrk3, Dyrk4). CMs were visualized with a-actinin staining (green); EdU staining (red) was used to identify proliferating cells. Nuclei are visualized with Hoechst 33342 (blue). **D.** CMs were treated with siRNAs against Dyrk1a, Dyrk2 and Dyrk4 and transfected with a TEAD luciferase reporter. Results were normalized to those obtained by a constitutively expressed Renilla luciferase plasmid and calculated as fold over control (non-coding siRNA). Data are mean ±SEM (n=4 independent experiments). **E-F.** Real-time RT-PCR quantification of YAP target genes, CTGF and Birc5, in CMs upon harmine treatment and Dyrk1a silencing. DMSO treatment and siRNA non-coding (nc) were used as controls. Data are mean ±SEM (n=3 independent experiments); *$P<0.01$; one-way ANOVA

4.14 Cardiac specific Dyrk1a KO induces cardiac proliferation in adult mice

To verify whether Dyrk1a silencing would also promote cardiac cell proliferation *in vivo*, an inducible mouse model of cardiomyocyte-specific Dyrk1a KO was created (MHC-MerCreMer-Dyrk1a f/f) by crossing a Dyrk1a floxed mouse (obtained from Prof. John D. Crispino, Robert H Lurie Medical Research Centre, US) with an MHC-MerCreMer driver mouse. The induction of Dyrk1a KO specifically in cardiomyocytes was obtained by 5 injections of 4-OH-tamoxifen, which was administrated intraperitoneally in two month-old mice (n=6) at the dosage of 40 mg/kg body weight (experimental scheme **Fig**. **4-17A**).

We verified the cardiac specific Dyrk1a ablation in the hearts of MHC-MerCreMer-Dyrk1a f/f mice and in the Dyrk1a f/f control group (n=6) using Real Time-qPCR **Fig. 4-17B**. Mice were monitored with echocardiography for functional cardiac parameters such as left ventricular ejection fraction (LVEF), left ventricular mass (LVmass) and left ventricular area of the wall in diastole, LVAWd, at different time points (week 0, 2, 4 and 8 weeks) (**Fig. 4-17D, -17E** and **-17F**). We referred to week 0 as the time point just after the injections of 4-OH-tamoxifen (week-1) and before the first EdU injection (week1). EdU was injected in mice from week 1 to the end of the follow-up period (2 months). As shown in **Fig**. **4-17D** and **-17F**, analysis of the left ventricular parameters of cardiomyocyte-specific Dyrk1a KO mice revealed a significant increase in LVAWd already at week 1 after the induction of the KO phenotype, which, in combination with an increase in LVmass, that becomes significant at week 2, was indicative of an increased thickness of the left ventricular wall without any correlation with an eventual increased in heart weight (**Fig.4-17C).**

In order to assess whether the observed phenotype was due to hyperhrophic remodelling of CMs or to an increase in CM number, wheat germ agglutinin staining (WGA) was used to identify plasma membranes and measure cardiac cell surface (**Fig 4-17G** and **-17H),** while EdU incorporation in α-actinin positive cells was used as a marker of proliferating cells, as

shown in **Fig. 4-17I**. The results obtained indicated that cardiac proliferation was responsible for the thickness of the heart wall (**Fig. 4-17F-17D)**, since CM size in the Dyrk1a KO mice was not different from that of the control group, as quantification in **Fig. 4-17H** shows. Collectively, these data show that the cardiomyocyte-specific Dyrk1a ablation leads to increased adult CM proliferation *in vivo*.

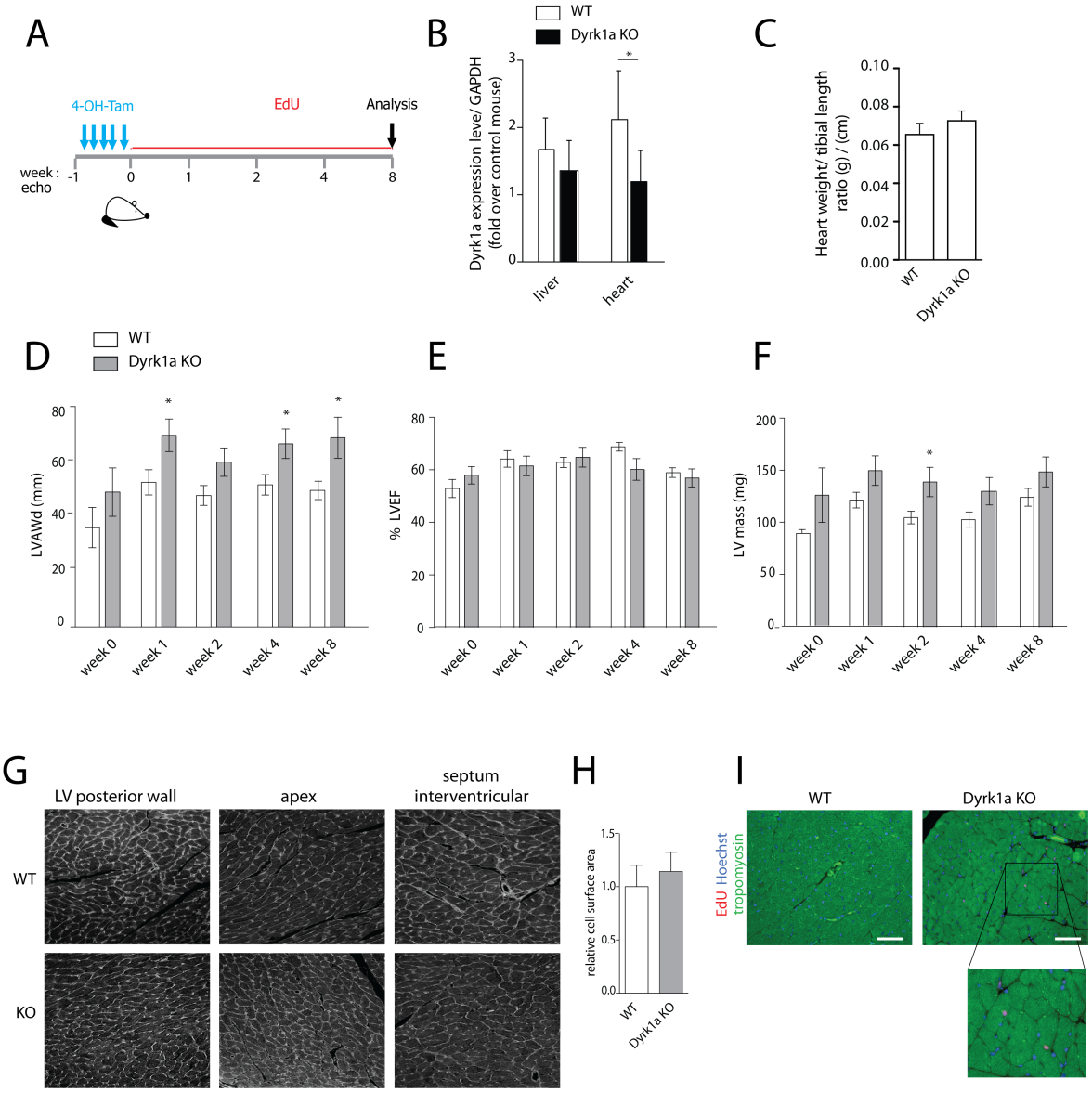

FIGURE 4-17. DYRK1A CARDIAC SPECIFIC KO PROMOTES CARDIOMYOCYTE PROLIFERATION IN VIVO

A. Schematic overview of the in vivo experiment. Three doses of 4-OH-tamoxifen were injected in MCM-CRE-f/f Dyrk1a mice to induce cardiac Dyrk1a knock out. Mice were monitored for a period of two months. **B**. Dyrk1a expression levels were evaluated in qRT-PCR in WT and Dyrk1a KO murine hearts. GAPDH was used as housekeeping gene. **C.** The weight of Dyrk1a WT and KO hearts were measured and normalized on tibia length. **D-F**. Left ventricular anterior wall thickness in diastolic phase was evaluated at at 0, 1, 2, 4 and 8 weeks. **E**. Left ventricle ejection fraction (LVEF) was evaluating at different time points to monitor heart functionality. **F**. Left ventricle mass, expressed in mg, was evaluated at 0, 1, 2, 4 and 8 weeks. **G.** Representative images of WGA staining showing CM area in WT and Dyrk1a KO hearts. **H**. Quantification of the relative cross-sectional area in WT and Dyrk1a KO mice. **I.** EdU staining (red) of tropomyosin positive cells (green) in paraffin sections of heart tissue of Dyrk1a KO or WT mice. Scale bar: 100μm.

5 DISCUSSION

The scanty information so far available on the molecular mechanisms that regulate cardiomyocyte cell cycle progression and those that are involved in physiological regeneration during the embryonic, fetal and early neonatal life still hamper the development of novel therapeutic approaches for the vast number of patients suffering of post-myocardial infarction heart failure. In the present work, we investigated the mechanism of action of two distinct pro-proliferative stimuli able to promote cardiomyocyte cell cycle re-entry: a series of microRNAs, identified in our previous work for their ability to stimulate neonatal rodent CM proliferation, and the neuroactive compound harmine, which had emerged from a high throughput screening using a library of FDA-registered drugs.

Our results clearly indicate that signaling from all investigated, pro-proliferative miRNAs converges towards nuclear translocation of the YAP transcriptional co-activator. This final molecular outcome is achieved through the modulation of different pathways, among which the regulation of actin cytoskeleton dynamics plays an essential role.

The Hippo-Yap signaling pathway is a master biochemical cascade in the control of organ size, as shown in YAP overexpression experiments (Camargo, Gokhale et al. 2007) or Hippo core component knock-down (Heallen, Morikawa et al. 2013). In particular, multiple evidence over the last few years has shown that this pathway is an essential regulator of physiological cell proliferation during normal heart development (Xiao, Leach et al. 2016). In adult hearts, YAP overexpression induces CM cell cycle re-entry (Lin, von Gise et al. 2014), while in the case of myocardial infarction, YAP activation drives heart tissue regeneration (Heallen, Morikawa et al. 2013) (Xin, Kim et al. 2013).

Our results, showing that the downregulation of YAP expression by RNAi blunts the pro-proliferative effect of all the 10 top effective miRNAs originally identified to stimulate CM proliferation, confirm that this pathway is also crucial for the exogenous stimulation of proliferation of post-natal CMs. This conclusion is reinforced by the observations that these pro-proliferative miRNAs promote the activation of a TEAD-responsive promoter, increase YAP-responsive gene expression and trigger nuclear import of active YAP.

Given the above discussed link between pro-proliferative microRNAs and YAP signaling, we investigated the molecular targets of these miRNAs, the downregulation of which might be eventually responsible for YAP functional activation in cardiomyocytes. Transcriptomic analysis of CMs in response to miRNA transfection revealed that 6 of the investigated miRNAs act through distinct pathways to achieve YAP activation. Indeed, all 6 of them determined downregulation of at least one of the kinases known to inactivate YAP (STK38L, LATS1/2 and TAOK1). Our results

further confirm previous findings from the Morrisey laboratory, showing that the miR-302/367 cluster - in our work, we analyzed miR-302c and miR-302d, belonging to this family - induces activation of the Hippo pathway in cardiac cells through the downregulation of MST1, MOB1b and LATS2 (Tian, Liu et al. 2015) MiR-199a-3p instead directly targets the 3'UTR of TAOK1 and β−TrCP, the latter acting as the E3 ubiquitin ligase driving YAP degradation through the proteasome (Zhao, Li et al. 2010) . Conversely, we found that the 3'UTR of STK38L is not directly bound by MiR-199a-3p: its downregulation upon miR-199a-3p, miR-302d and miR-373 transfection suggests either an indirect effect or an effect mediated by miRNA binding outside the 3'UTR region of the STK38L transcript.

Of interest, individual downregulation of either TAOK1 or β−TrCP by RNAi was sufficient to stimulate CM proliferation, indicating that the effect of miR-199a is likely the combinatorial outcome of downregulation of these (and likely other) genes, possibly impacting on the same pathway. Finally, consistent with their positive effect on the Hippo pathway, all the tested miRNAs upregulated the levels of the transcriptional enhancer factor TEF-4, TEAD2. This transcription factor belongs to the TEAD family: this isoform is highly expressed in muscles and mediates YAP coactivation of genes involved in DNA replication and cell cycle progression (Kapoor, Yao et al. 2014) (Zhao, Caretti et al. 2006).

Another molecular signature shared by most of the investigated miRNAs was the modulation of the actin cytoskeleton network. In particular, the levels of several factors preventing actin polymerization were significantly downregulated upon miRNA transfection in CMs: these included Cofilin2, Twinfilin1/2, Thymosin β4 and Profilin2. These regulatory proteins are important to maintain an active monomeric (G-actin) pool and prevent filamentous (F-actin) nucleation events (Xue and Robinson 2013). Few miRNAs dowregulated Csrp3, a Cofilin2-binding protein that enhances Cofilin2-dependent F-actin depolymerization (Papalouka, Arvanitis et al. 2009) and Mical3, known to destabilize F-actin, inhibiting local actin assembly (Fremont, Romet-Lemonne et al. 2017). Downregulation of these factors shifts the balance between F- and G-actin towards the polymerized state, as we observed in the case of transfection of individual miRNA mimics in cardiac cells, in particular miR-199a-3p, miR-302d, miR-373 and miR-33b*. Consistent with this effect, cells treated with miR-199a-3p or miR-373 macroscopically showed a rounded shape and displayed formation of layers of cortical, polymerized actin in bundles close to the cytoplasm periphery.

Interestingly, all the miRNAs we investigated, with the exception of miR-590-3p, were able to down-regulate the transcript of Cofilin2. This protein belongs to the muscle-specific ADF/Cofilin family, essential to modulate the equilibrium of actin assembly, thus being involved in all aspects of cell motility, locomotion and invasion (Bernstein and Bamburg 2010) (Bravo-Cordero, Magalhaes et al. 2013). In particular, Cofilin causes depolymerization of actin filaments, preventing their reassembly (Ghosh, Song et al. 2004). We found that four of the investigated

miRNAs (miR-199a-3p, miR-1825, miR-302d and miR-373) directly targeted the 3'UTR of Cofilin2 transcript. Even more notably, silencing of Cofilin2 by a specific siRNA was sufficient to stimulate CM proliferation and drive morphological changes in the treated cells, in terms of cortical actin accumulation and shape, which were superimposable to the phenotype triggered by miRNA transfection. We also found that the downregulation of Cofilin2 triggered YAP nuclear translocation with consequent activation of its transcriptional pathway, while inhibition of actin polymerization by cytochalasin D blocked this effect. Our results are perfectly consistent with previous findings showing that actin cytoskeleton dynamics is a strong activation signal for YAP in response to mechanical cues from the extracellular environment (Dupont, Morsut et al. 2011).

Keeping with the above experimental results and considerations, there is evidence that YAP activity is promoted and maintained by polymerized F-actin, essential for the maintenance of cellular homeostasis, resulting from a combination of extracellular hits affecting cell morphology and shape (Dupont, Morsut et al. 2011). The interplay between YAP activation and the cytoskeletal arrangement of CMs has an additional layer of complexity, since recent work has shown that YAP directly regulates genes encoding for proteins that promote F-actin polymerization and link the actin cytoskeleton to the extracellular environment, including components of the dystrophin glycoprotein complex (Morikawa, Zhang et al. 2015). Recent data also demonstrate that a component of this complex, Dag1, directly binds YAP and inhibits its pro-proliferative function (Morikawa, Heallen et al. 2017). Since the dystrophin glycoprotein complex connects the extracellular matrix to the actin cytoskeleton, it is conceivable that perturbing integrity of this connection at different levels might lead to YAP activation. This possibility is consistent with our observation that the individual Cofilin2 knockdown, which promotes actin rearrangement, is sufficient to activate YAP.

As far as miR-590 is concerned, although Cofilin2 was not a direct target of miR-590-3p, we cannot exclude that this miRNA interferes with cytoskeleton remodelling in exerting its pro-proliferative effect. Indeed, from the TargetScan prediction, in line with our RNaseq data, miR-590-3p downregulates the cysteine and glycine-rich protein 3 (Csrp3) mRNA levels, which encodes for the Muscle LIM Protein (MLP). As previously mentioned, this protein is involved in the maintenance of cytoarchitecture integrity of muscle cells and increases actin depolymerisation in a Cfl2-mediated manner (Papalouka, Arvanitis et al. 2009). We therefore can speculate that, although miR-590-3p is not directly affecting Cfl2 expression, it most likely acts on actin cytoskeleton remodeling through the silencing of Csrp3, in order to alter G-/F-actin balance to allow CM proliferation.

Recently, the study of actin dynamics has also unveiled a role of nuclear actin in the regulation of cellular transcriptional activity. In this context, additional molecular mechanisms of CM cell cycle regulation could be revealed by exploring the role of nuclear actin upon miRNA treatment, as it would shed lights in the understanding whether it is able to directly affect CM transcriptional activity in the proliferative effect exerted by microRNAs.

Finally, the interconnection between cytoskeletal dynamics, CM replication and YAP activation is further corroborated by the observation that all the pro-proliferative microRNAs under examination activated expression of Aurora A kinase, a protein that regulates G2/M phase transition during the cell cycle (Nikonova, Astsaturov et al. 2013). On the one hand, this serine/threonine kinase phosphorylates Cofilin at multiple sites during early mitosis resulting in the inactivation of its actin depolymerizing function (Ritchey and Chakrabarti 2014). On the other hand, recent work in cancer cells indicates that Aurora A kinase also acts as a direct, positive regulator to enhance YAP-mediated transcription (Chang, Yamaguchi et al. 2017).

In this work we also aimed at identifying small molecule drugs able to boost CM proliferation and thus potentially rescue myocardial function after ischemic injury. A library of 780 FDA-registered compounds was chosen for our screening, which was assembled by the vendor (Enzo) in order to ensure maximum heterogeneity in the chemical and pharmacological spectrum among all the available compounds. Our high-throughput, small molecule screening identified the neuroactive alokaloid drug harmine, as the most potent inducer of CM proliferation.

Harmine, is a small molecule historically isolated from *P. harmala* and *B. Caapi* and belonging to beta-carboline alkaloids family. Harmine was traditionally used in hallucinogen preparations in tribial cerimonies in the Central Asia, Middle East and South America. Besides its hallucinating properties of harmine, an interesting series of pharmacological effects have been attributed to this drug, including as anti-inflammatory, anti-microbial and anti-psychotic activities (reviewed in (Patel, Gadewar et al. 2012).

In the more recent literature, several papers report that harmine functions as a potent anti-tumor compound. In particular, in Hep3b and HuH7 hepatic cancer cell lines, harmine interferes with the double-stranded DNA break repair mechanism of cancer cells, which naturally allow these cells to survive and rapidly divide. In this context, harmine negatively affects the homologous recombination pathway by inhibiting the recruitment of Rad51 and consequentially determines failure of DNA damage repair mechanisms, with cytotoxicity as the ultimate result (Zhang, Zhang et al. 2015). Moreover, harmine was reported to inhibit tumor growth in head and neck squamous cell carcinoma (HNSCC) by inhibiting Dyrk1a-mediated Foxo3 phosphorylation, thereby promoting cell death (Radhakrishnan, Nanjappa et al. 2016).

In light of the above reported, known effect of harmine, it was quite surprising to us to discover that the drug was a powerful inducer of CM proliferation, in combination with miR-199a-3p or miR-590-3p, but also by itself. Moreover, *in vivo* and in neonatal mice harmine induced CM proliferation already at a dosage of 10mg/kg body weight. In addition, we found that harmine treatment significantly improve cardiac function after the induction of a myocardial infarction in mice, showing its beneficial potential in the heart regenerative process.

In considering the literature, however, one should mention that harmine was already reported to also stimulate proliferation of human neural progenitor cells in vitro (Dakic, Maciel et al. 2016) as

well as that of pancreatic β-cells, both in *in vitro* and *in vivo* (Wang, Alvarez-Perez et al. 2015). In both cases, inhibition of the ubiquitous kinase Dyrk-1a was found to mediate the proliferative effect of the drug. In particular, in pancreatic β-cells, inhibition of Dyrk1a was shown to result in NFAT nuclear translocation, which in turn induced expression of genes that stimulate cell cycle progression, such as c-Myc.

Our experimental data indicate that, among the alkaloid family members, harmine was the only tested compound able to promote CM proliferation, while the harmine analogues harmaline and harmane, which share a very similar biochemical structure with harmine, did not exert any significant effect.

The Dyrk1a gene is located on human chromosome 21, in the Down syndrome critical region (Shindoh, Kudoh et al. 1996) and is highly expressed in different tissues, such as brain and heart. It is considered to be crucial during early development of the nervous system and a master regulator in brain growth (Guedj, Pereira et al. 2012). Although, in neural cells, Dyrk1a has been described to regulate cell cycle progression and apoptosis, the detailed Dyrk1a downstream molecular mechanism still remains a topic of debate (Fernandez-Martinez, Zahonero et al. 2015). As for harmine, function of Dyrk1a seems to be dependent on the specific cell type and the cell proliferating status.

The role of Dyrk1a in cardiac myocytes is under investigation in various laboratories. One study has described Dyrk1a as a regulator of cardiac hypertrophy (Kuhn, Frank et al. 2009). Dyrk1a inhibition, mediated by a recombinant adenovirus carrying synthetic miRNAs targeting the kinase mRNA, was shown to induce *in vitro* cardiomyocyte hypertrophy induced by a 24 hr-pulse of phenylephrine. In addition, overexpression of Dyrk1a (AdDyrk1a) was reported to completely rescue the hypertrophic phenotype *in vitro*, while an inactive mutant of Dyrk1a (AdK188R) was ineffective. These findings were explained by the correlation between a decrease in Dyrk1a activity and the increased level of nuclear NFAT, the downstream transducer of calcineurin signaling responsible for CM hypertrophy.

There is an apparent contradiction between the above reported findings and those we obtained regarding the role of Dyrk1a as a negative regulator of CM proliferation. Indeed, we clearly observed that RNAi-mediated silencing of Dyrk1a stimulated CM proliferation without exerting obvious effects on either CM size or hypertrophic fetal gene expression. Differences in the experimental conditions and in timing of observation might explain these different results. In our experiments, Dyrk1a silencing was obtained by using a specific siRNA, which requires at least 72 hr to be effective, while the inactive mutant of Dyrk1a used by Hille and colleagues was evaluated 24 hr after transduction, which is a too short timeframe to appreciate any proliferative events in CMs. In addition, a recent line of though postulates that CM hypertrophy and proliferation are different sides of the same coin, which depends on the status of the cell that receives a given stimulation. In particular, CMs might require an increase in size (hypertrophic phase) before division; if adult CMs receive a pro-proliferative stimulus, they fail to proliferate and become

hypertrophic. Conversely, neonatal CMs are still capable to accomplish cell division therefore, once exposed to the same kind of stimulation, they overcome the "hypertrophic phase" and complete their mitosis.

The finding that harmine activates CM proliferation by targeting Dyrk1a raises the obvious question of which is the molecular mechanism by which this kinase controls cell proliferation. In this respect, the observation that harmine treatment did not exert any addictive effect with that of miR-199a-3p is consistent with the possibility that both the drug and this miRNA act through similar molecular mechanisms. Consistent with this possibility, we indeed found that harmine treatment resulted in YAP activation and that YAP was essential to mediate the pro-proliferative effect of the drug, again highlighting the essential role of the Hippo/YAP pathway in the regulation of cell cycle progression in CMs. However, how does Dyrk1 inhibition end up in YAP activation still remains a very interesting matter for future investigations. One might speculate that the kinase directly phosphorylates YAP thus inhibiting its activity or that, alternatively, it activates other known upstream kinases in the Hippo pathway, which are known to exert a negative role on YAP. Both possibilities appear to be experimentally testable.

The conclusion that Dyrk1a is an inhibitor of CM proliferation is fully consistent with the findings we observed in vivo in the Dyrk1a conditional knock-out mice. Full Dyrk1a knock-out is known to be embryonically lethal, while its overexpression during embryogenesis results in cardiovascular abnormalities (Fotaki, Dierssen et al. 2002). In our experiments, adult animals in which Dyrk1a was inactivated specifically in the heart, using tamoxifen-inducible Cre under the control of the MHC promoter, showed a significant increase in cardiomyocyte proliferation, with consequent hyperplastic increase in cardiac ventricle mass. These results might appear substantially different from those reported by the De Windt group in a haploinsufficient Dyrk1a mouse, in which pathologic hypertrophic growth after TAC was observed (da Costa Martins, Salic et al. 2010). However this discrepancy is only apparent, since the animal models used in the two studies are substantially different. Da Costa Martins and collaborators, to avoid embryonic lethality, took advantage of a haploinsufficient Dyrk1a mouse model, which is substantially different from the inducible cardiac specific knock-out used in our studies. Additionally, in the da Costa Martins study, analysis was performed at one week after transverse aortic constriction, while, in our case, mice were analysed in the absence of damage.

The effect of Dyrk1a overexpression was also recently studied in the heart (Hille, Dierck et al. 2016), showing that cardiac specific Dyrk1a transgenic mice developed dilated cardiomyopathy. In the same study, the hearts of neonatal transgenic mice, overexpressing Dyrk1a, presented decreased levels of CM proliferation, in agreement with our conclusions. At the molecular level, Hille et al. defined a new role for Dyrk1a as a negative regulator of Rb/E2F signalling mediated by cyclin-D and thus of cardiac myocyte proliferation. These conclusions appear to be fully consistent with our observation that Dyrk1a knock-out significantly increases CM proliferation.

Conclusions and translational perspectives

The discovery that individual miRNAs regulate post-natal CM proliferation is of particular interest towards the potential utilization of these molecules to promote cardiac regeneration. The identification of the molecular targets of the pro-proliferative miRNA is obviously important in this context. The results presented in this Thesis indicate that the stimulation of CM proliferation by miRNAs is a process that requires downregulation of multiple targets, with likely additive functions. In this respect, the pleiotropic effect of miRNAs appears to be of significant advantage compared to the use of single genes or siRNA knockdowns, provided, obviously, that the potential deleterious effects are minimized. For example, miR-199a-3p, one of the most effective miRNAs both ex vivo and in vivo, targets directly the 3'UTRs of Cofilin2 (modulation of actin cytoskeleton), TAOK1 (activation of the YAP inhibitory kinases) and β−TrCP (reduction of YAP degradation), in addition to the 3'UTRs of Hopx1 (a suppressor of embryonic CM proliferation (Trivedi, Zhu et al. 2010) and Homer1 (involved in the regulation of calcium signaling in cardiac cells (Jardin, Lopez et al. 2013), as shown in our previous work (Eulalio, Mano et al. 2012); other mRNAs are likely to be targeted as well. Despite these pleiotropic gene downregulation, however, it is of notice that all the proproliferative pathways appear to converge, and require, YAP activation. This conclusion is consistent with our previous observation, unexplained at the time, that combinatorial combinations of the four most effective miRNAs in our original HTS screen did not exert an effect that was superior to that of each individual miRNA when used at the same concentration of the combined molecules (Eulalio, Mano et al. 2012).

The pleiotropic function of miRNAs stimulating cardiac proliferation suggests that these molecules should be considered with caution in translational terms. While the permanent expression of miR-199a and miR-590 pri-miRNAs using AAV9 vectors in the mouse did not result in apparent deleterious effects (Eulalio, Mano et al. 2012), permanent expression of the miR-302/367 cluster led transgenic animals to develop cardiac dysfunction due to CM hyperproliferation coupled with cell de-differentiation (Tian, Liu et al. 2015). This observation is consistent with the finding that miR-302/367 enhances the reprogramming efficiency of mouse embryonic fibroblasts into induced pluripotent stem cells (iPSCs) (Judson, Babiarz et al. 2009) (Li, Yang et al. 2011). The pleiotropic effect of miRNAs and these observations, however, do not rule out that appropriate dose and schedule for the delivery of synthetic miRNA mimics would be effective and well tolerated. Available evidence already shows that single dose, systemic injection of miR302b/c itself (Tian, Liu et al. 2015) or intracardiac injection of miR-199a-3p mimics (Lesizza, Prosdocimo et al. 2017) determine significant beneficial effect in terms of recovery of myocardial tissue and function. These observations warrant further translation of these findings to large animals first and to the clinics later.

As far harmine is concerned, the potential beneficial effects of this molecule in the clinics was considered for different therapeutic approaches (Patel, Gadewar et al. 2012, Moloudizargari, Mikaili et al. 2013). In this regard, it is important to emphasize that pro-proliferative compounds, in

general, have the potential to promote cell cycle progression in a non-specific way, which could stimulate tumor growth at off-target sides. Harmine, however, appears to be quite peculiar in this respect, since its pro-proliferative effects are exerted in tissues with low proliferative capacity, such brain, β-cells and heart in our study. While this would be reassuring in terms of safety, however, it still needs to be considered that harmine itself exerts neuroexcitatory effects, which would prevent its direct clinical use. Other alkaloid compounds derived form harmine, might instaed prove equally effective in the downregulation of Dyrk1a but devoid of effects on the central nervous system and thus be more apt for clinical use. Thus, there is a translational perspective for this molecule, which would obviously require additional careful experimentation.

References

Aarons, D. H., G. V. Rossi and R. F. Orzechowski (1977). "Cardiovascular actions of three harmala alkaloids: harmine, harmaline, and harmalol." J Pharm Sci **66**(9): 1244-1248.

Agarwal, V., G. W. Bell, J. W. Nam and D. P. Bartel (2015). "Predicting effective microRNA target sites in mammalian mRNAs." Elife **4**.

Aguirre, A., N. Montserrat, S. Zacchigna, E. Nivet, T. Hishida, M. N. Krause, L. Kurian, A. Ocampo, E. Vazquez-Ferrer, C. Rodriguez-Esteban, S. Kumar, J. J. Moresco, J. R. Yates, 3rd, J. M. Campistol, I. Sancho-Martinez, M. Giacca and J. C. Izpisua Belmonte (2014). "In vivo activation of a conserved microRNA program induces mammalian heart regeneration." Cell Stem Cell **15**(5): 589-604.

Ahuja, P., E. Perriard, J. C. Perriard and E. Ehler (2004). "Sequential myofibrillar breakdown accompanies mitotic division of mammalian cardiomyocytes." J Cell Sci **117**(Pt 15): 3295-3306.

Aragona, M., T. Panciera, A. Manfrin, S. Giulitti, F. Michielin, N. Elvassore, S. Dupont and S. Piccolo (2013). "A mechanical checkpoint controls multicellular growth through YAP/TAZ regulation by actin-processing factors." Cell **154**(5): 1047-1059.

Aurora, A. B., E. R. Porrello, W. Tan, A. I. Mahmoud, J. A. Hill, R. Bassel-Duby, H. A. Sadek and E. N. Olson (2014). "Macrophages are required for neonatal heart regeneration." J Clin Invest **124**(3): 1382-1392.

Barry, E. R., T. Morikawa, B. L. Butler, K. Shrestha, R. de la Rosa, K. S. Yan, C. S. Fuchs, S. T. Magness, R. Smits, S. Ogino, C. J. Kuo and F. D. Camargo (2013). "Restriction of intestinal stem cell expansion and the regenerative response by YAP." Nature **493**(7430): 106-110.

Bartel, D. P. (2004). "MicroRNAs: genomics, biogenesis, mechanism, and function." Cell **116**(2): 281-297.

Basu, S., N. F. Totty, M. S. Irwin, M. Sudol and J. Downward (2003). "Akt phosphorylates the Yes-associated protein, YAP, to induce interaction with 14-3-3 and attenuation of p73-mediated apoptosis." Mol Cell **11**(1): 11-23.

Beltrami, A. P., L. Barlucchi, D. Torella, M. Baker, F. Limana, S. Chimenti, H. Kasahara, M. Rota, E. Musso, K. Urbanek, A. Leri, J. Kajstura, B. Nadal-Ginard and P. Anversa (2003). "Adult cardiac stem cells are multipotent and support myocardial regeneration." Cell **114**(6): 763-776.

Bergmann, O., R. D. Bhardwaj, S. Bernard, S. Zdunek, F. Barnabe-Heider, S. Walsh, J. Zupicich, K. Alkass, B. A. Buchholz, H. Druid, S. Jovinge and J. Frisen (2009). "Evidence for cardiomyocyte renewal in humans." Science **324**(5923): 98-102.

Bergmann, O., S. Zdunek, A. Felker, M. Salehpour, K. Alkass, S. Bernard, S. L. Sjostrom, M. Szewczykowska, T. Jackowska, C. Dos Remedios, T. Malm, M. Andra, R. Jashari, J. R. Nyengaard, G. Possnert, S. Jovinge, H. Druid and J. Frisen (2015). "Dynamics of Cell Generation and Turnover in the Human Heart." Cell **161**(7): 1566-1575.

Bernstein, B. W. and J. R. Bamburg (2010). "ADF/cofilin: a functional node in cell biology." Trends Cell Biol **20**(4): 187-195.

Berrougui, H., C. Martin-Cordero, A. Khalil, M. Hmamouchi, A. Ettaib, E. Marhuenda and M. D. Herrera (2006). "Vasorelaxant effects of harmine and harmaline extracted from Peganum harmala L. seeds in isolated rat aorta." Pharmacol Res **54**(2): 150-157.

Bersell, K., S. Arab, B. Haring and B. Kuhn (2009). "Neuregulin1/ErbB4 signaling induces cardiomyocyte proliferation and repair of heart injury." Cell **138**(2): 257-270.

Bhat, K. P., K. L. Salazar, V. Balasubramaniyan, K. Wani, L. Heathcock, F. Hollingsworth, J. D. James, J. Gumin, K. L. Diefes, S. H. Kim, A. Turski, Y. Azodi, Y. Yang, T. Doucette, H. Colman, E. P. Sulman, F. F. Lang, G. Rao, S. Copray, B. D. Vaillant and K. D. Aldape (2011). "The transcriptional coactivator TAZ regulates mesenchymal differentiation in malignant glioma." Genes Dev **25**(24): 2594-2609.

Boggiano, J. C., P. J. Vanderzalm and R. G. Fehon (2011). "Tao-1 phosphorylates Hippo/MST kinases to regulate the Hippo-Salvador-Warts tumor suppressor pathway." Dev Cell **21**(5): 888-895.

Brade, T., L. S. Pane, A. Moretti, K. R. Chien and K. L. Laugwitz (2013). "Embryonic heart progenitors and cardiogenesis." Cold Spring Harb Perspect Med **3**(10): a013847.

Bravo-Cordero, J. J., M. A. Magalhaes, R. J. Eddy, L. Hodgson and J. Condeelis (2013). "Functions of cofilin in cell locomotion and invasion." Nat Rev Mol Cell Biol **14**(7): 405-415.

Britschgi, A., S. Duss, S. Kim, J. P. Couto, H. Brinkhaus, S. Koren, D. De Silva, K. D. Mertz, D. Kaup, Z. Varga, H. Voshol, A. Vissieres, C. Leroy, T. Roloff, M. B. Stadler, C. H. Scheel, L. J. Miraglia, A. P. Orth, G. M. Bonamy, V. A. Reddy and M. Bentires-Alj (2017). "The Hippo kinases LATS1 and 2 control human breast cell fate via crosstalk with ERalpha." Nature **541**(7638): 541-545.

Buchmann, K. (2014). "Evolution of Innate Immunity: Clues from Invertebrates via Fish to Mammals." Front Immunol **5**: 459.

Cai, C. L., X. Liang, Y. Shi, P. H. Chu, S. L. Pfaff, J. Chen and S. Evans (2003). "Isl1 identifies a cardiac progenitor population that proliferates prior to differentiation and contributes a majority of cells to the heart." Dev Cell **5**(6): 877-889.

Cai, X., C. H. Hagedorn and B. R. Cullen (2004). "Human microRNAs are processed from capped, polyadenylated transcripts that can also function as mRNAs." RNA **10**(12): 1957-1966.

Camargo, F. D., S. Gokhale, J. B. Johnnidis, D. Fu, G. W. Bell, R. Jaenisch and T. R. Brummelkamp (2007). "YAP1 increases organ size and expands undifferentiated progenitor cells." Curr Biol **17**(23): 2054-2060.

Campa, V. M., R. Gutierrez-Lanza, F. Cerignoli, R. Diaz-Trelles, B. Nelson, T. Tsuji, M. Barcova, W. Jiang and M. Mercola (2008). "Notch activates cell cycle reentry and progression in quiescent cardiomyocytes." J Cell Biol **183**(1): 129-141.

Canseco, D. C., W. Kimura, S. Garg, S. Mukherjee, S. Bhattacharya, S. Abdisalaam, S. Das, A. Asaithamby, P. P. Mammen and H. A. Sadek (2015). "Human ventricular unloading induces cardiomyocyte proliferation." J Am Coll Cardiol **65**(9): 892-900.

Care, A., D. Catalucci, F. Felicetti, D. Bonci, A. Addario, P. Gallo, M. L. Bang, P. Segnalini, Y. Gu, N. D. Dalton, L. Elia, M. V. Latronico, M. Hoydal, C. Autore, M. A. Russo, G. W. Dorn, 2nd, O. Ellingsen, P. Ruiz-Lozano, K. L. Peterson, C. M. Croce, C. Peschle and G. Condorelli (2007). "MicroRNA-133 controls cardiac hypertrophy." Nat Med **13**(5): 613-618.

Chablais, F. and A. Jazwinska (2012). "The regenerative capacity of the zebrafish heart is dependent on TGFbeta signaling." Development **139**(11): 1921-1930.

Chang, S. S., H. Yamaguchi, W. Xia, S. O. Lim, Y. Khotskaya, Y. Wu, W. C. Chang, Q. Liu and M. C. Hung (2017). "Aurora A kinase activates YAP signaling in triple-negative breast cancer." Oncogene **36**(9): 1265-1275.

Chen, J., Z. P. Huang, H. Y. Seok, J. Ding, M. Kataoka, Z. Zhang, X. Hu, G. Wang, Z. Lin, S. Wang, W. T. Pu, R. Liao and D. Z. Wang (2013). "mir-17-92 cluster is required for and sufficient to induce cardiomyocyte proliferation in postnatal and adult hearts." Circ Res **112**(12): 1557-1566.

Chen, Q., R. Chao, H. Chen, X. Hou, H. Yan, S. Zhou, W. Peng and A. Xu (2005). "Antitumor and neurotoxic effects of novel harmine derivatives and structure-activity relationship analysis." Int J Cancer **114**(5): 675-682.

Chen, Z., G. A. Friedrich and P. Soriano (1994). "Transcriptional enhancer factor 1 disruption by a retroviral gene trap leads to heart defects and embryonic lethality in mice." Genes Dev **8**(19): 2293-2301.

Cheng, C., N. Bhardwaj and M. Gerstein (2009). "The relationship between the evolution of microRNA targets and the length of their UTRs." BMC Genomics **10**: 431.

Collesi, C., L. Zentilin, G. Sinagra and M. Giacca (2008). "Notch1 signaling stimulates proliferation of immature cardiomyocytes." J Cell Biol **183**(1): 117-128.

Coordinators, N. R. (2016). "Database resources of the National Center for Biotechnology Information." Nucleic Acids Res **44**(D1): D7-19.

Croquelois, A., A. A. Domenighetti, M. Nemir, M. Lepore, N. Rosenblatt-Velin, F. Radtke and T. Pedrazzini (2008). "Control of the adaptive response of the heart to stress via the Notch1 receptor pathway." J Exp Med **205**(13): 3173-3185.

da Costa Martins, P. A., K. Salic, M. M. Gladka, A. S. Armand, S. Leptidis, H. el Azzouzi, A. Hansen, C. J. Coenen-de Roo, M. F. Bierhuizen, R. van der Nagel, J. van Kuik, R. de Weger, A. de Bruin, G. Condorelli, M. L. Arbones, T. Eschenhagen and L. J. De Windt (2010). "MicroRNA-199b targets the nuclear kinase Dyrk1a in an auto-amplification loop promoting calcineurin/NFAT signalling." Nat Cell Biol **12**(12): 1220-1227.

Dakic, V., R. M. Maciel, H. Drummond, J. M. Nascimento, P. Trindade and S. K. Rehen (2016). "Harmine stimulates proliferation of human neural progenitors." PeerJ **4**: e2727.

Deng, Y., A. Wu, P. Li, G. Li, L. Qin, H. Song and K. K. Mak (2016). "Yap1 Regulates Multiple Steps of Chondrocyte Differentiation during Skeletal Development and Bone Repair." Cell Rep **14**(9): 2224-2237.

Dong, J., G. Feldmann, J. Huang, S. Wu, N. Zhang, S. A. Comerford, M. F. Gayyed, R. A. Anders, A. Maitra and D. Pan (2007). "Elucidation of a universal size-control mechanism in Drosophila and mammals." Cell **130**(6): 1120-1133.

Dorn, G. W., 2nd (2016). "Parkin-dependent mitophagy in the heart." J Mol Cell Cardiol **95**: 42-49.

Downward, J. and S. Basu (2008). "YAP and p73: a complex affair." Mol Cell **32**(6): 749-750.

Du, T. and P. D. Zamore (2005). "microPrimer: the biogenesis and function of microRNA." Development **132**(21): 4645-4652.

Dupont, S., L. Morsut, M. Aragona, E. Enzo, S. Giulitti, M. Cordenonsi, F. Zanconato, J. Le Digabel, M. Forcato, S. Bicciato, N. Elvassore and S. Piccolo (2011). "Role of YAP/TAZ in mechanotransduction." Nature **474**(7350): 179-183.

Egawa, H., K. Jingushi, T. Hirono, Y. Ueda, K. Kitae, W. Nakata, K. Fujita, M. Uemura, N. Nonomura and K. Tsujikawa (2016). "The miR-130 family promotes cell migration and invasion in bladder cancer through FAK and Akt phosphorylation by regulating PTEN." Sci Rep **6**: 20574.

Ehrman, L. A. and K. E. Yutzey (1999). "Lack of regulation in the heart forming region of avian embryos." Dev Biol **207**(1): 163-175.

Engel, F. B., P. C. Hsieh, R. T. Lee and M. T. Keating (2006). "FGF1/p38 MAP kinase inhibitor therapy induces cardiomyocyte mitosis, reduces scarring, and rescues function after myocardial infarction." Proc Natl Acad Sci U S A **103**(42): 15546-15551.

Engel, F. B., M. Schebesta, M. T. Duong, G. Lu, S. Ren, J. B. Madwed, H. Jiang, Y. Wang and M. T. Keating (2005). "p38 MAP kinase inhibition enables proliferation of adult mammalian cardiomyocytes." Genes Dev **19**(10): 1175-1187.

Epelman, S., P. P. Liu and D. L. Mann (2015). "Role of innate and adaptive immune mechanisms in cardiac injury and repair." Nat Rev Immunol **15**(2): 117-129.

Eschenhagen, T., R. Bolli, T. Braun, L. J. Field, B. K. Fleischmann, J. Frisen, M. Giacca, J. M. Hare, S. Houser, R. T. Lee, E. Marban, J. F. Martin, J. D. Molkentin, C. E. Murry, P. R. Riley, P. Ruiz-Lozano, H. A. Sadek, M. A. Sussman and J. A. Hill (2017). "Cardiomyocyte Regeneration: A Consensus Statement." Circulation **136**(7): 680-686.

Eulalio, A., M. Mano, M. Dal Ferro, L. Zentilin, G. Sinagra, S. Zacchigna and M. Giacca (2012). "Functional screening identifies miRNAs inducing cardiac regeneration." Nature **492**(7429): 376-381.

Farzin, D., A. Haghparast, S. Motaman, F. Baryar and N. Mansouri (2011). "Effects of harmane and other beta-carbolines on apomorphine-induced licking behavior in rat." Pharmacol Biochem Behav **98**(2): 215-219.

Felician, G., C. Collesi, M. Lusic, V. Martinelli, M. D. Ferro, L. Zentilin, S. Zacchigna and M. Giacca (2014). "Epigenetic modification at Notch responsive promoters blunts efficacy of inducing notch pathway reactivation after myocardial infarction." Circ Res **115**(7): 636-649.

Fernandez-Martinez, P., C. Zahonero and P. Sanchez-Gomez (2015). "DYRK1A: the double-edged kinase as a protagonist in cell growth and tumorigenesis." Mol Cell Oncol **2**(1): e970048.

Ferrigno, O., F. Lallemand, F. Verrecchia, S. L'Hoste, J. Camonis, A. Atfi and A. Mauviel (2002). "Yes-associated protein (YAP65) interacts with Smad7 and potentiates its inhibitory activity against TGF-beta/Smad signaling." Oncogene **21**(32): 4879-4884.

Fortunato, J. J., G. Z. Reus, T. R. Kirsch, R. B. Stringari, L. Stertz, F. Kapczinski, J. P. Pinto, J. E. Hallak, A. W. Zuardi, J. A. Crippa and J. Quevedo (2009). "Acute harmine administration induces antidepressive-like effects and increases BDNF levels in the rat hippocampus." Prog Neuropsychopharmacol Biol Psychiatry **33**(8): 1425-1430.

Fotaki, V., M. Dierssen, S. Alcantara, S. Martinez, E. Marti, C. Casas, J. Visa, E. Soriano, X. Estivill and M. L. Arbones (2002). "Dyrk1A haploinsufficiency affects viability and causes developmental delay and abnormal brain morphology in mice." Mol Cell Biol **22**(18): 6636-6647.

Fremont, S., G. Romet-Lemonne, A. Houdusse and A. Echard (2017). "Emerging roles of MICAL family proteins - from actin oxidation to membrane trafficking during cytokinesis." J Cell Sci **130**(9): 1509-1517.

Frost, D., B. Meechoovet, T. Wang, S. Gately, M. Giorgetti, I. Shcherbakova and T. Dunckley (2011). "beta-carboline compounds, including harmine, inhibit DYRK1A and tau phosphorylation at multiple Alzheimer's disease-related sites." PLoS One **6**(5): e19264.

Gao, J., Z. Zheng, B. Rawal, M. J. Schell, G. Bepler and E. B. Haura (2009). "Mirk/Dyrk1B, a novel therapeutic target, mediates cell survival in non-small cell lung cancer cells." Cancer Biol Ther **8**(17): 1671-1679.

Ghosh, M., X. Song, G. Mouneimne, M. Sidani, D. S. Lawrence and J. S. Condeelis (2004). "Cofilin promotes actin polymerization and defines the direction of cell motility." Science **304**(5671): 743-746.

Gilsbach, R., S. Preissl, B. A. Gruning, T. Schnick, L. Burger, V. Benes, A. Wurch, U. Bonisch, S. Gunther, R. Backofen, B. K. Fleischmann, D. Schubeler and L. Hein (2014). "Dynamic DNA methylation orchestrates cardiomyocyte development, maturation and disease." Nat Commun **5**: 5288.

Godwin, J. W., A. R. Pinto and N. A. Rosenthal (2013). "Macrophages are required for adult salamander limb regeneration." Proc Natl Acad Sci U S A **110**(23): 9415-9420.

Gomes, R. S., P. Skroblin, A. B. Munster, H. Tomlins, S. R. Langley, A. Zampetaki, X. Yin, F. C. Wardle and M. Mayr (2016). ""Young at heart": Regenerative potential linked to immature cardiac phenotypes." J Mol Cell Cardiol **92**: 105-108.

Gong, G., M. Song, G. Csordas, D. P. Kelly, S. J. Matkovich and G. W. Dorn, 2nd (2015). "Parkin-mediated mitophagy directs perinatal cardiac metabolic maturation in mice." Science **350**(6265): aad2459.

Grego-Bessa, J., L. Luna-Zurita, G. del Monte, V. Bolos, P. Melgar, A. Arandilla, A. N. Garratt, H. Zang, Y. S. Mukouyama, H. Chen, W. Shou, E. Ballestar, M. Esteller, A. Rojas, J. M. Perez-Pomares and J. L. de la Pompa (2007). "Notch signaling is essential for ventricular chamber development." Dev Cell **12**(3): 415-429.

Gregorieff, A., Y. Liu, M. R. Inanlou, Y. Khomchuk and J. L. Wrana (2015). "Yap-dependent reprogramming of Lgr5(+) stem cells drives intestinal regeneration and cancer." Nature **526**(7575): 715-718.

Grimsby, J., M. Toth, K. Chen, T. Kumazawa, L. Klaidman, J. D. Adams, F. Karoum, J. Gal and J. C. Shih (1997). "Increased stress response and beta-phenylethylamine in MAOB-deficient mice." Nat Genet **17**(2): 206-210.

Guedj, F., P. L. Pereira, S. Najas, M. J. Barallobre, C. Chabert, B. Souchet, C. Sebrie, C. Verney, Y. Herault, M. Arbones and J. M. Delabar (2012). "DYRK1A: a master regulatory protein controlling brain growth." Neurobiol Dis **46**(1): 190-203.

Gupta, V., M. Gemberling, R. Karra, G. E. Rosenfeld, T. Evans and K. D. Poss (2013). "An injury-responsive gata4 program shapes the zebrafish cardiac ventricle." Curr Biol **23**(13): 1221-1227.

Halder, G. and R. L. Johnson (2011). "Hippo signaling: growth control and beyond." Development **138**(1): 9-22.

Hamsa, T. P. and G. Kuttan (2010). "Harmine inhibits tumour specific neo-vessel formation by regulating VEGF, MMP, TIMP and pro-inflammatory mediators both in vivo and in vitro." Eur J Pharmacol **649**(1-3): 64-73.

Hariharan, I. K. (2006). "Growth regulation: a beginning for the hippo pathway." Curr Biol **16**(24): R1037-1039.

Harvey, K. F., X. Zhang and D. M. Thomas (2013). "The Hippo pathway and human cancer." Nat Rev Cancer **13**(4): 246-257.

Hatzistergos, K. E., H. Quevedo, B. N. Oskouei, Q. Hu, G. S. Feigenbaum, I. S. Margitich, R. Mazhari, A. J. Boyle, J. P. Zambrano, J. E. Rodriguez, R. Dulce, P. M. Pattany, D. Valdes, C. Revilla, A. W. Heldman, I. McNiece and J. M. Hare (2010). "Bone marrow mesenchymal stem cells stimulate cardiac stem cell proliferation and differentiation." Circ Res **107**(7): 913-922.

Haubner, B. J., J. Schneider, U. Schweigmann, T. Schuetz, W. Dichtl, C. Velik-Salchner, J. I. Stein and J. M. Penninger (2016). "Functional Recovery of a Human Neonatal Heart After Severe Myocardial Infarction." Circ Res **118**(2): 216-221.

Heallen, T., Y. Morikawa, J. Leach, G. Tao, J. T. Willerson, R. L. Johnson and J. F. Martin (2013). "Hippo signaling impedes adult heart regeneration." Development **140**(23): 4683-4690.

Heallen, T., M. Zhang, J. Wang, M. Bonilla-Claudio, E. Klysik, R. L. Johnson and J. F. Martin (2011). "Hippo pathway inhibits Wnt signaling to restrain cardiomyocyte proliferation and heart size." Science **332**(6028): 458-461.

Hedman, M., J. Hartikainen and S. Yla-Herttuala (2011). "Progress and prospects: hurdles to cardiovascular gene therapy clinical trials." Gene Ther **18**(8): 743-749.

Hergovich, A., R. S. Kohler, D. Schmitz, A. Vichalkovski, H. Cornils and B. A. Hemmings (2009). "The MST1 and hMOB1 tumor suppressors control human centrosome duplication by regulating NDR kinase phosphorylation." Curr Biol **19**(20): 1692-1702.

Hergovich, A., M. R. Stegert, D. Schmitz and B. A. Hemmings (2006). "NDR kinases regulate essential cell processes from yeast to humans." Nat Rev Mol Cell Biol **7**(4): 253-264.

Herraiz, T. and C. Chaparro (2006). "Human monoamine oxidase enzyme inhibition by coffee and beta-carbolines norharman and harman isolated from coffee." Life Sci **78**(8): 795-802.

Herraiz, T., D. Gonzalez, C. Ancin-Azpilicueta, V. J. Aran and H. Guillen (2010). "beta-Carboline alkaloids in Peganum harmala and inhibition of human monoamine oxidase (MAO)." Food Chem Toxicol **48**(3): 839-845.

Hille, S., F. Dierck, C. Kuhl, J. Sosna, S. Adam-Klages, D. Adam, R. Lullmann-Rauch, N. Frey and C. Kuhn (2016). "Dyrk1a regulates the cardiomyocyte cell cycle via D-cyclin-dependent Rb/E2f-signalling." Cardiovasc Res **110**(3): 381-394.

Hillman, N. H., S. G. Kallapur and A. H. Jobe (2012). "Physiology of transition from intrauterine to extrauterine life." Clin Perinatol **39**(4): 769-783.

Himpel, S., P. Panzer, K. Eirmbter, H. Czajkowska, M. Sayed, L. C. Packman, T. Blundell, H. Kentrup, J. Grotzinger, H. G. Joost and W. Becker (2001). "Identification of the autophosphorylation sites and characterization of their effects in the protein kinase DYRK1A." Biochem J **359**(Pt 3): 497-505.

Howell, M., C. Borchers and S. L. Milgram (2004). "Heterogeneous nuclear ribonuclear protein U associates with YAP and regulates its co-activation of Bax transcription." J Biol Chem **279**(25): 26300-26306.

Hsieh, P. C., V. F. Segers, M. E. Davis, C. MacGillivray, J. Gannon, J. D. Molkentin, J. Robbins and R. T. Lee (2007). "Evidence from a genetic fate-mapping study that stem cells refresh adult mammalian cardiomyocytes after injury." Nat Med **13**(8): 970-974.

Hulot, J. S., J. E. Salem, A. Redheuil, J. P. Collet, S. Varnous, P. Jourdain, D. Logeart, E. Gandjbakhch, C. Bernard, S. N. Hatem, R. Isnard, P. Cluzel, C. Le Feuvre, P. Leprince, N. Hammoudi, F. M. Lemoine, D. Klatzmann, E. Vicaut, M. Komajda, G. Montalescot, A. M. Lompre, R. J. Hajjar and A.-H. Investigators (2017). "Effect of intracoronary administration of AAV1/SERCA2a on ventricular remodelling in patients with advanced systolic heart failure: results from the AGENT-HF randomized phase 2 trial." Eur J Heart Fail **19**(11): 1534-1541.

Humphreys, D. T., B. J. Westman, D. I. Martin and T. Preiss (2005). "MicroRNAs control translation initiation by inhibiting eukaryotic initiation factor 4E/cap and poly(A) tail function." Proc Natl Acad Sci U S A **102**(47): 16961-16966.

Ieda, M., T. Tsuchihashi, K. N. Ivey, R. S. Ross, T. T. Hong, R. M. Shaw and D. Srivastava (2009). "Cardiac fibroblasts regulate myocardial proliferation through beta1 integrin signaling." Dev Cell **16**(2): 233-244.

Imokawa, Y., A. Simon and J. P. Brockes (2004). "A critical role for thrombin in vertebrate lens regeneration." Philos Trans R Soc Lond B Biol Sci **359**(1445): 765-776.

Jain, R., D. Li, M. Gupta, L. J. Manderfield, J. L. Ifkovits, Q. Wang, F. Liu, Y. Liu, A. Poleshko, A. Padmanabhan, J. C. Raum, L. Li, E. E. Morrisey, M. M. Lu, K. J. Won and J. A. Epstein (2015). "HEART DEVELOPMENT. Integration of Bmp and Wnt signaling by Hopx specifies commitment of cardiomyoblasts." Science **348**(6242): aaa6071.

Jardin, I., J. J. Lopez, A. Berna-Erro, G. M. Salido and J. A. Rosado (2013). "Homer proteins in Ca(2)(+) entry." IUBMB Life **65**(6): 497-504.

Jonker, S. S., L. Zhang, S. Louey, G. D. Giraud, K. L. Thornburg and J. J. Faber (2007). "Myocyte enlargement, differentiation, and proliferation kinetics in the fetal sheep heart." J Appl Physiol (1985) **102**(3): 1130-1142.

Jopling, C., E. Sleep, M. Raya, M. Marti, A. Raya and J. C. Izpisua Belmonte (2010). "Zebrafish heart regeneration occurs by cardiomyocyte dedifferentiation and proliferation." Nature **464**(7288): 606-609.

Judson, R. L., J. E. Babiarz, M. Venere and R. Blelloch (2009). "Embryonic stem cell-specific microRNAs promote induced pluripotency." Nat Biotechnol **27**(5): 459-461.

Justice, R. W., O. Zilian, D. F. Woods, M. Noll and P. J. Bryant (1995). "The Drosophila tumor suppressor gene warts encodes a homolog of human myotonic dystrophy kinase and is required for the control of cell shape and proliferation." Genes Dev **9**(5): 534-546.

Kadota, S., L. Pabon, H. Reinecke and C. E. Murry (2017). "In Vivo Maturation of Human Induced Pluripotent Stem Cell-Derived Cardiomyocytes in Neonatal and Adult Rat Hearts." Stem Cell Reports **8**(2): 278-289.

Kapoor, A., W. Yao, H. Ying, S. Hua, A. Liewen, Q. Wang, Y. Zhong, C. J. Wu, A. Sadanandam, B. Hu, Q. Chang, G. C. Chu, R. Al-Khalil, S. Jiang, H. Xia, E. Fletcher-Sananikone, C. Lim, G. I. Horwitz, A. Viale, P. Pettazzoni, N. Sanchez, H. Wang, A. Protopopov, J. Zhang, T. Heffernan, R. L. Johnson, L. Chin, Y. A. Wang, G. Draetta and R. A. DePinho (2014). "Yap1 activation enables bypass of oncogenic Kras addiction in pancreatic cancer." Cell **158**(1): 185-197.

Karakikes, I., A. H. Chaanine, S. Kang, B. N. Mukete, D. Jeong, S. Zhang, R. J. Hajjar and D. Lebeche (2013). "Therapeutic cardiac-targeted delivery of miR-1 reverses pressure overload-induced cardiac hypertrophy and attenuates pathological remodeling." J Am Heart Assoc **2**(2): e000078.

Khvorova, A., A. Reynolds and S. D. Jayasena (2003). "Functional siRNAs and miRNAs exhibit strand bias." Cell **115**(2): 209-216.

Kim, J., Q. Wu, Y. Zhang, K. M. Wiens, Y. Huang, N. Rubin, H. Shimada, R. I. Handin, M. Y. Chao, T. L. Tuan, V. A. Starnes and C. L. Lien (2010). "PDGF signaling is required for epicardial function and blood vessel formation in regenerating zebrafish hearts." Proc Natl Acad Sci U S A **107**(40): 17206-17210.

Kim, M., M. Kim, S. Lee, S. Kuninaka, H. Saya, H. Lee, S. Lee and D. S. Lim (2013). "cAMP/PKA signalling reinforces the LATS-YAP pathway to fully suppress YAP in response to actin cytoskeletal changes." EMBO J **32**(11): 1543-1555.

Kimura, W., F. Xiao, D. C. Canseco, S. Muralidhar, S. Thet, H. M. Zhang, Y. Abderrahman, R. Chen, J. A. Garcia, J. M. Shelton, J. A. Richardson, A. M. Ashour, A. Asaithamby, H. Liang, C. Xing, Z. Lu, C. Cheng Zhang and H. A. Sadek (2016). "Corrigendum: Hypoxia fate mapping identifies cycling cardiomyocytes in the adult heart." Nature **532**(7598): 268.

Komuro, A., M. Nagai, N. E. Navin and M. Sudol (2003). "WW domain-containing protein YAP associates with ErbB-4 and acts as a co-transcriptional activator for the carboxyl-terminal fragment of ErbB-4 that translocates to the nucleus." J Biol Chem **278**(35): 33334-33341.

Koontz, L. M., Y. Liu-Chittenden, F. Yin, Y. Zheng, J. Yu, B. Huang, Q. Chen, S. Wu and D. Pan (2013). "The Hippo effector Yorkie controls normal tissue growth by antagonizing scalloped-mediated default repression." Dev Cell **25**(4): 388-401.

Kratsios, P., C. Catela, E. Salimova, M. Huth, V. Berno, N. Rosenthal and F. Mourkioti (2010). "Distinct roles for cell-autonomous Notch signaling in cardiomyocytes of the embryonic and adult heart." Circ Res **106**(3): 559-572.

Kuhn, C., D. Frank, R. Will, C. Jaschinski, R. Frauen, H. A. Katus and N. Frey (2009). "DYRK1A is a novel negative regulator of cardiomyocyte hypertrophy." J Biol Chem **284**(25): 17320-17327.

Lallemand, D., M. Curto, I. Saotome, M. Giovannini and A. I. McClatchey (2003). "NF2 deficiency promotes tumorigenesis and metastasis by destabilizing adherens junctions." Genes Dev **17**(9): 1090-1100.

Lavine, K. J., S. Epelman, K. Uchida, K. J. Weber, C. G. Nichols, J. D. Schilling, D. M. Ornitz, G. J. Randolph and D. L. Mann (2014). "Distinct macrophage lineages contribute to disparate patterns of cardiac recovery and remodeling in the neonatal and adult heart." Proc Natl Acad Sci U S A **111**(45): 16029-16034.

Leach, J. P., T. Heallen, M. Zhang, M. Rahmani, Y. Morikawa, M. C. Hill, A. Segura, J. T. Willerson and J. F. Martin (2017). "Hippo pathway deficiency reverses systolic heart failure after infarction." Nature **550**(7675): 260-264.

Lee, K. P., J. H. Lee, T. S. Kim, T. H. Kim, H. D. Park, J. S. Byun, M. C. Kim, W. I. Jeong, D. F. Calvisi, J. M. Kim and D. S. Lim (2010). "The Hippo-Salvador pathway restrains hepatic oval cell proliferation, liver size, and liver tumorigenesis." Proc Natl Acad Sci U S A **107**(18): 8248-8253.

Lee, Y., C. Ahn, J. Han, H. Choi, J. Kim, J. Yim, J. Lee, P. Provost, O. Radmark, S. Kim and V. N. Kim (2003). "The nuclear RNase III Drosha initiates microRNA processing." Nature **425**(6956): 415-419.

Lenders, J. W., G. Eisenhofer, N. G. Abeling, W. Berger, D. L. Murphy, C. H. Konings, L. M. Wagemakers, I. J. Kopin, F. Karoum, A. H. van Gennip and H. G. Brunner (1996). "Specific genetic deficiencies of the A and B isoenzymes of monoamine oxidase are characterized by distinct neurochemical and clinical phenotypes." J Clin Invest **97**(4): 1010-1019.

Lepilina, A., A. N. Coon, K. Kikuchi, J. E. Holdway, R. W. Roberts, C. G. Burns and K. D. Poss (2006). "A dynamic epicardial injury response supports progenitor cell activity during zebrafish heart regeneration." Cell **127**(3): 607-619.

Lesizza, P., G. Prosdocimo, V. Martinelli, G. Sinagra, S. Zacchigna and M. Giacca (2017). "Single-Dose Intracardiac Injection of Pro-Regenerative MicroRNAs Improves Cardiac Function After Myocardial Infarction." Circ Res **120**(8): 1298-1304.

Lesurtel, M., R. Graf, B. Aleil, D. J. Walther, Y. Tian, W. Jochum, C. Gachet, M. Bader and P. A. Clavien (2006). "Platelet-derived serotonin mediates liver regeneration." Science **312**(5770): 104-107.

Li, F., X. Wang, J. M. Capasso and A. M. Gerdes (1996). "Rapid transition of cardiac myocytes from hyperplasia to hypertrophy during postnatal development." J Mol Cell Cardiol **28**(8): 1737-1746.

Li, Y., F. Liang, W. Jiang, F. Yu, R. Cao, Q. Ma, X. Dai, J. Jiang, Y. Wang and S. Si (2007). "DH334, a beta-carboline anti-cancer drug, inhibits the CDK activity of budding yeast." Cancer Biol Ther **6**(8): 1193-1199.

Li, Z., C. S. Yang, K. Nakashima and T. M. Rana (2011). "Small RNA-mediated regulation of iPS cell generation." EMBO J **30**(5): 823-834.

Lian, I., J. Kim, H. Okazawa, J. Zhao, B. Zhao, J. Yu, A. Chinnaiyan, M. A. Israel, L. S. Goldstein, R. Abujarour, S. Ding and K. L. Guan (2010). "The role of YAP transcription coactivator in regulating stem cell self-renewal and differentiation." Genes Dev **24**(11): 1106-1118.

Lin, C. W., Y. L. Chang, Y. C. Chang, J. C. Lin, C. C. Chen, S. H. Pan, C. T. Wu, H. Y. Chen, S. C. Yang, T. M. Hong and P. C. Yang (2013). "MicroRNA-135b promotes lung cancer metastasis by regulating multiple targets in the Hippo pathway and LZTS1." Nat Commun **4**: 1877.

Lin, L., A. J. Sabnis, E. Chan, V. Olivas, L. Cade, E. Pazarentzos, S. Asthana, D. Neel, J. J. Yan, X. Lu, L. Pham, M. M. Wang, N. Karachaliou, M. G. Cao, J. L. Manzano, J. L. Ramirez, J. M. Torres, F. Buttitta, C. M. Rudin, E. A. Collisson, A. Algazi, E. Robinson, I. Osman, E. Munoz-Couselo, J. Cortes, D. T. Frederick, Z. A. Cooper, M. McMahon, A. Marchetti, R. Rosell, K. T. Flaherty, J. A. Wargo and T. G. Bivona (2015). "The Hippo effector YAP promotes resistance to RAF- and MEK-targeted cancer therapies." Nat Genet **47**(3): 250-256.

Lin, Z., A. von Gise, P. Zhou, F. Gu, Q. Ma, J. Jiang, A. L. Yau, J. N. Buck, K. A. Gouin, P. R. van Gorp, B. Zhou, J. Chen, J. G. Seidman, D. Z. Wang and W. T. Pu (2014). "Cardiac-specific YAP activation improves cardiac function and survival in an experimental murine MI model." Circ Res **115**(3): 354-363.

Lin, Z., P. Zhou, A. von Gise, F. Gu, Q. Ma, J. Chen, H. Guo, P. R. van Gorp, D. Z. Wang and W. T. Pu (2015). "Pi3kcb links Hippo-YAP and PI3K-AKT signaling pathways to promote cardiomyocyte proliferation and survival." Circ Res **116**(1): 35-45.

Liu, J., Q. Li, Z. Liu, L. Lin, X. Zhang, M. Cao and J. Jiang (2016). "Harmine induces cell cycle arrest and mitochondrial pathway-mediated cellular apoptosis in SW620 cells via inhibition of the Akt and ERK signaling pathways." Oncol Rep **35**(6): 3363-3370.

Liu, P., H. Zhang, X. Liang, H. Ma, F. Luan, B. Wang, F. Bai, L. Gao and C. Ma (2015). "HBV preS2 promotes the expression of TAZ via miRNA-338-3p to enhance the tumorigenesis of hepatocellular carcinoma." Oncotarget **6**(30): 29048-29059.

Liu, X., L. F. Sempere, H. Ouyang, V. A. Memoli, A. S. Andrew, Y. Luo, E. Demidenko, M. Korc, W. Shi, M. Preis, K. H. Dragnev, H. Li, J. Direnzo, M. Bak, S. J. Freemantle, S. Kauppinen and E. Dmitrovsky (2010). "MicroRNA-31 functions as an oncogenic microRNA in mouse and human lung cancer cells by repressing specific tumor suppressors." J Clin Invest **120**(4): 1298-1309.

Low, B. C., C. Q. Pan, G. V. Shivashankar, A. Bershadsky, M. Sudol and M. Sheetz (2014). "YAP/TAZ as mechanosensors and mechanotransducers in regulating organ size and tumor growth." FEBS Lett **588**(16): 2663-2670.

Macmahon, H. E. (1937). "Hyperplasia and Regeneration of the Myocardium in Infants and in Children." Am J Pathol **13**(5): 845-854 845.

Mahmoud, A. I., F. Kocabas, S. A. Muralidhar, W. Kimura, A. S. Koura, S. Thet, E. R. Porrello and H. A. Sadek (2013). "Meis1 regulates postnatal cardiomyocyte cell cycle arrest." Nature **497**(7448): 249-253.

Mahmoud, A. I., C. C. O'Meara, M. Gemberling, L. Zhao, D. M. Bryant, R. Zheng, J. B. Gannon, L. Cai, W. Y. Choi, G. F. Egnaczyk, C. E. Burns, C. G. Burns, C. A. MacRae, K. D. Poss and R. T. Lee (2015). "Nerves Regulate Cardiomyocyte Proliferation and Heart Regeneration." Dev Cell **34**(4): 387-399.

Mahmoud, A. I. and E. R. Porrello (2012). "Turning back the cardiac regenerative clock: lessons from the neonate." Trends Cardiovasc Med **22**(5): 128-133.

Matsuki, T., G. Hori and T. Furuichi (2005). "Gene expression profiling during the embryonic development of mouse brain using an oligonucleotide-based microarray system." Brain Res Mol Brain Res **136**(1-2): 231-254.

Mattison, C. P., J. Stumpff, L. Wordeman and M. Winey (2011). "Mip1 associates with both the Mps1 kinase and actin, and is required for cell cortex stability and anaphase spindle positioning." Cell Cycle **10**(5): 783-793.

McCarthy, D. J., Y. Chen and G. K. Smyth (2012). "Differential expression analysis of multifactor RNA-Seq experiments with respect to biological variation." Nucleic Acids Res **40**(10): 4288-4297.

Meister, G., M. Landthaler, A. Patkaniowska, Y. Dorsett, G. Teng and T. Tuschl (2004). "Human Argonaute2 mediates RNA cleavage targeted by miRNAs and siRNAs." Mol Cell **15**(2): 185-197.

Meng, Z., T. Moroishi, V. Mottier-Pavie, S. W. Plouffe, C. G. Hansen, A. W. Hong, H. W. Park, J. S. Mo, W. Lu, S. Lu, F. Flores, F. X. Yu, G. Halder and K. L. Guan (2015). "MAP4K family kinases act in parallel to MST1/2 to activate LATS1/2 in the Hippo pathway." Nat Commun **6**: 8357.

Mitamura, T., H. Watari, L. Wang, H. Kanno, M. Kitagawa, M. K. Hassan, T. Kimura, M. Tanino, H. Nishihara, S. Tanaka and N. Sakuragi (2014). "microRNA 31 functions as an endometrial cancer oncogene by suppressing Hippo tumor suppressor pathway." Mol Cancer **13**: 97.

Molkentin, J. D., Q. Lin, S. A. Duncan and E. N. Olson (1997). "Requirement of the transcription factor GATA4 for heart tube formation and ventral morphogenesis." Genes Dev **11**(8): 1061-1072.

Mollova, M., K. Bersell, S. Walsh, J. Savla, L. T. Das, S. Y. Park, L. E. Silberstein, C. G. Dos Remedios, D. Graham, S. Colan and B. Kuhn (2013). "Cardiomyocyte proliferation contributes to heart growth in young humans." Proc Natl Acad Sci U S A **110**(4): 1446-1451.

Moloudizargari, M., P. Mikaili, S. Aghajanshakeri, M. H. Asghari and J. Shayegh (2013). "Pharmacological and therapeutic effects of Peganum harmala and its main alkaloids." Pharmacogn Rev **7**(14): 199-212.

Morikawa, Y., T. Heallen, J. Leach, Y. Xiao and J. F. Martin (2017). "Dystrophin-glycoprotein complex sequesters Yap to inhibit cardiomyocyte proliferation." Nature **547**(7662): 227-231.

Morikawa, Y., M. Zhang, T. Heallen, J. Leach, G. Tao, Y. Xiao, Y. Bai, W. Li, J. T. Willerson and J. F. Martin (2015). "Actin cytoskeletal remodeling with protrusion formation is essential for heart regeneration in Hippo-deficient mice." Sci Signal **8**(375): ra41.

Murakami, M., M. Nakagawa, E. N. Olson and O. Nakagawa (2005). "A WW domain protein TAZ is a critical coactivator for TBX5, a transcription factor implicated in Holt-Oram syndrome." Proc Natl Acad Sci U S A **102**(50): 18034-18039.

Nakada, Y., D. C. Canseco, S. Thet, S. Abdisalaam, A. Asaithamby, C. X. Santos, A. M. Shah, H. Zhang, J. E. Faber, M. T. Kinter, L. I. Szweda, C. Xing, Z. Hu, R. J. Deberardinis, G. Schiattarella, J. A. Hill, O. Oz, Z. Lu, C. C. Zhang, W. Kimura and H. A. Sadek (2017). "Hypoxia induces heart regeneration in adult mice." Nature **541**(7636): 222-227.

Nikonova, A. S., I. Astsaturov, I. G. Serebriiskii, R. L. Dunbrack, Jr. and E. A. Golemis (2013). "Aurora A kinase (AURKA) in normal and pathological cell division." Cell Mol Life Sci **70**(4): 661-687.

Nishio, M., K. Hamada, K. Kawahara, M. Sasaki, F. Noguchi, S. Chiba, K. Mizuno, S. O. Suzuki, Y. Dong, M. Tokuda, T. Morikawa, H. Hikasa, J. Eggenschwiler, N. Yabuta, H. Nojima, K. Nakagawa, Y. Hata, H. Nishina, K. Mimori, M. Mori, T. Sasaki, T. W. Mak, T. Nakano, S. Itami and A. Suzuki (2012). "Cancer susceptibility and embryonic lethality in Mob1a/1b double-mutant mice." J Clin Invest **122**(12): 4505-4518.

O'Leary, N. A., M. W. Wright, J. R. Brister, S. Ciufo, D. Haddad, R. McVeigh, B. Rajput, B. Robbertse, B. Smith-White, D. Ako-Adjei, A. Astashyn, A. Badretdin, Y. Bao, O. Blinkova, V. Brover, V. Chetvernin, J. Choi, E. Cox, O. Ermolaeva, C. M. Farrell, T. Goldfarb, T. Gupta, D. Haft, E. Hatcher, W. Hlavina, V. S. Joardar, V. K. Kodali, W. Li, D. Maglott, P. Masterson, K. M. McGarvey, M. R. Murphy, K. O'Neill, S.

Pujar, S. H. Rangwala, D. Rausch, L. D. Riddick, C. Schoch, A. Shkeda, S. S. Storz, H. Sun, F. Thibaud-Nissen, I. Tolstoy, R. E. Tully, A. R. Vatsan, C. Wallin, D. Webb, W. Wu, M. J. Landrum, A. Kimchi, T. Tatusova, M. DiCuccio, P. Kitts, T. D. Murphy and K. D. Pruitt (2016). "Reference sequence (RefSeq) database at NCBI: current status, taxonomic expansion, and functional annotation." Nucleic Acids Res **44**(D1): D733-745.

O'Meara, C. C., J. A. Wamstad, R. A. Gladstone, G. M. Fomovsky, V. L. Butty, A. Shrikumar, J. B. Gannon, L. A. Boyer and R. T. Lee (2015). "Transcriptional reversion of cardiac myocyte fate during mammalian cardiac regeneration." Circ Res **116**(5): 804-815.

Oberpriller, J. O. and J. C. Oberpriller (1974). "Response of the adult newt ventricle to injury." J Exp Zool **187**(2): 249-253.

Oie, E., W. J. Sandberg, M. S. Ahmed, A. Yndestad, O. D. Laerum, H. Attramadal, P. Aukrust and H. G. Eiken (2010). "Activation of Notch signaling in cardiomyocytes during post-infarction remodeling." Scand Cardiovasc J **44**(6): 359-366.

Oka, T., A. P. Schmitt and M. Sudol (2012). "Opposing roles of angiomotin-like-1 and zona occludens-2 on pro-apoptotic function of YAP." Oncogene **31**(1): 128-134.

Orlic, D., J. Kajstura, S. Chimenti, I. Jakoniuk, S. M. Anderson, B. Li, J. Pickel, R. McKay, B. Nadal-Ginard, D. M. Bodine, A. Leri and P. Anversa (2001). "Bone marrow cells regenerate infarcted myocardium." Nature **410**(6829): 701-705.

Osada, H. and T. Takahashi (2007). "MicroRNAs in biological processes and carcinogenesis." Carcinogenesis **28**(1): 2-12.

Papalouka, V., D. A. Arvanitis, E. Vafiadaki, M. Mavroidis, S. A. Papadodima, C. A. Spiliopoulou, D. T. Kremastinos, E. G. Kranias and D. Sanoudou (2009). "Muscle LIM protein interacts with cofilin 2 and regulates F-actin dynamics in cardiac and skeletal muscle." Mol Cell Biol **29**(22): 6046-6058.

Patel, K., M. Gadewar, R. Tripathi, S. K. Prasad and D. K. Patel (2012). "A review on medicinal importance, pharmacological activity and bioanalytical aspects of beta-carboline alkaloid "Harmine"." Asian Pac J Trop Biomed **2**(8): 660-664.

Penton, A. L., L. D. Leonard and N. B. Spinner (2012). "Notch signaling in human development and disease." Semin Cell Dev Biol **23**(4): 450-457.

Perez-Pomares, J. M., J. M. Gonzalez-Rosa and R. Munoz-Chapuli (2009). "Building the vertebrate heart - an evolutionary approach to cardiac development." Int J Dev Biol **53**(8-10): 1427-1443.

Philippen, L. E., E. Dirkx, P. A. da Costa-Martins and L. J. De Windt (2015). "Non-coding RNA in control of gene regulatory programs in cardiac development and disease." J Mol Cell Cardiol **89**(Pt A): 51-58.

Piccolo, S., S. Dupont and M. Cordenonsi (2014). "The biology of YAP/TAZ: hippo signaling and beyond." Physiol Rev **94**(4): 1287-1312.

Plouffe, S. W., Z. Meng, K. C. Lin, B. Lin, A. W. Hong, J. V. Chun and K. L. Guan (2016). "Characterization of Hippo Pathway Components by Gene Inactivation." Mol Cell **64**(5): 993-1008.

Porrello, E. R., A. I. Mahmoud, E. Simpson, J. A. Hill, J. A. Richardson, E. N. Olson and H. A. Sadek (2011). "Transient regenerative potential of the neonatal mouse heart." Science **331**(6020): 1078-1080.

Porrello, E. R., A. I. Mahmoud, E. Simpson, B. A. Johnson, D. Grinsfelder, D. Canseco, P. P. Mammen, B. A. Rothermel, E. N. Olson and H. A. Sadek (2013). "Regulation of neonatal and adult mammalian heart regeneration by the miR-15 family." Proc Natl Acad Sci U S A **110**(1): 187-192.

Poss, K. D., L. G. Wilson and M. T. Keating (2002). "Heart regeneration in zebrafish." Science **298**(5601): 2188-2190.

Pozo, N., C. Zahonero, P. Fernandez, J. M. Linares, A. Ayuso, M. Hagiwara, A. Perez, J. R. Ricoy, A. Hernandez-Lain, J. M. Sepulveda and P. Sanchez-Gomez (2013). "Inhibition of DYRK1A destabilizes EGFR and reduces EGFR-dependent glioblastoma growth." J Clin Invest **123**(6): 2475-2487.

Puente, B. N., W. Kimura, S. A. Muralidhar, J. Moon, J. F. Amatruda, K. L. Phelps, D. Grinsfelder, B. A. Rothermel, R. Chen, J. A. Garcia, C. X. Santos, S. Thet, E. Mori, M. T. Kinter, P. M. Rindler, S. Zacchigna, S. Mukherjee, D. J. Chen, A. I. Mahmoud, M. Giacca, P. S. Rabinovitch, A. Aroumougame, A. M. Shah, L. I. Szweda and H. A. Sadek (2014). "The oxygen-rich postnatal environment induces cardiomyocyte cell-cycle arrest through DNA damage response." Cell **157**(3): 565-579.

Qin, H., M. Hejna, Y. Liu, M. Percharde, M. Wossidlo, L. Blouin, J. Durruthy-Durruthy, P. Wong, Z. Qi, J. Yu, L. S. Qi, V. Sebastiano, J. S. Song and M. Ramalho-Santos (2016). "YAP Induces Human Naive Pluripotency." Cell Rep **14**(10): 2301-2312.

Radhakrishnan, A., V. Nanjappa, R. Raja, G. Sathe, V. N. Puttamallesh, A. P. Jain, S. M. Pinto, S. A. Balaji, S. Chavan, N. A. Sahasrabuddhe, P. P. Mathur, M. M. Kumar, T. S. Prasad, V. Santosh, G. Sukumar, J. A. Califano, A. Rangarajan, D. Sidransky, A. Pandey, H. Gowda and A. Chatterjee (2016). "A dual specificity kinase, DYRK1A, as a potential therapeutic target for head and neck squamous cell carcinoma." Sci Rep **6**: 36132.

Raya, A., C. M. Koth, D. Buscher, Y. Kawakami, T. Itoh, R. M. Raya, G. Sternik, H. J. Tsai, C. Rodriguez-Esteban and J. C. Izpisua-Belmonte (2003). "Activation of Notch signaling pathway precedes heart regeneration in zebrafish." Proc Natl Acad Sci U S A **100 Suppl 1**: 11889-11895.

Reese, D. E., T. Mikawa and D. M. Bader (2002). "Development of the coronary vessel system." Circ Res **91**(9): 761-768.

Rhoades, M. W., B. J. Reinhart, L. P. Lim, C. B. Burge, B. Bartel and D. P. Bartel (2002). "Prediction of plant microRNA targets." Cell **110**(4): 513-520.

Ritchey, L. and R. Chakrabarti (2014). "Aurora A kinase modulates actin cytoskeleton through phosphorylation of Cofilin: Implication in the mitotic process." Biochim Biophys Acta **1843**(11): 2719-2729.

Ruan, T., X. He, J. Yu and Z. Hang (2016). "MicroRNA-186 targets Yes-associated protein 1 to inhibit Hippo signaling and tumorigenesis in hepatocellular carcinoma." Oncol Lett **11**(4): 2941-2945.

Russell, J. L., S. C. Goetsch, H. R. Aguilar, H. Coe, X. Luo, N. Liu, E. van Rooij, D. E. Frantz and J. W. Schneider (2012). "Regulated expression of pH sensing G Protein-coupled receptor-68 identified through chemical biology defines a new drug target for ischemic heart disease." ACS Chem Biol **7**(6): 1077-1083.

Sahara, M., F. Santoro and K. R. Chien (2015). "Programming and reprogramming a human heart cell." EMBO J **34**(6): 710-738.

Saker, D. M., M. Walsh-Sukys, M. Spector and K. G. Zahka (1997). "Cardiac recovery and survival after neonatal myocardial infarction." Pediatr Cardiol **18**(2): 139-142.

Sasaki, T., H. Hwang, C. Nguyen, R. A. Kloner and M. Kahn (2013). "The small molecule Wnt signaling modulator ICG-001 improves contractile function in chronically infarcted rat myocardium." PLoS One **8**(9): e75010.

Sattler, S. and N. Rosenthal (2016). "The neonate versus adult mammalian immune system in cardiac repair and regeneration." Biochim Biophys Acta **1863**(7 Pt B): 1813-1821.

Schindler, Y. L., K. M. Garske, J. Wang, B. A. Firulli, A. B. Firulli, K. D. Poss and D. Yelon (2014). "Hand2 elevates cardiomyocyte production during zebrafish heart development and regeneration." Development **141**(16): 3112-3122.

Schuchardt, B. J., V. Bhat, D. C. Mikles, C. B. McDonald, M. Sudol and A. Farooq (2014). "Molecular basis of the binding of YAP transcriptional regulator to the ErbB4 receptor tyrosine kinase." Biochimie **101**: 192-202.

Senyo, S. E., R. T. Lee and B. Kuhn (2014). "Cardiac regeneration based on mechanisms of cardiomyocyte proliferation and differentiation." Stem Cell Res **13**(3 Pt B): 532-541.

Senyo, S. E., M. L. Steinhauser, C. L. Pizzimenti, V. K. Yang, L. Cai, M. Wang, T. D. Wu, J. L. Guerquin-Kern, C. P. Lechene and R. T. Lee (2013). "Mammalian heart renewal by pre-existing cardiomyocytes." Nature **493**(7432): 433-436.

Shao, D., P. Zhai, D. P. Del Re, S. Sciarretta, N. Yabuta, H. Nojima, D. S. Lim, D. Pan and J. Sadoshima (2014). "A functional interaction between Hippo-YAP signalling and FoxO1 mediates the oxidative stress response." Nat Commun **5**: 3315.

Shao, D. D., W. Xue, E. B. Krall, A. Bhutkar, F. Piccioni, X. Wang, A. C. Schinzel, S. Sood, J. Rosenbluh, J. W. Kim, Y. Zwang, T. M. Roberts, D. E. Root, T. Jacks and W. C. Hahn (2014). "KRAS and YAP1 converge to regulate EMT and tumor survival." Cell **158**(1): 171-184.

Shen, S., X. Guo, H. Yan, Y. Lu, X. Ji, L. Li, T. Liang, D. Zhou, X. H. Feng, J. C. Zhao, J. Yu, X. G. Gong, L. Zhang and B. Zhao (2015). "A miR-130a-YAP positive feedback loop promotes organ size and tumorigenesis." Cell Res **25**(9): 997-1012.

Shih, J. C., K. Chen and M. J. Ridd (1999). "Role of MAO A and B in neurotransmitter metabolism and behavior." Pol J Pharmacol **51**(1): 25-29.

Shimomura, T., N. Miyamura, S. Hata, R. Miura, J. Hirayama and H. Nishina (2014). "The PDZ-binding motif of Yes-associated protein is required for its co-activation of TEAD-mediated CTGF transcription and oncogenic cell transforming activity." Biochem Biophys Res Commun **443**(3): 917-923.

Shindoh, N., J. Kudoh, H. Maeda, A. Yamaki, S. Minoshima, Y. Shimizu and N. Shimizu (1996). "Cloning of a human homolog of the Drosophila minibrain/rat Dyrk gene from "the Down syndrome critical region" of chromosome 21." Biochem Biophys Res Commun **225**(1): 92-99.

Sirbulescu, R. F. and G. K. Zupanc (2010). "Effect of temperature on spinal cord regeneration in the weakly electric fish, Apteronotus leptorhynchus." J Comp Physiol A Neuroethol Sens Neural Behav Physiol **196**(5): 359-368.

Smith, A. M., K. K. Maguire-Nguyen, T. A. Rando, M. A. Zasloff, K. B. Strange and V. P. Yin (2017). "The protein tyrosine phosphatase 1B inhibitor MSI-1436 stimulates regeneration of heart and multiple other tissues." NPJ Regen Med **2**: 4.

Smith, R. R., L. Barile, H. C. Cho, M. K. Leppo, J. M. Hare, E. Messina, A. Giacomello, M. R. Abraham and E. Marban (2007). "Regenerative potential of cardiosphere-derived cells expanded from percutaneous endomyocardial biopsy specimens." Circulation **115**(7): 896-908.

Sobhani, A. M., S. A. Ebrahimi and M. Mahmoudian (2002). "An in vitro evaluation of human DNA topoisomerase I inhibition by Peganum harmala L. seeds extract and its beta-carboline alkaloids." J Pharm Pharm Sci **5**(1): 19-23.

Soonpaa, M. H. and L. J. Field (1997). "Assessment of cardiomyocyte DNA synthesis in normal and injured adult mouse hearts." Am J Physiol **272**(1 Pt 2): H220-226.

Stegert, M. R., A. Hergovich, R. Tamaskovic, S. J. Bichsel and B. A. Hemmings (2005). "Regulation of NDR protein kinase by hydrophobic motif phosphorylation mediated by the mammalian Ste20-like kinase MST3." Mol Cell Biol **25**(24): 11019-11029.

Storch, A., Y. I. Hwang, D. A. Gearhart, J. W. Beach, E. J. Neafsey, M. A. Collins and J. Schwarz (2004). "Dopamine transporter-mediated cytotoxicity of beta-carbolinium derivatives related to Parkinson's disease: relationship to transporter-dependent uptake." J Neurochem **89**(3): 685-694.

Sudol, M. (1994). "Yes-associated protein (YAP65) is a proline-rich phosphoprotein that binds to the SH3 domain of the Yes proto-oncogene product." Oncogene **9**(8): 2145-2152.

Sun, M., H. Song, S. Wang, C. Zhang, L. Zheng, F. Chen, D. Shi, Y. Chen, C. Yang, Z. Xiang, Q. Liu, C. Wei and B. Xiong (2017). "Integrated analysis identifies microRNA-195 as a suppressor of Hippo-YAP pathway in colorectal cancer." J Hematol Oncol **10**(1): 79.

Tattersall, G. J., T. M. Tyson, J. R. Lenchyshyn and R. L. Carlone (2012). "Temperature preference during forelimb regeneration in the red-spotted newt Notophthalmus viridescens." J Exp Zool A Ecol Genet Physiol **317**(4): 248-258.

Tian, Y., Y. Liu, T. Wang, N. Zhou, J. Kong, L. Chen, M. Snitow, M. Morley, D. Li, N. Petrenko, S. Zhou, M. Lu, E. Gao, W. J. Koch, K. M. Stewart and E. E. Morrisey (2015). "A microRNA-Hippo pathway that promotes cardiomyocyte proliferation and cardiac regeneration in mice." Sci Transl Med **7**(279): 279ra238.

Tomari, Y., C. Matranga, B. Haley, N. Martinez and P. D. Zamore (2004). "A protein sensor for siRNA asymmetry." Science **306**(5700): 1377-1380.

Tourneux, P., J. P. Libert, L. Ghyselen, A. Leke, S. Delanaud, L. Degrugilliers and V. Bach (2009). "[Heat exchanges and thermoregulation in the neonate]." Arch Pediatr **16**(7): 1057-1062.

Trivedi, C. M., W. Zhu, Q. Wang, C. Jia, H. J. Kee, L. Li, S. Hannenhalli and J. A. Epstein (2010). "Hopx and Hdac2 interact to modulate Gata4 acetylation and embryonic cardiac myocyte proliferation." Dev Cell **19**(3): 450-459.

Tsika, R. W., L. Ma, I. Kehat, C. Schramm, G. Simmer, B. Morgan, D. M. Fine, L. M. Hanft, K. S. McDonald, J. D. Molkentin, M. Krenz, S. Yang and J. Ji (2010). "TEAD-1 overexpression in the mouse heart promotes an age-dependent heart dysfunction." J Biol Chem **285**(18): 13721-13735.

Tumaneng, K., K. Schlegelmilch, R. C. Russell, D. Yimlamai, H. Basnet, N. Mahadevan, J. Fitamant, N. Bardeesy, F. D. Camargo and K. L. Guan (2012). "YAP mediates crosstalk between the Hippo and PI(3)K-TOR pathways by suppressing PTEN via miR-29." Nat Cell Biol **14**(12): 1322-1329.

Ueno, S., G. Weidinger, T. Osugi, A. D. Kohn, J. L. Golob, L. Pabon, H. Reinecke, R. T. Moon and C. E. Murry (2007). "Biphasic role for Wnt/beta-catenin signaling in cardiac specification in zebrafish and embryonic stem cells." Proc Natl Acad Sci U S A **104**(23): 9685-9690.

van Amerongen, M. J. and F. B. Engel (2008). "Features of cardiomyocyte proliferation and its potential for cardiac regeneration." J Cell Mol Med **12**(6A): 2233-2244.

van Rooij, E. and S. Kauppinen (2014). "Development of microRNA therapeutics is coming of age." EMBO Mol Med **6**(7): 851-864.

Vasudevan, S. and J. A. Steitz (2007). "AU-rich-element-mediated upregulation of translation by FXR1 and Argonaute 2." Cell **128**(6): 1105-1118.

von Gise, A., Z. Lin, K. Schlegelmilch, L. B. Honor, G. M. Pan, J. N. Buck, Q. Ma, T. Ishiwata, B. Zhou, F. D. Camargo and W. T. Pu (2012). "YAP1, the nuclear target of Hippo signaling, stimulates heart growth through cardiomyocyte proliferation but not hypertrophy." Proc Natl Acad Sci U S A **109**(7): 2394-2399.

Wada, K., K. Itoga, T. Okano, S. Yonemura and H. Sasaki (2011). "Hippo pathway regulation by cell morphology and stress fibers." Development **138**(18): 3907-3914.

Waki, H., K. W. Park, N. Mitro, L. Pei, R. Damoiseaux, D. C. Wilpitz, K. Reue, E. Saez and P. Tontonoz (2007). "The small molecule harmine is an antidiabetic cell-type-specific regulator of PPARgamma expression." Cell Metab **5**(5): 357-370.

Walte, A., K. Ruben, R. Birner-Gruenberger, C. Preisinger, S. Bamberg-Lemper, N. Hilz, F. Bracher and W. Becker (2013). "Mechanism of dual specificity kinase activity of DYRK1A." FEBS J **280**(18): 4495-4511.

Wang, P., J. C. Alvarez-Perez, D. P. Felsenfeld, H. Liu, S. Sivendran, A. Bender, A. Kumar, R. Sanchez, D. K. Scott, A. Garcia-Ocana and A. F. Stewart (2015). "A high-throughput chemical screen reveals that harmine-mediated inhibition of DYRK1A increases human pancreatic beta cell replication." Nat Med **21**(4): 383-388.

White, I. A., J. Gordon, W. Balkan and J. M. Hare (2015). "Sympathetic Reinnervation Is Required for Mammalian Cardiac Regeneration." Circ Res **117**(12): 990-994.

Willems, E., S. Spiering, H. Davidovics, M. Lanier, Z. Xia, M. Dawson, J. Cashman and M. Mercola (2011). "Small-molecule inhibitors of the Wnt pathway potently promote cardiomyocytes from human embryonic stem cell-derived mesoderm." Circ Res **109**(4): 360-364.

Writing Group, M., D. Mozaffarian, E. J. Benjamin, A. S. Go, D. K. Arnett, M. J. Blaha, M. Cushman, S. R. Das, S. de Ferranti, J. P. Despres, H. J. Fullerton, V. J. Howard, M. D. Huffman, C. R. Isasi, M. C. Jimenez, S. E. Judd, B. M. Kissela, J. H. Lichtman, L. D. Lisabeth, S. Liu, R. H. Mackey, D. J. Magid, D. K. McGuire, E. R. Mohler, 3rd, C. S. Moy, P. Muntner, M. E. Mussolino, K. Nasir, R. W. Neumar, G. Nichol, L. Palaniappan, D. K. Pandey, M. J. Reeves, C. J. Rodriguez, W. Rosamond, P. D. Sorlie, J. Stein, A. Towfighi, T. N. Turan, S. S. Virani, D. Woo, R. W. Yeh, M. B. Turner, C. American Heart Association Statistics and S. Stroke Statistics (2016). "Executive Summary: Heart Disease and Stroke Statistics--2016 Update: A Report From the American Heart Association." Circulation **133**(4): 447-454.

Wu, H., Y. Xiao, S. Zhang, S. Ji, L. Wei, F. Fan, J. Geng, J. Tian, X. Sun, F. Qin, C. Jin, J. Lin, Z. Y. Yin, T. Zhang, L. Luo, Y. Li, S. Song, S. C. Lin, X. Deng, F. Camargo, J. Avruch, L. Chen and D. Zhou (2013). "The Ets transcription factor GABP is a component of the hippo pathway essential for growth and antioxidant defense." Cell Rep **3**(5): 1663-1677.

Wu, S., Y. Liu, Y. Zheng, J. Dong and D. Pan (2008). "The TEAD/TEF family protein Scalloped mediates transcriptional output of the Hippo growth-regulatory pathway." Dev Cell **14**(3): 388-398.

Xiao, Y., J. Leach, J. Wang and J. F. Martin (2016). "Hippo/Yap Signaling in Cardiac Development and Regeneration." Curr Treat Options Cardiovasc Med **18**(6): 38.

Xin, M., Y. Kim, L. B. Sutherland, M. Murakami, X. Qi, J. McAnally, E. R. Porrello, A. I. Mahmoud, W. Tan, J. M. Shelton, J. A. Richardson, H. A. Sadek, R. Bassel-Duby and E. N. Olson (2013). "Hippo pathway effector Yap promotes cardiac regeneration." Proc Natl Acad Sci U S A **110**(34): 13839-13844.

Xin, M., Y. Kim, L. B. Sutherland, X. Qi, J. McAnally, R. J. Schwartz, J. A. Richardson, R. Bassel-Duby and E. N. Olson (2011). "Regulation of insulin-like growth factor signaling by Yap governs cardiomyocyte proliferation and embryonic heart size." Sci Signal **4**(196): ra70.

Xin, M., E. N. Olson and R. Bassel-Duby (2013). "Mending broken hearts: cardiac development as a basis for adult heart regeneration and repair." Nat Rev Mol Cell Biol **14**(8): 529-541.

Xu, T., W. Wang, S. Zhang, R. A. Stewart and W. Yu (1995). "Identifying tumor suppressors in genetic mosaics: the Drosophila lats gene encodes a putative protein kinase." Development **121**(4): 1053-1063.

Xue, B. and R. C. Robinson (2013). "Guardians of the actin monomer." Eur J Cell Biol **92**(10-11): 316-332.

Yamamoto, S., G. Yang, D. Zablocki, J. Liu, C. Hong, S. J. Kim, S. Soler, M. Odashima, J. Thaisz, G. Yehia, C. A. Molina, A. Yatani, D. E. Vatner, S. F. Vatner and J. Sadoshima (2003). "Activation of Mst1 causes dilated cardiomyopathy by stimulating apoptosis without compensatory ventricular myocyte hypertrophy." J Clin Invest **111**(10): 1463-1474.

Yenari, M. A. and H. S. Han (2013). "Influence of therapeutic hypothermia on regeneration after cerebral ischemia." Front Neurol Neurosci **32**: 122-128.

Yonezawa, T., S. Hasegawa, M. Asai, T. Ninomiya, T. Sasaki, B. Y. Cha, T. Teruya, H. Ozawa, K. Yagasaki, K. Nagai and J. T. Woo (2011). "Harmine, a beta-carboline alkaloid, inhibits osteoclast differentiation and bone resorption in vitro and in vivo." Eur J Pharmacol **650**(2-3): 511-518.

Yu, F. X., B. Zhao, N. Panupinthu, J. L. Jewell, I. Lian, L. H. Wang, J. Zhao, H. Yuan, K. Tumaneng, H. Li, X. D. Fu, G. B. Mills and K. L. Guan (2012). "Regulation of the Hippo-YAP pathway by G-protein-coupled receptor signaling." Cell **150**(4): 780-791.

Yuan, J., G. Xiao, G. Peng, D. Liu, Z. Wang, Y. Liao, Q. Liu, M. Wu and X. Yuan (2015). "MiRNA-125a-5p inhibits glioblastoma cell proliferation and promotes cell differentiation by targeting TAZ." Biochem Biophys Res Commun **457**(2): 171-176.

Zacchigna, S., L. Zentilin and M. Giacca (2014). "Adeno-associated virus vectors as therapeutic and investigational tools in the cardiovascular system." Circ Res **114**(11): 1827-1846.

Zaidi, S. K., A. J. Sullivan, R. Medina, Y. Ito, A. J. van Wijnen, J. L. Stein, J. B. Lian and G. S. Stein (2004). "Tyrosine phosphorylation controls Runx2-mediated subnuclear targeting of YAP to repress transcription." EMBO J **23**(4): 790-799.

Zangi, L., K. O. Lui, A. von Gise, Q. Ma, W. Ebina, L. M. Ptaszek, D. Spater, H. Xu, M. Tabebordbar, R. Gorbatov, B. Sena, M. Nahrendorf, D. M. Briscoe, R. A. Li, A. J. Wagers, D. J. Rossi, W. T. Pu and K. R. Chien (2013). "Modified mRNA directs the fate of heart progenitor cells and induces vascular regeneration after myocardial infarction." Nat Biotechnol **31**(10): 898-907.

Zeng, Y., R. Yi and B. R. Cullen (2005). "Recognition and cleavage of primary microRNA precursors by the nuclear processing enzyme Drosha." EMBO J **24**(1): 138-148.

Zhang, L., F. Tang, L. Terracciano, D. Hynx, R. Kohler, S. Bichet, D. Hess, P. Cron, B. A. Hemmings, A. Hergovich and D. Schmitz-Rohmer (2015). "NDR functions as a physiological YAP1 kinase in the intestinal epithelium." Curr Biol **25**(3): 296-305.

Zhang, L., F. Zhang, W. Zhang, L. Chen, N. Gao, Y. Men, X. Xu and Y. Jiang (2015). "Harmine suppresses homologous recombination repair and inhibits proliferation of hepatoma cells." Cancer Biol Ther **16**(11): 1585-1592.

Zhang, R., P. Han, H. Yang, K. Ouyang, D. Lee, Y. F. Lin, K. Ocorr, G. Kang, J. Chen, D. Y. Stainier, D. Yelon and N. C. Chi (2013). "In vivo cardiac reprogramming contributes to zebrafish heart regeneration." Nature **498**(7455): 497-501.

Zhao, B., L. Li, Q. Lei and K. L. Guan (2010). "The Hippo-YAP pathway in organ size control and tumorigenesis: an updated version." Genes Dev **24**(9): 862-874.

Zhao, B., L. Li, K. Tumaneng, C. Y. Wang and K. L. Guan (2010). "A coordinated phosphorylation by Lats and CK1 regulates YAP stability through SCF(beta-TRCP)." Genes Dev **24**(1): 72-85.

Zhao, B., X. Ye, J. Yu, L. Li, W. Li, S. Li, J. Yu, J. D. Lin, C. Y. Wang, A. M. Chinnaiyan, Z. C. Lai and K. L. Guan (2008). "TEAD mediates YAP-dependent gene induction and growth control." Genes Dev **22**(14): 1962-1971.

Zhao, K., C. Shen, Y. Lu, Z. Huang, L. Li, C. D. Rand, J. Pan, X. D. Sun, Z. Tan, H. Wang, G. Xing, Y. Cao, G. Hu, J. Zhou, W. C. Xiong and L. Mei (2017). "Muscle Yap Is a Regulator of Neuromuscular Junction Formation and Regeneration." J Neurosci **37**(13): 3465-3477.

Zhao, P., G. Caretti, S. Mitchell, W. L. McKeehan, A. L. Boskey, L. M. Pachman, V. Sartorelli and E. P. Hoffman (2006). "Fgfr4 is required for effective muscle regeneration in vivo. Delineation of a MyoD-Tead2-Fgfr4 transcriptional pathway." J Biol Chem **281**(1): 429-438.

Zhao, Y., E. Samal and D. Srivastava (2005). "Serum response factor regulates a muscle-specific microRNA that targets Hand2 during cardiogenesis." Nature **436**(7048): 214-220.

Zhou, Y., C. Zhang and W. Liang (2014). "Development of RNAi technology for targeted therapy--a track of siRNA based agents to RNAi therapeutics." J Control Release **193**: 270-281.

Zhu, G., Y. Wang, M. Mijiti, Z. Wang, P. F. Wu and D. Jiafu (2015). "Upregulation of miR-130b enhances stem cell-like phenotype in glioblastoma by inactivating the Hippo signaling pathway." Biochem Biophys Res Commun **465**(2): 194-199.

Zuo, Q. F., R. Zhang, B. S. Li, Y. L. Zhao, Y. Zhuang, T. Yu, L. Gong, S. Li, B. Xiao and Q. M. Zou (2015). "MicroRNA-141 inhibits tumor growth and metastasis in gastric cancer by directly targeting transcriptional co-activator with PDZ-binding motif, TAZ." Cell Death Dis **6**: e1623.

Table 1. Hippo-related genes. An update catalogue of genes known to have a role in the regulation of YAP-Hippo pathway are reported in the table. For each gene are reported its expression (RPKM) in fold changes (log2) for each miRNA treatment and the bioinformatic prediction according to TargetScan software.

Rat Gene Name	Entrez Gene ID	Ensembl Gene ID	NCBI Gene Description	Transcriptome Expression (RPKM)								log2(Fold Change)						Bioinformatic Targeting Prediction (TargetScan)						Function/Interaction	References
				lipo	mir.1825	mir.199	mir.302d	mir.33b	mir.373	mir.590	mir.67	mir.1825	mir.199	mir.302d	mir.33b	mir.373	mir.590	mir.1825	mir.199	mir.302d	mir.33b	mir.373	mir.590		
CORE HIPPO CASSETTE																									
Taok1	286993	ENSRNOG00000015692	TAO kinase 1	32,29	31,99	22,20	29,50	31,00	34,34	29,93	31,51	0,02	-0,51	-0,10	-0,02	0,12	-0,07	-0,02	-0,23	-0,10	-0,45	-0,10	-0,04	Phosphorylates Stk3/4 to activate Hippo Pathway	PMID: 22075147 PMID: 22075148 PMID: 23431053
Stk3	65189	ENSRNOG00000011278	serine/threonine kinase 3	1,54	1,50	1,88	2,07	1,84	2,05	1,62	1,57	-0,07	0,25	0,40	0,23	0,38	0,05	-	-	-	-	-	-	Forms a complex with Sav1 which can then phosphorylate Lats1/2-	PMID: 12941273 PMID: 15688006 PMID: 16930133 PMID:
Stk4	311622	ENSRNOG00000013529	serine/threonine kinase 4	8,85	11,49	11,35	9,45	8,16	10,03	10,41	8,35	0,46	0,44	0,18	-0,03	0,26	0,32	0,00	0,00	-0,15	-0,05	-0,15	-0,01	Forms a complex with Sav1 which can then phosphorylate Lats1/2-	PMID: 12941273 PMID: 15688006 PMID: 16930133 PMID:
Sav1	299116	ENSRNOG00000005264	salvador family WW domain containing protein 1	18,16	17,62	20,88	14,40	17,07	14,83	20,40	15,68	0,17	0,41	-0,12	0,12	-0,08	0,38	0,00	0,00	0,00	0,00	0,00	-0,11	Forms a complex with Stk3/4 which can then phosphorylate Lats1/2-	PMID: 16930133 PMID: 23431053
Lats1	308265	ENSRNOG00000014916	large tumor suppressor kinase 1	4,33	4,83	4,91	3,29	2,98	3,63	3,60	4,67	0,05	0,07	-0,50	-0,65	-0,36	-0,38	-	-	-	-	-	-	Forms a complex with Mob1 which phosphorylates	PMID: 15688006 PMID: 23431053
Lats2	305922	ENSRNOG00000056343	large tumor suppressor kinase 2	7,69	6,31	9,23	3,15	6,68	3,09	7,44	8,22	-0,38	0,17	-1,38	-0,30	-1,41	-0,14	0,00	0,00	-	0,00	-	-0,06	Forms a complex with Mob1 which phosphorylates	PMID: 15688006 PMID: 23431053
Mob1a	297387	ENSRNOG00000059474	MOB kinase activator 1A	22,23	26,30	23,30	17,41	21,60	20,40	25,29	22,71	0,21	0,04	-0,38	-0,07	-0,15	0,16	0,00	-0,15	0,00	0,00	0,00	-0,08	Forms a complex with Lats1/2	PMID: 15688006 PMID: 18328708 PMID: 23431053
Mob1b	360920	ENSRNOG00000010996	MOB kinase activator 1B	16,56	20,37	20,44	20,61	22,00	19,92	14,81	17,02	0,26	0,26	0,28	0,37	0,23	-0,20	-0,05	-0,23	-0,06	0,00	-0,06	-0,10	Forms a complex with Lats1/2	PMID: 15688006 PMID: 18328708 PMID: 23431053
Mob2	499288	ENSRNOG00000020044	MOB kinase activator 2	14,43	12,89	11,22	11,79	13,01	10,78	11,75	14,44	-0,16	-0,36	-0,29	-0,15	-0,42	-0,30	-0,24	0,00	0,00	0,00	0,00	0,00	Mediates an inhibitory interaction with NDR1/2	PMID: 20624913 PMID: 26728553
Yap1	363014	ENSRNOG00000005933	yes-associated protein 1	1,74	1,91	2,18	1,89	1,85	1,97	1,94	1,39	0,45	0,65	0,44	0,41	0,50	0,47	-	-	-	-	-	-	Phosphorylated form can be bound by 14-3-3 protein leading to	PMID: 20951342 PMID: 20439427 PMID: 23431053
Wwtr1	295062	ENSRNOG00000016617	WW domain containing transcription	24,07	30,59	25,25	18,32	19,13	15,47	21,21	20,76	0,56	0,28	-0,18	-0,12	-0,42	0,03	0,00	0,00	0,00	0,00	0,00	-0,10	Phosphorylated form can be bound by 14-3-3 protein leading to	PMID: 20951342 PMID: 20439427 PMID: 23431053
Tead1	361630	ENSRNOG00000015488	TEA domain transcription factor 1	0,85	0,86	1,00	0,75	0,83	0,77	0,85	0,84	-	-	-	-	-	-	-	-	-	-	-	-	Yap1/Wwtr1 are transcriptional coactivators of Tead1-4	PMID: 18579750 PMID: 23431053
Tead2	308582	ENSRNOG00000020695	TEA domain transcription factor 2	1,62	1,09	2,33	2,56	2,90	2,35	1,88	1,51	-0,48	0,62	0,76	0,94	0,63	0,31	-	-	-	-	-	-	Yap1/Wwtr1 are transcriptional coactivators of Tead1-4	PMID: 18579750 PMID: 23431053
Tead3	294299	ENSRNOG00000000506	TEA domain transcription factor 3	9,24	9,34	10,46	6,34	8,52	6,30	8,55	10,11	-0,11	0,05	-0,67	-0,25	-0,68	-0,24	0,00	0,00	0,00	0,00	0,00	0,00	Yap1/Wwtr1 are transcriptional coactivators of Tead1-4	PMID: 18579750 PMID: 23431053
Tead4	683522		TEA domain transcription factor 4	0,64	0,76	1,23	0,63	0,44	0,73	0,77	0,57	-	-	-	-	-	-	-	-	-	-	-	-	Yap1/Wwtr1 are transcriptional coactivators of Tead1-4	PMID: 18579750 PMID: 23431053
NON-CANONICAL PATHWAY																									
Abl2	304883	ENSRNOG00000004305	ABL proto-oncogene 2, non-receptor tyrosine kinase	0,40	0,36	0,30	0,47	0,44	0,49	0,45	0,35	0,04	-0,22	0,42	0,32	0,48	0,36	-0,25	-0,07	-0,12	-0,02	-0,12	-0,02	Phosphorylates Yap1 then	PMID: 26838548 PMID: 24
Akap8	116633	ENSRNOG00000006559	A-kinase anchoring protein 8	4,38	4,09	3,86	5,37	4,73	5,19	4,31	4,50	-0,14	-0,22	0,25	0,07	0,20	-0,06	-0,04	0,00	0,00	0,00	0,00	-0,03	Phosphorylates Yap1 then	PMID: 24362629
Epha7	171287	ENSRNOG00000007030	Eph receptor A7	0,36	0,50	0,54	0,39	0,37	0,35	0,36	0,53	-0,11	0,00	-0,46	-0,54	-0,62	-0,58	0,00	0,00	-0,17	-0,07	-0,17	-0,09	Phosphorylates Yap1 then	PMID: 24362629
Gak	81659	ENSRNOG00000000048	cyclin G associated kinase	2,55	2,59	2,95	3,08	2,14	3,04	2,48	2,62	-0,01	0,17	0,23	-0,29	0,22	-0,08	0,00	0,00	0,00	0,00	0,00	0,00	Phosphorylates Yap1 then	PMID: 24362629
Ly6g5b	406867	ENSRNOG00000027516	lymphocyte antigen 6 complex, locus G5B	0,03	0,11	0,01	0,04	0,03	0,07	0,01	0,03	1,76	-1,26	0,40	0,00	1,16	-1,11	0,00	0,00	0,00	0,00	0,00	0,00	Phosphorylates Yap1 then	PMID: 24362629
Magi1	500261	ENSRNOG00000022060	membrane associated guanylate kinase, WW and PDZ domain	1,44	1,58	1,41	1,87	1,80	1,56	1,61	1,79	-0,18	-0,34	0,06	0,01	-0,19	-0,15	0,00	-0,01	-0,09	-0,05	-0,09	0,00	Phosphorylates Yap1 then	PMID: 24362629
Map2k7	363855	ENSRNOG00000001047	mitogen activated protein kinase kinase 7	1,54	1,83	1,87	1,71	1,92	1,73	1,95	1,90	-0,05	-0,02	-0,15	0,01	-0,13	0,04	-0,02	0,00	0,00	0,00	0,00	0,00	Phosphorylates Yap1 then	PMID: 24362629
Map3k9	500690	ENSRNOG00000007271	mitogen-activated protein kinase kinase kinase 9	0,05	0,05	0,05	0,04	0,07	0,07	0,04	0,07	-0,58	-0,33	-0,68	0,00	0,08	-0,65	-0,02	0,00	-0,04	0,00	-0,04	-0,04	Phosphorylates Yap1 then	PMID: 24362629
Map4k4	301363	ENSRNOG00000014013	mitogen-activated protein kinase kinase kinase 4	0,95	1,10	1,18	1,04	0,98	0,96	0,93	0,79	0,48	0,57	0,40	0,30	0,28	0,23	0,00	0,00	0,00	-0,13	0,00	-0,02	Phosphorylates Yap1 then	PMID: 24362629
Map4k5	503027	ENSRNOG00000004923	mitogen-activated protein kinase kinase kinase 5	4,25	4,98	4,45	4,27	4,64	4,05	5,06	3,83	0,38	0,22	0,16	0,28	0,08	0,40	0,00	0,00	0,00	0,00	0,00	-0,02	Phosphorylates Yap1 then	PMID: 24362629
Mapkapk5	498183	ENSRNOG00000001345	mitogen-activated protein kinase-activated protein	9,26	8,86	10,50	10,29	6,20	8,04	7,73	8,09	0,13	0,38	0,35	-0,38	-0,01	-0,07	0,00	0,00	0,00	-0,01	0,00	-0,16	Phosphorylates Yap1 then	PMID: 24362629
Mylk2	117558	ENSRNOG00000008235	myosin light chain kinase 2	0,03	0,04	0,01	0,01	0,02	0,05	0,04	0,00	-	-	-	-	-	-	-0,15	0,00	-0,01	0,00	-0,01	0,00	Phosphorylates Yap1 then	PMID: 24362629
Nek4	306252	ENSRNOG00000017997	NIMA-related kinase 4	0,78	0,92	0,91	0,86	0,70	0,83	0,70	0,66	0,47	0,45	0,38	0,07	0,32	0,08	0,00	0,00	0,00	0,00	0,00	0,00	Phosphorylates Yap1 then	PMID: 24362629
Ripk3	246240	ENSRNOG00000020465	receptor-interacting serine-threonine kinase 3	7,04	5,17	5,51	3,24	4,49	3,88	6,63	5,61	-0,12	-0,03	-0,79	-0,32	-0,53	0,24	0,00	0,00	0,00	0,00	0,00	0,00	Phosphorylates Yap1 then	PMID: 24362629
Sgk1	29517	ENSRNOG00000011815	serum/glucocorticoid regulated kinase 1	1,08	1,61	1,21	0,63	1,11	0,75	1,35	1,45	0,15	-0,27	-1,21	-0,39	-0,96	-0,11	0,00	0,00	0,00	0,00	0,00	-0,02	Phosphorylates Yap1 then	PMID: 24362629
Stk10	29398	ENSRNOG00000004217	serine/threonine kinase 10	0,86	1,06	0,98	1,13	1,21	1,04	0,81	1,12	-0,08	-0,20	0,01	0,12	-0,11	-0,47	0,00	0,00	0,00	-0,01	0,00	0,00	Phosphorylates Yap1 then	PMID: 24362629
Stk11	314621	ENSRNOG00000014287	serine/threonine kinase 11	6,52	7,97	6,87	4,83	6,49	4,09	7,26	6,75	0,24	0,03	-0,48	-0,06	-0,73	0,10	0,00	0,00	0,00	0,00	0,00	0,00	Phosphorylates Yap1 then	PMID: 24362629
Stk33	690861	ENSRNOG00000014590	serine/threonine kinase 33	-	-	-	-	-	-	-	-	-	-	-	-	-	-	-	-	-	-	-	-	Phosphorylates Yap1 then	PMID: 24362629
Stk38l	691337	ENSRNOG00000001828	serine/threonine kinase 38 like	35,70	24,90	13,63	16,94	18,68	15,03	23,49	34,71	-0,48	-1,35	-1,04	-0,89	-1,21	-0,56	-0,25	-0,11	-0,14	0,00	-0,14	-0,15	Phosphorylates Yap1 then	PMID: 23985307
Tesk1	29460	ENSRNOG00000053729	testis-specific kinase 1	3,65	3,79	2,75	2,79	2,55	2,94	3,72	3,42	0,15	-0,32	-0,29	-0,42	-0,22	0,12	0,00	0,00	-0,15	0,00	-0,15	0,00	Phosphorylates Yap1 then	PMID: 24362629
Traf3ip3	360900	ENSRNOG00000005565	TRAF3 interacting protein 3	0,24	0,26	0,32	0,34	0,23	0,37	0,33	0,33	-0,36	-0,02	0,03	-0,50	0,16	0,00	0,00	0,00	0,00	0,00	0,00	0,00	Phosphorylates Yap1 then	PMID: 24362629
14-3-3 PROTEINS																									
Ywhab	56011	ENSRNOG00000010945	tyrosine 3-monooxygenase/tryptophan 5-	61,47	61,57	58,87	76,83	61,38	75,57	64,09	39,15	0,65	0,59	0,97	0,65	0,95	0,71	0,00	0,00	0,00	0,00	0,00	0,00	Forms a complex with phosphorylated Yap1/Wwtr1 leading to	PMID: 17974916 PMID: 23431053
Ywhae	29753	ENSRNOG00000005290	tyrosine 3-monooxygenase/tryptophan 5-	53,48	72,70	22,81	63,63	67,36	60,36	60,05	53,26	0,45	-1,22	0,26	0,34	0,18	0,17	0,00	-0,28	0,00	0,00	0,00	0,00	Forms a complex with phosphorylated Yap1/Wwtr1 leading to	PMID: 17974916 PMID: 23431053
Ywhag	56010	ENSRNOG00000001436	tyrosine 3-monooxygenase/tryptophan 5-	16,78	19,60	10,23	14,79	17,13	16,05	17,99	17,80	0,14	-0,80	-0,27	-0,06	-0,15	0,02	-0,07	-0,29	0,00	-0,13	0,00	-0,02	Forms a complex with phosphorylated Yap1/Wwtr1 leading to	PMID: 17974916 PMID: 23431053
Ywhah	25576	ENSRNOG00000055471	tyrosine 3-monooxygenase/tryptophan 5-	82,92	87,46	101,82	88,33	86,67	86,71	88,54	38,34	1,19	1,41	1,20	1,18	1,18	1,21	0,00	0,00	0,00	-0,36	0,00	0,00	Forms a complex with phosphorylated Yap1/Wwtr1 leading to	PMID: 17974916 PMID: 23431053
Ywhaq	25577	ENSRNOG00000051650	tyrosine 3-monooxygenase/tryptophan 5-	81,28	118,95	94,75	91,96	93,60	102,46	89,86	88,75	0,42	0,09	0,05	0,08	0,21	0,02	0,00	0,00	-0,15	0,00	-0,15	-0,02	Forms a complex with phosphorylated Yap1/Wwtr1 leading to	PMID: 17974916 PMID: 23431053
Ywhaz	25578	ENSRNOG00000008195	tyrosine 3-monooxygenase/tryptophan 5-	34,72	53,05	42,65	45,04	44,69	43,56	35,55	36,17	0,55	0,24	0,32	0,31	0,27	-0,02	0,00	-0,32	-0,28	-0,08	-0,28	-0,04	Forms a complex with phosphorylated Yap1/Wwtr1 leading to	PMID: 17974916 PMID: 23431053
Sfn	313017	ENSRNOG00000033153	stratifin	1,74	0,75	1,30	0,80	1,00	1,03	0,88	1,58	-1,08	-0,28	-0,98	-0,66	-0,62	-0,85	0,00	0,00	0,00	0,00	0,00	0,00	Forms a complex with phosphorylated Yap1/Wwtr1 leading to	PMID: 17974916 PMID: 23431053
CRUMBS COMPLEX																									
Crb1	304825	ENSRNOG00000010903	crumbs 1, cell polarity complex component	-	-	-	-	-	-	-	-	-	-	-	-	-	-	-	-	-	-	-	-	Binds to Frmd6	PMID: 20362447 PMID: 20498073 PMID: 23431053 PMID:
Crb2	366031	ENSRNOG00000025498	crumbs 2, cell polarity complex component	0,40	0,18	0,28	0,40	0,22	0,33	0,37	0,42	-1,23	-0,56	-0,06	-0,90	-0,35	-0,18	0,00	0,00	0,00	0,00	0,00	0,00	Binds to Frmd6	PMID: 20362447 PMID: 20498073 PMID: 23431053 PMID:
Crb3	301112	ENSRNOG00000047322	crumbs 3, cell polarity complex component	0,14	0,12	0,07	0,09	0,08	0,11	0,13	0,13	-0,05	-0,89	-0,50	-0,63	-0,24	-0,01	0,00	0,00	0,00	0,00	0,00	-0,19	Binds to Frmd6	PMID: 20362447 PMID: 20498073 PMID: 23431053 PMID:
Amot	300289	ENSRNOG00000007345	angiomotin	0,29	0,29	0,26	0,44	0,29	0,44	0,28	0,38	-0,39	-0,57	0,20	-0,40	0,20	-0,42	0,00	-0,21	0,00	0,00	0,00	0,00	Part of Crumbs Complex, Binds to Yap1/Wwtr1 to induce their	PMID: 21187284 PMID: 21205866 PMID: 21224387 PMID:
Amotl1	315430		angiomotin-like 1	6,89	5,72	6,92	4,39	5,38	4,34	6,22	5,72	0,00	0,28	-0,38	-0,09	-0,40	0,12	-0,10	0,00	-0,03	-0,01	-0,03	-0,02	Part of Crumbs Complex, Binds to Yap1/Wwtr1 to induce their	PMID: 21187284 PMID: 21205866 PMID: 21224387 PMID:
Amotl2	65157	ENSRNOG00000008487	angiomotin like 2	24,96	21,84	23,46	20,35	17,92	20,90	22,11	24,46	-0,16	-0,06	-0,27	-0,45	-0,23	-0,15	0,00	0,00	0,00	0,00	0,00	0,00	Part of Crumbs Complex, Binds to Yap1/Wwtr1 to induce their	PMID: 21187284 PMID: 21205866 PMID: 21224387 PMID:

Mpdz	29365	ENSRNOG00000007894	multiple PDZ domain crumbs cell polarity complex component	1,22	1,18	1,56	1,17	1,00	1,13	1,23	1,19	-0,01	0,39	-0,03	-0,24	-0,08	0,05	-0,20	0,00	0,00	0,00	0,00	-0,14	Part of Crumbs Complex, Binds to Yap1/Wwtr1	PMID: 21145499 PMID: 21187284 PMID: 23431053
Lin7a	85327	ENSRNOG00000004527	lin-7 homolog A, crumbs cell polarity complex component	-	-	-	-	-	-	-	-	-	-	-	-	-	-	-	-	-	-	-	-	Part of Crumbs Complex, Binds to Yap1/Wwtr1	PMID: 21145499 PMID: 21187284 PMID: 23431053
Lin7b	60377	ENSRNOG00000020746	lin-7 homolog B, crumbs cell polarity complex component	0,08	0,19	0,17	0,12	0,14	0,14	0,09	0,05	2,08	1,91	1,40	1,59	1,57	0,89	0,00	0,00	0,00	0,00	0,00	0,00	Part of Crumbs Complex, Binds to Yap1/Wwtr1	PMID: 21145499 PMID: 21187284 PMID: 23431053
Lin7c	60442	ENSRNOG00000045698	lin-7 homolog C, crumbs cell polarity complex component	36,70	25,92	29,07	42,83	36,34	41,10	23,74	31,93	-0,30	-0,14	0,42	0,19	0,36	-0,43	-0,14	0,00	0,00	-0,16	0,00	-0,45	Part of Crumbs Complex, Binds to Yap1/Wwtr1	PMID: 21145499 PMID: 21187284 PMID: 23431053
Patj	140581	ENSRNOG00000007551	PATJ, crumbs cell polarity complex component	0,51	0,33	0,62	0,52	0,47	0,55	0,48	0,46	-0,50	0,42	0,17	0,04	0,24	0,05	0,00	0,00	0,00	0,00	0,00	0,00	Part of Crumbs Complex, Binds to Yap1/Wwtr1	PMID: 21145499 PMID: 21187284 PMID: 23431053
Mpp5	314259	ENSRNOG00000008788	membrane palmitoylated protein 5	3,09	3,22	2,74	2,72	2,18	3,04	3,25	2,90	0,15	-0,08	-0,09	-0,41	0,07	0,17	-0,19	-0,11	-0,32	-0,01	-0,32	-0,08	Part of Crumbs Complex, Binds to Yap1/Wwtr1	PMID: 21145499 PMID: 21187284 PMID: 23431053
			SCRIBBLE COMPLEX																						
Scrib	362938	ENSRNOG00000032574	scribbled planar cell polarity protein	0,60	0,59	0,68	0,53	0,53	0,42	0,61	0,59	0,00	0,19	-0,17	-0,15	-0,50	0,04	-0,03	0,00	0,00	0,00	0,00	0,00	Part of the Scribble complex which represses the PAR complex	PMID: 22078877 PMID: 22169974 PMID: 23431053
Dlg1	25252	ENSRNOG00000038597	discs large MAGUK scaffold protein 1	10,50	11,18	10,73	9,25	9,16	9,48	9,11	8,68	0,37	0,31	0,09	0,08	0,13	0,07	0,00	0,00	0,00	0,00	0,00	-0,06	Part of the Scribble complex which represses the PAR complex	PMID: 22078877 PMID: 22169974 PMID: 23431053
Dlg2	64053	ENSRNOG00000022635	discs large MAGUK scaffold protein 2	0,02	0,03	0,13	0,04	0,09	0,05	0,02	0,09	-1,81	0,50	-1,30	-0,04	-0,92	-2,11	-0,10	0,00	0,00	-0,14	0,00	-0,04	Part of the Scribble complex which represses the PAR complex	PMID: 22078877 PMID: 22169974 PMID: 23431053
Dlg3	58948	ENSRNOG00000002767	discs large MAGUK scaffold protein 3	0,15	0,14	0,20	0,13	0,19	0,13	0,13	0,14	0,06	0,56	-0,09	0,47	-0,09	-0,03	0,00	0,00	-0,02	0,00	-0,02	-0,01	Part of the Scribble complex which represses the PAR complex	PMID: 22078877 PMID: 22169974 PMID: 23431053
Dlg4	29495	ENSRNOG00000018526	discs large MAGUK scaffold protein 4	0,36	0,34	0,27	0,30	0,31	0,28	0,35	0,36	-0,09	-0,43	-0,29	-0,20	-0,36	-0,07	0,00	0,00	0,00	-0,03	0,00	0,00	Part of the Scribble complex which represses the PAR complex	PMID: 22078877 PMID: 22169974 PMID: 23431053
Dlg5	305645	ENSRNOG00000005783	discs large MAGUK scaffold protein 5	0,95	0,81	1,44	1,15	1,11	1,01	1,17	0,97	-0,27	0,56	0,24	0,19	0,06	0,26	0,00	0,00	-0,07	0,00	-0,07	0,00	Part of the Scribble complex which represses the PAR complex	PMID: 22078877 PMID: 22169974 PMID: 23431053
Mpp2	85275	ENSRNOG00000059683	membrane palmitoylated protein 2	0,35	0,22	0,25	0,36	0,49	0,38	0,38	0,25	-0,20	0,00	0,53	0,98	0,60	0,62	0,00	0,00	0,00	0,00	0,00	0,00	Binds to Dlg1	PMID: 12351654
Mpp3	114202	ENSRNOG00000033653	membrane palmitoylated protein 3	0,06	0,01	0,02	0,02	0,05	0,04	0,04	0,02	-0,98	-0,58	-0,34	1,00	0,57	0,57	0,00	0,00	0,00	0,00	0,00	-0,01	Binds to Dlg1	PMID: 12351654
Mpp4	58808	ENSRNOG00000010486	membrane palmitoylated protein 4	0,03	0,02	0,02	0,02	0,03	0,02	0,03	0,03	-0,76	-0,41	-0,47	0,14	-0,17	0,27	0,00	0,00	0,00	0,00	0,00	0,00	Binds to Dlg1	PMID: 12351654
Llgl1	54265	ENSRNOG00000003948	LLGL1, scribble cell polarity complex component	3,55	2,65	3,56	3,23	3,38	2,86	3,54	3,79	-0,52	-0,09	-0,23	-0,17	-0,41	-0,10	-0,51	0,00	0,00	0,00	0,00	-0,03	Part of the Scribble complex which represses the PAR complex	PMID: 22078877 PMID: 22169974 PMID: 23431053
Llgl2	360661	ENSRNOG00000004834	LLGL2, scribble cell polarity complex component	0,57	0,48	0,27	0,80	0,60	0,65	0,43	0,62	-0,37	-1,20	0,38	-0,03	0,08	-0,52	0,00	-0,63	0,00	-0,09	0,00	0,00	Part of the Scribble complex which represses the PAR complex	PMID: 22078877 PMID: 22169974 PMID: 23431053
			PAR COMPLEX																						
Pard3	81918	ENSRNOG00000032437	par-3 family cell polarity regulator	0,58	0,54	0,68	0,66	0,61	0,63	0,63	0,57	-0,09	0,25	0,20	0,08	0,14	0,13	0,00	0,00	0,00	-0,04	0,00	0,00	Part of the PAR complex which represses Hippo pathway	PMID: 20362447 PMID: 21145886 PMID: 23431053 PMID:
Pard3b	301455	ENSRNOG00000024345	par-3 family cell polarity regulator beta	6,32	5,53	6,80	5,52	4,56	5,25	6,04	7,06	-0,35	-0,05	-0,35	-0,63	-0,43	-0,22	-0,45	-1,04	0,00	0,00	0,00	-0,28	Part of the PAR complex which represses Hippo pathway	PMID: 20362447 PMID: 21145886 PMID: 23431053 PMID:
Pard6a	307799	ENSRNOG00000017746	par-6 family cell polarity regulator alpha	0,22	0,15	0,09	0,17	0,10	0,17	0,15	0,09	0,76	-0,09	0,86	0,17	0,89	0,70	0,00	0,00	0,00	0,00	0,00	0,00	Part of the PAR complex which represses Hippo pathway	PMID: 20362447 PMID: 21145886 PMID: 23431053
Pard6b	362279	ENSRNOG00000010883	par-6 family cell polarity regulator beta	4,84	5,45	2,89	6,40	4,08	4,64	5,03	4,09	0,42	-0,50	0,65	0,00	0,18	0,30	0,00	0,00	0,00	-0,10	0,00	-0,02	Part of the PAR complex which represses Hippo pathway	PMID: 20362447 PMID: 21145886 PMID: 23431053
Pard6g	307237	ENSRNOG00000055157	par-6 family cell polarity regulator gamma	1,47	1,55	1,99	1,33	1,87	1,49	2,01	1,72	-0,15	0,21	-0,38	0,12	-0,20	0,22	0,00	0,00	0,00	0,00	0,00	-0,12	Part of the PAR complex which represses Hippo pathway	PMID: 20362447 PMID: 21145886 PMID: 23431053
Prkci	84006	ENSRNOG00000009652	protein kinase C, iota	8,90	10,29	8,82	11,36	9,66	9,68	9,55	7,23	0,51	0,29	0,65	0,42	0,42	0,40	0,00	-0,41	0,00	-0,39	0,00	-0,72	Part of the PAR complex which represses Hippo pathway	PMID: 20362447 PMID: 21145886 PMID: 23431053
			KIBRA COMPLEX																						
Frmd6	257646	ENSRNOG00000007329	FERM domain containing 6	2,68	2,87	2,94	1,80	2,34	1,58	2,28	2,23	0,36	0,39	-0,31	0,07	-0,50	0,03	0,00	0,00	0,00	0,00	0,00	-0,01	Frmd6, Nf2 and Wwc1 form a complex. Frmd6 and Nf2 associate	PMID: 20159598 PMID: 20159599 PMID: 20159600 PMID:
Nf2	25744	ENSRNOG00000007948	neurofibromin 2	3,41	3,52	3,06	2,38	2,38	2,20	3,13	3,31	0,09	-0,11	-0,48	-0,48	-0,59	-0,08	0,00	0,00	0,00	0,00	0,00	0,00	Frmd6, Nf2 and Wwc1 form a complex. Frmd6 and Nf2 associate	PMID: 20159598 PMID: 20159599 PMID: 20159600 PMID:
Wwc1	303039	ENSRNOG00000008065	WW and C2 domain containing 1	0,62	0,48	0,63	0,47	0,47	0,61	0,61	0,39	0,28	0,67	0,24	0,27	0,63	0,64	0,00	0,00	0,00	0,00	0,00	0,00	Frmd6, Nf2 and Wwc1 form a complex.	PMID: 20159598 PMID: 20159599 PMID: 20159600 PMID:
			OTHER APICAL-BASAL POLARITY PROTEINS																						
Ctnna1	307505	ENSRNOG00000005796	catenin alpha 1	100,04	80,33	64,15	81,03	74,97	69,98	85,55	87,86	-0,13	-0,45	-0,12	-0,23	-0,33	-0,04	-0,17	0,00	0,00	-0,14	0,00	-0,02	Forms a trimeric complex leading to sequesterization of	PMID: 21376238 PMID: 21610251 PMID: 23431053
Ctnna2	297357	ENSRNOG00000006003	catenin alpha 2	0,00	0,01	0,00	0,00	0,01	0,00	0,00	0,00	1,34	-0,26	-1,60	1,33	-	-1,11	0,00	0,00	0,00	0,00	0,00	0,00	Forms a trimeric complex leading to sequesterization of	PMID: 21376238 PMID: 21610251 PMID: 23431053
Ctnna3	361839	ENSRNOG00000000378	catenin alpha 3	5,34	4,60	3,75	4,35	4,11	4,72	4,72	5,01	-0,12	-0,42	-0,20	-0,28	-0,09	-0,09	0,00	0,00	0,00	0,00	0,00	-0,30	Forms a trimeric complex leading to sequesterization of	PMID: 21376238 PMID: 21610251 PMID: 23431053
Ctnnal1	298019	ENSRNOG00000010593	catenin alpha-like 1	4,38	4,62	4,47	5,59	5,49	4,77	4,26	5,10	-0,14	-0,19	0,13	0,11	-0,10	-0,26	0,00	0,00	0,00	0,00	0,00	0,00	Forms a trimeric complex leading to sequesterization of	PMID: 21376238 PMID: 21610251 PMID: 23431053
Ptpn14	305064	ENSRNOG00000003407	protein tyrosine phosphatase, non-receptor type 14	0,80	0,87	1,04	0,90	0,83	0,89	0,93	0,76	0,20	0,46	0,24	0,14	0,24	0,29	-0,01	0,00	0,00	-0,02	0,00	-0,03	Binds to Yap1/Wwtr1 leading to cytoplasmic retention. May also bind	PMID: 22689061 PMID: 22525271 PMID: 22948661 PMID:
Cdh1	83502	ENSRNOG00000020151	cadherin 1	0,55	0,53	0,57	0,36	0,29	0,50	0,48	0,77	-0,52	-0,43	-1,09	-1,41	-0,60	-0,67	0,00	0,00	0,00	0,00	0,00	0,00	Leads to Yap1 inactivation	PMID: 21730131 PMID: 23431053
Ajuba	85265	ENSRNOG00000012791	ajuba LIM protein	22,69	16,64	19,14	21,07	17,85	19,68	23,18	19,57	-0,23	-0,03	0,11	-0,13	0,01	0,24	0,00	0,00	-0,23	0,00	-0,23	0,00	Leads to Yap1 inactivation	PMID: 20303269 PMID: 23431053
Nphp4	313749	ENSRNOG00000011967	nephronophthisis 4	0,02	0,03	0,02	0,02	0,02	0,02	0,02	0,02	0,42	0,02	-0,29	-0,23	0,15	0,10	0,00	0,00	0,00	0,00	0,00	-0,21	Inhibits LATS1	PMID: 21555462 PMID: 23431053
Tjp1	292994	ENSRNOG00000011077	tight junction protein 1	1,35	1,82	1,54	1,15	1,56	1,24	1,39	1,05	0,80	0,56	0,14	0,58	0,25	0,41	0,00	0,00	0,00	0,00	0,00	0,00	Represses Wwtr1 activation	PMID: 20850437 PMID: 23431053
Tjp2	115769	ENSRNOG00000015030	tight junction protein 2	1,19	1,17	1,40	1,03	0,92	1,07	1,32	1,37	-0,22	0,03	-0,41	-0,57	-0,36	-0,05	0,00	0,00	0,00	-0,11	0,00	0,00	Induce Yap1 nuclear localization	PMID: 20868367 PMID: 23431053
Tjp3	314640	ENSRNOG00000020501	tight junction protein 3	0,14	0,18	0,18	0,13	0,19	0,11	0,11	0,16	0,18	0,17	-0,23	0,26	-0,46	-0,53	0,00	0,00	0,00	0,00	0,00	0,00	Predicted to interact with Yap1	PMID: 19371381
Tjap1	316233	ENSRNOG00000018980	tight junction associated protein 1	0,54	0,45	0,55	0,45	0,49	0,52	0,44	0,49	-0,13	0,14	-0,12	-0,02	0,08	-0,17	0,00	0,00	0,00	0,00	0,00	0,00	Predicted to regulate Hippo pathway	PMID: 27236618
			GPCR SIGNALLING																						
Gna11	81662	ENSRNOG00000005446	guanine nucleotide binding protein, alpha 11	12,96	13,47	15,34	15,92	10,70	14,11	12,48	13,67	-0,02	0,17	0,22	-0,35	0,05	-0,13	-0,01	0,00	-0,02	0,00	-0,02	0,00	Activates Rhoa	PMID: 22863277 PMID: 23431053
Gna12	81663	ENSRNOG00000001235	G protein subunit alpha 12	14,31	14,66	5,71	16,76	13,73	15,58	12,00	15,45	-0,08	-1,44	0,12	-0,17	0,01	-0,36	0,00	-1,47	0,00	0,00	0,00	0,00	Activates Rhoa	PMID: 22863277 PMID: 23431053
Gna13	303634	ENSRNOG00000036745	G protein subunit alpha 13	10,95	14,11	11,31	12,21	14,66	11,40	13,31	9,18	0,62	0,30	0,41	0,68	0,31	0,54	-0,18	0,00	0,00	0,00	0,00	-0,13	Activates Rhoa	PMID: 22863277 PMID: 23431053
Gna14	309242	ENSRNOG00000014840	G protein subunit alpha 14	0,06	0,05	0,06	0,02	0,03	0,03	0,05	0,05	0,00	0,46	-1,26	-0,65	-0,72	0,24	-0,25	0,00	0,00	0,00	0,00	-0,03	Activates Rhoa	PMID: 22863277 PMID: 23431053
Gna15	89788	ENSRNOG00000005378	guanine nucleotide binding protein, alpha 15	0,10	0,11	0,04	0,04	0,05	0,05	0,07	0,18	-0,66	-2,26	-2,02	-2,00	-1,84	-1,30	0,00	0,00	0,00	0,00	0,00	0,00	Activates Rhoa	PMID: 22863277 PMID: 23431053
Gnaq	81666	ENSRNOG00000014183	G protein subunit alpha q	17,29	21,81	21,32	19,58	13,64	19,53	18,80	16,14	0,43	0,40	0,28	-0,24	0,27	0,22	0,00	0,00	0,00	-0,11	0,00	-0,06	Activates Rhoa	PMID: 22863277 PMID: 23431053
Gnao1	50664	ENSRNOG00000019482	G protein subunit alpha o1	2,10	2,80	1,39	2,20	3,01	2,08	1,56	2,57	0,12	-0,89	-0,22	0,23	-0,30	-0,72	-0,03	0,00	0,00	-0,11	0,00	-0,01	Activates Rhoa	PMID: 22863277 PMID: 23431053
Gnai1	25686	ENSRNOG00000057096	G protein subunit alpha i1	7,49	6,27	5,15	4,68	4,72	4,36	7,73	6,26	0,00	-0,28	-0,42	-0,41	-0,52	0,30	0,00	0,00	0,00	-0,15	0,00	-0,12	Activates Rhoa	PMID: 22863277 PMID: 23431053
Gnai2	81664	ENSRNOG00000016592	G protein subunit alpha i2	31,36	31,28	35,98	29,16	23,15	26,37	31,06	27,64	0,18	0,38	0,08	-0,26	-0,07	0,17	0,00	0,00	0,00	0,00	0,00	0,00	Activates Rhoa	PMID: 22863277 PMID: 23431053
Gnai3	25643	ENSRNOG00000019465	G protein subunit alpha i3	27,45	40,80	36,91	43,64	37,38	42,68	29,56	29,00	0,49	0,35	0,59	0,37	0,56	0,03	-0,61	0,00	0,00	-0,38	0,00	-0,18	Activates Rhoa	PMID: 22863277 PMID: 23431053
Gnaz	25740	ENSRNOG00000001313	G protein subunit alpha z	0,01	0,01	0,01	0,01	0,02	0,02	0,03	0,00	-	-	-	-	-	-	0,00	0,00	0,00	0,00	0,00	0,00	Activates Rhoa	PMID: 22863277 PMID: 23431053
Gnal	24611	ENSRNOG00000010440	G protein subunit alpha L	0,39	0,60	0,44	0,32	0,78	0,31	0,61	0,65	-0,12	-0,56	-1,03	0,26	-1,08	-0,11	0,00	-0,13	-0,07	0,00	-0,07	-0,01	Activates Rhoa	PMID: 22863277 PMID: 23431053
Gnas	24896	ENSRNOG00000025889	GNAS complex locus	7,87	9,86	7,29	7,85	11,38	7,92	8,53	7,68	0,36	-0,08	0,03	0,57	0,04	0,15	0,00	-0,11	0,00	0,00	0,00	-0,05	Inhibits Rhoa	PMID: 22863277 PMID: 23431053
Rhoa	117273	ENSRNOG00000050519	ras homolog family member A	45,30	41,42	52,35	43,39	41,50	43,30	44,96	44,40	-0,10	0,24	-0,03	-0,10	-0,04	0,02	0,00	0,00	0,00	0,00	0,00	0,00	Inhibits Lats1/2	PMID: 22863277 PMID: 23431053
			PLANAR CELL POLARITY																						
Fat1	83720	ENSRNOG00000030954	FAT atypical cadherin 1	4,116	3,903	4,564	3,390	3,505	3,574	4,320	4,276	-0,132	0,094	-0,335	-0,287	-0,259	0,015	-0,055	-0,159	0,000	0,000	0,000	-0,020	Regulates Hippo pathway	PMID: 22399682 PMID: 23250217 PMID: 23318637 PMID:

Fat2	65048	ENSRNOG00000012575	FAT atypical cadherin 2	0,010	0,076	0,022	0,059	0,012	0,052	0,030	0,032	1,253	-0,545	0,891	-1,456	0,696	-0,107	0,000	0,000	0,000	0,000	0,000	0,000	Regulates Hippo pathway	PMID: 22399682 PMID: 23250217 PMID: 23318637 PMID:
Fat3	191571	ENSRNOG00000011585	FAT atypical cadherin 3	0,107	0,071	0,117	0,053	0,082	0,052	0,107	0,132	-0,892	-0,178	-1,330	-0,697	-1,353	-0,311	-0,010	-0,071	0,000	-0,020	0,000	-0,313	Regulates Hippo pathway	PMID: 22399682 PMID: 23250217 PMID: 23318637 PMID:
Fat4	310341	ENSRNOG00000028335	FAT atypical cadherin 4	1,477	2,153	3,469	1,038	1,749	0,971	1,288	1,776	0,278	0,966	-0,774	-0,022	-0,871	-0,463	0,000	0,000	-0,136	0,000	-0,136	0,000	Regulates Hippo pathway	PMID: 22399682 PMID: 23250217 PMID: 23318637 PMID:
Dchs1	308912	ENSRNOG00000031643	dachsous cadherin-related 1	0,194	0,138	0,244	0,226	0,256	0,257	0,222	0,295	-1,094	-0,275	-0,387	-0,206	-0,196	-0,409	0,000	0,000	0,000	0,000	0,000	0,000	Regulates Hippo pathway	PMID: 22399682 PMID: 23250217 PMID: 23318637 PMID:
Dchs2	310550		dachsous cadherin-related 2	0,014	0,049	0,029	0,042	0,128	0,059	0,030	0,036	0,436	-0,329	0,204	1,811	0,708	-0,259	0,000	0,000	0,000	0,000	0,000	0,000	Regulates Hippo pathway	PMID: 22399682 PMID: 23250217 PMID: 23318637 PMID:
Fjx1	366140	ENSRNOG00000005347	four jointed box 1	3,778	2,047	3,705	2,713	2,547	2,287	3,716	3,922	-0,938	-0,082	-0,532	-0,623	-0,778	-0,078	0,000	0,000	0,000	0,000	0,000	-0,050	Regulates Hippo pathway	PMID: 22499807 PMID: 23592229
Zyx	114636	ENSRNOG00000017354	zyxin	6,373	5,771	5,338	4,212	3,569	3,818	5,000	5,486	0,073	-0,039	-0,381	-0,620	-0,523	-0,134	0,000	0,000	0,000	0,000	0,000	0,000	Regulates Hippo pathway	PMID: 21666802 PMID: 27030211
Zdhhc1	291967	ENSRNOG00000017045	zinc finger, DHHC-type containing 1	0,378	0,286	0,375	0,156	0,284	0,223	0,359	0,416	-0,542	-0,149	-1,416	-0,552	-0,899	-0,211	0,000	0,000	0,000	0,000	0,000	0,000	Regulates cell polarity	PMID: 22174083 PMID: 23592229
Zdhhc2	246326	ENSRNOG00000022686	zinc finger, DHHC-type containing 2	26,180	25,532	13,609	26,045	20,109	30,728	22,837	18,432	0,470	-0,438	0,499	0,126	0,737	0,309	0,000	0,000	0,000	-0,092	0,000	-0,032	Regulates cell polarity	PMID: 22174083 PMID: 23592229
Zdhhc3	301081	ENSRNOG00000004344	zinc finger, DHHC-type containing 3	3,270	3,489	3,567	3,269	2,911	3,156	3,585	3,273	0,092	0,124	-0,002	-0,169	-0,053	0,131	-0,169	0,000	0,000	-0,080	0,000	-0,030	Regulates cell polarity	PMID: 22174083 PMID: 23592229
Zdhhc4	304291	ENSRNOG00000051699	zinc finger, DHHC-type containing 4	2,210	3,684	2,620	3,718	2,846	3,493	2,561	2,727	0,434	-0,058	0,447	0,062	0,357	-0,091	0,000	0,000	0,000	0,000	0,000	0,000	Regulates cell polarity	PMID: 22174083 PMID: 23592229
Zdhhc5	362156	ENSRNOG00000006832	zinc finger, DHHC-type containing 5	5,731	5,594	5,622	5,372	4,552	5,316	5,670	5,731	-0,035	-0,028	-0,093	-0,332	-0,109	-0,016	0,000	0,000	0,000	0,000	0,000	0,000	Regulates cell polarity	PMID: 22174083 PMID: 23592229
Zdhhc6	361771	ENSRNOG00000036576	zinc finger, DHHC-type containing 6	17,412	18,543	18,712	19,813	15,020	18,000	16,294	15,319	0,276	0,289	0,371	-0,028	0,233	0,089	0,000	0,000	-0,081	0,000	-0,081	0,000	Regulates cell polarity	PMID: 22174083 PMID: 23592229
Zdhhc7	170906	ENSRNOG00000017342	zinc finger, DHHC-type containing 7	6,574	6,099	4,824	5,570	4,265	5,707	7,213	6,327	-0,053	-0,391	-0,184	-0,569	-0,149	0,189	0,000	0,000	0,000	0,000	0,000	-0,030	Regulates cell polarity	PMID: 22174083 PMID: 23592229
Zdhhc8	303796	ENSRNOG00000021891	zinc finger, DHHC-type containing 8	0,927	0,848	1,113	0,946	1,075	0,692	1,032	0,798	0,087	0,480	0,245	0,430	-0,206	0,370	0,000	0,000	-0,170	0,000	-0,170	-0,020	Regulates cell polarity	PMID: 22174083 PMID: 23592229
Zdhhc9	302808	ENSRNOG00000004581	zinc finger, DHHC-type containing 9	2,060	2,326	2,075	1,194	1,991	1,802	1,671	1,452	0,680	0,516	-0,282	0,456	0,312	0,203	-0,122	-0,066	-0,203	-0,101	-0,203	0,000	Regulates cell polarity	PMID: 22174083 PMID: 23592229
Zdhhc11	499000	ENSRNOG00000039743	zinc finger, DHHC-type containing 11	-	-	-	-	-	-	-	-	-	-	-	-	-	-	-	-	-	-	-	-	Regulates cell polarity	PMID: 22174083 PMID: 23592229
Zdhhc12	366014	ENSRNOG00000015791	zinc finger, DHHC-type containing 12	4,858	6,561	4,711	8,487	6,651	7,319	5,570	5,436	0,271	-0,206	0,643	0,291	0,429	0,035	0,000	0,000	0,000	0,000	0,000	0,000	Regulates cell polarity	PMID: 22174083 PMID: 23592229
Zdhhc13	365252	ENSRNOG00000014277	zinc finger, DHHC-type containing 13	4,495	3,729	5,713	4,577	4,939	4,501	5,211	4,375	-0,230	0,385	0,065	0,175	0,041	0,252	0,000	0,000	0,000	0,000	0,000	0,000	Regulates cell polarity	PMID: 22174083 PMID: 23592229
Zdhhc14	499014	ENSRNOG00000029049	zinc finger, DHHC-type containing 14	0,240	0,205	0,305	0,147	0,207	0,200	0,245	0,304	-0,574	0,004	-1,053	-0,556	-0,608	-0,314	0,000	0,000	-0,192	0,000	-0,192	0,000	Regulates cell polarity	PMID: 22174083 PMID: 23592229
Zdhhc15	317235	ENSRNOG00000002751	zinc finger, DHHC-type containing 15	0,326	0,369	0,529	0,712	0,513	0,671	0,403	0,576	-0,641	-0,122	0,307	-0,166	0,221	-0,515	0,000	0,000	-0,049	-0,034	-0,049	-0,100	Regulates cell polarity	PMID: 22174083 PMID: 23592229
Zdhhc16	654495	ENSRNOG00000046530	zinc finger, DHHC-type containing 16	2,897	2,545	2,637	2,927	2,115	2,854	2,812	2,968	-0,222	-0,171	-0,020	-0,489	-0,057	-0,078	-0,382	0,000	0,000	0,000	0,000	0,000	Regulates cell polarity	PMID: 22174083 PMID: 23592229
Zdhhc17	366889	ENSRNOG00000003803	zinc finger, DHHC-type containing 17	4,023	5,836	4,474	4,251	6,782	4,731	5,064	4,698	0,313	-0,070	-0,144	0,530	0,010	0,108	0,000	0,000	-0,111	-0,094	-0,111	0,000	Regulates cell polarity	PMID: 22174083 PMID: 23592229
Zdhhc18	362613	ENSRNOG00000058156	zinc finger, DHHC-type containing 18	2,005	2,563	2,307	2,352	2,093	1,929	2,313	1,717	0,578	0,426	0,454	0,286	0,168	0,430	-0,125	0,000	0,000	0,000	0,000	0,000	Regulates cell polarity	PMID: 22174083 PMID: 23592229
Zdhhc19	288045	ENSRNOG00000025055	zinc finger, DHHC-type containing 19	0,000	0,025	0,018	0,053	0,088	0,022	0,034	0,022	0,173	-0,255	1,271	2,003	-0,015	0,630	0,000	0,000	0,000	0,000	0,000	0,000	Regulates cell polarity	PMID: 22174083 PMID: 23592229
Zdhhc20	305923	ENSRNOG00000011024	zinc finger, DHHC-type containing 20	2,645	4,118	3,101	3,599	3,754	3,244	3,478	3,164	0,380	-0,029	0,186	0,247	0,036	0,136	0,000	0,000	0,000	-0,073	0,000	-0,020	Regulates cell polarity	PMID: 22174083 PMID: 23592229
Zdhhc21	298184	ENSRNOG00000010484	zinc finger, DHHC-type containing 21	1,975	1,962	2,029	1,677	2,115	1,827	1,798	2,200	-0,165	-0,117	-0,392	-0,057	-0,268	-0,291	0,000	-0,225	-0,109	-0,031	-0,109	-0,384	Regulates cell polarity	PMID: 22174083 PMID: 23592229
Zdhhc22	299211	ENSRNOG00000011285	zinc finger, DHHC-type containing 22	-	-	-	-	-	-	-	-	-	-	-	-	-	-	-	-	-	-	-	-	Regulates cell polarity	PMID: 22174083 PMID: 23592229
Zdhhc23	363783	ENSRNOG00000060348	zinc finger, DHHC-type containing 23	0,079	0,042	0,034	0,152	0,046	0,118	0,080	0,039	0,132	-0,203	1,973	0,249	1,610	1,045	0,000	-0,090	-0,020	0,000	-0,020	-0,040	Regulates cell polarity	PMID: 22174083 PMID: 23592229
Zdhhc24	293665	ENSRNOG00000019825	zinc finger, DHHC-type containing 24	1,235	0,729	0,678	1,437	0,811	1,101	1,202	1,051	-0,528	-0,634	0,451	-0,375	0,066	0,193	0,000	0,000	0,000	0,000	0,000	0,000	Regulates cell polarity	PMID: 22174083 PMID: 23592229
Zdhhc25	300323	ENSRNOG00000046044	zinc finger, DHHC-type containing 25	-	-	-	-	-	-	-	-	-	-	-	-	-	-	-	-	-	-	-	-	Regulates cell polarity	PMID: 22174083 PMID: 23592229
OTHER MODULATORS																									
Prkaca	25636	ENSRNOG00000005257	protein kinase cAMP-activated catalytic subunit alpha	34,82	26,66	41,08	42,41	35,53	36,83	37,67	35,81	-0,43	0,20	0,24	-0,01	0,04	0,07	0,00	0,00	0,00	0,00	0,00	0,00	Activates Hippo pathway	PMID: 23752589
Prkacb	293508	ENSRNOG00000004978	protein kinase cAMP-activated catalytic subunit beta	6,12	6,24	6,27	5,45	6,48	5,66	6,01	6,45	-0,05	-0,04	-0,24	0,01	-0,19	-0,10	0,00	-0,13	-0,26	0,00	-0,26	-0,12	Activates Hippo pathway	PMID: 23752589
Ppp1ca	24668	ENSRNOG00000018708	protein phosphatase 1 catalytic subunit alpha	147,00	181,08	140,39	167,87	155,04	160,71	155,48	133,19	0,44	0,08	0,33	0,22	0,27	0,22	0,00	0,00	0,00	0,00	0,00	0,00	Regulates Yap1 activity	PMID: 21909427
Ppp1cb	25594	ENSRNOG00000004612	protein phosphatase 1 catalytic subunit beta	63,94	51,78	57,65	59,02	53,41	64,61	65,46	68,26	-0,40	-0,24	-0,21	-0,35	-0,08	-0,06	0,00	0,00	0,00	0,00	0,00	-0,04	Regulates Yap1 activity	PMID: 21909427
Ppp1cc	24669	ENSRNOG00000001269	protein phosphatase 1 catalytic subunit gamma	31,86	41,00	37,55	36,42	37,93	33,69	39,28	35,09	0,22	0,10	0,05	0,11	-0,06	0,16	0,00	0,00	0,00	0,00	0,00	0,00	Regulates Yap1 activity	PMID: 21909427
Ppp2ca	24672	ENSRNOG00000005389	protein phosphatase 2, catalytic subunit, alpha isozyme	42,84	42,84	39,16	43,90	38,98	42,38	48,27	45,65	-0,09	-0,22	-0,06	-0,23	-0,11	0,08	0,00	0,00	0,00	0,00	0,00	0,00	Forms a complex which dephosphorylates Stk3/4 and Yap1	PMID: 17174922 PMID: 20797625 PMID: 23431053
Ppp2cb	24673	ENSRNOG00000015182	protein phosphatase 2 catalytic subunit beta	47,02	50,21	36,71	50,19	61,15	48,76	51,57	49,02	0,03	-0,42	0,03	0,32	-0,01	0,07	0,00	0,00	0,00	0,00	0,00	0,00	Forms a complex which dephosphorylates Stk3/4 and Yap1	PMID: 17174922 PMID: 20797625 PMID: 23431053
Ppp1r13b	314465	ENSRNOG00000012653	protein phosphatase 1, regulatory subunit 13B	0,47	0,58	0,52	0,87	0,63	0,71	0,57	0,55	0,08	-0,09	0,66	0,19	0,37	0,06	0,00	0,00	0,00	0,00	0,00	0,00	Facilitates dephosphorylation of PP1 complex	PMID: 21041411
Tp53bp2	305025	ENSRNOG00000003237	tumor protein p53 binding protein, 2	3,37	3,49	3,62	3,39	3,89	3,52	3,28	3,48	0,00	0,06	-0,04	0,16	0,02	-0,08	0,00	0,00	0,00	0,00	0,00	0,00	Facilitates dephosphorylation of PP1 complex	PMID: 21189257
Rassf1	363140	ENSRNOG00000021548	Ras association domain family member 1	4,44	5,77	5,05	4,23	4,17	4,33	5,33	4,69	0,30	0,11	-0,15	-0,17	-0,12	0,18	-0,09	0,00	0,00	0,00	0,00	0,00	Prevents Stk3/4 dephosphorylation by Ppp2ca	PMID: 17517604 PMID: 15109305 PMID: 23431053
Rassf2	311437	ENSRNOG00000021261	Ras association domain family member 2	0,05	0,03	0,04	0,03	0,04	0,03	0,07	0,07	-1,31	-0,69	-1,04	-0,71	-1,05	-0,05	-0,12	-0,05	-0,28	-0,04	-0,28	-0,03	Activates Stk3	PMID: 19962960
Rassf3	362886	ENSRNOG00000005388	Ras association domain family member 3	11,04	13,17	9,65	6,10	7,43	4,95	10,50	10,66	0,30	-0,14	-0,80	-0,52	-1,11	-0,02	0,00	-0,08	0,00	0,00	0,00	0,00	Regulates Hippo pathway	PMID: 17517604
Rassf4	362423	ENSRNOG00000013526	Ras association domain family member 4	5,43	1,83	3,02	3,77	1,93	4,45	2,84	5,09	-1,48	-0,75	-0,43	-1,40	-0,19	-0,84	-0,15	0,00	0,00	0,00	0,00	0,00	Regulates Hippo pathway	PMID: 17517604
Rassf5	54355	ENSRNOG00000005342	Ras association domain family member 5	0,11	0,13	0,13	0,27	0,31	0,55	0,15	0,15	-0,17	-0,15	0,90	1,10	1,91	0,00	-0,27	0,00	0,00	-0,02	0,00	-0,01	May inhibit or activate Stk4 depending on the context	PMID: 27643882
Rassf6	305251	ENSRNOG00000002866	Ras association domain family member 6	0,02	0,01	0,01	0,01	0,00	0,02	0,01	0,00	0,76	0,33	1,40	0,00	2,03	0,89	0,00	-0,03	0,00	-0,02	0,00	-0,08	Inhibits Stk3 by direct binding	PMID: 19797269 PMID: 23431053
Rassf7	293623	ENSRNOG00000017109	Ras association domain family member 7	0,86	0,45	1,41	0,59	0,58	0,58	0,72	0,35	0,37	2,01	0,75	0,72	0,72	1,04	0,00	0,00	0,00	0,00	0,00	0,00	Regulates Hippo pathway	PMID: 17517604
Rassf8	312846	ENSRNOG00000015986	Ras association domain family member 8	4,15	4,07	4,08	3,25	3,67	3,30	3,64	4,33	-0,09	-0,08	-0,42	-0,24	-0,39	-0,25	0,00	0,00	0,00	-0,16	0,00	-0,08	Regulates Hippo pathway	PMID: 17517604
Rassf9	65053	ENSRNOG00000038574	Ras association domain family member 9	0,61	0,40	0,67	0,47	0,31	0,80	0,44	0,64	-0,68	0,08	-0,45	-1,05	0,34	-0,54	0,00	0,00	-0,09	-0,11	-0,09	-0,34	Regulates Hippo pathway	PMID: 17517604
Rassf10	308894	ENSRNOG00000014847	Ras association domain family member 10	0,04	0,13	0,09	0,37	0,13	0,20	0,07	0,15	-0,24	-0,70	1,30	-0,24	0,41	-1,03	0,00	0,00	0,00	0,00	0,00	0,00	Regulates Hippo pathway	PMID: 17517604
Btrc	361765	ENSRNOG00000016280	beta-transducin repeat containing E3 ubiquitin protein	0,39	0,36	0,33	0,68	0,45	0,56	0,37	0,42	-0,22	-0,37	0,69	0,11	0,42	-0,19	-0,12	-0,17	-0,07	-0,05	-0,07	-0,02	Facilitates Yap1/Wwtr1 degradation	PMID: 20048001 PMID: 20858893
Fbxw11	303024	ENSRNOG00000004395	F-box and WD repeat domain containing 11	1,36	1,17	0,90	1,11	1,03	1,19	1,57	1,38	-0,24	-0,62	-0,32	-0,42	-0,21	0,18	-0,23	-0,29	-0,04	0,00	-0,04	0,00	Regulates Hippo pathway	PMID: 27124581
Wbp2	192645	ENSRNOG00000007971	WW domain binding protein 2	2,08	2,57	1,94	1,95	2,22	1,99	1,70	2,02	0,35	-0,06	-0,05	0,14	-0,02	-0,25	0,00	0,00	0,00	0,00	0,00	0,00	Activates Yap1/Wwtr1	PMID: 21311569 PMID: 20972459
Hipk2	362342	ENSRNOG00000007034	homeodomain interacting protein kinase 2	1,02	0,82	0,72	1,01	0,89	1,08	0,89	1,16	-0,49	-0,69	-0,20	-0,38	-0,10	-0,39	-0,01	0,00	0,00	-0,06	0,00	-0,04	Promotes Yap1 Activity	PMID: 20514025
Itch	311567	ENSRNOG00000059043	itchy E3 ubiquitin protein ligase	8,70	10,78	10,08	10,59	9,75	10,28	9,38	8,87	0,28	0,18	0,25	0,14	0,21	0,08	0,00	0,00	0,00	0,00	0,00	-0,07	Degrades Lats1/2 and promotes Yap1/Wwtr1 activity	PMID: 21383157
TRANSCRIPTION FACTORS BOUND TO YAP/TAZ																									
Smad1	25671	ENSRNOG00000018483	SMAD family member 1	1,13	1,10	1,00	1,00	1,07	0,83	1,16	1,26	-0,20	-0,34	-0,33	-0,24	-0,60	-0,13	0,00	0,00	0,00	0,00	0,00	-0,04	Yap1/Wwtr1 are transcriptional coactivators of	PMID: 26961347

Smad2	29357	ENSRNOG00000018140	SMAD family member 2	3,95	3,21	3,57	3,46	3,45	3,64	3,04	3,30	-0,04	0,11	0,07	0,06	0,14	-0,12	0,00	-0,15	-0,27	-0,01	-0,27	-0,08	Yap1/Wwtr1 are transcriptional coactivators of	PMID: 26961347
Smad3	25631	ENSRNOG00000008620	SMAD family member 3	3,21	3,32	2,85	3,69	3,37	3,47	3,06	3,74	-0,17	-0,39	-0,02	-0,15	-0,11	-0,29	0,00	0,00	0,00	0,00	0,00	0,00	Yap1/Wwtr1 are transcriptional coactivators of	PMID: 26961347
Smad7	81516	ENSRNOG00000018359	SMAD family member 7	1,58	1,48	1,28	1,44	1,37	1,30	1,72	1,79	-0,28	-0,49	-0,32	-0,39	-0,47	-0,06	0,00	0,00	0,00	-0,14	0,00	0,00	Yap1/Wwtr1 are transcriptional coactivators of	PMID: 26961347
Runx1	50662	ENSRNOG00000001704	runt-related transcription factor 1	0,12	0,10	0,08	0,03	0,12	0,05	0,11	0,09	0,23	-0,15	-1,38	0,43	-0,79	0,32	-0,02	-0,50	-0,20	0,00	-0,20	-0,02	Yap1/Wwtr1 are transcriptional coactivators of	PMID: 10228168 PMID: 14765127
Runx2	367218	ENSRNOG00000020193	runt-related transcription factor 2	0,02	0,04	0,05	0,02	0,03	0,01	0,03	0,01	1,50	1,76	0,78	1,27	0,11	1,33	-0,11	-0,11	-0,27	-0,03	-0,27	-0,02	Yap1/Wwtr1 are transcriptional coactivators of	PMID: 10228168 PMID: 14765127
Tp63	246334	ENSRNOG00000001924	tumor protein p63	-	-	-	-	-	-	-	-	-	-	-	-	-	-	-	-	-	-	-	-	Yap1/Wwtr1 are transcriptional coactivators of	PMID: 21364617
Tp73	362675	ENSRNOG00000024707	tumor protein p73	-	-	-	-	-	-	-	-	-	-	-	-	-	-	-	-	-	-	-	-	Yap1/Wwtr1 are transcriptional coactivators of	PMID: 17110958
Erbb4	59323	ENSRNOG00000014248	erb-b2 receptor tyrosine kinase 4	4,88	3,42	3,51	3,91	4,92	3,92	5,45	5,43	-0,66	-0,63	-0,47	-0,14	-0,47	0,00	-0,03	-0,38	-0,16	0,00	-0,16	-0,14	Yap1/Wwtr1 are transcriptional coactivators of	PMID: 25492965
Mkl1	315151	ENSRNOG00000018803	megakaryoblastic leukemia (translocation) 1	0,16	0,20	0,18	0,20	0,25	0,22	0,18	0,17	0,20	0,08	0,22	0,55	0,32	0,05	0,00	0,00	0,00	0,00	0,00	0,00	Yap1/Wwtr1 are transcriptional coactivators of	PMID: 27689009
TRANSCRIPTIONAL TARGETS OF YAP/TEAD																									
Ccna1	295052	ENSRNOG00000014052	cyclin A1	0,00	0,01	0,01	0,01	0,01	0,01	0,01	0,01	1,08	1,07	0,57	1,46	0,38	1,48	0,00	0,00	0,00	0,00	0,00	0,00		PMID: 26258633
Cdc25a	171102	ENSRNOG00000020737	cell division cycle 25A	2,54	3,25	3,04	2,44	2,74	2,45	2,77	3,08	0,08	-0,02	-0,34	-0,17	-0,33	-0,16	0,00	0,00	-0,05	-0,08	-0,05	0,00		PMID: 26258633
Cdc6	360621	ENSRNOG00000027787	cell division cycle 6	2,46	1,24	2,72	2,31	1,97	2,68	2,26	1,86	-0,59	0,55	0,31	0,08	0,53	0,28	0,00	-0,19	0,00	-0,09	0,00	0,00		PMID: 26258633
Cdca5	684771	ENSRNOG00000046635	cell division cycle associated 5	2,60	2,97	2,53	2,52	1,96	2,76	3,12	1,90	0,64	0,41	0,40	0,05	0,53	0,71	0,00	0,00	0,00	0,00	0,00	0,00		PMID: 26258633
Cdca8	500545	ENSRNOG00000031431	cell division cycle associated 8	6,94	15,09	9,71	7,39	6,96	8,09	9,82	4,74	1,67	1,03	0,64	0,55	0,77	1,05	0,00	0,00	0,00	0,00	0,00	0,00		PMID: 26258633
Cenpf	257649	ENSRNOG00000003388	centromere protein F	8,50	29,47	12,52	13,04	14,62	15,29	19,01	5,52	2,42	1,18	1,24	1,41	1,47	1,79	-0,14	0,00	0,00	0,00	0,00	0,00		PMID: 26258633
Cenpv	501702		centromere protein V	0,83	1,20	1,32	0,85	0,79	0,57	1,52	1,06	0,18	0,31	-0,32	-0,43	-0,90	0,52	0,00	0,00	0,00	0,00	0,00	0,00		PMID: 26258633
Edn1	24323	ENSRNOG00000014361	endothelin 1	6,90	5,85	4,52	8,38	4,23	8,57	6,83	11,03	-0,92	-1,29	-0,40	-1,38	-0,36	-0,69	0,00	0,00	0,00	-0,12	0,00	-0,03		PMID: 26258633
Ets1	24356	ENSRNOG00000008941	ETS proto-oncogene 1, transcription factor	1,74	1,20	1,70	1,71	1,31	1,58	1,46	1,97	-0,72	-0,22	-0,21	-0,59	-0,32	-0,43	-0,22	-0,07	0,00	-0,07	0,00	-0,08		PMID: 26258633
Ets2	304063	ENSRNOG00000001647	ETS proto-oncogene 2, transcription factor	3,13	3,13	3,76	1,49	2,53	1,51	2,26	3,03	0,05	0,31	-1,02	-0,26	-1,01	-0,42	-0,13	0,00	0,00	-0,11	0,00	0,00		PMID: 26258633
Fosl1	25445	ENSRNOG00000020552	FOS like 1, AP-1 transcription factor subunit	2,40	2,59	1,86	1,50	1,90	1,75	2,28	1,62	0,68	0,20	-0,11	0,23	0,11	0,49	-0,08	0,00	0,00	0,00	0,00	0,00		PMID: 26258633
Gadd45b	299626	ENSRNOG00000019822	growth arrest and DNA-damage-inducible, beta	6,21	7,97	5,47	4,01	5,02	3,75	5,71	6,17	0,37	-0,17	-0,62	-0,30	-0,72	-0,11	0,00	0,00	0,00	0,00	0,00	0,00		PMID: 26258633
Gins1	499914	ENSRNOG00000008091	GINS complex subunit 1	8,52	8,15	8,59	5,94	7,31	8,37	9,37	7,21	0,17	0,25	-0,28	0,02	0,21	0,38	0,00	0,00	0,00	0,00	0,00	0,00		PMID: 26258633
Kif14	360849	ENSRNOG00000037211	kinesin family member 14	2,08	4,26	2,80	1,81	2,26	2,41	3,51	1,30	1,71	1,10	0,47	0,79	0,89	1,43	0,00	0,00	-0,10	0,00	-0,10	-0,01		PMID: 26258633
Kif20b	309523	ENSRNOG00000018929	kinesin family member 20B	1,33	3,46	1,72	1,48	1,70	1,84	2,58	0,84	2,04	1,03	0,81	1,01	1,13	1,61	0,00	0,00	0,00	0,00	0,00	0,00		PMID: 26258633
Kif23	315740	ENSRNOG00000014080	kinesin family member 23	7,95	16,66	13,31	10,15	9,86	11,54	14,46	5,09	1,71	1,39	1,00	0,95	1,18	1,51	0,00	0,00	0,00	0,00	0,00	0,00		PMID: 26258633
Kntc1	304477	ENSRNOG00000033658	kinetochore associated 1	3,25	3,56	4,85	2,57	2,49	2,84	3,50	2,60	0,46	0,90	-0,02	-0,06	0,13	0,43	0,00	0,00	0,00	0,00	0,00	0,00		PMID: 26258633
Mcm3	316273	ENSRNOG00000012543	minichromosome maintenance complex component 3	24,95	17,33	26,13	19,69	24,30	22,80	23,83	20,94	-0,27	0,32	-0,09	0,21	0,12	0,19	0,00	0,00	-0,06	0,00	-0,06	0,00		PMID: 26258633
Mcm7	288532	ENSRNOG00000001349	minichromosome maintenance complex component 7	8,43	7,39	9,50	7,60	7,04	8,84	7,86	7,62	-0,04	0,32	0,00	-0,11	0,22	0,05	0,00	0,00	-0,22	0,00	-0,22	0,00		PMID: 26258633
Mre11a	64046	ENSRNOG00000009506	MRE11 homolog A, double strand break reoair nuclease	1,68	1,64	1,81	2,15	1,63	2,03	1,66	1,67	-0,03	0,11	0,36	-0,04	0,28	-0,01	0,00	0,00	-0,05	-0,09	-0,05	-0,04		PMID: 26258633
Mybl1	297783	ENSRNOG00000021669	myeloblastosis oncogene-like 1	2,31	2,14	1,46	0,56	1,11	0,76	1,83	2,08	0,04	-0,51	-1,89	-0,90	-1,45	-0,18	0,00	0,00	-0,28	0,00	-0,28	-0,03		PMID: 26258633
Myc	24577	ENSRNOG00000004500	myelocytomatosis oncogene	2,47	1,81	2,15	2,03	1,91	1,53	1,95	2,69	-0,58	-0,32	-0,41	-0,50	-0,81	-0,47	0,00	0,00	0,00	-0,22	0,00	0,00		PMID: 26258633
Pola2	85242	ENSRNOG00000020906	DNA polymerase alpha 2, accessory subunit	6,83	5,05	7,44	9,02	5,04	7,24	7,40	6,54	-0,37	0,19	0,46	-0,38	0,15	0,18	0,00	0,00	0,00	0,00	0,00	0,00		PMID: 26258633
Pole3	298098	ENSRNOG00000055277	polymerase (DNA directed), epsilon 3, accessory subunit	10,21	14,48	9,29	11,39	11,36	11,89	10,63	8,09	0,84	0,20	0,49	0,49	0,56	0,39	0,00	0,00	-0,53	0,00	-0,53	0,00		PMID: 26258633
Polh	316235	ENSRNOG00000019195	DNA polymerase eta	2,77	2,71	2,71	1,60	2,12	2,07	3,22	2,26	0,26	0,26	-0,50	-0,09	-0,13	0,51	0,00	0,00	0,00	0,00	0,00	0,00		PMID: 26258633
Psmc3ip	140938	ENSRNOG00000020022	PSMC3 interacting protein	4,00	4,90	4,91	3,79	3,51	3,91	3,88	3,75	0,39	0,39	0,01	-0,09	0,06	0,05	-0,64	0,00	0,00	0,00	0,00	0,00		PMID: 26258633
Psmg1	288236	ENSRNOG00000001643	proteasome assembly chaperone 1	6,10	5,73	3,08	6,37	5,97	5,90	5,62	4,94	0,21	-0,68	0,37	0,27	0,26	0,19	0,00	0,00	0,00	0,00	0,00	-0,22		PMID: 26258633
Rad18	362412	ENSRNOG00000005907	RAD18 E3 ubiquitin protein ligase	2,76	3,94	2,24	1,24	1,80	2,00	3,01	2,06	0,93	0,12	-0,74	-0,19	-0,04	0,55	0,00	0,00	-0,47	0,00	-0,47	-0,03		PMID: 26258633
Rrm2	362720	ENSRNOG00000054286	ribonucleotide reductase regulatory subunit M2	40,39	65,09	46,44	26,95	21,29	36,66	55,61	31,04	1,07	0,58	-0,20	-0,54	0,24	0,84	0,00	0,00	0,00	0,00	0,00	0,00		PMID: 26258633
Ruvbl2	292907	ENSRNOG00000020793	RuvB-like AAA ATPase 2	9,24	9,99	11,37	11,14	9,21	11,38	10,37	9,22	0,11	0,30	0,27	0,00	0,30	0,17	0,00	0,00	0,00	0,00	0,00	0,00		PMID: 26258633
Sgol1	363174	ENSRNOG00000022499	shugoshin 1	-	-	-	-	-	-	-	-	-	-	-	-	-	-	-	-	-	-	-	-		PMID: 26258633
Smc3	29486	ENSRNOG00000014173	structural maintenance of chromosomes 3	20,55	22,77	25,89	21,70	23,32	23,10	21,99	18,62	0,29	0,48	0,22	0,32	0,31	0,24	0,00	0,00	-0,09	0,00	-0,09	0,00		PMID: 26258633
Suv39h2	364785	ENSRNOG00000015585	suppressor of variegation 3-9 homolog 2	0,49	0,73	0,71	0,66	0,59	0,64	0,90	0,56	0,39	0,33	0,23	0,08	0,19	0,68	0,00	0,00	-0,23	0,00	-0,23	-0,10		PMID: 26258633
Timeless	83508	ENSRNOG00000031916	timeless circadian clock	3,99	2,44	4,96	4,02	3,46	3,81	3,68	3,52	-0,53	0,50	0,19	-0,03	0,12	0,06	0,00	0,00	0,00	0,00	0,00	0,00		PMID: 26258633
Tk1	24834	ENSRNOG00000047314	thymidine kinase 1	6,17	5,37	7,21	5,09	5,92	5,17	8,01	2,49	1,11	1,53	1,03	1,25	1,05	1,68	0,00	0,00	0,00	0,00	0,00	0,00		PMID: 26258633
Top2a	360243	ENSRNOG00000053047	topoisomerase (DNA) II alpha	59,77	158,05	81,57	54,36	70,39	66,40	106,43	35,91	2,14	1,18	0,60	0,97	0,89	1,57	0,00	0,00	0,00	0,00	0,00	-0,01		PMID: 26258633
Zwilch	691493	ENSRNOG00000009303	zwilch kinetochore protein	14,80	21,67	16,18	16,53	12,90	17,58	16,58	10,73	1,01	0,59	0,62	0,27	0,71	0,63	0,00	0,00	0,00	0,00	0,00	0,00		PMID: 26258633

Table 2. Actin-related genes. An update catalouge of genes known to be involved in the actin cytoskeleton remodeling is shown in the table below. The fold changes (log2) of gene expression (RPKM) upon transfection of miR-1825, miR-199a, miR-302d, miR-373, miR-590 are reported here along with the bioinformatic predictions (TargetsScan software); cel-miR-67 was used as control.

Rat Gene Name	Entrez Gene ID	Ensembl Gene ID	NCBI Gene Description	Transcriptome Expression (RPKM)								log2(Fold Change)						Bioinformatic Targeting Prediction (TargetScan)						Function/Interaction	Notes	References
				lipo	mir.1825	mir.199	mir.302d	mir.33b	mir.373	mir.590	mir.67	mir.1825	mir.199	mir.302d	mir.33b	mir.373	mir.590	mir.1825	mir.199	mir.302d	mir.33b	mir.373	mir.590			
ACTIN																										
Acta1	29437	ENSRNOG00000017786	actin, alpha 1, skeletal muscle	383,41	583,65	463,90	783,20	626,88	747,34	487,18	558,62	0,06	-0,27	0,49	0,17	0,42	-0,20	0,00	0,00	0,00	0,00	0,00	0,00		actin component in skeletal striated muscle tissue	
Acta2	81633	ENSRNOG00000058039	actin, alpha 2, smooth muscle, aorta	240,42	177,94	269,73	110,02	132,95	120,41	202,55	155,73	0,19	0,79	-0,50	-0,23	-0,37	0,38	0,00	0,00	0,00	-0,12	0,00	0,00		actin component in smoot muscle tissue	
Actb	81822	ENSRNOG00000034254	actin, beta	1210,69	1263,93	1044,71	1164,71	858,20	1046,15	971,76	1162,83	0,12	-0,15	0,00	-0,44	-0,15	-0,26	0,00	0,00	0,00	-0,15	0,00	0,00		codes for cytoskeleton	
Actc1	29275	ENSRNOG00000008536	actin, alpha, cardiac muscle 1	7975,25	6725,44	5645,82	5365,51	6442,26	5446,97	6371,87	6745,00	0,00	-0,26	-0,33	-0,07	-0,31	-0,08	0,00	0,00	0,00	0,00	0,00	0,00		actin component in cardiac muscles	
Actg1	287876	ENSRNOG00000036701	actin, gamma 1	195,85	124,78	163,44	207,81	130,37	188,14	155,17	189,06	-0,60	-0,21	0,14	-0,54	-0,01	-0,29	-0,53	0,00	0,00	0,00	0,00	0,00		codes for cytoskeleton	
Actg2	25365	ENSRNOG00000029401	actin, gamma 2, smooth muscle, enteric	21,76	11,17	22,38	12,57	9,34	12,36	14,45	23,07	-1,05	-0,04	-0,88	-1,31	-0,90	-0,67	0,00	0,00	0,00	0,00	0,00	0,00		actin component in the intestinal muscles	
Actbl2	294732	ENSRNOG00000043292	actin, beta-like 2	0,07	0,04	0,03	0,06	0,11	0,02	0,06	0,03	0,34	-0,26	0,98	1,81	-0,43	0,89	0,00	0,00	0,00	0,00	0,00	-0,10			
THYMOSINS																										
Tmsb4x	81814	ENSRNOG00000047931	thymosin beta 4, X-linked	695,76	553,95	322,24	575,05	671,76	562,40	725,25	673,02	-0,28	-1,06	-0,23	0,00	-0,26	0,11	0,00	-0,81	0,00	0,00	0,00	0,00	binds and sequesters G-actin		PMID: 15039431, 8506348, 17947588
Tmsb10	50665	ENSRNOG00000042499	thymosin, beta 10	118,40	70,49	140,13	137,56	87,80	143,61	99,55	99,62	-0,50	0,49	0,47	-0,18	0,53	0,00	0,00	0,00	0,00	0,00	0,00	-0,15	binds and sequesters G-actin		PMID: 6578703
Tmsbl1	286978	ENSRNOG00000037661	thymosin beta-like protein 1	13,42	14,47	16,13	15,55	19,40	22,15	16,08	15,17	-0,07	0,09	0,04	0,35	0,55	0,08	0,00	0,00	0,00	0,00	0,00	0,00	binds and sequesters G-actin	(by similarity)	
PROFILINS																										
Pfn1	64303	ENSRNOG00000003975	profilin 1	211,56	246,24	232,00	229,45	215,54	222,57	225,43	197,85	0,32	0,23	0,21	0,12	0,17	0,19	0,00	0,00	0,00	0,00	0,00	0,00	prevents formation of G-actin nuclei thereby inhibiting the formation of actin filaments		PMID: 8252614, 8413665
Pfn2	81531	ENSRNOG00000017427	profilin 2	2,54	3,02	3,21	1,65	1,76	1,97	2,76	2,61	0,21	0,30	-0,66	-0,57	-0,41	0,08	0,00	0,00	-0,46	-0,13	-0,46	-0,02	prevents formation of G-actin nuclei thereby inhibiting the formation of actin filaments		PMID: 8252614, 8413665
Pfn3	685936	ENSRNOG00000047752	profilin 3	-	-	-	-	-	-	-	-	-	-	-	-	-	-	-	-	-	-	-	-	prevents formation of G-actin nuclei thereby inhibiting the formation of actin filaments		PMID: 8252614, 8413665
Pfn4	494222	ENSRNOG00000050386	profilin family, member 4	-	-	-	-	-	-	-	-	-	-	-	-	-	-	-	-	-	-	-	-	prevents formation of G-actin nuclei thereby inhibiting the formation of actin filaments		PMID: 8252614, 8413665
TWINFILINS																										
Twf1	315265	ENSRNOG00000022507	twinfilin actin-binding protein 1	16,29	21,98	10,49	12,81	19,99	13,87	13,50	18,71	0,23	-0,83	-0,55	0,10	-0,43	-0,47	0,00	0,00	-0,34	0,00	-0,34	-0,18	binds to G-actin and promotes its sequestration thereby inhibiting actin polymerization		PMID: 11870207, 12207032, 12429826
Twf2	684352	ENSRNOG00000048915	twinfilin actin-binding protein 2	17,14	9,15	10,98	12,90	12,13	11,76	13,88	20,05	-1,13	-0,87	-0,64	-0,73	-0,77	-0,53	0,00	0,00	0,00	0,00	0,00	0,00	binds to G-actin and promotes its sequestration thereby inhibiting actin polymerization		PMID: 11870207, 12207032, 12429826
SEVERING PROTEINS																										
Gsn	296654	ENSRNOG00000018991	gelsolin	9,94	12,85	19,62	8,54	10,67	10,01	13,49	7,96	0,69	1,30	0,10	0,42	0,33	0,76	0,00	0,00	0,00	0,00	0,00	0,00	severing protein; caps the actin filament at (+) end		PMID: 3021782
Cfl1	29271	ENSRNOG00000020660	cofilin 1	337,07	340,04	235,34	423,38	313,58	389,25	310,88	319,65	0,09	-0,44	0,41	-0,03	0,28	-0,04	-0,10	0,00	0,00	0,00	0,00	0,00	severing protein	non-muscle cofilin	PMID: 9265645, 9087445
Cfl2	366624	ENSRNOG00000045892	cofilin 2	82,18	37,55	35,05	27,73	51,10	32,81	93,01	73,21	-0,96	-1,06	-1,40	-0,52	-1,16	0,35	-0,36	-0,61	-0,52	0,00	-0,52	-0,07	severing protein	muscle cofilin	PMID: 9265645, 9087445
Dstn	502674	502674ENSRNOG00000005924	destrin, actin depolymerizing factor	513,24	529,62	561,02	468,28	512,72	458,89	550,29	451,99	0,23	0,31	0,05	0,18	0,02	0,28	0,00	0,00	0,00	-0,17	0,00	-0,07	severing protein		PMID: 9265645, 9087445
Dstnl1	296197		destrin-like 1	251,57	284,07	280,05	232,44	266,28	231,67	279,94	223,31	0,35	0,33	0,06	0,25	0,05	0,33	0,00	0,00	0,00	0,00	0,00	0,00	(by similarity)		
CAPPING PROTEINS																										
Capza3	29324	ENSRNOG00000008727	capping actin protein of muscle Z-line alpha subunit 3	-	-	-	-	-	-	-	-	-	-	-	-	-	-	-	-	-	-	-	-	caps the actin filament at (+) end		PMID: 9915586
Capzb	298584	ENSRNOG00000007330	capping actin protein of muscle Z-line beta subunit	9,52	7,80	10,52	9,71	10,04	9,74	8,99	9,40	-0,27	0,16	0,05	0,10	0,05	-0,06	0,00	0,00	0,00	-0,22	0,00	0,00	caps the actin filament at (+) end		PMID: 9915586
Capg	297339	ENSRNOG00000013668	capping actin protein, gelsolin like	2,34	1,75	1,56	1,40	1,63	1,84	1,76	1,81	-0,05	-0,21	-0,37	-0,15	0,02	-0,04	0,00	0,00	0,00	0,00	0,00	0,00	caps the actin filament at (+) end		PMID: 2255912
Tmod1	25566	ENSRNOG00000009761	tropomodulin 1	28,32	18,29	23,07	26,66	22,87	28,13	25,07	29,92	-0,71	-0,38	-0,17	-0,39	-0,09	-0,25	0,00	-0,07	0,00	0,00	0,00	0,00	caps the actin filament at (-) end		PMID: 7798317
Tmod2	58814	ENSRNOG00000010447	tropomodulin 2	0,04	0,05	0,02	0,24	0,21	0,17	0,03	0,05	0,02	-1,12	2,35	2,16	1,85	-0,62	-0,31	-0,19	-0,33	0,00	-0,33	-0,11	caps the actin filament at (-) end		PMID: 7798317
Tmod3	300838	ENSRNOG00000032436	tropomodulin 3	15,53	17,90	15,99	19,02	16,63	19,70	17,43	15,49	0,21	0,05	0,30	0,10	0,35	0,17	0,00	0,00	0,00	0,00	0,00	-0,17	caps the actin filament at (-) end		PMID: 7798317
Tmod4	295261	ENSRNOG00000021088	tropomodulin 4	0,05	0,03	0,06	0,11	0,06	0,04	0,04	0,04	-0,24	0,82	1,69	0,74	0,31	0,05	-0,54	0,00	0,00	0,00	0,00	0,00	caps the actin filament at (-) end		PMID: 7798317
Mtpn	79215	ENSRNOG00000011857	myotrophin	97,44	120,51	72,68	73,15	90,70	79,24	104,28	82,45	0,55	-0,18	-0,17	0,14	-0,06	0,34	0,00	0,00	-0,16	-0,09	-0,16	-0,19	uncapping protein		PMCID: PMC2277501; PMID: 12488317
Carmil1	306941	ENSRNOG00000016576	capping protein regulator and myosin 1 linker 1	0,44	0,62	0,48	0,67	0,87	0,89	0,45	0,45	0,47	0,10	0,58	0,95	0,98	0,01	0,00	0,00	0,00	0,00	0,00	0,00	uncapping protein		PMID: 16054028
Carmil2	307797	ENSRNOG00000024452	capping protein regulator and myosin 1 linker 2	0,10	0,12	0,10	0,14	0,10	0,13	0,13	0,07	0,85	0,55	1,07	0,53	0,96	0,94	0,00	0,00	0,00	0,00	0,00	0,00	uncapping protein		PMID: 16054028
Carmil3	361041	ENSRNOG00000025518	capping protein regulator and myosin 1 linker 3	0,03	0,03	0,02	0,12	0,06	0,07	0,03	0,03	-0,15	-0,46	1,77	0,89	1,09	-0,01	0,00	0,00	0,00	0,00	0,00	0,00	uncapping protein		PMID: 16054028
ACTIN NUCLEATORS																										
Fmn1	296512		formin 1	0,13	0,18	0,16	0,14	0,11	0,13	0,15	0,21	-0,28	-0,40	-0,57	-0,89	-0,74	-0,46	-0,25	-0,05	-0,03	-0,05	-0,03	-0,09	nucleating/elongation factors mediating the assembly of unbranched actin networks		PMCID: PMC2854303
Fmn2	1E+08		formin 2	-	-	-	-	-	-	-	-	-	-	-	-	-	-	-	-	-	-	-	-	nucleating/elongation factors mediating the assembly of unbranched actin networks	facilitates binding of formins	PMCID: PMC2854303
Fmnl1	287746	ENSRNOG00000003207	formin-like 1	0,02	0,01	0,01	0,01	0,01	0,01	0,01	0,02	-0,83	-0,26	-0,28	-1,26	-0,56	-0,37	0,00	0,00	0,00	0,00	0,00	0,00	(by similarity)		
Fmnl2	311033		formin-like 2	-	-	-	-	-	-	-	-	-	-	-	-	-	-	-	-	-	-	-	-	(by similarity)		
Fmnl3	300225	ENSRNOG00000056297	formin-like 3	0,68	0,68	0,76	0,66	0,64	0,73	0,58	0,74	-0,11	0,05	-0,16	-0,21	-0,01	-0,34	0,00	0,00	-0,12	0,00	-0,12	0,00	(by similarity)		
Diaph1	307483	ENSRNOG00000019688	diaphanous-related formin 1	1,19	1,35	1,12	1,47	1,45	1,64	1,17	1,44	-0,09	-0,36	0,03	0,01	0,19	-0,30	-0,04	-0,01	0,00	-0,02	0,00	0,00	nucleating/elongation factors mediating the assembly of unbranched actin networks	catalyzes filament elongation	PMCID: PMC2854303
Diaph2	317189		diaphanous-related formin 2	1,14	1,21	1,04	0,87	0,75	1,00	0,97	0,94	0,36	0,15	-0,12	-0,32	0,09	0,04	0,00	-0,07	-0,04	0,00	-0,04	-0,02	nucleating/elongation factors mediating the assembly of unbranched actin networks		PMCID: PMC2854303
Diaph3	290396	ENSRNOG00000008986	diaphanous-related formin 3	5,30	7,18	6,73	3,05	3,08	3,75	5,79	3,47	1,05	0,96	-0,19	-0,17	0,11	0,74	-0,02	0,00	0,00	0,00	0,00	-0,02	nucleating/elongation factors mediating the assembly of unbranched actin networks		PMCID: PMC2854303
Daam1	314212	ENSRNOG00000004345	dishevelled associated activator of morphogenesis 1	1,92	2,12	1,82	2,77	2,05	2,63	2,62	2,28	-0,11	-0,32	0,28	-0,15	0,21	0,20	0,00	0,00	0,00	-0,09	0,00	-0,08	nucleating/elongation factors mediating the assembly of unbranched actin networks		PMCID: PMC2854303
Daam2	316201	ENSRNOG00000053945	dishevelled associated activator of morphogenesis 2	2,14	1,17	2,39	1,98	1,17	1,96	1,83	2,37	-1,02	0,01	-0,26	-1,02	-0,28	-0,37	0,00	0,00	-0,02	0,00	-0,02	-0,02	nucleating/elongation factors mediating the assembly of unbranched actin networks		PMCID: PMC2854303
Actr2	289820	ENSRNOG00000004959	ARP2 actin related protein 2 homolog	25,31	28,87	26,60	26,58	29,23	27,79	21,54	26,84	0,10	-0,01	-0,01	0,12	0,05	-0,32	0,00	0,00	0,00	-0,26	0,00	-0,81	creates new nucleation cores to stimulate actin polymerization	major constituents of the Arp2/3 complex	PMID: 16262445
Actr3	81732	ENSRNOG00000003206	ARP3 actin related protein 3 homolog	167,62	166,32	157,66	140,23	150,10	136,38	175,82	165,76	0,00	-0,07	-0,24	-0,14	-0,28	0,09	0,00	0,00	0,00	0,00	0,00	0,00	creates new nucleation cores to stimulate actin polymerization	major constituents of the Arp2/3 complex	PMID: 16262445
Arpc1a	81824	ENSRNOG00000000996	actin related protein 2/3 complex, subunit 1A	31,09	30,90	28,19	29,36	28,41	31,42	29,27	29,82	0,05	-0,08	-0,02	-0,07	0,08	-0,03	0,00	0,00	0,00	0,00	0,00	-0,05	creates new nucleation cores to stimulate actin polymerization	major constituents of the Arp2/3 complex	PMID: 16262445
Arpc1b	54227	ENSRNOG00000000991	actin related protein 2/3 complex, subunit 1B	83,99	69,86	81,23	56,68	69,21	63,32	65,30	76,30	-0,13	0,09	-0,43	-0,14	-0,27	-0,22	0,00	0,00	0,00	-0,32	0,00	0,00	creates new nucleation cores to stimulate actin polymerization	major constituents of the Arp2/3 complex	PMID: 16262445
Arpc2	301511	ENSRNOG00000014289	actin related protein 2/3 complex, subunit 2	33,13	22,18	32,54	32,87	32,68	31,37	30,54	31,74	-0,52	0,04	0,05	0,04	-0,02	-0,06	0,00	0,00	0,00	0,00	0,00	0,00	creates new nucleation cores to stimulate actin polymerization	major constituents of the Arp2/3 complex	PMID: 16262445
Arpc3	288669	ENSRNOG00000008673	actin related protein 2/3 complex, subunit 3	57,66	52,77	53,63	62,86	62,56	65,63	48,29	57,20	-0,12	-0,09	0,14	0,13	0,20	-0,24	0,00	0,00	0,00	0,00	0,00	0,00	creates new nucleation cores to stimulate actin polymerization	major constituents of the Arp2/3 complex	PMID: 16262445
Arpc4	297518	ENSRNOG00000008994	actin related protein 2/3 complex, subunit 4	51,15	41,93	49,93	50,56	43,40	52,22	42,55	50,13	-0,26	-0,01	0,01	-0,21	0,06	-0,24	-0,27	0,00	0,00	0,00	0,00	0,00	creates new nucleation cores to stimulate actin polymerization	major constituents of the Arp2/3 complex	PMID: 16262445
Arpc5	360854	ENSRNOG00000028062	actin related protein 2/3 complex, subunit 5	50,66	65,54	61,97	55,22	32,26	54,47	34,95	49,96	0,39	0,31	0,14	-0,63	0,12	-0,52	0,00	0,00	0,00	0,00	0,00	-0,07	creates new nucleation cores to stimulate actin polymerization	major constituents of the Arp2/3 complex	PMID: 16262445
Arpc5l	296710	ENSRNOG00000014317	actin related protein 2/3 complex, subunit 5-like	39,99	28,84	37,77	38,50	37,41	36,05	39,98	42,06	-0,54	-0,16	-0,13	-0,17	-0,22	-0,07	-0,18	0,00	0,00	0,00	0,00	0,00	creates new nucleation cores to stimulate actin polymerization	major constituents of the Arp2/3 complex	PMID: 16262445
Was	317371	ENSRNOG00000031058	Wiskott-Aldrich syndrome	0,28	0,05	0,13	0,23	0,22	0,28	0,32	0,19	-1,83	-0,52	0,27	0,23	0,57	0,77	0,00	0,00	0,00	0,00	0,00	0,00	binds and activates Arp2/3 complex		PMID: 19625501
Wasf1	294568	ENSRNOG00000047476	WAS protein family, member 1	0,20	0,20	0,13	0,30	0,29	0,34	0,19	0,14	0,48	-0,15	1,09	1,06	1,26	0,44	0,00	0,00	0,00	-0,13	0,00	0,00	binds and activates Arp2/3 complex	contains WASp domains	PMID: 19625501
Wasf2	313024	ENSRNOG00000009805	WAS protein family, member 2	1,39	2,02	1,68	1,83	1,76	1,51	1,36	1,29	0,65	0,39	0,50	0,45	0,23	0,08	0,00	0,00	0,00	-0,05	0,00	0,00	binds and activates Arp2/3 complex	contains WASp domains	PMID: 19625501
Wasf3	682937		WAS protein family, member 3	0,01	0,02	0,00	0,03	0,01	0,02	0,02	0,01	0,76	#NAME?	1,40	0,00	0,57	0,89	0,00	0,00	-0,55	0,00	-0,55	-1,45	binds and activates Arp2/3 complex	contains WASp domains	PMID: 19625501

Wash1	367328	ENSRNOG00000053306	WAS protein family homolog 1	6,14	6,09	5,86	6,53	6,29	6,82	6,28	6,69	-0,13	-0,19	-0,04	-0,09	0,03	-0,09	0,00	0,00	0,00	0,00	0,00	0,00	binds and activates Arp2/3 complex	contains WASp domains	PMID: 19625501
Wasl	682507	ENSRNOG00000006975	Wiskott-Aldrich syndrome-like	2,41	3,51	2,79	2,15	3,13	2,56	2,23	3,15	0,16	-0,17	-0,55	-0,01	-0,30	-0,50	-0,30	0,00	0,00	0,00	0,00	-0,14	binds and activates Arp2/3 complex	contains WASp domains	PMID: 19625501
Spire1	307348	ENSRNOG00000025324	spire-type actin nucleation factor 1	0,61	0,55	0,67	0,63	0,74	0,70	0,51	0,65	-0,23	0,04	-0,03	0,19	0,12	-0,34	0,00	-0,42	0,00	0,00	0,00	-0,09	creates new nucleation cores with their G-actin binding motifs	tandem-monomer-binding nucleators	PMID: 15674283
Spire2	307925	ENSRNOG00000016920	spire-type actin nucleation factor 2	-	-	-	-	-	-	-	-	-	-	-	-	-	-	-	-	-	-	-	-	creates new nucleation cores with their G-actin binding motifs	tandem-monomer-binding nucleators	PMID: 15674283
Cobl	305497	ENSRNOG00000004281	cordon-bleu WH2 repeat protein	0,32	0,19	0,30	0,16	0,19	0,23	0,24	0,16	0,27	0,95	0,05	0,25	0,54	0,62	-0,02	0,00	0,00	0,00	0,00	0,00	creates new nucleation cores with their G-actin binding motifs	tandem-monomer-binding nucleators	PMID: 17956734
Cobl1	311088	ENSRNOG00000027016	cordon-bleu WH2 repeat protein-like 1	0,09	0,08	0,10	0,09	0,09	0,10	0,09	0,09	-0,23	0,08	-0,06	-0,05	0,14	-0,10	-0,02	-0,18	0,00	0,00	0,00	-0,03	creates new nucleation cores with their G-actin binding motifs	tandem-monomer-binding nucleators	PMID: 17956734
Lmod1	304816	ENSRNOG00000051548	leiomodin 1	2,08	0,94	1,67	0,79	0,60	0,84	1,48	1,65	-0,82	0,01	-1,06	-1,46	-0,98	-0,16	-0,37	0,00	0,00	0,00	0,00	0,00	creates new nucleation cores with their G-actin binding motifs	tandem-monomer-binding nucleators	PMID: 19406642
Lmod2	296935	ENSRNOG00000045831	leiomodin 2	168,81	139,07	103,93	104,57	108,30	86,73	152,98	160,95	-0,21	-0,63	-0,62	-0,57	-0,89	-0,07	0,00	0,00	0,00	0,00	0,00	0,00	creates new nucleation cores with their G-actin binding motifs	tandem-monomer-binding nucleators	PMID: 19406642
Lmod3	500267	ENSRNOG00000032443	leiomodin 3	0,18	0,06	0,25	0,11	0,11	0,16	0,36	0,20	-1,78	0,36	-0,80	-0,91	-0,34	0,87	0,00	0,00	0,00	0,00	0,00	0,00	creates new nucleation cores with their G-actin binding motifs	tandem-monomer-binding nucleators	PMID: 19406642
Jmy	683593		junction mediating and regulatory protein, p53 cofactor	1,23	1,64	0,90	0,75	1,54	0,79	0,82	1,47	0,15	-0,71	-0,97	0,06	-0,89	-0,84	0,00	-0,02	-0,17	-0,05	-0,17	-0,13	creates new nucleation cores with their G-actin binding motifs	tandem-monomer-binding nucleators	PMID: 19287377
Apc	24205	ENSRNOG00000020423	APC, WNT signaling pathway regulator	0,54	0,54	0,59	0,55	0,52	0,58	0,49	0,56	-0,03	0,08	-0,01	-0,10	0,06	-0,19	-0,01	0,00	-0,19	-0,04	-0,19	-0,07	creates new nucleation cores with their G-actin binding motifs	tandem-monomer-binding nucleators	PMID: 20566685
Apc2	299611	ENSRNOG00000033791	APC2, WNT signaling pathway regulator	0,11	0,10	0,11	0,12	0,12	0,11	0,10	0,14	-0,42	-0,41	-0,17	-0,17	-0,34	-0,51	0,00	0,00	0,00	0,00	0,00	0,00	creates new nucleation cores with their G-actin binding motifs	tandem-monomer-binding nucleators	PMID: 20566685
																OTHER PROTEINS									
Tpm1	24851	ENSRNOG00000018184	tropomyosin 1, alpha	74,33	62,51	71,31	58,17	54,99	61,73	64,40	69,80	-0,16	0,03	-0,26	-0,34	-0,18	-0,12	0,00	0,00	0,00	0,00	0,00	0,00	inhibits the rate of actin polymerization by stabilization		PMID: 3242622
Tpm2	500450	ENSRNOG00000016731	tropomyosin 2, beta	67,88	52,56	59,34	44,80	45,28	46,29	59,03	52,01	0,02	0,19	-0,22	-0,20	-0,17	0,18	-0,48	-0,05	-0,25	0,00	-0,25	0,00	inhibits the rate of actin polymerization by stabilization		PMID: 3242622
Tpm3	117557	ENSRNOG00000017441	tropomyosin 3	3,79	4,45	3,82	4,26	3,80	4,38	3,43	3,37	0,40	0,18	0,34	0,17	0,38	0,02	0,00	0,00	0,00	0,00	0,00	0,00	inhibits the rate of actin polymerization by stabilization		PMID: 3242622
Tpm4	24852	ENSRNOG00000015496	tropomyosin 4	421,67	327,25	477,71	401,48	296,20	387,40	396,18	382,11	-0,22	0,32	0,07	-0,37	0,02	0,05	0,00	0,00	0,00	0,00	0,00	0,00	inhibits the rate of actin polymerization by stabilization		PMID: 3242622
Mical1	294520	ENSRNOG00000000307	microtubule associated monooxygenase, microtubule associated monooxygenase, microtubule associated monooxygenase,	4,92	2,81	5,97	4,49	3,82	3,89	3,48	4,59	-0,71	-0,38	-0,03	-0,27	-0,24	-0,40	0,00	0,00	0,00	0,00	0,00	0,00	synergizes with Cfl2 to depolymerize F-actin		PMID: 27454820
Mical2	365352	ENSRNOG00000016244		4,36	4,15	3,68	3,56	3,64	3,48	3,73	4,30	-0,05	-0,22	-0,27	-0,24	-0,31	-0,20	0,00	0,00	0,00	0,00	0,00	0,00	synergizes with Cfl2 to depolymerize F-actin		PMID: 27454820
Mical3	362427	ENSRNOG00000053203		11,57	12,32	10,00	9,91	10,80	8,99	12,29	13,96	-0,18	-0,48	-0,49	-0,37	-0,63	-0,18	-0,22	0,00	-0,05	0,00	-0,05	-0,02	synergizes with Cfl2 to depolymerize F-actin		PMID: 27454820
Micall1	362958	ENSRNOG00000026212	MICAL-like 1	1,63	1,54	1,47	2,26	1,79	2,18	1,63	1,66	-0,11	-0,17	0,44	0,11	0,39	-0,03	-0,12	0,00	-0,05	0,00	-0,05	0,00	(by similarity)		
Micall2	288515	ENSRNOG00000022533	MICAL-like 2	1,07	1,28	0,87	0,93	0,98	0,88	0,89	0,94	0,44	-0,11	-0,03	0,05	-0,10	-0,09	0,00	0,00	0,00	0,00	0,00	0,00	(by similarity)		
Csrp3	117505	ENSRNOG00000014327	cysteine and glycine rich protein 3	353,87	247,12	142,86	231,14	196,24	221,96	222,90	330,86	-0,42	-1,21	-0,52	-0,75	-0,58	-0,57	0,00	0,00	0,00	0,00	0,00	-0,12	interacts with Cfl2 and aids in F-actin depolymerization	contains two LIM domains	PMID: 19752190
Aurka	261730	ENSRNOG00000004479	aurora kinase A	3,23	11,17	3,76	4,49	4,38	4,86	7,53	2,08	2,43	0,86	1,11	1,08	1,23	1,86	0,00	-0,19	0,00	0,00	0,00	0,00	phosphorylates Cfl2 thereby inhibiting its function	target gene of Yap/TEAD transcription activation	PMID: 25090971, 22308401
Aurkb	114592	ENSRNOG00000005659	aurora kinase B	3,02	4,92	3,64	3,55	3,11	3,35	4,24	1,94	1,34	0,91	0,87	0,68	0,79	1,13	0,00	0,00	0,00	0,00	0,00	0,00	phosphorylates Cfl2 thereby inhibiting its function	target gene of Yap/TEAD transcription activation	PMID: 25090971, 22308401
Mkl1	315151	ENSRNOG00000018803	megakaryoblastic leukemia (translocation) 1	0,16	0,20	0,18	0,20	0,25	0,22	0,18	0,17	0,20	0,08	0,22	0,55	0,32	0,05	0,00	0,00	0,00	0,00	0,00	0,00	bound to free G-actin and is released upon nucleation, initiates transcription with its interaction of transnucleated Yap		PMID: 12732141, 12732141, 28028053

Table 3. FDA-registered drug screening results. Each drug is characterized by the FDA-registration number and with the name of the compound.

The z-score mean value obtained by the evaluation of EdU+CMs in fold changes over control (for column 1= miR-67, column 2= miR-199a-3p, column 3= n

n=3 indipendent experiments.

cel-miR-67	*z-score mean*	*hsa-miR-199a-3p*	*z-score mean*	*hsa-miR-590-3p*	*z-score mean*
442-51-3 - Harmine, [H04]	4,302209435	442-51-3 - Harmine, [H04]	4,835986201	442-51-3 - Harmine, [H04]	5,288410519
16320-04-0 - Gestrinone, [L15]	3,609728936	50-91-9 - Floxuridine, [J11]	2,523485819	1400-61-9 - Nystatin, [E06]	3,00315612
135046-48-9 - Clopidogrel sulfate, [O21]	3,16249897	555-30-6 - Methyldopa, [A12]	2,357681895	1421-86-9 - Strychnine HCl, [D03]	2,996807097
63-92-3 - Phenoxybenzamine HCl, [I10]	3,0704343	102767-28-2 - Levetiracetam, [L20]	2,332820399	75847-73-3 - Enalapril, [F07]	2,923657741
127045-41-4 - Pazufloxacin, [G08]	2,970817217	59804-37-4 - Tenoxicam, [O20]	2,320392418	51-48-9 - L-thyroxine [(3-[4-(4-hydroxy-3	2,870190593
22494-42-4 - Diflunisal, [D15]	2,907878738	298-46-4 - Carbamazepine, [M07]	2,298257552	68475-42-3 - Anagrelide, [C22]	2,764688972
cel-67, [L02]	2,823268192	34911-55-2 - Amfebutamone, [H13]	2,296888605	1744-22-5 - Riluzole HCl, [O19]	2,695375756
64-47-1 - Physostigmine sulfate, [M11]	2,796058859	81-24-3 - Taurocholic acid, sodium salt hydrate, [N18]	2,138529634	112964-99-5 - Hydroxytacrine maleate, [	2,686969862
11018-89-6 - Ouabain, [I20]	2,521178645	93479-97-1 - Glimepiride, [L17]	2,128706656	115956-12-2 - Dolasetron, [N22]	2,678050227
139264-17-8 - zolmitriptan, [O13]	2,465211256	54-85-3 - Isoniazid, [J15]	1,961600176	93479-97-1 - Glimepiride, [L17]	2,656415576
56-53-1 - Diethylstilbestrol, [D13]	2,317817115	24729-96-2 - Clindamycin palmitate, [N16]	1,955836289	70458-96-7 - Norfloxacin, [E04]	2,586417727
21535-47-7 - Mianserin hcl, [B03]	2,254082464	73210-73-8 - Xamoterol hemifumarate, [I13]	1,889477934	32828-81-2 - Picotamide, [L18]	2,580532569
68373-14-8 - Sulbactam, [E07]	2,249205068	134308-13-7 - Tolcapone, [L13]	1,860628704	104227-87-4 - Famciclovir, [H09]	2,551573735
53885-35-1 - Ticlopidine HCl, [J17]	2,108451047	20537-88-6 - Amifostine, [I03]	1,806075822	68-35-9 - Sulfadiazine, [O10]	2,53878607
26807-65-8 - Indapamide, [N15]	2,097717673	645-05-6 - Altretamine, [G17]	1,749431883	41859-67-0 - Bezafibrate, [F04]	2,508372407
53-16-7 - Estrone, [F21]	2,071084733	19728-88-2 - Methiothepin maleate, [O12]	1,719849363	54-42-2 - Idoxuridine, [N09]	2,435270078
124832-27-5 - Valaciclovir, [D20]	2,062832738	73590-58-6 - Omeprazole, [E12]	1,67329992	28721-07-5 - Oxcarbazepine, [E14]	2,431940378
5536-17-4 - Vidarabine, [F06]	2,053082531	93106-60-6 - Enrofloxacin, [F11]	1,667314975	53-43-0 - Dehydroepiandrosterone, [D0	2,418653261
139481-59-7 - Candesartan, [N21]	2,02530921	1501-84-4 - Rimantadine HCl, [K20]	1,664883143	68550-75-4 - Cilostamide, [J06]	2,384203156
581-88-4 - Debrisoquin sulfate, [O10]	2,022893494	74011-58-8 - Enoxacin, [F09]	1,663026965	19387-91-8 - Tinidazole, [B14]	2,375552942
93479-97-1 - Glimepiride, [L17]	1,978782304	5536-17-4 - Vidarabine, [F06]	1,657320145	115344-47-3 - Siguazodan, [J18]	2,354910367
124750-99-8 - Losartan potassium, [P21]	1,958478025	36330-85-5 - Fenbufen, [H13]	1,547951178	2963-78-2 - Butyrylcholine Cl, [J09]	2,322087608
69004-03-1 - Toltrazuril, [D08]	1,924130818	95635-56-6 - Ranolazine 2HCl, [K10]	1,531358122	13710-19-5 - Tolfenamic acid, [D04]	2,309798117
16676-29-2 - Naltrexone HCl, [O11]	1,913104378	50-12-4 - Mephenytoin, [J22]	1,509375397	81110-73-8 - Racecadotril, [K08]	2,246864088
35208-55-0 - Clindamycin PO4, [A07]	1,882864461	135046-48-9 - Clopidogrel sulfate, [O21]	1,501867801	161814-49-9 - Amprenavir, [N10]	2,203855566
73590-58-6 - Omeprazole, [E12]	1,865262026	149-64-4 - Scopolamine n-butylbromide, [M12]	1,472369974	2078-54-8 - Propofol, [O21]	2,159406811
18046-21-4 - Fentiazac, [J20]	1,853208683	13710-19-5 - Tolfenamic acid, [D04]	1,451384181	73590-58-6 - Omeprazole, [E12]	2,156869554
590-63-6 - Carbamyl-beta-methylcholine Cl, [J07]	1,835542093	1405-41-0 - Gentamycin sulfate, [L11]	1,450249533	124832-27-5 - Valaciclovir, [D20]	2,150171963
10118-90-8 - Minocycline HCl, [C04]	1,800908069	51-48-9 - L-thyroxine [(3-[4-(4-hydroxy-3,5-diiodopheno	1,447595474	20537-88-6 - Amifostine, [I03]	2,130884137
33386-08-2 - Buspirone HCl, [K19]	1,760548193	1405-10-3 - Neomycin sulfate, [O16]	1,441692529	114-49-8 - Scopolamine HBr, [M14]	2,126549725
65141-46-0 - Nicorandil, [L12]	1,744530781	84-16-2 - Hexestrol, [L21]	1,41109735	298-46-4 - Carbamazepine, [M07]	2,125258686
74764-40-2 - Bepridil, [C05]	1,741441615	590-63-6 - Carbamyl-beta-methylcholine Cl, [J07]	1,410595833	57-94-3 - Tubocurarine Cl (+), [D05]	2,112398868
139755-83-2 - Sildenafil, [N11]	1,723146024	93793-83-0 - Roxatidine acetate HCl, [M04]	1,367488738	62893-19-0 - Cefoperazone acid, [M09]	2,092274112
84625-61-6 - Itraconazole, [N19]	1,673956842	70458-96-7 - Norfloxacin, [E04]	1,349538816	139755-83-2 - Sildenafil, [N11]	2,078878959
151615 - Oxymetazoline HCl, [G03]	1,654779029	87333-19-5 - Ramipril, [K12]	1,339677251	82009-34-5 - Cilastatin, [L14]	2,06733222
115344-47-3 - Siguazodan, [J18]	1,574371767	53902-12-8 - Tranilast, [K08]	1,323318125	85622-93-1 - Temozolomide, [B08]	2,050923472
78415-72-2 - Milrinone, [J14]	1,573719823	28721-07-5 - Oxcarbazepine, [E14]	1,300927606	5104-49-4 - Flurbiprofen, [J05]	2,047711567
59729-33-8 - Citalopram, [O09]	1,5693853	93-14-1 - Guaifenesin, [L19]	1,273895036	91161-71-6 - Terbinafine HCl, [B20]	2,039370819
64490-92-2 - Tolmetin Na, [D06]	1,567525952	7177-48-2 - Ampicillin trihydrate, [I11]	1,262699711	57381-26-7 - Irsogladine maleate, [J12]	1,998735769
72599-27-0 - Miglustat, [N20]	1,566005107	14838-15-4 - Phenylpropanolamine, [P12]	1,25525547	24390-14-5 - Doxycycline HCl, [F05]	1,963278781
61-68-7 - Mefenamic acid, [A08]	1,565476017	59277-89-3 - Acycloguanosine, [G09]	1,248197706	60-54-8 - Tetracycline, [B04]	1,961661186
37321-09-8 - Apramycin, [I15]	1,565155129	25812-30-0 - Gemfibrozil, [L13]	1,247801943	42924-53-8 - Nabumetone, [C14]	1,935502307
72558-82-8 - Ceftazidime, [M13]	1,562765435	112811-59-3 - Gatifloxacin, [L09]	1,236435388	19453 - Galanthamine HBr, [G04]	1,924470557
121268-17-5 - Alendronate, [G15]	1,538515787	39809-25-1 - Penciclovir, [G12]	1,229936063	16676-29-2 - Naltrexone HCl, [O11]	1,917644454
88040-23-7 - Cefepime, [N17]	1,536867208	84625-61-6 - Itraconazole, [N19]	1,226440176	125-69-9 - Dextromethorphan HBr, [D07	1,917140012
154-21-2 - Lincomycin, [A13]	1,524107521	99-66-1 - Valproic acid, [J06]	1,213510926	17360-35-9 - Oxotremorine sesquifumar	1,907510325
55528-07-9 - Butaclamol (+), [D07]	1,523213485	32828-81-2 - Picotamide, [L18]	1,202980261	112811-59-3 - Gatifloxacin, [L09]	1,899607247
158966-92-8 - Montelukast, [C08]	1,50960949	33386-08-2 - Buspirone HCl, [K19]	1,198812035	132539-06-1 - Olanzapine, [N03]	1,879075245
50-12-4 - Mephenytoin, [J22]	1,497887931	82419-36-1 - Ofloxacin, [E08]	1,184132874	111406-87-2 - Zileuton, [J12]	1,861088482
106017-08-7 - Rufloxacin, [M08]	1,477293324	78613-35-1 - Amorolfine, [J19]	1,180603079	21187-98-4 - Gliclazide, [L15]	1,843666802
68550-75-4 - Cilostamide, [J06]	1,47420242	2068-78-2 - Vincristine sulfate, [E19]	1,178240007	636-54-4 - Clopamide, [I22]	1,837922345
75330-75-5 - Lovastatin, [N05]	1,441221105	106463-17-6 - Tamsulosin HCl, [O16]	1,170182394	7481-89-2 - 2',3' - dideoxycytidine, [D11	1,823923639
81103-11-9 - Clarithromycin, [O11]	1,42150393	1677687 - Pentoxifylline, [G14]	1,148647879	84371-65-3 - Mifepristone, [L22]	1,820252447
21462-39-5 - Clindamycin HCl, [A05]	1,418945496	hsa-199, [E02]	1,136056592	26807-65-8 - Indapamide, [N15]	1,817605171
52-01-7 - Spironolactone, [M22]	1,414420153	152459-95-5 - Imatinib, [C04]	1,134293347	29094-61-9 - Glipizide, [C21]	1,817470104
99-66-1 - Valproic acid, [J06]	1,407698829	1156-19-0 - Tolazamide, [L10]	1,122233376	84-16-2 - Hexestrol, [L21]	1,817314922
15826-37-6 - Disodium cromoglycate, [M10]	1,407477365	517- 89- 5 - Shikonin, [K10]	1,109332549	15291-75-5 - Ginkgolide a, [P12]	1,81550645
59277-89-3 - Acycloguanosine, [G09]	1,403199289	82586-55-8 - Quinapril HCl, [K06]	1,108982995	24729-96-2 - Clindamycin palmitate, [N1	1,790195563
50-28-2 - Estradiol, [F17]	1,398190836	19453 - Galanthamine HBr, [G04]	1,086217684	95635-56-6 - Ranolazine 2HCl, [K10]	1,788113213
73-31-4 - Melatonin, [E10]	1,368199081	7240-38-2 - Oxacillin sodium monohydrate, [E18]	1,077839461	113712-98-4 - Tenatoprazole, [B06]	1,784939517
111406-87-2 - Zileuton, [J12]	1,364271841	67227-56-9 - Fenoldopam mesylate, [H15]	1,051288339	72432-10-1 - Aniracetam, [O17]	1,784153004
114-80-7 - Neostigmine Br, [B21]	1,361510968	hsa-199, [F02]	1,047284422	379-79-3 - Ergotamine D-tartrate, [H22]	1,776432922
2393-92-2 - Thiamphenicol glycinate, [E09]	1,33181623	110871-86-8 - Sparfloxacin, [M20]	1,046940315	113806-05-6 - Olopatadine, [L09]	1,774067668
63527-52-6 - Cefotaxime acid, [M11]	1,319063163	4394-00-7 - Niflumic acid, [C20]	1,039837802	58066-85-6 - Miltefosine, [I16]	1,751725036
146-48-5 - Yohimbine HCl, [G19]	1,309818249	64490-92-2 - Tolmetin Na, [D06]	1,027566562	50700-72-6 - Vecuronium Br, [D22]	1,723252074
7414-83-7 - Etidronate 2Na, [H03]	1,306350327	13523-86-9 - Pindolol, [I21]	1,0100818	110871-86-8 - Sparfloxacin, [M20]	1,71724195
91161-71-6 - Terbinafine HCl, [B20]	1,295125687	69004-03-1 - Toltrazuril, [D08]	0,990396527	50-28-2 - Estradiol, [F17]	1,712217142
56392-17-7 - Metoprolol tartrate, [A16]	1,25196	436349 - Doxifluridine, [D21]	0,988077038	60142-96-3 - Gabapentin, [I04]	1,707550068
112529-15-4 - Pioglitazone, [H14]	1,247203105	26921-17-5 - Timolol maleate (s), [I11]	0,985642784	17230-88-5 - Danazol, [B21]	1,703013798
115956-12-2 - Dolasetron, [N22]	1,240556994	105956-99-8 - Clinafloxacin HCl, [O15]	0,982894364	53885-35-1 - Ticlopidine HCl, [J17]	1,700206297
20537-88-6 - Amifostine, [I03]	1,236009569	147-24-0 - Diphenhydramine HCl, [F05]	0,976100002	146-48-5 - Yohimbine HCl, [G19]	1,694836442
64221-86-9 - Imipenem, [A15]	1,216067973	54029-12-8 - Ricobendazole, [E05]	0,971376289	69655-05-6 - Didanosine, [N20]	1,693844678
74863-84-6 - Argatroban, [L12]	1,202209182	50-28-2 - Estradiol, [F17]	0,96480993	59052-16-3 - Nalbuphine HCl, [J03]	1,683896332
33069-62-4 - Taxol, [C08]	1,196361838	78415-72-2 - Milrinone, [J14]	0,957420018	1156-19-0 - Tolazamide, [L10]	1,683773093
114084-78-5 - Ibandronate, [A13]	1,19585598	59052-16-3 - Nalbuphine HCl, [J03]	0,938337477	hsa-590, [J23]	1,672104129
50-91-9 - Floxuridine, [J11]	1,191840065	2971-90-6 - Clopidol, [O19]	0,931223698	73210-73-8 - Xamoterol hemifumarate,	1,667142487

79794-75-5 - Loratadine, [P17]	1,190805403	130929-57-6 - Entacapone, [P15]	0,928687704	84057-84-1 - Lamotrigine, [N07]	1,663204784
65-49-6 - 4-aminosalicylic acid, [I07]	1,182762521	82009-34-5 - Cilastatin, [L14]	0,928687704	41570-61-0 - Tulobuterol, [E11]	1,660271787
57381-26-7 - Irsogladine maleate, [J12]	1,181805021	23672-07-3 - Sulpiride s (-), [F03]	0,92330011	51037-30-0 - Acipimox, [G05]	1,655978064
60-54-8 - Tetracycline, [B04]	1,176890199	158966-92-8 - Montelukast, [C08]	0,919235402	57773-63-4 - Triptorelin, [C17]	1,638686475
16595-80-5 - Levamisole HCl, [P03]	1,176396055	hsa-199, [F23]	0,917012546	69975-86-6 - Doxofylline, [F03]	1,634282474
51037-30-0 - Acipimox, [G05]	1,157225515	21498-08-8 - Lofexidine, [C03]	0,916745395	83150-76-9 - Octreotide, [C09]	1,634169714
70458-96-7 - Norfloxacin, [E04]	1,12955987	22204-53-1 - Naproxen, [M22]	0,915752438	65-49-6 - 4-aminosalicylic acid, [I07]	1,630874358
379-79-3 - Ergotamine D-tartrate, [H22]	1,1233296	22494-42-4 - Diflunisal, [D15]	0,912656338	590-63-6 - Carbamyl-beta-methylcholine	1,630674451
2078-54-8 - Propofol, [O21]	1,114332806	62929-91-3 - Procaterol hcl, [I17]	0,902218674	93793-83-0 - Roxatidine acetate HCl, [M	1,629492602
125-84-8 - Dl-aminoglutethimide, [I05]	1,104507527	357-08-4 - Naloxone HCl, [F20]	0,900460899	49562-28-9 - Fenofibrate, [H19]	1,623342138
6673-35-4 - Practolol, [I09]	1,10094875	66357-59-3 - Ranitidine HCl, [F09]	0,899658684	103628-48-4 - Sumatriptan Succinate, [C	1,612660942
88671-89-0 - Myclobutanil, [C10]	1,093038589	38776-75-9 - Rifampicin, [F12]	0,897492534	124750-99-8 - Losartan potassium, [P21	1,593233861
28395-03-1 - Bumetanide, [O14]	1,090138976	56-75-7 - Chloramphenicol, [M15]	0,884810487	106463-17-6 - Tamsulosin HCl, [O16]	1,580235484
50-78-2 - Acetylsalicylic acid, [G03]	1,090021821	143491-57-0 - Emtricitabine, [I05]	0,88092172	85721-33-1 - Ciprofloxacin, [O07]	1,579256869
53716-50-0 - Oxfendazole, [E20]	1,088523277	154598-52-4 - Efavirenz, [N16]	0,866590367	41575-94-4 - Carboplatin, [M05]	1,568916888
50-33-9 - Phenylbutazone, [G18]	1,080678852	58-33-3 - Promethazine HCl, [F07]	0,824782079	56-75-7 - Chloramphenicol, [M15]	1,543239689
69975-86-6 - Doxofylline, [F03]	1,051012405	16320-04-0 - Gestrinone, [L15]	0,824326263	7240-38-2 - Oxacillin sodium monohydra	1,528228131
603-50-9 - Bisacodyl, [K15]	1,048143875	315-30-0 - Allopurinol, [G13]	0,819012388	78110-38-0 - Aztreonam, [K09]	1,514534445
198904-31-3 - Atazanavir, [P22]	1,043678886	144701-48-4 - Telmisartan, [O18]	0,811518202	149676-40-4 - Pefloxacine mesylate, [G1	1,510789429
92623-83-1 - Pravadoline, [K06]	1,037830676	106017-08-7 - Rufloxacin, [M08]	0,800264943	13523-86-9 - Pindolol, [I21]	1,468820601
66357-59-3 - Ranitidine HCl, [F09]	1,037377356	60-81-1 - Phloridzin, [P10]	0,79801603	165800-03-3 - Linezolid, [L05]	1,445159302
224785-90-4 - Vardenafil, [L03]	1,030400848	40600-13-3 - Cirazoline HCl, [E21]	0,771540684	105462-24-6 - Risedronic acid, [C21]	1,435013485
54029-12-8 - Ricobendazole, [E05]	1,022866319	147416-96-4 - Telenzepine 2HCl, [M03]	0,762904865	65-29-2 - Gallamine triethiodide, [E22]	1,426970333
357-08-4 - Naloxone HCl, [F20]	1,003221121	75847-73-3 - Enalapril, [F07]	0,758203737	25717-80-0 - Molsidomine, [K04]	1,421699287
306-40-1 - Succinylcholine, [P14]	0,996368955	130636-43-0 - Nifekalant HCl, [C07]	0,754789037	78613-35-1 - Amorolfine, [J19]	1,406873967
95734-82-0 - Nedaplatin, [P16]	0,988138985	28395-03-1 - Bumetanide, [O14]	0,749253708	497-30-3 - Ergothioneine, [D04]	1,396829759
120092-68-4 - Manidipine, [L11]	0,975304037	15307-79-6 - Diclofenac, Na, [D09]	0,748275993	147416-96-4 - Telenzepine 2HCl, [M03]	1,396029774
2971-90-6 - Clopidol, [O19]	0,974618602	37321-09-8 - Apramycin, [I15]	0,745118539	357-08-4 - Naloxone HCl, [F20]	1,394066285
29520-14-7 - Guanfacine HCl, [P21]	0,961041079	hsa-199, [E23]	0,744554143	106017-08-7 - Rufloxacin, [M08]	1,385447683
305-03-3 - Chlorambucil, [M19]	0,959611859	51803-78-2 - Nimesulide, [B14]	0,742115412	568-72-9 - Tanshinone iia, [H08]	1,37511341
97964-56-2 - Lorglumide, [P19]	0,945462256	50-27-1 - Estriol, [F19]	0,736639182	69004-03-1 - Toltrazuril, [D08]	1,373259585
2216-88-5 - Ketoprofen (s), [N21]	0,942132005	151615 - Oxymetazoline HCl, [G03]	0,736639043	738-70-5 - Trimethoprim, [D14]	1,371767444
57754-86-6 - Nisoxetine HCl, [K13]	0,929474101	7232-21-5 - Metoclopramide HCl, [H15]	0,707442693	25812-30-0 - Gemfibrozil, [L13]	1,365600915
cel-67, [D23]	0,923868998	14222-60-7 - Prothionamide, [I12]	0,701234128	57-41-0 - Phenytoin, [E11]	1,363991543
1421-86-9 - Strychnine HCl, [D03]	0,908763393	41859-67-0 - Bezafibrate, [F04]	0,696389453	81732-65-2 - Bambuterol, [J18]	1,35395249
61413-54-5 - Rolipram, [J16]	0,906831192	6055-19-2 - Cyclophosphamide monohydrate, [B11]	0,691376583	hsa-590, [M23]	1,347986866
32828-81-2 - Picotamide, [L18]	0,906404757	113806-05-6 - Olopatadine, [L09]	0,683894381	154598-52-4 - Efavirenz, [N16]	1,347884577
366-70-1 - Procarbazine HCl, [I10]	0,90615979	65-49-6 - 4-aminosalicylic acid, [I07]	0,673190928	50-91-9 - Floxuridine, [J11]	1,347612226
3778-73-2 - Ifosfamide, [N11]	0,90150199	29122-68-7 - Atenolol, [I19]	0,671407671	1791337 - Carbadox, [M03]	1,340698907
98079-52-8 - Lomefloxacin HCl, [P15]	0,897356694	27203-92-5 - Tramadol HCl, [D10]	0,658983126	50-63-5 - Chloroquine phosphate, [O03]	1,336237305
83150-76-9 - Octreotide, [C09]	0,89693375	3366-95-8 - Secnidazole, [M16]	0,653478966	14838-15-4 - Phenylpropanolamine, [P1	1,332951789
14222-60-7 - Prothionamide, [I12]	0,896754444	68291-97-4 - Zonisamide, [O07]	0,645482977	530-78-9 - Flufenamic acid, [E07]	1,322528308
98-92-0 - Medroxyprogesterone 17-acetate, [A06]	0,896453174	28822-58-4 - Isobutylmethylxanthine, [J10]	0,640769917	78415-72-2 - Milrinone, [J14]	1,319262741
89197-32-0 - Efaroxan, [C16]	0,892363245	36322-90-4 - Piroxicam, [B06]	0,636552388	40391-99-9 - Pamidronic acid, [C13]	1,300034848
58066-85-6 - Miltefosine, [I16]	0,886452929	41575-94-4 - Carboplatin, [M05]	0,631283562	56-53-1 - Diethylstilbestrol, [D13]	1,289879637
68291-97-4 - Zonisamide, [O07]	0,885932268	54-71-7 - Pilocarpine HCl, [K17]	0,625160293	64490-92-2 - Tolmetin Na, [D06]	1,288032153
53-86-1 - Indomethacin, [M20]	0,883574251	119141-88-7 - Esomeprazole potassium, [F15]	0,624905813	61413-54-5 - Rolipram, [J16]	1,279885511
10238-21-8 - Glyburide, [L06]	0,88227408	79855-88-2 - Trequinsin, [J20]	0,617637118	15307-79-6 - Diclofenac, Na, [D09]	1,273911988
73210-73-8 - Xamoterol hemifumarate, [I13]	0,880296416	57381-26-7 - Irsogladine maleate, [J12]	0,601994842	63590-64-7 - Terazosin HCl, [O22]	1,266875441
34580-14-8 - Ketotifen fumarate, [F16]	0,874159085	89-57-6 - 5-aminosalicylic acid, [I09]	0,598415986	614-39-1 - Procainamide, [E13]	1,263586235
54-85-3 - Isoniazid, [J15]	0,871633233	603-50-9 - Bisacodyl, [K15]	0,584410014	15687-27-1 - Ibuprofen, [O06]	1,2606048
81409-90-7 - Cabergoline, [A09]	0,862010261	hsa-199, [F01]	0,576067669	68291-97-4 - Zonisamide, [O07]	1,242416271
98048-97-6 - Fosinopril, [P08]	0,856870257	84057-84-1 - Lamotrigine, [N07]	0,570817197	99464-64-9 - Ampiroxicam, [I13]	1,240736983
cel-67, [D23]	0,853002779	54-31-9 - Furosemide, [L05]	0,55138641	50-27-1 - Estriol, [F19]	1,240049295
3160-91-6 - Moroxydine HCl, [A03]	0,841900605	60-54-8 - Tetracycline, [B04]	0,543420348	122892-31-3 - Itopride HCl, [N17]	1,228444817
1716-12-7 - Sodium phenylbutyrate, [B22]	0,831205686	73-31-4 - Melatonin, [E10]	0,536999633	39809-25-1 - Penciclovir, [G12]	1,226998603
99300-78-4 - Venlafaxine HCl, [F04]	0,828364081	891986 - Dacarbazine, [B19]	0,536915663	566-48-3 - Formestane, [J21]	1,224119188
16170-76-6 - Bromebric acid, [L16]	0,824704208	1791337 - Carbadox, [M03]	0,53499909	427-51-0 - Cyproterone acetate, [B13]	1,212247691
10596-23-3 - Clodronate disodium, [N14]	0,822464968	50-35-1 - Thalidomide, [O05]	0,531177194	2216-88-5 - Ketoprofen (s), [N21]	1,198994467
122-11-2 - Sulfadimethoxine, [O12]	0,820785653	15826-37-6 - Disodium cromoglycate, [M10]	0,51669484	91296-87-6 - Sarafloxacin HCl, [M10]	1,179761989
1400-61-9 - Nystatin, [E06]	0,819166048	122892-31-3 - Itopride HCl, [N17]	0,513373315	98079-52-8 - Lomefloxacin HCl, [P15]	1,174889225
cel-67, [L23]	0,815384798	2216-88-5 - Ketoprofen (s), [N21]	0,512513908	73-31-4 - Melatonin, [E10]	1,174818477
107753-78-6 - Zafirlukast, [J10]	0,812888164	hsa-199, [F02]	0,495100531	69014-14-8 - Tiotidine, [O05]	1,173331172
5786-21-0 - Clozapine, [K14]	0,798728287	81110-73-8 - Racecadotril, [K08]	0,482706257	81-24-3 - Taurocholic acid, sodium salt h	1,173241397
54-31-9 - Furosemide, [L05]	0,794359047	24390-14-5 - Doxycycline HCl, [F05]	0,464497843	364-98-7 - Diazoxide, [L04]	1,172566545
322-35-0 - Benserazide HCl, [O08]	0,794032195	104632-26-0 - Pramipexole, [C15]	0,463555221	19728-88-2 - Methiothepin maleate, [O1	1,166105766
104632-26-0 - Pramipexole, [C15]	0,791512524	162011-90-7 - Rofecoxib, [H20]	0,460729659	125-84-8 - Dl-aminoglutethimide, [I05]	1,163890529
530-78-9 - Flufenamic acid, [E07]	0,787438249	657-24-9 - Metformin, [C20]	0,45746628	7361-61-7 - Xylazine HCl, [F19]	1,161117253
125494-59-9 - Sibutramine HCl, [M18]	0,782633751	10118-90-8 - Minocycline HCl, [C04]	0,45739471	59277-89-3 - Acycloguanosine, [G09]	1,149699543
15307-79-6 - Diclofenac, Na, [D09]	0,767395477	79547-78-7 - Levocabastine HCl, [F18]	0,445506723	434-03-7 - Ethisterone, [F13]	1,143218252
90357-06-5 - Bicalutamide, [N12]	0,763293879	3810-74-0 - Streptomycin sulfate, [O06]	0,433723976	6673-35-4 - Practolol, [I09]	1,137604216
cel-67, [K23]	0,761386409	153559-49-0 - Bexarotene, [L14]	0,426873788	54-92-2 - Iproniazid, [F08]	1,135933935
22204-24-6 - Pyrantel pamoate, [I22]	0,758986674	80288-49-9 - Furafylline, [B07]	0,423704648	99011-02-6 - Imiquimod, [N13]	1,133325044
95233-18-4 - Atovaquone, [N13]	0,752977831	99464-64-9 - Ampiroxicam, [I13]	0,418086926	1508-75-4 - Tropicamide, [M05]	1,13057883
106463-17-6 - Tamsulosin HCl, [O16]	0,743387795	132539-06-1 - Olanzapine, [N03]	0,416722536	1405-54-5 - Tylosin tartrate, [D18]	1,128343581
54-71-7 - Pilocarpine HCl, [K17]	0,716956573	51-12-7 - Nialamide, [M13]	0,415283786	17902-23-7 - Ftorafur, [L03]	1,109844
22071-15-4 - Ketoprofen, [B16]	0,716390049	53-86-1 - Indomethacin, [M20]	0,414870794	90098-04-7 - Rebamipide, [K14]	1,107501404
99011-02-6 - Imiquimod, [N13]	0,71582756	611-75-6 - Bromhexine HCl, [K17]	0,413724668	976-71-6 - Canrenone, [K21]	1,1043615
74011-58-8 - Enoxacin, [F09]	0,714920613	74863-84-6 - Argatroban, [L12]	0,411402443	hsa-590, [J24]	1,101762669
105956-99-8 - Clinafloxacin HCl, [O15]	0,707031412	80214-83-1 - Roxithromycin, [M06]	0,405624343	hsa-590, [I24]	1,098823168
cel-67, [K24]	0,704521222	541-22-0 - Decamethonium 2Br, [B17]	0,402306457	15500-66-0 - Pancuronium Br, [M07]	1,072675718
1649-18-9 - Azaperone, [K03]	0,70275246	568-72-9 - Tanshinone iia, [H08]	0,400296854	73-05-2 - PhentolamineHCl, [E03]	1,072467691
555-30-6 - Methyldopa, [A12]	0,700827552	2078-54-8 - Propofol, [O21]	0,38244441	132-98-9 - Pencillin v potassium, [G16]	1,060236127

89796-99-6 - Aceclofenac, [G07]	0,698428216	81732-65-2 - Bambuterol, [J18]	0,372986132	60-81-1 - Phloridzin, [P10]	1,052524505
4205-91-8 - Clonidine HCl, [G11]	0,687981017	133040-01-4 - Eprosartan, [P09]	0,356871172	90-05-1 - Guaiacol, [D18]	1,049813903
71-82-9 - Levallorphan tartrate, [H21]	0,681319723	101975-10-4 - Zardaverine, [L06]	0,35072254	53902-12-8 - Tranilast, [K08]	1,046612913
26921-17-5 - Timolol maleate (s), [I11]	0,677765731	25717-80-0 - Molsidomine, [K04]	0,350171004	82419-36-1 - Ofloxacin, [E08]	1,030238653
14611-51-9 - Selegiline, [C10]	0,675141514	14252-80-3 - Bupivacaine HCl, [F12]	0,341166052	123948-87-8 - Topotecan, [B20]	1,024528621
105826-92-4 - Tropisetron HCl, [D16]	0,671439979	88040-23-7 - Cefepime, [N17]	0,34076535	3366-95-8 - Secnidazole, [M16]	1,023472138
105816-04-4 - nateglinide, [B09]	0,670970871	51-02-5 - Pronethalol HCl, [K07]	0,340200472	65141-46-0 - Nicorandil, [L12]	1,022443355
6119-47-7 - Quinine, [E05]	0,667927479	599-79-1 - Sulfasalazine, [O14]	0,338037457	145-13-1 - Pregnenolone, [I16]	1,02187646
80288-49-9 - Furafylline, [B07]	0,666075091	72558-82-8 - Ceftazidime, [M13]	0,337720468	99-66-1 - Valproic acid, [J06]	1,020382364
56-75-7 - Chloramphenicol, [M15]	0,666049965	4205-91-8 - Clonidine HCl, [G11]	0,336955103	1405-10-3 - Neomycin sulfate, [O16]	1,019322235
404-86-4 - Capsaicin, [M12]	0,66572771	63-92-3 - Phenoxybenzamine HCl, [I10]	0,335901993	99300-78-4 - Venlafaxine HCl, [F04]	1,0038296
315-30-0 - Allopurinol, [G13]	0,648310146	145-13-1 - Pregnenolone, [I16]	0,332213748	97964-56-2 - Lorglumide, [P19]	1,002910897
26786-84-5 - Lomofungin, [A15]	0,645018868	83150-76-9 - Octreotide, [C09]	0,331842024	81147-92-4 - Esmolol, [P06]	1,000321676
5104-49-4 - Flurbiprofen, [J05]	0,643970348	637-07-0 - Clofibrate, [O04]	0,32747031	54029-12-8 - Ricobendazole, [E05]	0,999747685
99464-64-9 - Ampiroxicam, [I13]	0,642783653	49745-95-1 - Dobutamine HCl, [K05]	0,319356283	7232-21-5 - Metoclopramide HCl, [H15]	0,982566538
32986-56-4 - Tobramycin (free base), [B16]	0,639943394	10238-21-8 - Glyburide, [L06]	0,313892855	637-07-0 - Clofibrate, [O04]	0,977425694
133-67-5 - Trichloromethiazide, [H07]	0,62969035	139481-59-7 - Candesartan, [N21]	0,308173654	119302-91-9 - Rocuronium bromide, [E0	0,973933541
57-94-3 - Tubocurarine Cl (+), [D05]	0,626224704	40391-99-9 - Pamidronic acid, [C13]	0,305018783	86386-73-4 - Fluconazole, [J19]	0,973406978
cel-67, [D01]	0,612211022	120511-73-1 - Anastrozole, [N10]	0,296560342	101975-10-4 - Zardaverine, [L06]	0,969591361
34911-55-2 - Amfebutamone, [H13]	0,611877592	122-11-2 - Sulfadimethoxine, [O12]	0,296275316	2393-92-2 - Thiamphenicol glycinate, [E(	0,969573561
53-03-2 - Prednisone, [I14]	0,61178274	21187-98-4 - Gliclazide, [L15]	0,290278392	144701-48-4 - Telmisartan, [O18]	0,964809604
364-98-7 - Diazoxide, [L04]	0,604700999	64795-35-3 - Mesulergine HCl, [H11]	0,288260075	1716-12-7 - Sodium phenylbutyrate, [B2	0,964751102
13311-84-7 - Flutamide, [J17]	0,587118165	129-46-4 - Suramin sodium, [D14]	0,286103386	1476-53-5 - Novobiocin Na, [A19]	0,961978394
89-57-6 - 5-aminosalicylic acid, [I09]	0,582378556	18046-21-4 - Fentiazac, [J20]	0,284755834	366-70-1 - Procarbazine HCl, [I10]	0,956186643
59804-37-4 - Tenoxicam, [O20]	0,570228988	103177-37-3 - Pranlukast, [H16]	0,281894832	38776-75-9 - Rifampicin, [F12]	0,951320494
202409-33-4 - Etoricoxib, [A05]	0,570194823	81103-11-9 - Clarithromycin, [O11]	0,279077346	29520-14-7 - Guanfacine HCl, [P21]	0,943657653
111469-81-9 - Naltrindole HCl, [F11]	0,56555021	113-92-8 - Chlorpheniramine maleate, [M21]	0,271097784	27203-92-5 - Tramadol HCl, [D10]	0,940780431
97322-87-7 - Troglitazone, [D22]	0,565344894	69014-14-8 - Tiotidine, [O05]	0,267433883	143491-57-0 - Emtricitabine, [I05]	0,939691318
657-24-9 - Metformin, [C20]	0,564851855	76824-35-6 - Famotidine, [J11]	0,264472813	133040-01-4 - Eprosartan, [P09]	0,935605481
24729-96-2 - Clindamycin palmitate, [N16]	0,558820477	7361-61-7 - Xylazine HCl, [F19]	0,253702394	22204-53-1 - Naproxen, [M22]	0,934519374
58-33-3 - Promethazine HCl, [F07]	0,554610863	11018-89-6 - Ouabain, [I20]	0,250934959	hsa-590, [I23]	0,930815152
50700-72-6 - Vecuronium Br, [D22]	0,554399209	10418-03-8 - Stanozolol, [O04]	0,249669871	76824-35-6 - Famotidine, [J11]	0,920118681
79660-72-3 - Fleroxacin, [J07]	0,552291432	hsa-199, [E01]	0,243025396	51-12-7 - Nialamide, [M13]	0,918517133
1476-53-5 - Novobiocin Na, [A19]	0,551644327	50-40-1 - Norepinephrine-(+)-tartrate l (-), [F21]	0,236889232	436349 - Doxifluridine, [D21]	0,91685391
80809-81-0 - Docebenone, [O22]	0,549422632	65141-46-0 - Nicorandil, [L12]	0,235794191	61-68-7 - Mefenamic acid, [A08]	0,914011462
65277-42-1 - Ketoconazole, [M06]	0,547146831	114-49-8 - Scopolamine HBr, [M14]	0,229533008	22254-24-6 - Ipratropium Br, [K19]	0,9015711
3810-74-0 - Streptomycin sulfate, [O06]	0,516697179	125-84-8 - Dl-aminoglutethimide, [I05]	0,213127063	53-16-7 - Estrone, [F21]	0,899140788
93793-83-0 - Roxatidine acetate HCl, [M04]	0,514165133	2393-92-2 - Thiamphenicol glycinate, [E09]	0,208124293	22204-24-6 - Pyrantel pamoate, [I22]	0,897148562
41575-94-4 - Carboplatin, [M05]	0,505147026	16676-29-2 - Naltrexone HCl, [O11]	0,202812544	159989-64-7 - Nelfinavir Mesylate, [K18	0,895761063
78613-35-1 - Amorolfine, [J19]	0,505109588	483-63-6 - Crotamiton, [B09]	0,20019634	54-71-7 - Pilocarpine HCl, [K17]	0,893245889
124858-35-1 - Nadifloxacin, [C12]	0,500929796	1649-18-9 - Azaperone, [K03]	0,197621776	514-78-3 - Canthaxanthin, [K15]	0,885922284
17230-88-5 - Danazol, [B21]	0,481012981	19982-08-2 - Memantine HCl, [O15]	0,193814697	517- 89- 5 - Shikonin, [K10]	0,880486855
cel-67, [D24]	0,474822463	50-07-7 - Mitomycin c, [F16]	0,193743031	24730-10-7 - Dihydroergocristine mesyl	0,880395213
cel-67, [D01]	0,472700995	68475-42-3 - Anagrelide, [C22]	0,185390626	50-33-9 - Phenylbutazone, [G18]	0,874324303
96036-03-2 - Meropenem, [C05]	0,467992558	57773-63-4 - Triptorelin, [C17]	0,168049539	105816-04-4 - nateglinide, [B09]	0,87332771
28721-07-5 - Oxcarbazepine, [E14]	0,467983406	55268-74-1 - Praziquantel, [I20]	0,167642035	34580-14-8 - Ketotifen fumarate, [F16]	0,869135976
53-43-0 - Dehydroepiandrosterone, [D03]	0,466703655	99300-78-4 - Venlafaxine HCl, [F04]	0,146980396	891986 - Dacarbazine, [B19]	0,846116548
82419-36-1 - Ofloxacin, [E08]	0,465078147	49562-28-9 - Fenofibrate, [H19]	0,129294809	96036-03-2 - Meropenem, [C05]	0,8460852
78755-81-4 - Flumazenil, [A16]	0,462680979	56-53-1 - Diethylstilbestrol, [D13]	0,127112776	149-64-4 - Scopolamine n-butylbromide	0,844786333
132-98-9 - Pencillin v potassium, [G16]	0,46098356	129-03-3 - Cyproheptadine, [P20]	0,126820209	119141-88-7 - Esomeprazole potassium,	0,833820162
103745-39-7 - Fasudil, [E14]	0,458436371	976-71-6 - Canrenone, [K21]	0,120984684	100643-71-8 - Desloratadine, [D05]	0,83049229
58-54-8 - Ethacrynic acid, [M18]	0,458186915	84225-95-6 - Raclopride l-tartrate s(-), [D19]	0,120359652	64-47-1 - Physostigmine sulfate, [M11]	0,825317144
75706-12-6 - Leflunomide, [P11]	0,457670729	315-80-0 - Dibenzepine HCl, [H08]	0,10650889	28822-58-4 - Isobutylmethylxanthine, [J	0,823453824
93-14-1 - Guaifenesin, [L19]	0,453672652	41570-61-0 - Tulobuterol, [E11]	0,105240152	hsa-590, [J02]	0,822474391
87333-19-5 - Ramipril, [K12]	0,452727624	37762-06-4 - Zaprinast, [L04]	0,10198785	1166-34-3 - Cinanserin, [H06]	0,819230968
50-07-7 - Mitomycin c, [F16]	0,45140219	113712-98-4 - Tenatoprazole, [B06]	0,095852016	79-83-4 - Pantothenic acid, [P08]	0,818939309
78919-13-8 - Iloprost, [A19]	0,445135934	364-98-7 - Diazoxide, [L04]	0,091841	603-50-9 - Bisacodyl, [K15]	0,817094243
90098-04-7 - Rebamipide, [K14]	0,443978185	68-35-9 - Sulfadiazine, [O10]	0,091492851	28797-61-7 - Pirenzepine 2HCl, [K21]	0,816215955
69655-05-6 - Didanosine, [N20]	0,440846041	hsa-199, [E24]	0,091369429	6108-05-0 - Lidocaine, [E15]	0,814883178
95635-56-6 - Ranolazine 2HCl, [K10]	0,438115094	1716-12-7 - Sodium phenylbutyrate, [B22]	0,084652523	hsa-590, [I23]	0,813116526
51803-78-2 - Nimesulide, [B14]	0,437749094	85622-93-1 - Temozolomide, [B08]	0,077623946	145781-92-6 - Goserelin acetate, [D16]	0,799014505
102625-70-7 - Pantoprazole, [G04]	0,433241611	2038-35-9 - Phenamil, [E19]	0,072534705	315-80-0 - Dibenzepine HCl, [H08]	0,785489777
2447-57-6 - Sulfadoxine, [O08]	0,431829513	22254-24-6 - Ipratropium Br, [K19]	0,066967199	4205-91-8 - Clonidine HCl, [G11]	0,779969393
361-37-5 - Methysergide, [P04]	0,431379622	119-36-8 - Methyl salicylate, [H12]	0,061314812	68373-14-8 - Sulbactam, [E07]	0,77648438
497-30-3 - Ergothioneine, [D04]	0,418834592	95233-18-4 - Atovaquone, [N13]	0,054079969	89-57-6 - 5-aminosalicylic acid, [I09]	0,776432745
18683-91-5 - Ambroxol, [D06]	0,413581713	83915-83-7 - Lisinopril, [P13]	0,050759382	hsa-590, [N23]	0,756747583
33286-22-5 - Diltiazem, [G10]	0,401923714	614-39-1 - Procainamide, [E13]	0,046609546	3810-74-0 - Streptomycin sulfate, [O06]	0,75342654
14252-80-3 - Bupivacaine HCl, [F12]	0,379005232	111406-87-2 - Zileuton, [J12]	0,031850641	37148-27-9 - Clenbuterol, [I15]	0,749391654
82586-55-8 - Quinapril HCl, [K06]	0,375030477	29094-61-9 - Glipizide, [C21]	0,021408919	hsa-590, [N01]	0,743948203
1166-34-3 - Cinanserin, [H06]	0,369200107	434-03-7 - Ethisterone, [F13]	0,020894615	93-14-1 - Guaifenesin, [L19]	0,739297603
27203-92-5 - Tramadol HCl, [D10]	0,35591877	124832-27-5 - Valaciclovir, [D20]	0,011316357	53716-50-0 - Oxfendazole, [E20]	0,738678548
7232-21-5 - Metoclopramide HCl, [H15]	0,35057556	21736-83-4 - Spectinomycin, [C03]	0,008533744	54-31-9 - Furosemide, [L05]	0,73457836
15687-27-1 - Ibuprofen, [O06]	0,342426721	26807-65-8 - Indapamide, [N15]	0,005406089	10596-23-3 - Clodronate disodium, [N14	0,726106533
25717-80-0 - Molsidomine, [K04]	0,342039789	161814-49-9 - Amprenavir, [N10]	0,004127709	826-39-1 - Mecamylamine HCl, [B19]	0,716972837
147-24-0 - Diphenhydramine HCl, [F05]	0,338403859	53885-35-1 - Ticlopidine HCl, [J17]	0,001115637	1405-41-0 - Gentamycin sulfate, [L11]	0,705341058
147536-97-8 - Bosentan, [N14]	0,337557345	61413-54-5 - Rolipram, [J16]	-0,008743516	67121-76-0 - Fluperlapine, [H12]	0,697341306
24390-14-5 - Doxycycline HCl, [F05]	0,329211502	54-92-2 - Iproniazid, [F08]	-0,013266137	22494-42-4 - Diflunisal, [D15]	0,694040265
38194-50-2 - Sulindac, [J04]	0,327660753	835-31-4 - Naphazoline HCl, [C16]	-0,014152012	53-86-1 - Indomethacin, [M20]	0,688696005
64-77-7 - Tolbutamide, [C17]	0,32253609	366-70-1 - Procarbazine HCl, [I10]	-0,015517897	139481-59-7 - Candesartan, [N21]	0,68595205
50-63-5 - Chloroquine phosphate, [O03]	0,310281594	50-33-9 - Phenylbutazone, [G18]	-0,019476722	93106-60-6 - Enrofloxacin, [F11]	0,676617159
93106-60-6 - Enrofloxacin, [F11]	0,304670956	53-16-7 - Estrone, [F21]	-0,020424665	114-80-7 - Neostigmine Br, [B21]	0,676255856
28822-58-4 - Isobutylmethylxanthine, [J10]	0,30433401	75706-12-6 - Leflunomide, [P11]	-0,021145462	7414-83-7 - Etidronate 2Na, [H03]	0,668061184
1501-84-4 - Rimantadine HCl, [K20]	0,303092154	1986-47-6 - Tranylcypromine, [B04]	-0,023759977	317-34-0 - Aminophylline, [B05]	0,666526732

113-52-0 - Imipramine HCl, [H07]	0,302889185	115344-47-3 - Siguazodan, [J18]	-0,031585334	88040-23-7 - Cefepime, [N17]	0,665847355
144701-48-4 - Telmisartan, [O18]	0,298042851	53716-50-0 - Oxfendazole, [E20]	-0,041575958	118072-93-8 - Zoledronic acid, [O09]	0,665684158
cel-67, [C01]	0,294721734	85371-64-8 - Pinacidil, [C19]	-0,04482604	80214-83-1 - Roxithromycin, [M06]	0,66308971
112811-59-3 - Gatifloxacin, [L09]	0,294640199	144689-63-4 - Olmesartan, [L17]	-0,045857042	224785-90-4 - Vardenafil, [L03]	0,661482135
81147-92-4 - Esmolol, [P06]	0,293711557	73220-03-8 - Remoxipride, [K20]	-0,059299997	306-40-1 - Succinylcholine, [P14]	0,660289942
315-80-0 - Dibenzepine HCl, [H08]	0,288628346	88150-42-9 - Amlodipine, [G08]	-0,062180308	82586-55-8 - Quinapril HCl, [K06]	0,65683106
64795-35-3 - Mesulergine HCl, [H11]	0,28849575	105826-92-4 - Tropisetron HCl, [D16]	-0,070462083	52549-17-4 - Pranoprofen, [I04]	0,654053356
170729-80-3 - Aprepitant, [N12]	0,288028279	hsa-199, [E24]	-0,070582585	305-03-3 - Chlorambucil, [M19]	0,638001834
114-70-5 - Sodium phenylacetate, [P11]	0,287295134	51481-61-9 - Cimetidine, [O03]	-0,083944006	hsa-590, [J23]	0,633202528
196618-13-0 - Oseltamivir, [C11]	0,278012087	19216-56-9 - Prazosin HCl, [G09]	-0,084918397	147536-97-8 - Bosentan, [N14]	0,630212658
37762-06-4 - Zaprinast, [L04]	0,277528115	85721-33-1 - Ciprofloxacin, [O07]	-0,090765431	14222-60-7 - Prothionamide, [I12]	0,624915459
3521-84-4 - Meglumine, [A06]	0,27192163	17360-35-9 - Oxotremorine sesquifumarate, [E18]	-0,09664317	74863-84-6 - Argatroban, [L12]	0,609530729
90-05-1 - Guaiacol, [D18]	0,268401894	68-22-4 - Norethindrone, [C22]	-0,098436727	53164-05-9 - Acemetacin, [E21]	0,596055157
123441-03-2 - Rivastigmine, [H18]	0,26645581	77883-43-3 - Doxazosin mesylate, [D19]	-0,104121567	14252-80-3 - Bupivacaine HCl, [F12]	0,594705898
1684-40-8 - Tacrine HCl, [E20]	0,256218109	63527-52-6 - Cefotaxime acid, [M11]	-0,116528606	50-78-2 - Acetylsalicylic acid, [G03]	0,594540342
62929-91-3 - Procaterol hcl, [I17]	0,255362339	119302-91-9 - Rocuronium bromide, [E03]	-0,120680785	85371-64-8 - Pinacidil, [C19]	0,590690052
82410-32-0 - Ganciclovir, [L07]	0,25282087	125-69-9 - Dextromethorphan HBr, [D07]	-0,121671539	16170-76-6 - Bromebric acid, [L16]	0,578178456
19728-88-2 - Methiothepin maleate, [O12]	0,251569589	59-92-7 - Levodopa, [P07]	-0,133434015	135046-48-9 - Clopidogrel sulfate, [O21]	0,574814752
60-81-1 - Phloridzin, [P10]	0,244732565	68550-75-4 - Cilostamide, [J06]	-0,13571606	90357-06-5 - Bicalutamide, [N12]	0,573281813
31879-05-7 - Fenoprofen, [H17]	0,234829104	224785-90-4 - Vardenafil, [L03]	-0,137897751	50-35-1 - Thalidomide, [O05]	0,554813825
13710-19-5 - Tolfenamic acid, [D04]	0,234559433	5104-49-4 - Flurbiprofen, [J05]	-0,140141131	22071-15-4 - Ketoprofen, [B16]	0,545074881
57808-65-8 - Closantel, [B05]	0,234504881	62893-19-0 - Cefoperazone acid, [M09]	-0,145805339	74011-58-8 - Enoxacin, [F09]	0,541881646
81732-65-2 - Bambuterol, [J18]	0,233504609	379-79-3 - Ergotamine D-tartrate, [H22]	-0,149816419	89796-99-6 - Aceclofenac, [G07]	0,539676484
28860-95-9 - Carbidopa, [B12]	0,2289996	514-78-3 - Canthaxanthin, [K15]	-0,152608921	81103-11-9 - Clarithromycin, [O11]	0,525026039
110871-86-8 - Sparfloxacin, [M20]	0,227920856	42924-53-8 - Nabumetone, [C14]	-0,1550297	103745-39-7 - Fasudil, [E14]	0,523286272
105462-24-6 - Risedronic acid, [C21]	0,226305389	113-52-0 - Imipramine HCl, [H07]	-0,156948577	1501-84-4 - Rimantadine HCl, [K20]	0,518987516
112809-51-5 - Letrozole, [L22]	0,220645624	738-70-5 - Trimethoprim, [D14]	-0,157834447	hsa-590, [N01]	0,518305316
13707-88-5 - Alprenolol HCl, [H05]	0,21809245	65-29-2 - Gallamine triethiodide, [E22]	-0,166463216	104-46-1 - Anethole, trans-, [P20]	0,515284802
79547-78-7 - Levocabastine HCl, [F18]	0,217508215	305-03-3 - Chlorambucil, [M19]	-0,17687322	72599-27-0 - Miglustat, [N20]	0,508663376
50-35-1 - Thalidomide, [O05]	0,216250756	636-54-4 - Clopamide, [I22]	-0,180284673	541-22-0 - Decamethonium 2Br, [B17]	0,505878782
32672-69-8 - Mesoridazine besylate, [H22]	0,209479459	104227-87-4 - Famciclovir, [H09]	-0,186403157	139264-17-8 - zolmitriptan, [O13]	0,500304337
29122-68-7 - Atenolol, [I19]	0,209110376	50700-72-6 - Vecuronium Br, [D22]	-0,202974498	16595-80-5 - Levamisole HCl, [P03]	0,492573346
738-70-5 - Trimethoprim, [D14]	0,200464778	54187-04-1 - Rilmenidine hemifumarate, [G15]	-0,204386186	4394-00-7 - Niflumic acid, [C20]	0,4886123
143491-57-0 - Emtricitabine, [I05]	0,197031583	57-41-0 - Phenytoin, [E11]	-0,212642301	51-83-2 - Carbamylcholine Cl, [J05]	0,486793682
134308-13-7 - Tolcapone, [L13]	0,188861699	17230-88-5 - Danazol, [B21]	-0,21500352	57808-65-8 - Closantel, [B05]	0,475852405
152459-95-5 - Imatinib, [C04]	0,188400038	15687-27-1 - Ibuprofen, [O06]	-0,225195226	1649-18-9 - Azaperone, [K03]	0,468920915
cel-67, [L24]	0,180813033	hsa-199, [F24]	-0,227577533	89365-50-4 - Salmeterol, [E17]	0,468314194
147221-93-0 - Delavirdine mesylate, [F20]	0,175657474	31879-05-7 - Fenoprofen, [H17]	-0,260408642	144689-63-4 - Olmesartan, [L17]	0,466790174
cel-67, [L01]	0,166004945	114-70-5 - Sodium phenylacetate, [P11]	-0,276864955	645-05-6 - Altretamine, [G17]	0,462811164
84-16-2 - Hexestrol, [L21]	0,163983668	497-30-3 - Ergothioneine, [D04]	-0,27739855	28395-03-1 - Bumetanide, [O14]	0,456330807
55-48-1 - Atropine sulfate, [B15]	0,163610499	55-48-1 - Atropine sulfate, [B15]	-0,288111506	55268-74-1 - Praziquantel, [I20]	0,452332123
749-13-3 - Trifluperidol 2HCl, [P16]	0,162862068	551-11-1 - Dinoprost, [E12]	-0,294642837	38304-91-5 - Minoxidil, [L08]	0,44872727
66085-59-4 - Nimodipine, [G14]	0,159342225	107753-78-6 - Zafirlukast, [J10]	-0,296469942	121268-17-5 - Alendronate, [G15]	0,448269441
81110-73-8 - Racecadotril, [K08]	0,152795223	96036-03-2 - Meropenem, [C05]	-0,303395807	133-67-5 - Trichloromethiazide, [H07]	0,444347587
69-09-0 - Chlorpromazine HCl, [D11]	0,145142467	24730-10-7 - Dihydroergocristine mesylate, [H10]	-0,306426533	59804-37-4 - Tenoxicam, [O20]	0,442146512
cel-67, [L01]	0,14094485	154-21-2 - Lincomycin, [A13]	-0,309154155	33286-22-5 - Diltiazem, [G10]	0,440456702
60142-96-3 - Gabapentin, [I04]	0,140302398	34580-14-8 - Ketotifen fumarate, [F16]	-0,318764753	51803-78-2 - Nimesulide, [B14]	0,432125487
52549-17-4 - Pranoprofen, [I04]	0,137620389	2447-57-6 - Sulfadoxine, [O08]	-0,31986199	88671-89-0 - Myclobutanil, [C10]	0,427375337
85721-33-1 - Ciprofloxacin, [O07]	0,134611636	54-42-2 - Idoxuridine, [N09]	-0,32102834	657-24-9 - Metformin, [C20]	0,425894548
7361-61-7 - Xylazine HCl, [F19]	0,133647346	10596-23-3 - Clodronate disodium, [N14]	-0,330134024	1986-47-6 - Tranylcypromine, [B04]	0,422340539
cel-67, [C23]	0,11683242	hsa-199, [E02]	-0,333188826	2971-90-6 - Clopidol, [O19]	0,419179683
51022-70-9 - Salbutamol sulfate, [I19]	0,11586686	97964-56-2 - Lorglumide, [P19]	-0,341065195	82410-32-0 - Ganciclovir, [L07]	0,39412333
976-71-6 - Canrenone, [K21]	0,111687029	63659-19-8 - Betaxolol HCl, [I07]	-0,35013368	79660-72-3 - Fleroxacin, [J07]	0,392628319
130929-57-6 - Entacapone, [P15]	0,110277734	566-48-3 - Formestane, [J21]	-0,360656017	53-03-2 - Prednisone, [I14]	0,384335819
1405-41-0 - Gentamycin sulfate, [L11]	0,103777857	124750-99-8 - Losartan potassium, [P21]	-0,372897639	hsa-590, [M01]	0,375542208
42924-53-8 - Nabumetone, [C14]	0,102608998	1400-61-9 - Nystatin, [E06]	-0,373888014	581-88-4 - Debrisoquin sulfate, [O10]	0,372067967
20559-55-1 - Oxibendazole, [E22]	0,09520962	112809-51-5 - Letrozole, [L22]	-0,381782329	68-22-4 - Norethindrone, [C22]	0,369763564
103177-37-3 - Pranlukast, [H16]	0,090108291	121268-17-5 - Alendronate, [G15]	-0,406090776	3778-73-2 - Ifosfamide, [N11]	0,368876935
74050-98-9 - Ketanserin tartrate, [H18]	0,084848557	51-83-2 - Carbamylcholine Cl, [J05]	-0,411127504	18683-91-5 - Ambroxol, [D06]	0,364273864
3366-95-8 - Secnidazole, [M16]	0,081496637	hsa-199, [E01]	-0,417281921	107753-78-6 - Zafirlukast, [J10]	0,359247277
38776-75-9 - Rifampicin, [F12]	0,079890249	57-94-3 - Tubocurarine Cl (+), [D05]	-0,428324267	114-70-5 - Sodium phenylacetate, [P11]	0,357757116
10418-03-8 - Stanozolol, [O04]	0,078519346	53-43-0 - Dehydroepiandrosterone, [D03]	-0,44331458	79547-78-7 - Levocabastine HCl, [F18]	0,351282693
443-48-1 - Metronidazole, [A20]	0,074461639	58186-27-9 - Idebenone, [D08]	-0,451331808	54-85-3 - Isoniazid, [J15]	0,350561629
599-79-1 - Sulfasalazine, [O14]	0,074404856	118072-93-8 - Zoledronic acid, [O09]	-0,451770743	10118-90-8 - Minocycline HCl, [C04]	0,350320805
122892-31-3 - Itopride HCl, [N17]	0,07111076	78110-38-0 - Aztreonam, [K09]	-0,480088586	23672-07-3 - Sulpiride s (-), [F03]	0,333853837
23672-07-3 - Sulpiride s (-), [F03]	0,070182169	11032-41-0 - Dihydroergotamine mesylate, [G21]	-0,491436499	104632-26-0 - Pramipexole, [C15]	0,331739956
101828-21-1 - Butenafine, [P03]	0,060020937	3778-73-2 - Ifosfamide, [N11]	-0,491756203	32672-69-8 - Mesoridazine besylate, [H2	0,326750234
43210-67-9 - Fenbendazole, [H11]	0,056698719	55528-07-9 - Butaclamol (+), [D07]	-0,504549686	98-92-0 - Medroxyprogesterone 17-acet	0,326170329
13523-86-9 - Pindolol, [I21]	0,054903314	125494-59-9 - Sibutramine HCl, [M18]	-0,506015826	21736-83-4 - Spectinomycin, [C03]	0,298182436
54-92-2 - Iproniazid, [F08]	0,053804696	hsa-199, [F23]	-0,508908801	120279-95-0 - Dorzolamide, [P05]	0,297194227
149676-40-4 - Pefloxacine mesylate, [G10]	0,050507116	145781-92-6 - Goserelin acetate, [D16]	-0,509153387	60-31-1 - Acetylcholine Cl, [B13]	0,290661668
50-27-1 - Estriol, [F19]	0,049606982	7481-89-2 - 2',3' - dideoxycytidine, [D11]	-0,513143925	hsa-590, [M24]	0,28915566
1156-19-0 - Tolazamide, [L10]	0,049093588	6108-05-0 - Lidocaine, [E15]	-0,514276821	55528-07-9 - Butaclamol (+), [D07]	0,284616379
104-46-1 - Anethole, trans-, [P20]	0,028810133	29520-14-7 - Guanfacine HCl, [P21]	-0,519672933	51-30-9 - Isoproterenol HCl (rac), [B11]	0,277837419
79-83-4 - Pantothenic acid, [P08]	0,02750672	7414-83-7 - Etidronate 2Na, [H03]	-0,523187098	54239-37-1 - Cimaterol, [K03]	0,266931882
118072-93-8 - Zoledronic acid, [O09]	0,026488809	58066-85-6 - Miltefosine, [I16]	-0,523540459	361-37-5 - Methysergide, [P04]	0,266781161
568-72-9 - Tanshinone iia, [H08]	0,026301653	82571-53-7 - Ozagrel, [P13]	-0,524072693	hsa-590, [N02]	0,246671994
149-64-4 - Scopolamine n-butylbromide, [M12]	0,026024137	68373-14-8 - Sulbactam, [E07]	-0,526634466	87333-19-5 - Ramipril, [K12]	0,241214176
68-35-9 - Sulfadiazine, [O10]	0,023994775	3521-84-4 - Meglumine, [A06]	-0,527288395	202409-33-4 - Etoricoxib, [A05]	0,240236223
80214-83-1 - Roxithromycin, [M06]	0,021163651	89197-32-0 - Efaroxan, [C16]	-0,528248557	66357-59-3 - Ranitidine HCl, [F09]	0,228665223
51-02-5 - Pronethalol HCl, [K07]	0,015517442	69975-86-6 - Doxofylline, [F03]	-0,544435369	3506-09-0 - Propranolol, [K22]	0,225299508
427-51-0 - Cyproterone acetate, [B13]	0,01463297	88671-89-0 - Myclobutanil, [C10]	-0,547174052	26921-17-5 - Timolol maleate (s), [I11]	0,225011634
30484-77-6 - Flunarizine-2HCl, [G22]	0,014008533	58-54-8 - Ethacrynic acid, [M18]	-0,548740348	101828-21-1 - Butenafine, [P03]	0,224412984

19453 - Galanthamine HBr, [G04]	0,012356217	59729-33-8 - Citalopram, [O09]	-0,558440733	105956-99-8 - Clinafloxacin HCl, [O15]	0,216138241
69014-14-8 - Tiotidine, [O05]	0,012000553	79660-72-3 - Fleroxacin, [J07]	-0,559936574	31431-39-7 - Mebendazol, [A04]	0,186876579
120511-73-1 - Anastrozole, [N10]	0,008951278	133-67-5 - Trichloromethiazide, [H07]	-0,560844341	102767-28-2 - Levetiracetam, [L20]	0,173187671
19216-56-9 - Prazosin HCl, [G09]	0,0066543	82410-32-0 - Ganciclovir, [L07]	-0,562016377	51022-77-6 - Etazolate, [J08]	0,158899097
84371-65-3 - Mifepristone, [L22]	0,005916612	123441-03-2 - Rivastigmine, [H18]	-0,56572917	85760-74-3 - Quinpirole HCl (-)-, [K18]	0,136524693
1677687 - Pentoxifylline, [G14]	0,005440114	21535-47-7 - Mianserin hcl, [B03]	-0,573209132	99614-01-4 - Ondansetron, [H16]	0,122283916
835-31-4 - Naphazoline HCl, [C16]	-0,00132272	16595-80-5 - Levamisole HCl, [P03]	-0,584923679	6055-19-2 - Cyclophosphamide monohy	0,122281968
15291-75-5 - Ginkgolide a, [P12]	-0,012034754	65277-42-1 - Ketoconazole, [M06]	-0,58588149	2447-57-6 - Sulfadoxine, [O08]	0,116590669
91296-87-6 - Sarafloxacin HCl, [M10]	-0,012103648	72599-27-0 - Miglustat, [N20]	-0,5890872	42971-09-5 - Vinpocetine, [J22]	0,111681183
78110-38-0 - Aztreonam, [K09]	-0,020488986	57808-65-8 - Closantel, [B05]	-0,593423458	97322-87-7 - Troglitazone, [D22]	0,103005765
113-92-8 - Chlorpheniramine maleate, [M21]	-0,021062482	103745-39-7 - Fasudil, [E14]	-0,598360581	196618-13-0 - Oseltamivir, [C11]	0,102876398
100-33-4 - Pentamidine, [J14]	-0,023992084	139264-17-8 - zolmitriptan, [O13]	-0,599968188	6119-47-7 - Quinine, [E05]	0,09471332
483-63-6 - Crotamiton, [B09]	-0,024718794	530-78-9 - Flufenamic acid, [E07]	-0,601071802	315-30-0 - Allopurinol, [G13]	0,090970808
59052-16-3 - Nalbuphine HCl, [J03]	-0,029398627	90-05-1 - Guaiacol, [D18]	-0,607560649	36330-85-5 - Fenbufen, [H13]	0,086750342
11032-41-0 - Dihydroergotamine mesylate, [G21]	-0,031489055	103628-48-4 - Sumatriptan Succinate, [G21]	-0,610451293	83905-01-5 - Azithromycin, [K07]	0,079605223
81-24-3 - Taurocholic acid, sodium salt hydrate, [N1	-0,038931011	212141-54-3 - Vatalanib, [C12]	-0,611512753	10418-03-8 - Stanozolol, [O04]	0,074936541
97825-25-7 - Ractopamine, [N09]	-0,040047532	22204-24-6 - Pyrantel pamoate, [I22]	-0,612863836	151615 - Oxymetazoline HCl, [G03]	0,072894926
cel-67, [L02]	-0,049940331	32986-56-4 - Tobramycin (free base), [B16]	-0,62215839	21462-39-5 - Clindamycin HCl, [A05]	0,06824526
1791337 - Carbadox, [M03]	-0,050325489	60-31-1 - Acetylcholine Cl, [B13]	-0,627600909	170729-80-3 - Aprepitant, [N12]	0,060959865
23210-56-2 - Ifenprodil, [G05]	-0,051346974	69655-05-6 - Didanosine, [N20]	-0,644257403	hsa-590, [M02]	0,056322265
51-48-9 - L-thyroxine [(3-[4-(4-hydroxy-3,5-diiodoph	-0,060407206	97322-87-7 - Troglitazone, [D22]	-0,657966358	11032-41-0 - Dihydroergotamine mesyla	0,051849583
29094-61-9 - Glipizide, [C21]	-0,071944773	51-30-9 - Isoproterenol HCl (rac), [B11]	-0,670785271	88150-42-9 - Amlodipine, [G08]	0,047616509
184475-35-2 - Gefitinib, [A20]	-0,074677374	64-47-1 - Physostigmine sulfate, [M11]	-0,672343485	84225-95-6 - Raclopride l-tartrate s(-), [I	0,045067519
82571-53-7 - Ozagrel, [P13]	-0,075264491	51322-75-9 - Tizanidine HCl, [A04]	-0,675038027	hsa-590, [N23]	0,038374191
19982-08-2 - Memantine HCl, [O15]	-0,07540171	146-48-5 - Yohimbine HCl, [G19]	-0,677932247	51022-70-9 - Salbutamol sulfate, [I19]	0,035448705
17902-23-7 - Ftorafur, [L03]	-0,076960517	98079-52-8 - Lomefloxacin HCl, [P15]	-0,692524312	147221-93-0 - Delavirdine mesylate, [F2	0,031252743
51-83-2 - Carbamylcholine Cl, [J05]	-0,081029074	hsa-199, [E23]	-0,702867497	124858-35-1 - Nadifloxacin, [C12]	0,028958464
113806-05-6 - Olopatadine, [L09]	-0,081105517	22071-15-4 - Ketoprofen, [B16]	-0,70751917	611-75-6 - Bromhexine HCl, [K17]	0,016792772
cel-67, [C01]	-0,084904974	13707-88-5 - Alprenolol HCl, [H05]	-0,707560924	64-77-7 - Tolbutamide, [C17]	0,006835664
62893-19-0 - Cefoperazone acid, [M09]	-0,08677488	84371-65-3 - Mifepristone, [L22]	-0,70933524	51-02-5 - Pronethalol HCl, [K07]	-0,001153498
298-46-4 - Carbamazepine, [M07]	-0,088463239	959-24-0 - Sotalol HCl, [K09]	-0,713839303	29122-68-7 - Atenolol, [I19]	-0,00233951
145-13-1 - Pregnenolone, [I16]	-0,089193093	90098-04-7 - Rebamipide, [K14]	-0,725634053	599-79-1 - Sulfasalazine, [O14]	-0,007528215
73-05-2 - PhentolamineHCl, [E03]	-0,097285724	99011-02-6 - Imiquimod, [N13]	-0,736507525	835-31-4 - Naphazoline HCl, [C16]	-0,016024473
68475-42-3 - Anagrelide, [C22]	-0,102917286	33286-22-5 - Diltiazem, [G10]	-0,745498294	95233-18-4 - Atovaquone, [N13]	-0,017341099
125-69-9 - Dextromethorphan HBr, [D07]	-0,106208915	51022-70-9 - Salbutamol sulfate, [I19]	-0,750858038	hsa-590, [M02]	-0,021753695
54143-56-5 - Flecainide, [E17]	-0,11175307	99614-01-4 - Ondansetron, [H16]	-0,765147524	32986-56-4 - Tobramycin (free base), [B	-0,023234437
642-72-8 - Benzydamine, [P22]	-0,112052447	91161-71-6 - Terbinafine HCl, [B20]	-0,766450783	55-48-1 - Atropine sulfate, [B15]	-0,027607609
112964-99-5 - Hydroxytacrine maleate, [E16]	-0,115652495	143-67-9 - Vinblastine sulfate, [K05]	-0,776577294	84625-61-6 - Itraconazole, [N19]	-0,036259406
53164-05-9 - Acemetacin, [E21]	-0,117648753	136310-93-5 - Tiotropium Br, [H20]	-0,777185879	hsa-590, [J02]	-0,068043698
595-33-5 - Megestrol acetate, [N04]	-0,123384236	114-80-7 - Neostigmine Br, [B21]	-0,781648771	hsa-590, [M23]	-0,068070651
130636-43-0 - Nifekalant HCl, [C07]	-0,123740822	165800-03-3 - Linezolid, [L05]	-0,784764623	hsa-590, [M24]	-0,08188818
49562-28-9 - Fenofibrate, [H19]	-0,124095361	85760-74-3 - Quinpirole HCl (-)-, [K18]	-0,785093388	hsa-590, [I01]	-0,09271933
cel-67, [D02]	-0,130108265	147221-93-0 - Delavirdine mesylate, [F20]	-0,795394913	hsa-590, [J01]	-0,095872649
79855-88-2 - Trequinsin, [J20]	-0,134600169	38083-17-9 - Climbazole, [O13]	-0,802451457	2898-76-2 - Benzamil, [F10]	-0,110358276
cel-67, [C24]	-0,137344385	91296-87-6 - Sarafloxacin HCl, [M10]	-0,808775378	36322-90-4 - Piroxicam, [B06]	-0,113652306
144689-63-4 - Olmesartan, [L17]	-0,142566166	61-68-7 - Mefenamic acid, [A08]	-0,809375206	95734-82-0 - Nedaplatin, [P16]	-0,128531384
63590-64-7 - Terazosin HCl, [O22]	-0,150704686	54965-21-8 - Albendazole, [G19]	-0,819722068	21535-47-7 - Mianserin hcl, [B03]	-0,12933726
83905-01-5 - Azithromycin, [K07]	-0,155876223	361-37-5 - Methysergide, [P04]	-0,823362334	13707-88-5 - Alprenolol HCl, [H05]	-0,134565207
636-54-4 - Clopamide, [I22]	-0,160119661	63-45-6 - Primaquine phosphate, [I18]	-0,830410781	hsa-590, [I02]	-0,146848507
76420-72-9 - Enalaprilat, [P04]	-0,161454754	53164-05-9 - Acemetacin, [E21]	-0,83668514	80288-49-9 - Furafylline, [B07]	-0,152101331
132539-06-1 - Olanzapine, [N03]	-0,162158647	63590-64-7 - Terazosin HCl, [O22]	-0,84003	113-92-8 - Chlorpheniramine maleate, [I	-0,15481155
25812-30-0 - Gemfibrozil, [L13]	-0,163321896	1508-75-4 - Tropicamide, [M05]	-0,841272619	83915-83-7 - Lisinopril, [P13]	-0,17142516
85622-93-1 - Temozolomide, [B08]	-0,17644662	36791-04-5 - Ribavirin, [K16]	-0,844593638	37321-09-8 - Apramycin, [I15]	-0,173339139
317-34-0 - Aminophylline, [B05]	-0,187426532	132203-70-4 - Cilnidipine, [I08]	-0,850022436	14611-51-9 - Selegiline, [C10]	-0,176750791
73220-03-8 - Remoxipride, [K20]	-0,189184507	52-01-7 - Spironolactone, [M22]	-0,855770831	122-11-2 - Sulfadimethoxine, [O12]	-0,178436599
119141-88-7 - Esomeprazole potassium, [F15]	-0,192786106	100490-36-6 - Tosufloxacin, [B18]	-0,861442725	7177-48-2 - Ampicillin trihydrate, [I11]	-0,190826236
cel-67, [D24]	-0,192952657	15291-75-5 - Ginkgolide a, [P12]	-0,86190389	125494-59-9 - Sibutramine HCl, [M18]	-0,196507798
36330-85-5 - Fenbufen, [H13]	-0,195019926	15500-66-0 - Pancuronium Br, [M07]	-0,876212441	62929-91-3 - Procaterol hcl, [I17]	-0,198344266
38304-91-5 - Minoxidil, [L08]	-0,195443277	28797-61-7 - Pirenzepine 2HCl, [K21]	-0,882041405	57076-71-8 - Denbufylline, [I14]	-0,234022994
cel-67, [K01]	-0,201566758	38304-91-5 - Minoxidil, [L08]	-0,883510551	119-36-8 - Methyl salicylate, [H12]	-0,241879713
39562-70-4 - Nitrendipine, [G16]	-0,202115818	64-77-7 - Tolbutamide, [C17]	-0,884962231	hsa-590, [I01]	-0,245490304
514-78-3 - Canthaxanthin, [K15]	-0,206438943	79-83-4 - Pantothenic acid, [P08]	-0,886114404	797-63-7 - Levonorgestrel, [P05]	-0,246177145
64490-92-2 - Tolmetin Na, [D06]	-0,213573042	60-56-0 - Methimazole, [A18]	-0,89094017	18046-21-4 - Fentiazac, [J20]	-0,248182942
21187-98-4 - Gliclazide, [L15]	-0,217411329	98048-97-6 - Fosinopril, [P08]	-0,895635428	443-48-1 - Metronidazole, [A20]	-0,255441713
cel-67, [K02]	-0,220413672	149676-40-4 - Pefloxacine mesylate, [G10]	-0,911513144	64795-35-3 - Mesulergine HCl, [H11]	-0,255510458
311074 - Troleandomycin, [B10]	-0,221976562	86386-73-4 - Fluconazole, [J19]	-0,916021627	130929-57-6 - Entacapone, [P15]	-0,256660455
cel-67, [C02]	-0,223655815	16170-76-6 - Bromebric acid, [L16]	-0,92366332	40600-13-3 - Cirazoline HCl, [E21]	-0,260849067
40600-13-3 - Cirazoline HCl, [E21]	-0,224298504	595-33-5 - Megestrol acetate, [N04]	-0,926294756	71125-38-7 - Meloxicam, [B18]	-0,265688892
57-41-0 - Phenytoin, [E11]	-0,229632061	5051-62-7 - Guanabenz acetate, [G13]	-0,93447803	78919-13-8 - Iloprost, [A19]	-0,275204741
7240-38-2 - Oxacillin sodium monohydrate, [E18]	-0,231512217	306-40-1 - Succinylcholine, [P14]	-0,937621523	82571-53-7 - Ozagrel, [P13]	-0,278271483
cel-67, [C02]	-0,236077837	1744-22-5 - Riluzole HCl, [O19]	-0,938379812	80809-81-0 - Docebenone, [O22]	-0,278670897
23313-68-0 - Verapamil, [G18]	-0,240250237	3506-09-0 - Propranolol, [K22]	-0,960359158	63527-52-6 - Cefotaxime acid, [M11]	-0,30665489
6108-05-0 - Lidocaine, [E15]	-0,251050494	745-65-3 - Alprostadil, [L08]	-0,960489548	123441-03-2 - Rivastigmine, [H18]	-0,327388459
41859-67-0 - Bezafibrate, [F04]	-0,256409047	21462-39-5 - Clindamycin HCl, [A05]	-0,960809108	67227-56-9 - Fenoldopam mesylate, [H1	-0,347932439
13010-47-4 - Lomustine, [A17]	-0,257674321	52549-17-4 - Pranoprofen, [I04]	-1,035034449	103177-37-3 - Pranlukast, [H16]	-0,354019495
51481-61-9 - Cimetidine, [O03]	-0,258227638	317-34-0 - Aminophylline, [B05]	-1,040413045	14611-52-0 - Deprenyl HCl r (-), [B08]	-0,370527609
797-63-7 - Levonorgestrel, [P05]	-0,272792767	30484-77-6 - Flunarizine-2HCl, [G22]	-1,041281485	959-24-0 - Sotalol HCl, [K09]	-0,379334131
436349 - Doxifluridine, [D21]	-0,275898497	581-88-4 - Debrisoquin sulfate, [O10]	-1,056625706	127045-41-4 - Pazufloxacin, [G08]	-0,388350268
51-12-7 - Nialamide, [M13]	-0,276668982	18683-91-5 - Ambroxol, [D06]	-1,083626307	98048-97-6 - Fosinopril, [P08]	-0,388839342
75847-73-3 - Enalapril, [F07]	-0,278515509	19387-91-8 - Tinidazole, [B14]	-1,086201817	595-33-5 - Megestrol acetate, [N04]	-0,393836926
53902-12-8 - Tranilast, [K08]	-0,293802316	53643-48-4 - Vindesine, [E15]	-1,09226914	hsa-590, [I02]	-0,42211626
cel-67, [C23]	-0,294205076	32672-69-8 - Mesoridazine besylate, [H22]	-1,101380063	72558-82-8 - Ceftazidime, [M13]	-0,449488114
161814-49-9 - Amprenavir, [N10]	-0,301588332	443-48-1 - Metronidazole, [A20]	-1,110344108	56296-78-7 - Fluoxetine HCl, [H14]	-0,455471603

99614-01-4 - Ondansetron, [H16]	-0,309170362	60142-96-3 - Gabapentin, [I04]	-1,134776175	58186-27-9 - Idebenone, [D08]	-0,455888783
120279-95-0 - Dorzolamide, [P05]	-0,314167466	98319-26-7 - Finasteride, [H21]	-1,138215345	50-07-7 - Mitomycin c, [F16]	-0,460435245
6055-19-2 - Cyclophosphamide monohydrate, [B11]	-0,327530719	112529-15-4 - Pioglitazone, [H14]	-1,138774803	73231-34-2 - Florfenicol, [J09]	-0,463018668
15500-66-0 - Pancuronium Br, [M07]	-0,329886464	13311-84-7 - Flutamide, [J17]	-1,144640159	NA - Pravastatin lactone, [G22]	-0,47295972
84225-95-6 - Raclopride l-tartrate s(-), [D19]	-0,332780175	123948-87-8 - Topotecan, [B20]	-1,15963749	1677687 - Pentoxifylline, [G14]	-0,490047842
1986-47-6 - Tranylcypromine, [B04]	-0,334099985	42971-09-5 - Vinpocetine, [J22]	-1,16889753	114084-78-5 - Ibandronate, [A13]	-0,49881485
637-07-0 - Clofibrate, [O04]	-0,3356481	28860-95-9 - Carbidopa, [B12]	-1,174519375	129-46-4 - Suramin sodium, [D14]	-0,499958374
60607-34-3 - Oxatomide, [M08]	-0,341745518	1405-54-5 - Tylosin tartrate, [D18]	-1,185060347	15826-37-6 - Disodium cromoglycate, [N	-0,500818948
22204-53-1 - Naproxen, [M22]	-0,344590429	196618-13-0 - Oseltamivir, [C11]	-1,203522933	75706-12-6 - Leflunomide, [P11]	-0,512370189
6998-60-3 - Rifamycin sv, [C19]	-0,35219622	61477-96-1 - Piperacillin, [G20]	-1,204427196	79855-88-2 - Trequinsin, [J20]	-0,534048075
59-92-7 - Levodopa, [P07]	-0,369646985	6119-47-7 - Quinine, [E05]	-1,220863147	63-92-3 - Phenoxybenzamine HCl, [I10]	-0,541574066
54063-53-5 - Propafenone, [E09]	-0,370979721	2963-78-2 - Butyrylcholine Cl, [J09]	-1,221848311	28860-95-9 - Carbidopa, [B12]	-0,54374821
109889-09-0 - Granisetron, [P14]	-0,379954078	139755-83-2 - Sildenafil, [N11]	-1,223199999	38083-17-9 - Climbazole, [O13]	-0,551440338
21736-83-4 - Spectinomycin, [C03]	-0,380467194	95734-82-0 - Nedaplatin, [P16]	-1,224670795	162011-90-7 - Rofecoxib, [H20]	-0,552662148
133040-01-4 - Eprosartan, [P09]	-0,38659441	112964-99-5 - Hydroxytacrine maleate, [E16]	-1,225616785	73220-03-8 - Remoxipride, [K20]	-0,553957529
79944-56-2 - Idazoxan, [F13]	-0,391273085	71125-38-7 - Meloxicam, [B18]	-1,232756061	120511-73-1 - Anastrozole, [N10]	-0,557409038
40391-99-9 - Pamidronic acid, [C13]	-0,399324231	64221-86-9 - Imipenem, [A15]	-1,25379485	65277-42-1 - Ketoconazole, [M06]	-0,563728919
119302-91-9 - Rocuronium bromide, [E03]	-0,424803994	132-98-9 - Pencillin v potassium, [G16]	-1,255494996	50-40-1 - Norepinephrine-(+)-tartrate l (	-0,581358009
103628-48-4 - Sumatriptan Succinate, [G21]	-0,434981629	749-13-3 - Trifluperidol 2HCl, [P16]	-1,257183003	198904-31-3 - Atazanavir, [P22]	-0,599449971
cel-67, [K02]	-0,437809336	124858-35-1 - Nadifloxacin, [C12]	-1,25834064	136310-93-5 - Tiotropium Br, [H20]	-0,605480858
88150-42-9 - Amlodipine, [G08]	-0,446936376	101477-55-8 - Lomerizine HCl, [A21]	-1,261545763	134308-13-7 - Tolcapone, [L13]	-0,607535929
119-36-8 - Methyl salicylate, [H12]	-0,448984639	826-39-1 - Mecamylamine HCl, [B19]	-1,261704604	37762-06-4 - Zaprinast, [L04]	-0,612305786
37148-27-9 - Clenbuterol, [I15]	-0,453561805	62658-64-4 - Bopindolol malonate, [P19]	-1,26353201	31879-05-7 - Fenoprofen, [H17]	-0,639815733
90-69-7 - Lobeline, [E08]	-0,467339262	81147-92-4 - Esmolol, [P06]	-1,266040922	31430-15-6 - Flubendazole, [J15]	-0,662665877
60-31-1 - Acetylcholine Cl, [B13]	-0,468952086	hsa-199, [F01]	-1,270962252	212141-54-3 - Vatalanib, [C12]	-0,662791431
31431-39-7 - Mebendazol, [A04]	-0,484262689	17902-23-7 - Ftorafur, [L03]	-1,286695555	749-13-3 - Trifluperidol 2HCl, [P16]	-0,669513898
112965-21-6 - Calcipotriene, [J08]	-0,486324241	57076-71-8 - Denbufylline, [I14]	-1,288193404	147-24-0 - Diphenhydramine HCl, [F05]	-0,669738934
183321-74-6 - Erlotinib, [E06]	-0,486976046	115956-12-2 - Dolasetron, [N22]	-1,300456305	hsa-590, [I24]	-0,67299733
611-75-6 - Bromhexine HCl, [K17]	-0,493432127	31430-15-6 - Flubendazole, [J15]	-1,30247477	311074 - Troleandomycin, [B10]	-0,708050606
04199-10-4 - Propranolol HCl s(-), [A08]	-0,503062216	100986-85-4 - Levofloxacin HCl, [P09]	-1,302677415	hsa-590, [M01]	-0,716870373
14611-52-0 - Deprenyl HCl r (-), [B08]	-0,505599711	1951-25-3 - Amiodarone, [C07]	-1,325156323	158966-92-8 - Montelukast, [C08]	-0,728338128
106266-06-2 - Risperidone, [D21]	-0,520540719	80809-81-0 - Docebenone, [O22]	-1,357386141	154-21-2 - Lincomycin, [A13]	-0,729413771
165800-03-3 - Linezolid, [L05]	-0,528863899	92623-83-1 - Pravadoline, [K06]	-1,379853661	16320-04-0 - Gestrinone, [L15]	-0,744625315
54965-21-8 - Albendazole, [G19]	-0,532780846	hsa-199, [F24]	-1,38395237	555-30-6 - Methyldopa, [A12]	-0,762136485
28797-61-7 - Pirenzepine 2HCl, [K21]	-0,533077761	5786-21-0 - Clozapine, [K14]	-1,392476705	63659-19-8 - Betaxolol HCl, [I07]	-0,780914978
113712-98-4 - Tenatoprazole, [B06]	-0,533967404	6673-35-4 - Practolol, [I09]	-1,393070009	59-92-7 - Levodopa, [P07]	-0,782230458
891986 - Dacarbazine, [B19]	-0,535239734	105816-04-4 - nateglinide, [B09]	-1,411916296	36791-04-5 - Ribavirin, [K16]	-0,788946307
154598-52-4 - Efavirenz, [N16]	-0,550248761	198904-31-3 - Atazanavir, [P22]	-1,415167689	111469-81-9 - Naltrindole HCl, [F11]	-0,793651934
434-03-7 - Ethisterone, [F13]	-0,556741248	83366-66-9 - Nefazodone, [C18]	-1,417567442	83366-66-9 - Nefazodone, [C18]	-0,802636812
959-24-0 - Sotalol HCl, [K09]	-0,566697416	100643-71-8 - Desloratadine, [D05]	-1,418495261	112809-51-5 - Letrozole, [L22]	-0,822837946
cel-67, [D02]	-0,568527097	50-63-5 - Chloroquine phosphate, [O03]	-1,432058995	34911-55-2 - Amfebutamone, [H13]	-0,839694225
1405-10-3 - Neomycin sulfate, [O16]	-0,570278376	50-41-9 - Clomiphene citrate, [O17]	-1,441835054	51481-61-9 - Cimetidine, [O03]	-0,846714802
2963-78-2 - Butyrylcholine Cl, [J09]	-0,57134726	59122-46-2 - Misoprostol, [L10]	-1,452170601	49745-95-1 - Dobutamine HCl, [K05]	-0,85961058
100986-85-4 - Levofloxacin HCl, [P09]	-0,579564068	38194-50-2 - Sulindac, [J04]	-1,454873498	100986-85-4 - Levofloxacin HCl, [P09]	-0,877983481
24730-10-7 - Dihydroergocristine mesylate, [H10]	-0,581811963	311074 - Troleandomycin, [B10]	-1,463718285	58-33-3 - Promethazine HCl, [F07]	-0,881993356
72432-10-1 - Aniracetam, [O17]	-0,584614227	66104-23-2 - Pergolide mesylate, [D17]	-1,46500608	30484-77-6 - Flunarizine-2HCl, [G22]	-0,911073825
57773-63-4 - Triptorelin, [C17]	-0,584880847	183321-74-6 - Erlotinib, [E06]	-1,476457881	60-56-0 - Methimazole, [A18]	-0,919903827
cel-67, [K01]	-0,598924171	50-78-2 - Acetylsalicylic acid, [G03]	-1,483828438	6998-60-3 - Rifamycin sv, [C19]	-0,924677865
83915-83-7 - Lisinopril, [P13]	-0,599594552	NA - Pravastatin lactone, [G22]	-1,498193703	101477-55-8 - Lomerizine HCl, [A21]	-0,93458154
1405-54-5 - Tylosin tartrate, [D18]	-0,599735541	57754-86-6 - Nisoxetine HCl, [K13]	-1,503093003	100-33-4 - Pentamidine, [J14]	-0,939989012
114977-28-5 - Docetaxil, [L07]	-0,602192209	97825-25-7 - Ractopamine, [N09]	-1,503119877	5536-17-4 - Vidarabine, [F06]	-0,947133612
302-22-7 - Chlormadinone acetate, [M17]	-0,607319564	114084-78-5 - Ibandronate, [A13]	-1,539283885	13311-84-7 - Flutamide, [J17]	-0,957814004
93957-54-1 - Fluvastatin Na, [P06]	-0,614154087	105462-24-6 - Risedronic acid, [C21]	-1,554322941	2016-88-8 - Amiloride, [G06]	-0,973227024
614-39-1 - Procainamide, [E13]	-0,617517568	72432-10-1 - Aniracetam, [O17]	-1,563642373	98319-26-7 - Finasteride, [H21]	-0,97831354
101975-10-4 - Zardaverine, [L06]	-0,617698075	322-35-0 - Benserazide HCl, [O08]	-1,575733623	hsa-590, [N24]	-0,979997541
67121-76-0 - Fluperlapine, [H12]	-0,629754486	73-05-2 - PhentolamineHCl, [E03]	-1,582528642	51322-75-9 - Tizanidine HCl, [A04]	-0,989058606
76824-35-6 - Famotidine, [J11]	-0,630156127	1166-34-3 - Cinanserin, [H06]	-1,583609012	113-52-0 - Imipramine HCl, [H07]	-1,016590645
85371-64-8 - Pinacidil, [C19]	-0,632789715	109889-09-0 - Granisetron, [P14]	-1,585116635	483-63-6 - Crotamiton, [B09]	-1,017850262
143-67-9 - Vinblastine sulfate, [K05]	-0,633328025	76420-72-9 - Enalaprilat, [P04]	-1,601952696	97825-25-7 - Ractopamine, [N09]	-1,023578168
54-42-2 - Idoxuridine, [N09]	-0,638773301	56296-78-7 - Fluoxetine HCl, [H14]	-1,645272062	5051-62-7 - Guanabenz acetate, [G13]	-1,029815006
114-49-8 - Scopolamine HBr, [M14]	-0,650309754	2016-88-8 - Amiloride, [G06]	-1,648614792	109889-09-0 - Granisetron, [P14]	-1,03613347
38083-17-9 - Climbazole, [O13]	-0,656393624	73231-34-2 - Florfenicol, [J09]	-1,666252266	21498-08-8 - Lofexidine, [C03]	-1,044167622
83366-66-9 - Nefazodone, [C18]	-0,666548125	6998-60-3 - Rifamycin sv, [C19]	-1,674714134	hsa-590, [J24]	-1,054713283
2016-88-8 - Amiloride, [G06]	-0,666669358	1421-86-9 - Strychnine HCl, [D03]	-1,678137245	hsa-590, [N02]	-1,062754296
39809-25-1 - Penciclovir, [G12]	-0,672093815	127045-41-4 - Pazufloxacin, [G08]	-1,683305415	71-82-9 - Levallorphan tartrate, [H21]	-1,078257288
86386-73-4 - Fluconazole, [J19]	-0,674102666	78755-81-4 - Flumazenil, [A16]	-1,690959102	79944-56-2 - Idazoxan, [F13]	-1,086629011
826-39-1 - Mecamylamine HCl, [B19]	-0,684680357	71-82-9 - Levallorphan tartrate, [H21]	-1,714973342	110429-49-8 - Paroxetine HCl, [G06]	-1,089806882
102767-28-2 - Levetiracetam, [L20]	-0,688801711	98-92-0 - Medroxyprogesterone 17-acetate, [A06]	-1,741997839	77883-43-3 - Doxazosin mesylate, [D19]	-1,098933579
100490-36-6 - Tosufloxacin, [B18]	-0,69314901	14611-52-0 - Deprenyl HCl r (-), [B08]	-1,749569803	50-12-4 - Mephenytoin, [J22]	-1,142884208
36791-04-5 - Ribavirin, [K16]	-0,697234576	90357-06-5 - Bicalutamide, [N12]	-1,769176353	90-69-7 - Lobeline, [E08]	-1,157912651
41570-61-0 - Tulobuterol, [E11]	-0,706828959	83905-01-5 - Azithromycin, [K07]	-1,778254325	61477-96-1 - Piperacillin, [G20]	-1,165454768
54239-37-1 - Cimaterol, [K03]	-0,712215772	130209-82-4 - Latanoprost, [I18]	-1,779775843	89197-32-0 - Efaroxan, [C16]	-1,173074861
169590-42-5 - Celecoxib, [L18]	-0,722442093	89796-99-6 - Aceclofenac, [G07]	-1,795680615	23210-56-2 - Ifenprodil, [G05]	-1,18952063
145781-92-6 - Goserelin acetate, [D16]	-0,722588132	120279-95-0 - Dorzolamide, [P05]	-1,815190129	33386-08-2 - Buspirone HCl, [K19]	-1,223120398
cel-67, [K24]	-0,723649422	79944-56-2 - Idazoxan, [F13]	-1,856661813	11018-89-6 - Ouabain, [I20]	-1,262421655
14028-44-5 - Amoxapine, [H09]	-0,739356134	14611-51-9 - Selegiline, [C10]	-1,866395216	52-01-7 - Spironolactone, [M22]	-1,265993601
63-45-6 - Primaquine phosphate, [I18]	-0,75016066	1476-53-5 - Novobiocin Na, [A19]	-1,870570406	35208-55-0 - Clindamycin PO4, [A07]	-1,28486691
6138-79-0 - Trans-triprolidine HCl, [M21]	-0,751282498	81409-90-7 - Cabergoline, [A09]	-1,906878094	551-11-1 - Dinoprost, [E12]	-1,295078568
57808-66-9 - Domperidone, [D13]	-0,754385523	57149-07-2 - Naftopidil 2HCl, [G07]	-1,939671555	2038-35-9 - Phenamil, [E19]	-1,302746748
NA - Pravastatin lactone, [G22]	-0,766208084	202409-33-4 - Etoricoxib, [A05]	-1,968293625	54143-56-5 - Flecainide, [E17]	-1,329556492
17360-35-9 - Oxotremorine sesquifumarate, [E18]	-0,772369186	302-22-7 - Chlormadinone acetate, [M17]	-1,98079901	10238-21-8 - Glyburide, [L06]	-1,357688701
55268-74-1 - Praziquantel, [I20]	-0,783404738	797-63-7 - Levonorgestrel, [P05]	-1,984362478	64221-86-9 - Imipenem, [A15]	-1,362001169
101477-55-8 - Lomerizine HCl, [A21]	-0,796105873	170729-80-3 - Aprepitant, [N12]	-1,999656425	59-33-6 - Mepyramine maleate, [M19]	-1,421407571

566-48-3 - Formestane, [J21]	-0,810531026	31431-39-7 - Mebendazol, [A04]	-2,009480338	3521-84-4 - Meglumine, [A06]	-1,426254449
147416-96-4 - Telenzepine 2HCl, [M03]	-0,811662777	79794-75-5 - Loratadine, [P17]	-2,020568205	04199-10-4 - Propranolol HCl s(-), [A08]	-1,43461035
cel-67, [C24]	-0,813816167	90-69-7 - Lobeline, [E08]	-2,131981149	115256-11-6 - Dofetilide, [E04]	-1,45972104
73231-34-2 - Florfenicol, [J09]	-0,814072265	115256-11-6 - Dofetilide, [E04]	-2,138750805	130636-43-0 - Nifekalant HCl, [C07]	-1,474615843
49745-95-1 - Dobutamine HCl, [K05]	-0,815238512	10347-81-6 - Maprotiline HCl, [K11]	-2,209739089	30516-87-1 - 3'-azido-3'-deoxythymidine	-1,477110815
22254-24-6 - Ipratropium Br, [K19]	-0,817314997	51-40-1 - Epinephrine-(+)-tartrate l (-), [F17]	-2,246889065	129-03-3 - Cyproheptadine, [P20]	-1,498809598
51-21-8 - 5-fluorouracil, [J03]	-0,829799693	427-51-0 - Cyproterone acetate, [B13]	-2,271608412	100490-36-6 - Tosufloxacin, [B18]	-1,507801847
21498-08-8 - Lofexidine, [C03]	-0,838711802	89778-26-7 - Toremifene, [B22]	-2,283126642	19982-08-2 - Memantine HCl, [O15]	-1,540496108
1508-75-4 - Tropicamide, [M05]	-0,84652753	101828-21-1 - Butenafine, [P03]	-2,331358931	38194-50-2 - Sulindac, [J04]	-1,591787763
58186-27-9 - Idebenone, [D08]	-0,848398024	184475-35-2 - Gefitinib, [A20]	-2,373120238	112529-15-4 - Pioglitazone, [H14]	-1,616708692
cel-67, [L23]	-0,855115688	104-46-1 - Anethole, trans-, [P20]	-2,383558138	302-22-7 - Chlormadinone acetate, [M1	-1,637449587
4394-00-7 - Niflumic acid, [C20]	-0,857204735	74050-98-9 - Ketanserin tartrate, [H18]	-2,38879806	1054-88-2 - Spiroxatrine, [G17]	-1,665680424
59865-13-3 - Cyclosporin a, [A09]	-0,858032594	100-33-4 - Pentamidine, [J14]	-2,412628085	hsa-590, [J01]	-1,665836394
3506-09-0 - Propranolol, [K22]	-0,85855482	749-02-0 - Spiperone, [F15]	-2,436538178	642-72-8 - Benzydamine, [P22]	-1,709894199
22260-51-1 - Bromocriptine mesylate, [K12]	-0,864034657	67121-76-0 - Fluperlapine, [H12]	-2,460628089	54350-48-0 - Etretinate, [H05]	-1,746097802
68-96-2 - 17- hydroxyprogesterone, [N07]	-0,864679195	51022-77-6 - Etazolate, [J08]	-2,463830637	153559-49-0 - Bexarotene, [L14]	-1,787866005
103890-78-4 - Lacidipine, [L21]	-0,869600228	363-24-6 - Dinoprostone, [C18]	-2,476824035	105826-92-4 - Tropisetron HCl, [D16]	-1,804342404
27848-84-6 - Nicergoline, [I03]	-0,875258394	111469-81-9 - Naltrindole HCl, [F11]	-2,489457037	26786-84-5 - Lomofungin, [A15]	-1,812080389
2068-78-2 - Vincristine sulfate, [E19]	-0,885667477	13010-47-4 - Lomustine, [A17]	-2,54993727	184475-35-2 - Gefitinib, [A20]	-1,816591498
71125-38-7 - Meloxicam, [B18]	-0,921364871	120092-68-4 - Manidipine, [L11]	-2,550663851	43210-67-9 - Fenbendazole, [H11]	-1,898295264
67227-56-9 - Fenoldopam mesylate, [H15]	-0,927783402	54239-37-1 - Cimaterol, [K03]	-2,562222457	56392-17-7 - Metoprolol tartrate, [A16]	-1,902626603
153559-49-0 - Bexarotene, [L14]	-0,935406248	59-33-6 - Mepyramine maleate, [M19]	-2,587093809	128196-01-0 - Escitalopram, [P07]	-1,917032925
66104-23-2 - Pergolide mesylate, [D17]	-0,947062621	2919-66-6 - Melengestrol acetate, [N06]	-2,594598727	749-02-0 - Spiperone, [F15]	-2,024325568
54350-48-0 - Etretinate, [H05]	-0,952829386	147536-97-8 - Bosentan, [N14]	-2,601439988	50-41-9 - Clomiphene citrate, [O17]	-2,12579507
50-40-1 - Norepinephrine-(+)-tartrate l (-), [F21]	-0,953547919	26786-84-5 - Lomofungin, [A15]	-2,606871141	106266-06-2 - Risperidone, [D21]	-2,133518701
314-19-2 - Apomorphine r (-), [D09]	-0,977192411	54143-56-5 - Flecainide, [E17]	-2,622420361	78755-81-4 - Flumazenil, [A16]	-2,149517138
123948-87-8 - Topotecan, [B20]	-0,990979967	103890-78-4 - Lacidipine, [L21]	-2,65149149	hsa-590, [N24]	-2,162857949
5051-62-7 - Guanabenz acetate, [G13]	-0,994451276	35208-55-0 - Clindamycin PO4, [A07]	-2,66065464	111555-58-9 - Naltriben mesylate, [H17]	-2,223640301
77883-43-3 - Doxazosin mesylate, [D19]	-1,022179258	169590-42-5 - Celecoxib, [L18]	-2,672098898	1684-40-8 - Tacrine HCl, [E20]	-2,232752482
cel-67, [L24]	-1,023577353	51037-30-0 - Acipimox, [G05]	-2,789680891	92623-83-1 - Pravadoline, [K06]	-2,260238205
10347-81-6 - Maprotiline HCl, [K11]	-1,027217886	2898-76-2 - Benzamil, [F10]	-2,805641671	6138-79-0 - Trans-triprolidine HCl, [M21	-2,274732956
73573-88-3 - Mevastatin, [D10]	-1,027217886	04199-10-4 - Propranolol HCl s(-), [A08]	-2,806418239	102625-70-7 - Pantoprazole, [G04]	-2,276655126
115256-11-6 - Dofetilide, [E04]	-1,035700525	23210-56-2 - Ifenprodil, [G05]	-2,82127001	148-82-3 - Melphalan, [A10]	-2,277761115
65-29-2 - Gallamine triethiodide, [E22]	-1,040520287	71486-22-1 - Vinorelbine, [E13]	-2,8251249	57754-86-6 - Nisoxetine HCl, [K13]	-2,280047479
84057-84-1 - Lamotrigine, [N07]	-1,047898552	37148-27-9 - Clenbuterol, [I15]	-2,833813194	50847-11-5 - Ibudilast, [A22]	-2,332484429
cel-67, [K23]	-1,054079897	62571-86-2 - Captopril, [O20]	-2,838303491	81409-90-7 - Cabergoline, [A09]	-2,380815837
129-46-4 - Suramin sodium, [D14]	-1,069543081	89365-50-4 - Salmeterol, [E17]	-2,884195419	59122-46-2 - Misoprostol, [L10]	-2,402881382
82009-34-5 - Cilastatin, [L14]	-1,074002476	54350-48-0 - Etretinate, [H05]	-2,914658277	130-61-0 - Thioridazine HCl, [J04]	-2,414101818
59-33-6 - Mepyramine maleate, [M19]	-1,074916624	3160-91-6 - Moroxydine HCl, [A03]	-2,965613551	76420-72-9 - Enalaprilat, [P04]	-2,431565975
51022-77-6 - Etazolate, [J08]	-1,08894672	65899-73-2 - Tioconazole, [B12]	-2,970048554	89778-26-7 - Toremifene, [B22]	-2,597731643
98319-26-7 - Finasteride, [H21]	-1,095426461	39562-70-4 - Nitrendipine, [G16]	-2,971233754	62658-64-4 - Bopindolol malonate, [P19	-2,611758606
551-11-1 - Dinoprost, [E12]	-1,09617521	23313-68-0 - Verapamil, [G18]	-2,974028042	66085-59-4 - Nimodipine, [G14]	-2,620744011
51-40-1 - Epinephrine-(+)-tartrate l (-), [F17]	-1,106558134	51-21-8 - 5-fluorouracil, [J03]	-2,982927387	59729-33-8 - Citalopram, [O09]	-2,657951477
54527-84-3 - Nicardipine, [C09]	-1,116519874	66085-59-4 - Nimodipine, [G14]	-3,002838527	57149-07-2 - Naftopidil 2HCl, [G07]	-2,663215036
14838-15-4 - Phenylpropanolamine, [P12]	-1,148296945	78919-13-8 - Iloprost, [A19]	-3,032603953	5786-21-0 - Clozapine, [K14]	-2,66960054
50847-11-5 - Ibudilast, [A22]	-1,148756185	1684-40-8 - Tacrine HCl, [E20]	-3,044986375	75330-75-5 - Lovastatin, [N05]	-2,809163071
440-17-5 - Trifluoperazine, [I12]	-1,173378168	14028-44-5 - Amoxapine, [H09]	-3,108226496	13010-47-4 - Lomustine, [A17]	-2,870360074
31430-15-6 - Flubendazole, [J15]	-1,173749841	68-26-8 - Vitamin a (acetate), [H19]	-3,157729971	152459-95-5 - Imatinib, [C04]	-2,890810847
57-83-0 - Progesterone, [I08]	-1,189538872	54063-53-5 - Propafenone, [E09]	-3,158585744	73573-88-3 - Mevastatin, [D10]	-2,929328729
100643-71-8 - Desloratadine, [D05]	-1,212810843	74764-40-2 - Bepridil, [C05]	-3,193818168	63-45-6 - Primaquine phosphate, [I18]	-2,951019093
23110-15-8 - Fumagillone, [C14]	-1,214283429	64228-81-5 - Atracurium besylate, [I21]	-3,207120814	114977-28-5 - Docetaxil, [L07]	-3,002668994
517- 89- 5 - Shikonin, [K10]	-1,224012698	129453-61-8 - Fulvestrant, [N22]	-3,231023549	79794-75-5 - Loratadine, [P17]	-3,006670087
129453-61-8 - Fulvestrant, [N22]	-1,231789035	111555-58-9 - Naltriben mesylate, [H17]	-3,269513893	39562-70-4 - Nitrendipine, [G16]	-3,051419207
57076-71-8 - Denbufylline, [I14]	-1,233008902	302-79-4 - Retinoic acid, [D20]	-3,36237223	2068-78-2 - Vincristine sulfate, [E19]	-3,100434686
51322-75-9 - Tizanidine HCl, [A04]	-1,23379549	50847-11-5 - Ibudilast, [A22]	-3,38043317	57-83-0 - Progesterone, [I08]	-3,19974392
54187-04-1 - Rilmenidine hemifumarate, [G15]	-1,267511088	53-03-2 - Prednisone, [I14]	-3,399520597	74050-98-9 - Ketanserin tartrate, [H18]	-3,231846084
541-22-0 - Decamethonium 2Br, [B17]	-1,269304293	60607-34-3 - Oxatomide, [M08]	-3,402773897	93957-54-1 - Fluvastatin Na, [P06]	-3,250168009
51-30-9 - Isoproterenol HCl (rac), [B11]	-1,270867867	129722-12-9 - Aripiprazole, [N19]	-3,416495483	3160-91-6 - Moroxydine HCl, [A03]	-3,280695306
645-05-6 - Altretamine, [G17]	-1,293072107	130-61-0 - Thioridazine HCl, [J04]	-3,429824789	20559-55-1 - Oxibendazole, [E22]	-3,293489262
30516-87-1 - 3'-azido-3'-deoxythymidine, [G11]	-1,302520579	106266-06-2 - Risperidone, [D21]	-3,482148219	78213-63-5 - Piribedil HCl, [M17]	-3,327089703
130209-82-4 - Latanoprost, [I18]	-1,323116231	114977-28-5 - Docetaxil, [L07]	-3,495714142	71486-22-1 - Vinorelbine, [E13]	-3,32867328
72656-09-3 - Carvedilol, [A10]	-1,346272005	57-83-0 - Progesterone, [I08]	-3,517228452	130209-82-4 - Latanoprost, [I18]	-3,397512212
60-56-0 - Methimazole, [A18]	-1,36119697	78213-63-5 - Piribedil HCl, [M17]	-3,540246393	74764-40-2 - Bepridil, [C05]	-3,412328291
85760-74-3 - Quinpirole HCl (-)-, [K18]	-1,361676351	404-86-4 - Capsaicin, [M12]	-3,569897527	132203-70-4 - Cilnidipine, [I08]	-3,44522634
61825-94-3 - Oxaliplatin, [P18]	-1,369481951	1054-88-2 - Spiroxatrine, [G17]	-3,607429169	23313-68-0 - Verapamil, [G18]	-3,477658618
128196-01-0 - Escitalopram, [P07]	-1,390020368	63968-64-9 - Artemisinin, [I17]	-3,612426618	54187-04-1 - Rilmenidine hemifumarate	-3,488602789
104227-87-4 - Famciclovir, [H09]	-1,401334444	33069-62-4 - Taxol, [C08]	-3,641439376	58-54-8 - Ethacrynic acid, [M18]	-3,50720529
148-82-3 - Melphalan, [A10]	-1,434669569	22260-51-1 - Bromocriptine mesylate, [K12]	-3,649239777	745-65-3 - Alprostadil, [L08]	-3,527813806
68-22-4 - Norethindrone, [C22]	-1,479028802	110429-49-8 - Paroxetine HCl, [G06]	-3,688151221	129453-61-8 - Fulvestrant, [N22]	-3,572332423
63659-19-8 - Betaxolol HCl, [I07]	-1,484841191	5630-53-5 - Tibolone, [B10]	-3,692517542	63968-64-9 - Artemisinin, [I17]	-3,577053412
61477-96-1 - Piperacillin, [G20]	-1,494001563	314-19-2 - Apomorphine r (-), [D09]	-3,702036341	65899-73-2 - Tioconazole, [B12]	-3,583471247
2898-76-2 - Benzamil, [F10]	-1,507490748	54527-84-3 - Nicardipine, [C09]	-3,732284197	54527-84-3 - Nicardipine, [C09]	-3,595213852
53643-48-4 - Vindesine, [E15]	-1,527753385	60628-96-8 - Bifonazole, [K13]	-3,73572177	35898-87-4 - Dilazep, [A11]	-3,610930012
36322-90-4 - Piroxicam, [B06]	-1,557661207	30516-87-1 - 3'-azido-3'-deoxythymidine, [G11]	-3,744140752	68-96-2 - 17- hydroxyprogesterone, [N0	-3,759522452
50-41-9 - Clomiphene citrate, [O17]	-1,598549584	20559-55-1 - Oxibendazole, [E22]	-3,769248473	64228-81-5 - Atracurium besylate, [I21]	-3,848950855
111555-58-9 - Naltriben mesylate, [H17]	-1,601638462	2058-52-8 - Clothiapine, [K16]	-3,893406321	145599-86-6 - Cerivastatin, [A12]	-3,934405994
78213-63-5 - Piribedil HCl, [M17]	-1,605014731	642-72-8 - Benzydamine, [P22]	-3,983170647	51-40-1 - Epinephrine-(+)-tartrate l (-), [I	-3,954042984
50-03-3 - Hydrocortisone 21-acetate, [N05]	-1,616856632	57808-66-9 - Domperidone, [D13]	-4,033548444	27848-84-6 - Nicergoline, [I03]	-4,107041131
749-02-0 - Spiperone, [F15]	-1,617659483	14976-57-9 - Clemastine fumarate, [J21]	-4,107423202	53643-48-4 - Vindesine, [E15]	-4,119350389
363-24-6 - Dinoprostone, [C18]	-1,618652502	159989-64-7 - Nelfinavir Mesylate, [K18]	-4,117923473	54965-21-8 - Albendazole, [G19]	-4,124625903
1841-19-6 - Fluspirilene, [C15]	-1,627247654	43210-67-9 - Fenbendazole, [H11]	-4,136788133	54063-53-5 - Propafenone, [E09]	-4,136317486
62571-86-2 - Captopril, [O20]	-1,651796505	69-09-0 - Chlorpromazine HCl, [D11]	-4,170424074	14028-44-5 - Amoxapine, [H09]	-4,242079216
42971-09-5 - Vinpocetine, [J22]	-1,65259001	6138-79-0 - Trans-triprolidine HCl, [M21]	-4,311911165	10347-81-6 - Maprotiline HCl, [K11]	-4,341882724

132203-70-4 - Cilnidipine, [I08]	-1,658298533
146-56-5 - Fluphenazine 2HCl, [D15]	-1,673872996
57149-07-2 - Naftopidil 2HCl, [G07]	-1,688655921
65646-68-6 - Fenretinide, [A18]	-1,707587451
162011-90-7 - Rofecoxib, [H20]	-1,722307582
145599-86-6 - Cerivastatin, [A12]	-1,737889194
2058-52-8 - Clothiapine, [K16]	-1,76132158
10212-25-6 - Cyclocytidine HCl, [B15]	-1,763994066
53123-88-9 - Rapamycin, [A21]	-1,798103788
56296-78-7 - Fluoxetine HCl, [H14]	-1,829977383
62658-64-4 - Bopindolol malonate, [P19]	-1,860056957
159989-64-7 - Nelfinavir Mesylate, [K18]	-1,872025792
7177-48-2 - Ampicillin trihydrate, [I11]	-1,943022361
7481-89-2 - 2',3' - dideoxycytidine, [D11]	-1,946314285
2062-78-4 - Pimozide, [C11]	-1,950252778
1951-25-3 - Amiodarone, [C07]	-1,963008713
72509-76-3 - Felodipine, [I06]	-1,970575347
6980-18-3 - Kasugamycin, [A11]	-1,974987292
50-24-8 - Prednisolone, [I06]	-1,982492139
101831-37-2 - Diclazuril, [N18]	-2,412496445
1054-88-2 - Spiroxatrine, [G17]	-2,464021131
123318-82-1 - Clofarabine, [A07]	-4,679720453
124-94-7 - Triamcinolone, [D12]	-4,156131038
128794-94-5 - Mycophenolate mofetil, [A03]	-3,040684611
129-03-3 - Cyproheptadine, [P20]	-2,618499386
129722-12-9 - Aripiprazole, [N19]	-2,086122514
136310-93-5 - Tiotropium Br, [H20]	-2,338727467
147-94-4 - Cytarabine, [B17]	-2,089686979
14976-57-9 - Clemastine fumarate, [J21]	-2,079521016
1744-22-5 - Riluzole HCl, [O19]	-2,713082361
179324-69-7 - Bortezomib, [J16]	-3,015270441
18378-89-7 - Plicamycin, [F10]	-3,167902847
19387-91-8 - Tinidazole, [B14]	-2,19384767
2038-35-9 - Phenamil, [E19]	-2,186787868
2114454 - Camptothecin, [F08]	-3,296464655
212141-54-3 - Vatalanib, [C12]	-1,863031286
21829-25-4 - Nifedipine, [G12]	-2,683305711
24280-93-1 - Mycophenolic acid, [A17]	-3,048519267
25122-46-7 - Clobetasol propionate, [B03]	-3,565756495
25316-40-9 - Doxorubicin HCl, [H06]	-3,150532788
2919-66-6 - Melengestrol acetate, [N06]	-3,708496771
302-79-4 - Retinoic acid, [D20]	-2,226628684
33419-42-0 - Etoposide, [F14]	-3,499571095
34031-32-8 - Auranofin, [O18]	#DIV/0!
34552-83-5 - Loperamide, [C13]	-2,093303875
35898-87-4 - Dilazep, [A11]	-2,083438558
378-44-9 - Betamethasone, [K11]	-3,073322386
388082-78-8 - Lapatinib, [H10]	-2,950669511
50-02-2 - Dexamethasone, [M14]	-2,876858819
50-22-6 - Corticosterone, [B07]	-2,869934473
50-23-7 - Hydrocortisone, [N03]	-2,952012955
52-86-8 - Haloperidol HCl, [M15]	-3,557291946
532-11-6 - Anethole-trithione (anetholtrithion), [N0	-2,519226247
57576-44-0 - Aclarubicin, [A14]	-4,443454244
58-32-2 - Dipyridamole, [M16]	-2,713397016
58-58-2 - Puromycin 2HCl, [F18]	-4,407247755
63675-72-9 - Nisoldipine, [L19]	-4,373582488
64228-81-5 - Atracurium besylate, [I21]	-2,543174205
64439-81-2 - 10-hydroxycamptothecin, [F22]	-4,421122452
67-73-2 - Fluocinolone acetonide, [J13]	-3,392729164
70288-86-7 - Ivermectin, [M09]	-4,223805583
71486-22-1 - Vinorelbine, [E13]	-2,68844862
71751-41-2 - Abamectin, [N04]	-3,783970267
79902-63-9 - Simvastatin, [D12]	-2,2285194
82640-04-8 - Raloxifene HCl, [F06]	-3,246125729
83-43-2 - Methylprednisolone, [A14]	-3,193503671
89365-50-4 - Salmeterol, [E17]	-2,632171275
9041-93-4 - Bleomycin sulfate, [P17]	-4,228834502
95058-81-4 - Gemcitabine HCl, [P10]	-5,243414738
128196-01-0 - Escitalopram, [P07]	-4,348691255
148-82-3 - Melphalan, [A10]	-4,380946082
73573-88-3 - Mevastatin, [D10]	-4,542685462
56392-17-7 - Metoprolol tartrate, [A16]	-4,586154805
65646-68-6 - Fenretinide, [A18]	-4,636644728
68-96-2 - 17- hydroxyprogesterone, [N07]	-4,640666328
54965-24-1 - Tamoxifen citrate, [N08]	-4,667778388
102625-70-7 - Pantoprazole, [G04]	-4,831092524
27848-84-6 - Nicergoline, [I03]	-5,166670497
61825-94-3 - Oxaliplatin, [P18]	-5,380333123
64211-46-7 - Oxiconazole nitrate, [E16]	-5,446745621
146-56-5 - Fluphenazine 2HCl, [D15]	-5,45372414
440-17-5 - Trifluoperazine, [I12]	-5,509163736
59865-13-3 - Cyclosporin a, [A09]	-5,56828918
72656-09-3 - Carvedilol, [A10]	-5,840993834
23110-15-8 - Fumagillone, [C14]	-5,893168356
35898-87-4 - Dilazep, [A11]	-6,019391899
88495-63-0 - Artesunate, [L16]	-6,06335834
75330-75-5 - Lovastatin, [N05]	-6,175711268
53123-88-9 - Rapamycin, [A21]	-6,226683313
68844-77-9 - Astemizole, [F14]	-6,320613344
34552-83-5 - Loperamide, [C13]	-6,447958939
111974-72-2 - Quetiapine fumarate, [H03]	-6,528937604
50-03-3 - Hydrocortisone 21-acetate, [N05]	-6,621380758
1841-19-6 - Fluspirilene, [C15]	-6,675666317
22916-47-8 - Miconazole, [A22]	-6,684982783
532-11-6 - Anethole-trithione (anetholtrithion), [N08]	-6,715142192
21829-25-4 - Nifedipine, [G12]	-6,868219637
83-43-2 - Methylprednisolone, [A14]	-6,900965154
93957-54-1 - Fluvastatin Na, [P06]	-6,919531501
112965-21-6 - Calcipotriene, [J08]	-6,982124976
79902-63-9 - Simvastatin, [D12]	-7,120379632
6090-95-5 - Conduritol b epoxide, [L20]	-7,171014555
124-94-7 - Triamcinolone, [D12]	-7,227471021
50-24-8 - Prednisolone, [I06]	-7,288258235
72509-76-3 - Felodipine, [I06]	-7,375232216
50-22-6 - Corticosterone, [B07]	-7,385588653
145599-86-6 - Cerivastatin, [A12]	-7,689297796
50-02-2 - Dexamethasone, [M14]	-7,793755342
99592-32-2 - Sertaconazole, [N15]	-7,823956759
67-73-2 - Fluocinolone acetonide, [J13]	-7,845403695
25122-46-7 - Clobetasol propionate, [B03]	-7,988057693
378-44-9 - Betamethasone, [K11]	-7,996017477
58-32-2 - Dipyridamole, [M16]	-8,260641052
82640-04-8 - Raloxifene HCl, [F06]	-8,518015591
52-86-8 - Haloperidol HCl, [M15]	-8,575966221
50-23-7 - Hydrocortisone, [N03]	-8,693503142
32222-06-3 - Calcitriol, [M04]	-8,695449699
6980-18-3 - Kasugamycin, [A11]	-8,787413337
9041-93-4 - Bleomycin sulfate, [P17]	-9,182072291
71751-41-2 - Abamectin, [N04]	-9,227092162
41294-56-8 - Alfacalcidol, [N06]	-9,281740272
101831-37-2 - Diclazuril, [N18]	-9,858517114
33419-42-0 - Etoposide, [F14]	-10,16807669
18378-89-7 - Plicamycin, [F10]	-10,36683155
2114454 - Camptothecin, [F08]	-10,38439828
24280-93-1 - Mycophenolic acid, [A17]	-10,39786554
19356-17-3 - Calcifediol, [K22]	-10,81083145
57576-44-0 - Aclarubicin, [A14]	-10,89137923
10212-25-6 - Cyclocytidine HCl, [B15]	-10,98716709
63675-72-9 - Nisoldipine, [L19]	-11,03076084
128794-94-5 - Mycophenolate mofetil, [A03]	-11,260195
64439-81-2 - 10-hydroxycamptothecin, [F22]	-11,64875062
25316-40-9 - Doxorubicin HCl, [H06]	-12,55865101
82824-01-9 - Naloxonazine 2HCl, [F22]	-12,80217749
147-94-4 - Cytarabine, [B17]	-13,05973305
179324-69-7 - Bortezomib, [J16]	-13,43047506
95058-81-4 - Gemcitabine HCl, [P10]	-14,18071655
34031-32-8 - Auranofin, [O18]	-14,22761407
123318-82-1 - Clofarabine, [A07]	-14,4267973
66104-23-2 - Pergolide mesylate, [D17]	-4,480513077
33069-62-4 - Taxol, [C08]	-4,704647158
183321-74-6 - Erlotinib, [E06]	-4,812956684
2058-52-8 - Clothiapine, [K16]	-4,952503331
2919-66-6 - Melengestrol acetate, [N06]	-4,955795643
404-86-4 - Capsaicin, [M12]	-4,984239699
19216-56-9 - Prazosin HCl, [G09]	-5,085367045
50-03-3 - Hydrocortisone 21-acetate, [N	-5,179393518
111974-72-2 - Quetiapine fumarate, [H0	-5,211860437
143-67-9 - Vinblastine sulfate, [K05]	-5,35146573
129722-12-9 - Aripiprazole, [N19]	-5,383766434
72656-09-3 - Carvedilol, [A10]	-5,406870987
60607-34-3 - Oxatomide, [M08]	-5,416973688
51-21-8 - 5-fluorouracil, [J03]	-5,462890658
302-79-4 - Retinoic acid, [D20]	-5,560910033
22260-51-1 - Bromocriptine mesylate, [K	-5,613407338
59865-13-3 - Cyclosporin a, [A09]	-5,824208725
120092-68-4 - Manidipine, [L11]	-5,849585017
69-09-0 - Chlorpromazine HCl, [D11]	-5,861944608
22916-47-8 - Miconazole, [A22]	-5,942964735
169590-42-5 - Celecoxib, [L18]	-6,214257812
68844-77-9 - Astemizole, [F14]	-6,593958517
61825-94-3 - Oxaliplatin, [P18]	-6,711872524
64211-46-7 - Oxiconazole nitrate, [E16]	-6,792794402
363-24-6 - Dinoprostone, [C18]	-6,957775607
57808-66-9 - Domperidone, [D13]	-7,066895078
322-35-0 - Benserazide HCl, [O08]	-7,14444039
50-22-6 - Corticosterone, [B07]	-7,190789059
14976-57-9 - Clemastine fumarate, [J21]	-7,193368207
50-23-7 - Hydrocortisone, [N03]	-7,417465037
6980-18-3 - Kasugamycin, [A11]	-7,466715751
6090-95-5 - Conduritol b epoxide, [L20]	-7,501642691
62571-86-2 - Captopril, [O20]	-7,566220573
54965-24-1 - Tamoxifen citrate, [N08]	-7,748372573
50-02-2 - Dexamethasone, [M14]	-7,797504504
24280-93-1 - Mycophenolic acid, [A17]	-7,984665238
72509-76-3 - Felodipine, [I06]	-8,151807525
378-44-9 - Betamethasone, [K11]	-8,241101721
58-32-2 - Dipyridamole, [M16]	-8,242266196
25122-46-7 - Clobetasol propionate, [B0	-8,327311915
124-94-7 - Triamcinolone, [D12]	-8,389690181
50-24-8 - Prednisolone, [I06]	-8,60027043
5630-53-5 - Tibolone, [B10]	-8,62906355
88495-63-0 - Artesunate, [L16]	-8,794969568
9041-93-4 - Bleomycin sulfate, [P17]	-8,795995075
83-43-2 - Methylprednisolone, [A14]	-8,907313297
128794-94-5 - Mycophenolate mofetil, [	-8,978259133
18378-89-7 - Plicamycin, [F10]	-9,272037484
23110-15-8 - Fumagillone, [C14]	-9,423104294
82640-04-8 - Raloxifene HCl, [F06]	-9,451220741
82824-01-9 - Naloxonazine 2HCl, [F22]	-9,61770223
65646-68-6 - Fenretinide, [A18]	-9,890495687
52-86-8 - Haloperidol HCl, [M15]	-10,18917905
53123-88-9 - Rapamycin, [A21]	-10,37960221
68-26-8 - Vitamin a (acetate), [H19]	-10,64390541
67-73-2 - Fluocinolone acetonide, [J13]	-10,89881841
60628-96-8 - Bifonazole, [K13]	-10,90999842
99592-32-2 - Sertaconazole, [N15]	-10,94757686
33419-42-0 - Etoposide, [F14]	-11,55755237
83-89-6 - Quinacrine 2HCl dihydrate, [K0	-11,71935787
64439-81-2 - 10-hydroxycamptothecin, [	-11,90258798
2114454 - Camptothecin, [F08]	-12,05472795
79902-63-9 - Simvastatin, [D12]	-12,10387524
10212-25-6 - Cyclocytidine HCl, [B15]	-12,45210348
147-94-4 - Cytarabine, [B17]	-12,74169909
101831-37-2 - Diclazuril, [N18]	-12,98094443
64224-21-1 - Oltipraz, [E10]	-13,32259029
32222-06-3 - Calcitriol, [M04]	-13,3689594
57576-44-0 - Aclarubicin, [A14]	-13,52553917
41294-56-8 - Alfacalcidol, [N06]	-13,61439792
112965-21-6 - Calcipotriene, [J08]	-13,63865965
21829-25-4 - Nifedipine, [G12]	-14,05693049
123318-82-1 - Clofarabine, [A07]	-14,0604983
25316-40-9 - Doxorubicin HCl, [H06]	-14,06383757
19356-17-3 - Calcifediol, [K22]	-14,30257387
71751-41-2 - Abamectin, [N04]	-14,39741541
34031-32-8 - Auranofin, [O18]	-14,52859068
95058-81-4 - Gemcitabine HCl, [P10]	-14,542782
179324-69-7 - Bortezomib, [J16]	-14,72653871
	-19,2316631